UNIVERSIDADE FEDERAL DE SANTA CATARINA
CENTRO DE CIÊNCIAS BIOLÓGICAS
PROGRAMA DE PÓS-GRADUAÇÃO EM BIOTECNOLOGIA E BIOCIÊNCIAS

Geniane Schneider

Prospecção e regulação fotobiológica em macroalgas

Florianópolis
2021

Geniane Schneider

Prospecção e regulação fotobiológica em macroalgas

Tese submetida ao Programa de Pós-Graduação em Biotecnologia e Biociências da Universidade Federal de Santa Catarina para a obtenção do título de Doutor em Biotecnologia e Biociências
Orientador: Prof. José Bonomi Barufi, Dr.
Coorientador: Prof. Félix López Figueroa, Dr.

Florianópolis
2021

Ficha de identificação da obra elaborada pelo autor,
através do Programa de Geração Automática da Biblioteca Universitária da UFSC.

Schneider, Geniane
Prospecção e regulação fotobiológica em macroalgas / Geniane Schneider ; orientador, José Bonomi Barufi, coorientador, Félix López Figueroa, 2021.
237 p.

Tese (doutorado) - Universidade Federal de Santa Catarina, Centro de Ciências Biológicas, Programa de Pós Graduação em Biotecnologia e Biociências, Florianópolis, 2021.

Inclui referências.

1. Biotecnologia e Biociências. 2. Macroalgas. 3. Fotoproteção. 4. Radiação UV-visível. 5. Fotossíntese. I. Barufi, José Bonomi . II. Figueroa, Félix López . III. Universidade Federal de Santa Catarina. Programa de Pós Graduação em Biotecnologia e Biociências. IV. Título.

Geniane Schneider

Prospecção e regulação fotobiológica em macroalgas

O presente trabalho em nível de doutorado foi avaliado e aprovado por banca examinadora composta pelos seguintes membros:

Prof. Marcelo Maraschin, Dr.
Instituição: Universidade Federal de Santa Catarina

Prof. Nelso Patricio Navarro Martínez, Dr.
Instituição: Universidad de Magallanes

Prof.(a) Valéria Laneuville Teixeira, Dr.(a)
Instituição: Universidade Federal Fluminense

Prof. Rubens Tadeu Delgado Duarte, Dr.
Instituição: Universidade Federal de Santa Catarina

Prof. Fábio de Farias Neves, Dr.
Instituição: Universidade do Estado de Santa Catarina

Certificamos que esta é a **versão original e final** do trabalho de conclusão que foi julgado adequado para obtenção do título de doutora em Biotecnologia e Biociências.

ICP-Edu
Documento assinado digitalmente
Glauber Wagner
Data: 23/12/2021 15:11:41-0300
CPF: 007.019.139-59
Verifique as assinaturas em https://v.ufsc.br

Coordenação do Programa de Pós-Graduação

ICP-Edu
Documento assinado digitalmente
Jose Bonomi Barufi
Data: 23/12/2021 09:31:02-0300
CPF: 295.777.208-62
Verifique as assinaturas em https://v.ufsc.br

Prof. José Bonomi Barufi, Dr.
Orientador

Florianópolis, 2021.

Este trabalho é dedicado aos meus professores José Bonomi Barufi e Paulo Antunes Horta, aos meus queridos pais Lorivo Schneider e Rosani C. Schneider, ao meu esposo Alcione Miguel Franz e ao meu filho Miguel Schneider Franz.

AGRADECIMENTOS

Agradeço, primeiramente, meu esposo Alcione Miguel Franz pelo seu apoio e dedicação em todos os momentos. Também aos meus pais e irmãs pelos aconselhamentos, pelo apoio e suporte quando precisei. Obrigada por terem cuidado do Miguel, assim pude finalizar minha pesquisa sabendo que meu filho querido estava em boas mãos.

Agradeço aos meus professores e orientadores Félix López Figueroa, Nathalie Korbee, Nadine Schubert, João Silva e, especialmente, José Bonomi Barufi e Paulo Antunes Horta. A esses professores agradeço imensamente pelo conhecimento transmitido e pelo apoio em todos os momentos, como pesquisadora e como ser humano.

Um agradecimento especial ao professor Paulo e sua esposa Ana Claudia Rodrigues e ao professor José, pois graças a eles atravessei fronteiras e conheci novos horizontes. Por um tempo, além de meus professores foram minha família.

Agradeço aos professores, colegas e toda equipe de técnicos do laboratório LAFIC da UFSC, do laboratório FYBOA da Universidade de Málaga e do Grupo de Pesquisa em Ecologia de Plantas Marinhas da Universidade do Algarve.

Agradeço a CAPES e o CNPq pelo financiamento da pesquisa. Também agradeço o programa de Pós-Graduação em Biotecnologia e Biociências e a UFSC responsáveis, juntamente com os professores, pela minha formação. Sem esses o presente estudo não teria sido possível.

Agradeço a todos que ajudaram para que este doutorado fosse possível, pois foi outro grande desafio para mim...

Muito Obrigada!!

A vida é... um pequeno fluxo, mantido pela luz do Sol.
(Szent-Györgyi, 1937)

RESUMO

As algas são importantes ecologicamente e economicamente, pois desempenham papéis importantes nos diferentes ecossistemas e podem ser fontes potenciais de recursos naturais. Por serem em sua maioria fotossintetizantes, a luz, ou radiação visível, assim como a radiação ultravioleta (UV) são fatores importantes para esses organismos, pois induzem diferentes respostas fisiológicas e bioquímicas. Essas respostas ocorrem graças aos pigmentos fotossintetizantes, responsáveis pela captação da luz, e aos fotorreceptores, proteínas sensíveis à luz e capazes de perceberem a qualidade e quantidade de radiações no ambiente, desencadeando cascatas de reações biológicas. A aclimatação às condições de luz do ambiente leva a mudanças fisiológicas que podem resultar na maior ou menor produção de alguns compostos que captam luz sob baixa luminosidade ou fotoprotegem sob luz excessiva. Algas que ocorrem em regiões entremarés estão mais expostas à luz do que aquelas presentes em maiores profundidades. Assim, buscou-se identificar nessas regiões espécies que naturalmente produzem maior quantidade de compostos de fotoproteção. Além disso, experimentos em laboratório foram conduzidos com duas macroalgas vermelhas (*Gracilaria cornea* e *Osmundea pinnatifida*) para testar os efeitos da qualidade e da fluência de diferentes radiações UV-visível sobre a fotossíntese, a calcificação e a produção de compostos, especialmente os fotoprotetores, tais como: carotenoides, MAAs e fenólicos. A existência e atuação de possíveis fotorreceptores foi também investigada. Duas espécies de macroalgas foram identificadas como as melhores fontes potenciais de substâncias de fotoproteção *Sargassum vulgare* e *Porphyra umbilicalis*. Nos experimentos realizados, observou-se que a radiação UV induz respostas em *G. cornea* e *O. pinnatifida*. Essas respostas podem estar relacionadas com a presença de fotorreceptores sensíveis à luz azul e às radiações UV-A e UV-B. A radiação UV-A parece promover efeitos positivos sobre o crescimento e a produção de compostos alguns compostos (zeaxantina e palitina), enquanto a radiação UV-B promove a produção de alguns compostos (anteraxantina, zeaxantina, luteína e violaxantina) às custas do crescimento. A fotossíntese e a calcificação da alga coralina vermelha *Lithophyllum hibernicum* variaram em relação às diferentes intensidades de luz. A fotossíntese consumiu o CO_2, aumentado o pH e a saturação da calcita e da aragonita, o que favoreceu a calcificação. Taxas positivas e negativas de calcificação foram observadas no escuro. Calcificou no escuro, os espécimes de algas coletados dentro de bancos de gramas marinhas. Além disso, *L. hibernicum* apresentou faces diferentemente pigmentadas. A face adaxial (exposta à luz) das algas coletadas fora dos bancos de gramas marinhas apresentou maior quantidade de substâncias fotoprotetoras e clorofila *a*, enquanto a face abaxial (adjacente ao sedimento) das algas coletadas dentro dos bancos de gramas marinhas apresentou maior quantidade de ficobiliproteínas, especialmente ficoeritrina. Finalmente, foi possível verificar que as macroalgas podem ser importantes fontes de compostos para fins cosmecêuticos, como verificado na bioprospecção que identificou espécies relevantes (*S. vulgare* e *P. umbilicalis*). Além disso, as macroalgas podem ter suas respostas fisiológicas e bioquímicas reguladas como foi visto para *O. pinnatifida* e *G. cornea*, especialmente em relação a radiação UV e luz azul. É importante destacar ainda que a fisiologia das algas precisa ser mais bem compreendida como foi observado para a alga coralina *L. hibernicum*. De forma geral, esta tese contribui com o entendimento sobre compostos produzidos pelas macroalgas, regulação dos mesmos e aspectos ecofisiológicos da alga coralina *L. hibernicum*.

Palavras-chave: Radiação UV-visível. Fotossíntese. Calcificação. Macroalgas. Fotorreceptores. Fotoproteção. MAAs. Carotenoides. Fenólicos.

ABSTRACT

Algae are important ecologically and economically, as they play important roles in different ecosystems and can be potential sources of natural resources. As they are mostly photosynthesizing, the light, or visible radiation, as well as ultraviolet (UV) radiation are important factors for these organisms because they induce different physiological and biochemical responses. These responses occur due to photosynthetic pigments, responsible for capturing light, and photoreceptors, light-sensitive proteins capable of perceiving the quality and quantity of radiation in the environment, triggering cascades of biological reactions. Acclimatization to ambient light conditions leads to physiological changes that can result in greater or lesser production of some compounds that capture light under low light or photoprotect under excessive light. Algae that occur in intertidal regions are more exposed to light than those present at greater depths. Thus, we sought to identify species in these regions that naturally produce a greater amount of photoprotection compounds. Furthermore, laboratory experiments were performed with two species of red macroalgae (*Gracilaria cornea* e *Osmundea pinnatifida*) to test the effects of quality and fluence of different UV-visible radiations on photosynthesis, calcification and production of compounds, especially photoprotectors, such as: carotenoids, MAAs and phenolics. The existence and performance of possible photoreceptors were also investigated. Two macroalgal species were identified as potential sources of photoprotective substances: *Sargassum vulgare* and *Porphyra umbilicalis*. In the experiments carried out, we observed that UV radiation induces responses in *G. cornea* and *O. pinnatifida*. These responses may be related to the presence of photoreceptors sensitive to blue light and UV-A and UV-B radiation. UV-A radiation seems to promote positive effects on the growth and production of some compounds (zeaxanthin and palythine), while UV-B radiation promotes the production of certain compounds (violaxanthin, antheraxanthin, zeaxanthin and lutein) at the expense of growth. Photosynthesis and calcification of the red coralline alga *Lithophyllum hibernicum* varied according to different light intensities. Photosynthesis consumed CO_2, increasing the pH and saturation of calcite and aragonite, which favored calcification. Positive and negative calcification rates were observed in the dark. Calcified in the dark, algae specimens collected from seagrass meadows. In addition, *L. hibernicum* had different pigmented faces. The adaxial face (exposed to light) of the algae collected outside the seagrass meadows showed a higher amount of photoprotective substances and chlorophyll *a*, while the abaxial face (adjacent to the sediment) of the algae collected inside the seagrass meadows showed a higher amount of phycobiliproteins, especially phycoerythrin. Finally, it was possible to verify that macroalgae can be important sources of compounds for cosmeceutical purposes, as verified in the bioprospecting that identified relevant species (*S. vulgare* and *P. umbilicalis*). Furthermore, macroalgae can have their physiological and biochemical responses regulated as seen for *O. pinnatifida* and *G. cornea*, especially in relation to UV radiation and blue light. And lastly, we found that the physiology of algae needs to be better understood as observed for the coralline alga *L. hibernicum*. In general, this thesis contributes to the understanding of compounds produced by macroalgae, their regulation and ecophysiological aspects of the coralline alga *L. hibernicum*.

Keywords: UV-visible radiation. Photosynthesis. Calcification. Macroalgae. Photoreceptors. Photoprotection. MAAs. Carotenoids. Phenolics.

LISTA DE FIGURAS

LISTA DE TABELAS

LISTA DE ABREVIATURAS E SIGLAS

AC: anidrase carbônica

APC: Aloficocianina

AT: Alcalinidade total

BEPFs: Fator de proteção biologicamente efetivo

BSA: Albumina sérica bovina

CCA: Algas coralinas crostosas

Chl*a:* Clorofila *a*

Chl*b:* Clorofila *b*

Chl*c:* Clorofila c

CRA: Algas coralinas vermelhas

DIC: Carbono inorgânico dissolvido

DNA: Ácido desoxirribonucleico

DW: Peso seco

EPI: Índice de fotoproteção do extrato

ESAR: Radiação solar efetiva absorvida

ETR: Taxa de transporte de elétrons

ETR_{max}: Taxa máxima de transporte de elétrons

F_v/F_m: Rendimento quântico máximo do fotossistema II

FW: Peso fresco

HPLC: Cromatografia líquida de alta eficiência

I_k: Irradiância de saturação

LEDs: Diodos emissores de luz

LHCs: Complexos coletores de luz

MAAs: Aminoácidos tipo micosporinas

MCCs: Mecanismos de concentração de carbono

MF: Massa fresca

MS: Massa seca

OCP: *Orange carotenoid protein*

PAR: Radiação fotossinteticamente ativa

PC: Ficocianina

PE: Ficoeritrina

pH: Potencial hidrogeniônico

PMMA: Polimetilmetacrilato

PPD: Escurecimento Persistente do Pigmento

PSI: Fotossistema I

PSII: Fotossistema II

RLC: Curva rápida de luz

RNA: Ácido ribonucleico

ROS: Espécies Reativas de Oxigênio

SOX: Lâmpada de sódio de baixa pressão

SPF: Fator de proteção solar

TC: Taxa de crescimento

UTM: Universal Transversa de Mercator

UV: Radiação ultravioleta

UV-A: Radiação ultravioleta A

UVAPF: Fator de proteção UV-A

UV-B: Radiação ultravioleta B

UV-C: Radiação ultravioleta C

XC: Ciclo de xantofila

α_{ETR}: Eficiência fotossintética

Φ_{PSII}: Rendimento quântico efetivo do fotossistema II

SUMÁRIO

1 INTRODUÇÃO GERAL

As algas constituem um grupo bastante heterogêneo, incluindo organismos que variam de uma única célula até aqueles pluricelulares gigantes. A maioria das algas são fotossintetizantes e vivem em ambientes aquáticos. As exceções incluem organismos heterotróficos, como alguns protistas euglenóides, e outros que toleram ambientes secos e frios mesmo que em estado dormente (GRAHAM et al., 2016a). As algas visíveis a olho nu são denominadas de macroalgas, possuindo corpos parenquimatosos, filamentosos (pseudoparenquimatosos) e cenocíticos. As macroalgas lembram as plantas em algumas características, pois são fotossintetizantes, possuem estratégias parecidas de defesa contra parasitas e predadores e possuem algumas similaridades morfológicas, porém com menor grau de diferenciação e especialização dos seus tecidos (BARSANTI; GUALTIERI, 2005; GRAHAM et al., 2016a).

Os aspectos fundamentais da fotossíntese são similares entre plantas e algas, embora no ambiente terrestre a disponibilidade de dióxido de carbono (CO_2) seja maior. Na água o CO_2 se difunde 10.000 vezes mais lentamente do que no ar. Como resposta, as algas desenvolveram mecanismos de concentração de carbono (MCCs), os quais otimizam a captura de CO_2 garantindo quantidades suficientes para a fotossíntese. Um dos mecanismos consiste em obter o CO_2 a partir do bicarbonato (HCO_3^-) por meio da seguinte reação: $HCO_3^- + H^+ \leftrightarrow CO_2 + H_2O$. Como essa reação é muito lenta, as algas usam uma enzima conhecida como anidrase carbônica (AC) para acelerar drasticamente a taxa de reação (GRAHAM et al., 2016a, 2016b). Outras diferenças importantes estão relacionadas com disponibilidade de luz nos ambientes aquáticos.

A luz como conhecemos se refere à radiação visível que está contida no espectro de radiação emitido pelo Sol, sendo a principal fonte de energia para a fotossíntese. A radiação solar que atinge a superfície terrestre é constituída principalmente pela radiação ultravioleta (UV), visível e infravermelha (ondas de calor). A radiação pode ser representada como ondas que apresentam comprimentos inversamente proporcionais a sua energia. A radiação UV é composta por ondas com comprimentos de 100 a 400 nanômetros (nm), subdividida em UV-A (400 a 315 nm), UV-B (315 a 280 nm) e UV-C (280-100 nm). A UV-C que é quase totalmente absorvida pelos gases estratosféricos, praticamente não afeta os seres vivos. A radiação visível compreende ondas de 400 a 700 nm e a radiação infravermelha acima de 700 nm (BJÖRN, 2008; KIRK, 2010). Essa classificação é arbitrária e pode variar entre autores.

A radiação visível corresponde a luz branca que ao sofrer difração se decompõe em diferentes cores, tais como: roxo, azul, verde, amarelo, laranja e o vermelho, que apresentam diferentes quantidades de energia (MCCLUNEY, 1994). A radiação fotossinteticamente ativa (PAR) engloba os comprimentos de ondas visíveis, por isso na literatura a radiação visível também é chamada de radiação PAR (BJÖRN, 2008). O intervalo de radiação visível e PAR pode variar entre autores, mas para fins deste estudo será considerado como PAR o intervalo entre 400 e 700 nm. A Figura 1 apresenta o espectro eletromagnético, onde é possível visualizar os diferentes tipos de radiações.

Figura 1 - Espectro eletromagnético.

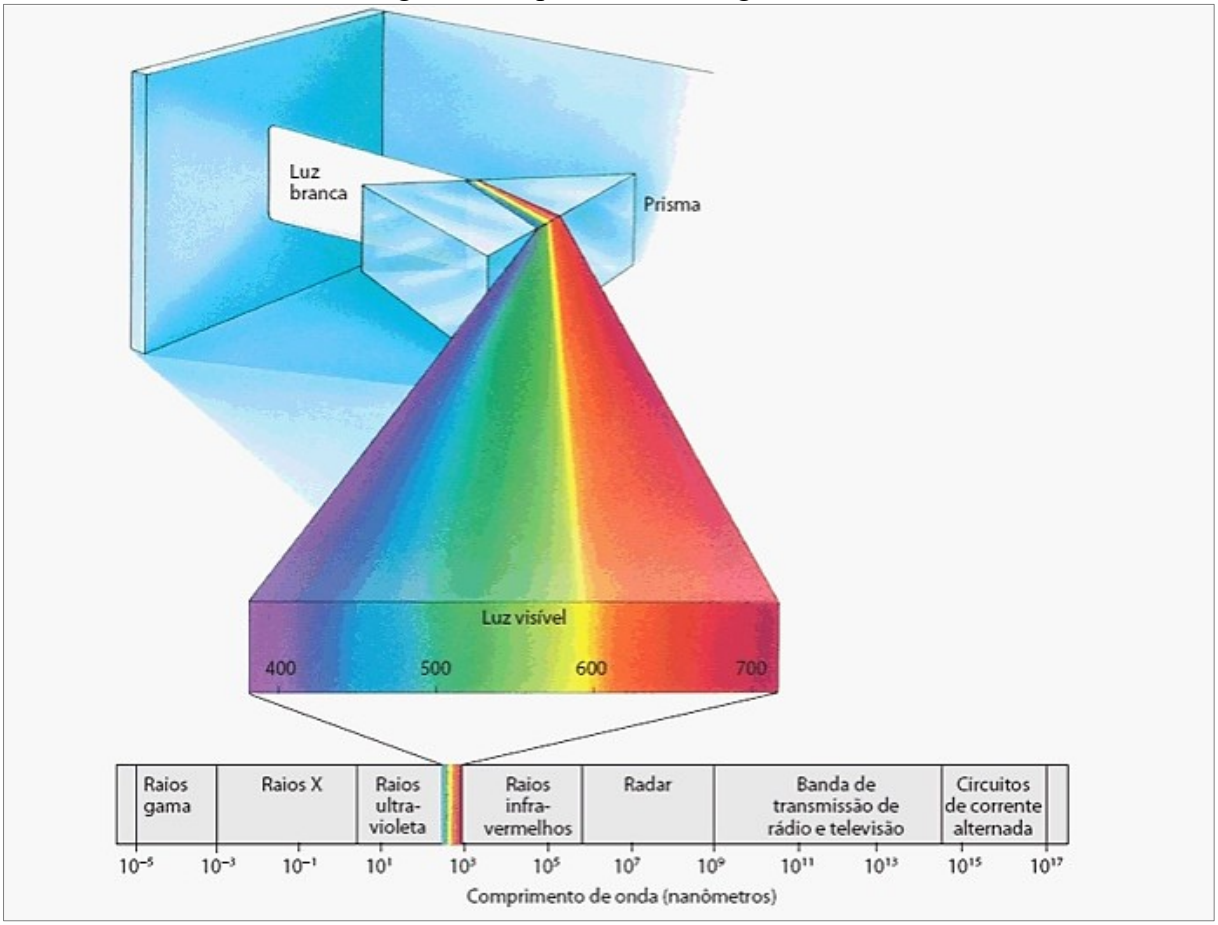

Ao passar por um prisma, a luz branca se decompõe em diferentes cores que são visíveis ao olho humano, por isso é chamada de radiação visível. Fonte: (RAVEN; EVERT; EICHHORN, 2014).

No ambiente terrestre, as plantas estão sujeitas ao espectro de luz total que chega à superfície da Terra, incluindo os comprimentos de onda azuis e vermelhos absorvidos pela clorofila *a* (Chl*a*), pigmento essencial para fotossíntese. Nos ecossistemas aquáticos, a qualidade e fluência da radiação varia, dependendo das características da água e das substâncias dissolvidas, as quais podem absorver alguns comprimentos de ondas (KARSTEN, 2008). A luz

vermelha, por exemplo, é absorvida ainda próximo a superfície, estando ausente em profundidades maiores. Isso explica o porquê em águas mais profundas a qualidade de luz é azul-esverdeada. Nesses ambientes a quantidade de luz absorvida pela Chl*a* pode não ser suficiente para a fotossíntese (GRAHAM et al., 2016a).

Em resposta ao espectro diferenciado de luz no ambiente aquático, as algas desenvolveram algumas estratégias e uma delas foi diversificar os pigmentos para coleta de luz. Assim, além da Chl*a* e Chl*b* algumas algas também possuem as clorofilas *c* e *d* (Chl*c* e Chl*d*). Também diversificaram os pigmentos acessórios (carotenoides e ficobiliproteínas), os quais são capazes de coletar a energia de diferentes comprimentos de ondas (diferentes cores) e repassar para a Chl*a* (Figura 2). Parte desses pigmentos, como os carotenoides e clorofilas, estão organizados em complexos coletores de luz "*light-harvesting complexes"* (LHCs), também conhecidos como antenas (GRAHAM et al., 2016a; KIRK, 2011a).

Figura 2 - Espectro de absorção de pigmentos.

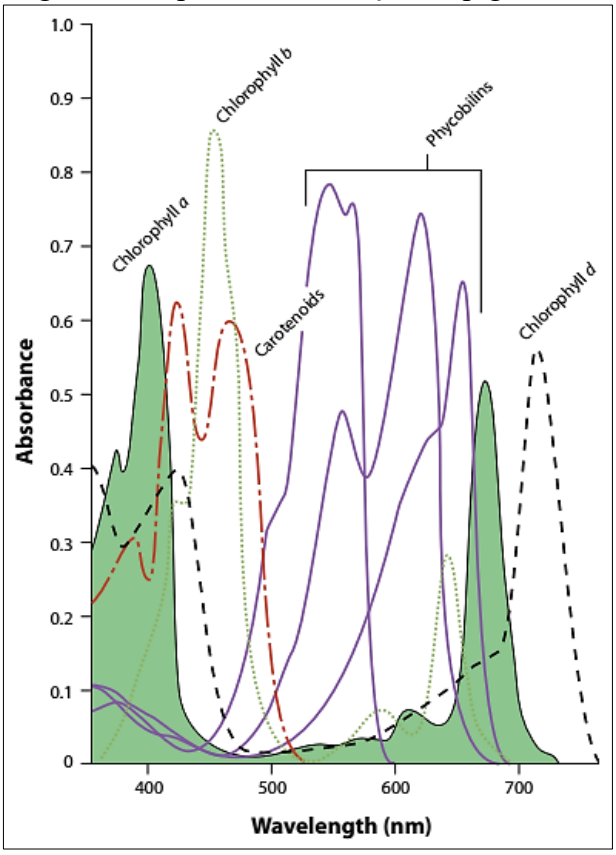

Espectro de absorção das clorofilas *a*, *b* e *d* (*Chlorophyll a*, *Chlorophyll b* e *Chlorophyll d*), carotenoides (*carotenoids*) e das ficobiliproteínas (*phycobilins*). Absorbância (*absorbance*) e comprimento de onda (nm) (*wavelength*). Fonte: (GRAHAM et al., 2016a).

As ficobiliproteínas estão presentes em organismos como algas vermelhas e cianobactérias, e incluem: a ficoeritrina (PE), a ficocianina (PC) e a aloficocianina (APC). Esses pigmentos estão organizados em estruturas conhecidas como ficobilissomos. A PE fica na periferia do ficobilissomo, abaixo desta a PC e na região central a APC. A entrada de energia também ocorre nesta ordem (Figura 3A), ou seja, a luz é captada pela PE e conduzida através da PC e APC até o centro de reação do fotossistema II (PSII) (GRAHAM et al., 2016c; GROSSMAN et al., 1993). Os picos de absorção variam em torno de 560 nm para PE, 620 nm para PC e 650 nm para APC, podendo englobar mais ou menos nanômetros nas regiões azul-esverdeada, verde, amarelo e laranja do espectro, ver Figura 3B (GRAHAM et al., 2016c; GROSSMAN et al., 1993; KIRK, 2011b).

Figura 3 - Pigmentos acessórios das algas vermelhas e cianobactérias e sua capacidade de absorção de luz.

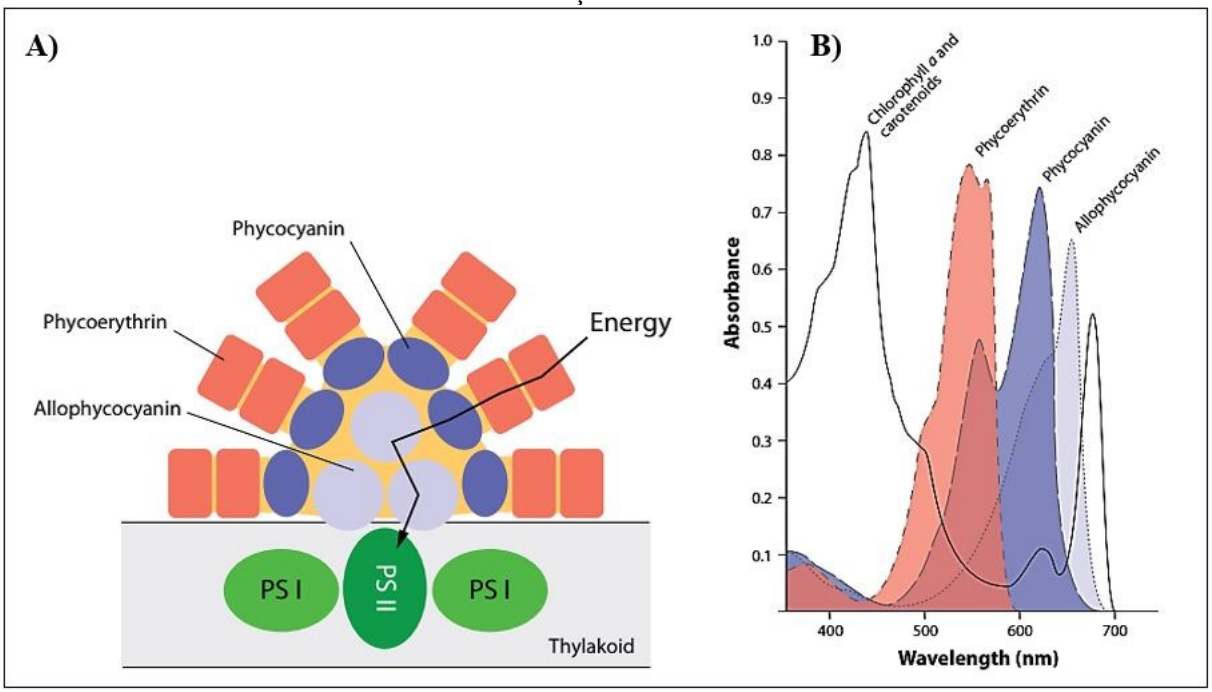

A) Estrutura geral do ficobilissomo, com ficoeritrina (phycoerythrin) na periferia, seguida da ficocianina (phycocyanin) e aloficocianina (allophycocyanin) na porção central. PS II (fotossistema II), PS I (fotossistema I). B) Espectros de absorção da clorofila *a* e carotenoides (chlorophyll *a* and carotenoids) e das ficobiliproteínas (phycoerythrin, phycocyanin, allophycocyanin). Fonte: (GRAHAM et al., 2016c).

Outra forma das algas lidarem com o espectro diferenciado de luz na água é utilizando fotorreceptores. Os fotorreceptores são proteínas sensíveis à luz que estão ligadas a diferentes vias de sinalização, permitindo que organismos se aclimatem às condições de luz do ambiente (KIANIANMOMENI; HALLMANN, 2014). Essas moléculas sensíveis à luz são capazes de perceber a qualidade (nm), quantidade (fluência), direção e duração de diferentes qualidades de

radiação, tanto visível quanto ultravioleta. Assim, mudanças nas condições espectrais do ambiente podem desencadear cascatas de reações biológicas que em plantas controlam o crescimento e outros processos, tais como: ritmos circadianos, respostas ao sombreamento, germinação, movimento dos cloroplastos, germinação, fototropismos e outros (JIAO; LAU; DENG, 2007).

Em algas, a evolução das ferramentas de sequenciamento na última década permitiu identificar a presença de fotorreceptores, tais como: fitocromo, criptocromo, fototropinas, auricromos, neocromos, UVR8 (fotorreceptor sensível a radiação UV-B) e até mesmo a rodopsina, estruturalmente semelhante a um receptor de luz presente em animais. Embora ainda pouco entendido, em algas os fotorreceptores parecem controlar processos como crescimento, reprodução, fotoproteção, fotossíntese e fotoorientação ou fototaxia, no caso de algas flageladas que podem se movimentar em direção a luz (ALLORENT; PETROUTSOS, 2017; COLLÉN et al., 2013; DRING, 1988; FERNÁNDEZ et al., 2016; GRAHAM et al., 2016a; HEGEMANN, 2008; KIANIANMOMENI; HALLMANN, 2014; OLIVERI et al., 2014a; ROCKWELL et al., 2014).

Os organismos fotossintetizantes podem ser afetados negativamente tanto pela falta quanto pelo excesso de luz. Energia (fótons) acima da capacidade de utilização pela fotossíntese pode resultar em uma condição de estresse conhecida como fotoinibição. O PSII é a parte mais afetada do aparato fotossintético. Isso está associado ao alto poder redutor deste sistema, o qual possibilita a oxidação da água, mas ao mesmo tempo pode gerar espécies reativas de oxigênio (ROS), como O_2 singleto, peróxidos e superóxidos (ARAÚJO; DEMINICIS, 2009). Ao ser absorvida pelos pigmentos, a energia entra na via fotoquímica, mas também pode ser perdida na forma de fluorescência ou dissipada na forma de calor (dissipação não-fotoquímica) (MAXWELL; JOHNSON, 2000). A perda do excesso de energia por meio da dissipação térmica tem um papel importante na fotoproteção e pode ser considerada uma defesa inicial. Além deste, muitos outros mecanismos de fotoproteção foram desenvolvidos pelos organismos fotossintetizantes.

Os carotenoides atuam capturando luz e na fotoproteção, pois são poderosos antioxidantes, capazes neutralizar e/ou reduzir os efeitos negativos dos radicais livres. Além disso, em plantas e algumas algas ocorre o ciclo das xantofilas (XC), o qual permite dissipar o excesso de energia absorvido pelo aparato fotossintético. Nas plantas, três carotenoides participam deste ciclo: a violaxantina, a anteraxantina e a zeaxantina. Sob altos níveis de luz, a violaxantina é convertida em zeaxantina, tendo a anteraxantina como intermediária, tal processo

é chamado de deepoxidação. O menor nível de energia da zeaxantina é 704 nm, o que permite absorção de energia a partir da Chl*a.* Essa energia é degradada em pequenas quantidades, na forma de calor, evitando a quebra de ligações e reações químicas indesejadas (BJÖRN, 2015a; SCHUBERT; GARCÍA-MENDOZA; PACHECO-RUIZ, 2006). Em cianobactérias, ocorre uma proteína fotoativa, a "*orange carotenoid protein"* (OCP). Esta proteína é sensível à luz azul-esverdeada, quando ativada ela sofre uma mudança estrutural que permite interagir com os LHCs, reduzindo a energia que entra nos centros de reação (KIRILOVSKY; KERFELD, 2013). Na literatura, há ainda outros exemplos de moléculas sensíveis a diferentes qualidades de radiação (fotorreceptores), as quais atuam na dissipação de energia em algas (ALLORENT; PETROUTSOS, 2017; PETROUTSOS et al., 2016).

É importante falar ainda sobre a proteína D1. Quando os mecanismos iniciais de defesa falham ou não conseguem lidar com o excesso de luz, o PSII pode sofrer danos, precisando ser desmontado e consertado. Os danos ocorrem principalmente na proteína D1 que faz parte do centro de reação. Essa proteína apresenta um rápido "*turnover"*, ou seja, ela sofre uma regeneração rápida. Segundo Araújo e Deminicis (2009), quando isso acontece é porque a fotoinibição foi crônica e sua duração é relativamente longa, resultando na diminuição da eficiência quântica e da taxa fotossintética máxima. Quando a fotoinibição é moderada e ocorre nos estágios iniciais, ela chamada de fotoinibição dinâmica. Neste caso, ocorre a redução da eficiência quântica, mas a taxa fotossintética máxima permanece inalterada (ARAÚJO; DEMINICIS, 2009).

As algas respiram, fotossintetizam e algumas também podem calcificar. A calcificação é o processo pelo qual certas espécies de algas produzem carbonato de cálcio ($CaCO_3$), por exemplo, as algas coralinas vermelhas - CRA (GRAHAM et al., 2016b). A fotossíntese, respiração e calcificação são processos interativos. Embora vários aspectos desta interação ainda precisam ser melhor entendidos (HOFMANN; KOCH; BEER, 2016), sabe-se que a relação acontece em torno da química do carbono, uma vez que a respiração libera dióxido de carbono (CO_2) e a fotossíntese consome CO_2 na presença de luz. O CO_2 no ambiente aquoso se transforma em ácido carbônico (H_2CO_3), um elemento instável que rapidamente pode formar bicarbonato (HCO_3^-), liberando íons de hidrogênio (H^+). O HCO_3^- pode ser quebrado e resultar na formação de íons carbonato (CO_3^{2-}) mais H^+ ou ser convertido diretamente em $CaCO_3$, na presença do cálcio (Ca^{2+}), liberando água (H_2O) e CO_2, ver Figura 4 (DE BEER; LARKUM, 2001; DONEY et al., 2009; HOFMANN; BISCHOF, 2014; HOFMANN; SCHOENROCK; DE BEER, 2018; MARTIN et al., 2013; MARTIN; CASTETS; CLAVIER, 2006; MARTIN;

CHARNOZ; GATTUSO, 2013; MCCONNAUGHEY, 1991). O consumo do CO_2 pela fotossíntese faz aumentar variáveis, tais como o pH e o estado de saturação dos íons CO_3^{-2} e Ca^{2+}, favorecendo a calcificação. Deste modo, ocorre uma relação positiva entre fotossíntese e calcificação (DE BEER; LARKUM, 2001; SEMESI; BEER; BJÖRK, 2009). Luz e calcificação também apresentam relação positiva (DE BEER; LARKUM, 2001; MARTIN; CASTETS; CLAVIER, 2006; MARTIN; CHARNOZ; GATTUSO, 2013), não apenas porque a fotossíntese depende de luz, mas também porque a luz parece induzir bombas iônicas complexas que desempenham um papel importante na calcificação (HOFMANN; KOCH; BEER, 2016).

Figura 4 - Reações da química do carbono na água e a relação com fotossíntese, respiração e calcificação.

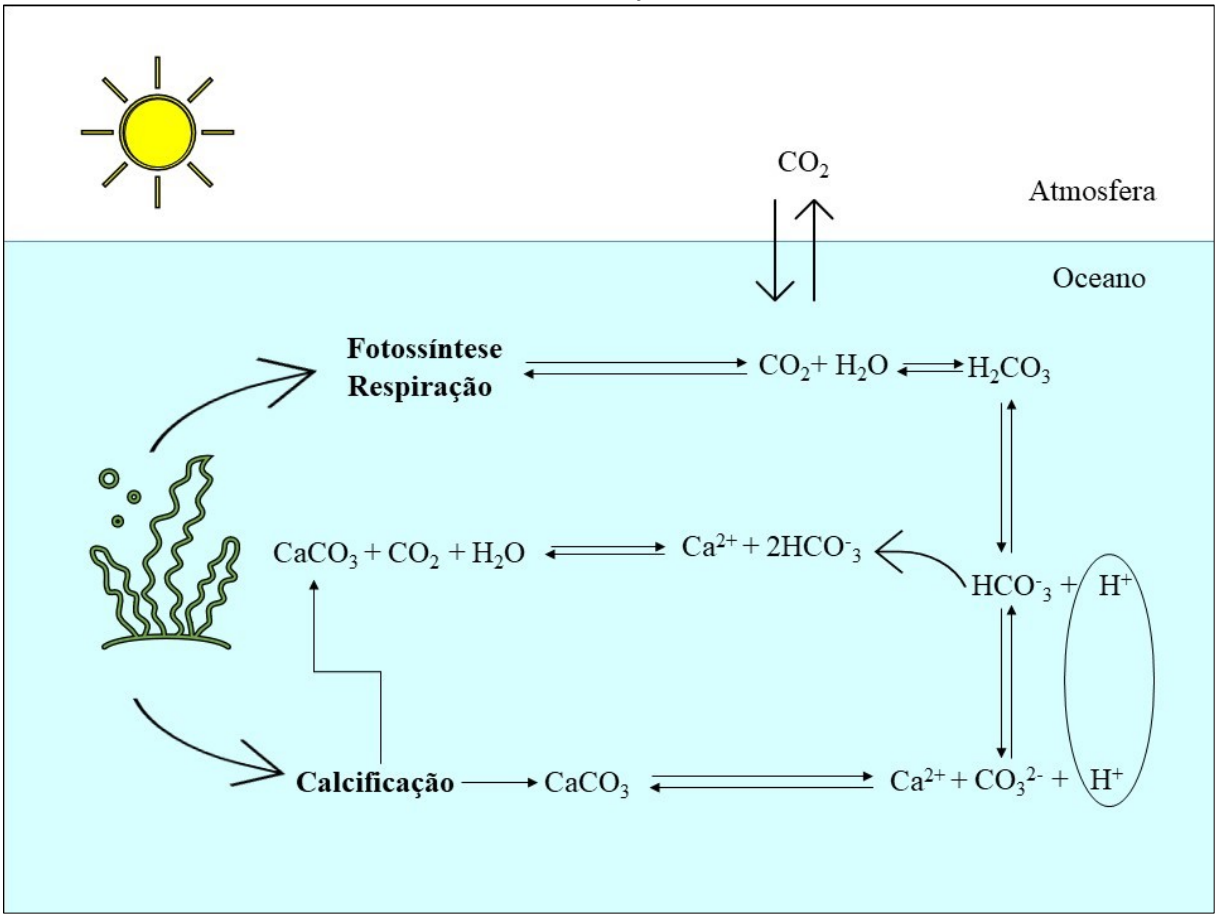

A fotossíntese consome CO_2 enquanto a respiração libera. O CO_2 se transforma em ácido carbônico (H_2CO_3) que é transformado em bicarbonato (HCO^-_3) ou carbonato (CO_3^{2-}), os quais na presença do cálcio vão formar o carbonato de cálcio ($CaCO_3$). A formação do HCO^-_3 e CO_3^{2-} causa a liberação de íons de hidrogênio (H^+), quando a quantidade destes íons aumenta o pH diminui, então o $CaCO_3$ pode ser quebrado para formação do HCO^-_3, o qual eleva o pH. Como pode ser observado todas as reações são dinâmicas e reversíveis. Fonte: elaborada pela autora.

Por meio da fotossíntese e da calcificação, as algas vêm desempenhando papéis importantes na biogeoquímica da Terra. Há bilhões de anos as cianobactérias geraram a primeira atmosfera contendo oxigênio. Esses organismos também armazenaram muito carbono por meio das formações rochosas de carbonato e dos depósitos de combustível fóssil. Atualmente, as algas produzem cerca de metade do oxigênio da atmosfera e influenciam a ciclagem de carbono, nitrogênio, fósforo, silício e outros elementos. Biotecnologicamente falando, as algas poderiam ser usadas como sistemas de engenharia nos quais seu crescimento poderia ser manipulado para mitigar os efeitos humanos sobre a química da atmosfera, amenizando os impactos das mudanças climáticas (GRAHAM et al., 2016b).

1.1 ALGAS CORALINAS CROSTOSAS (CCA)

As CCA são um grupo cosmopolita de algas vermelhas calcificantes que desempenham papéis ecológicos importantes. Essas algas e outros organismos calcificadores transformaram grandes quantidades de CO_2 atmosférico em sedimentos carbonáticos e rochas como o calcário, tendo papel fundamental no ciclo do carbono. Além disso, as algas coralinas ajudam a construir e manter recifes de corais, que abrigam diversos organismos. Assim a perda das CCA em alguns ambientes poderia causar o colapso de comunidades inteiras (GRAHAM et al., 2016b; HOFMANN; KOCH; BEER, 2016).

Os rodolitos são um grupo muito peculiar de CCA. São macroalgas não geniculadas (livre de articulações não calcificadas), com crescimento lento e podem ter uma vida longa. A morfologia externa e as faixas de crescimento são arquivos potenciais de variação ambiental em escalas de dezenas de anos. Além disso, a estrutura complexa e rígida dessas algas pode servir como microhabitats para outros organismos, por isso os rodolitos são conhecidos "modificadores de habitats" ou "bioengenheiros" (Figura 5). Essas algas podem ocorrer em altas concentrações em grandes áreas, formando os "leitos ou bancos" de rodolitos (em inglês *rhodolith beds*), que podem ser considerados uma das quatro grandes comunidades bentônicas da Terra (Figura 6), desempenhando um papel ecológico de sustentação de cadeias tróficas. Os bancos de rodolitos abrigam populações de invertebrados de vida livre, por exemplo, briozoários, hidróides, esponjas; entre outros (FOSTER, 2001).

Figura 5 - Complexidade estrutural dos rodolitos.

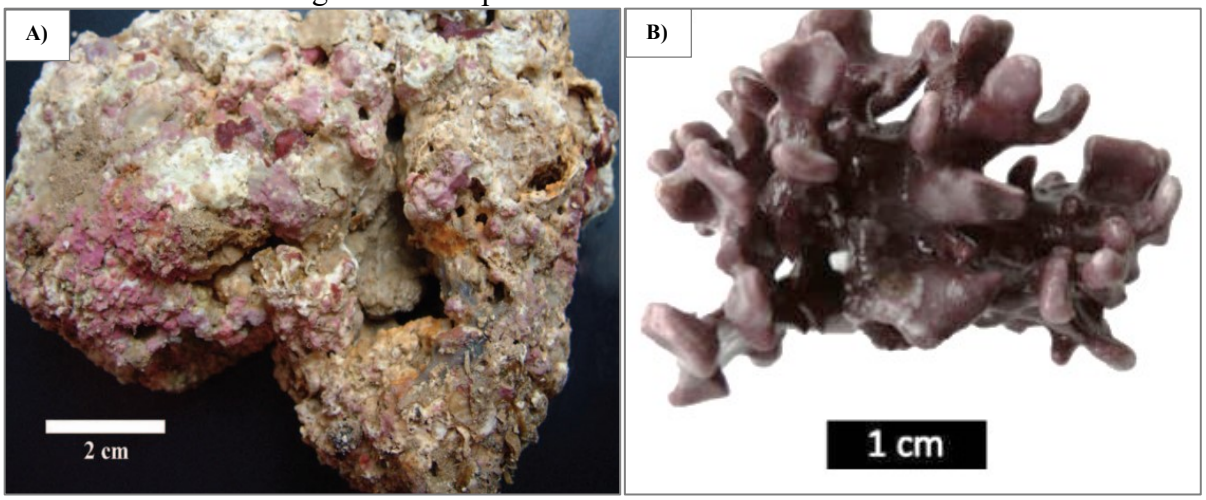

Nas imagens é possível visualizar a complexidade estrutural dos rodolitos, por isso são considerados "Bioengenheiros". As reentrâncias formadas pela estrutura dessas algas podem servir de microhabitats estáveis para outros organismos. A) rodolitos, espécie não identificada (PEREIRA-FILHO et al., 2012a), B) *Lithothammion corallioides* (QUI-MINET et al., 2019).

Figura 6 - Bancos de rodolitos existentes na laguna Ria Formosa, na cidade de Faro, Portugal.

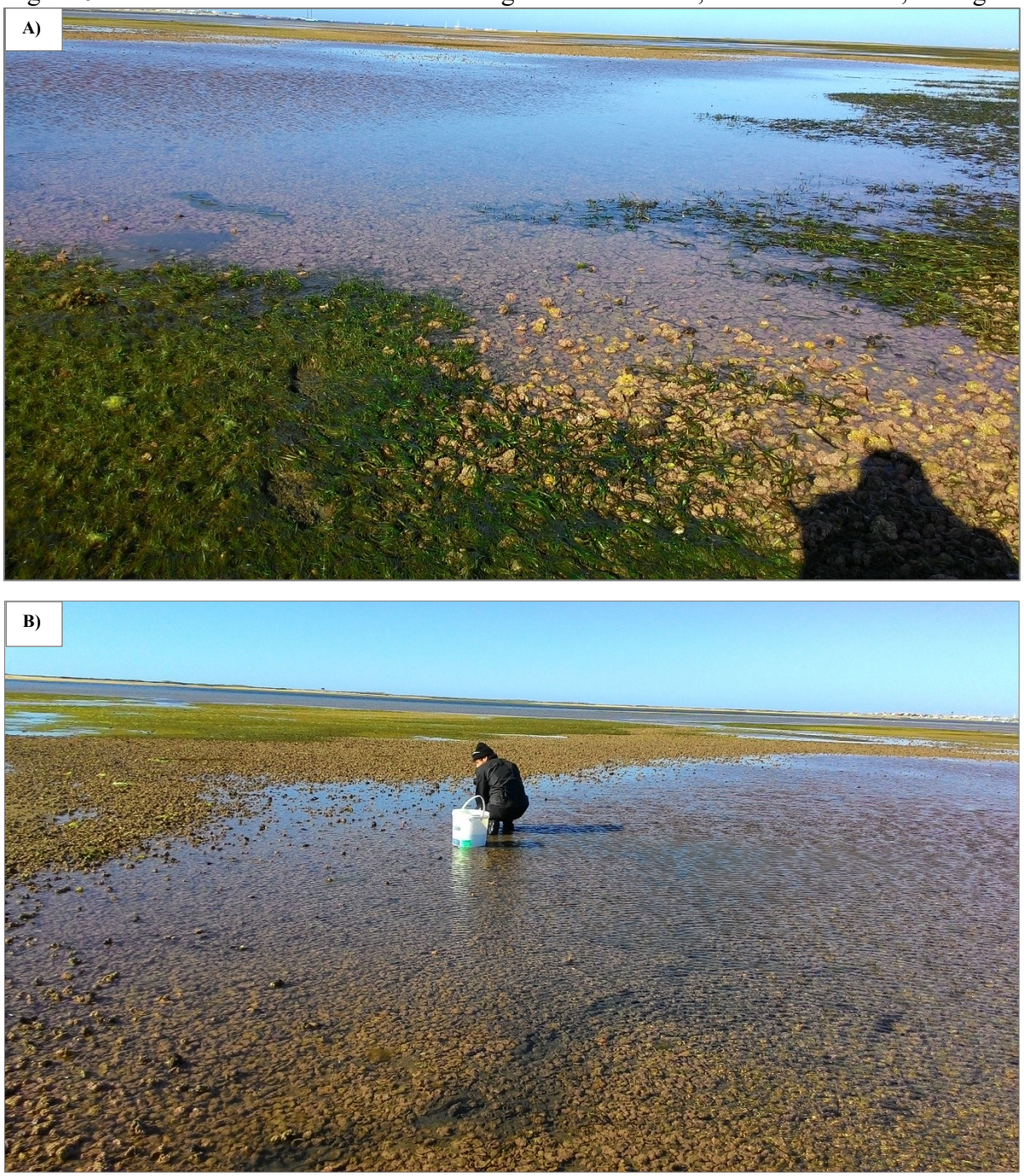

Os rodolitos formam bancos dentro (A) e fora (B) dos prados de ervas marinhas. As fotos foram tiradas durante a maré baixa. Fonte: a autora.

Os bancos de rodolitos contêm recursos de importância econômica e a extração desses recursos pode resultar na perda de comunidades inteiras. Há ainda outras ameaças como a pesca de arrasto e alterações como a sedimentação, o aumento de turbidez, a eutrofização, além das mudanças climáticas, especialmente, a acidificação dos oceanos, a qual afeta diretamente a

química do carbono e, consequentemente, a calcificação (DONEY et al., 2009; FOSTER, 2001; FOSTER et al., 2013; HOFMANN; SCHOENROCK; DE BEER, 2018).

1.2 COMPOSTOS NATURAIS DE ALGAS

As algas desempenham diversos papéis ecológicos importantes. Por outro lado, esses organismos também apresentam amplo potencial biotecnológico. Nas últimas décadas, as algas vêm se destacando como fonte de compostos bioativos que contribuem com a indústria alimentícia e cosmecêutica (CHAROENSIDDHI et al., 2017a; SINGH et al., 2017). Estima-se que só as macroalgas são responsáveis por 3000 compostos naturais, representando 20% da química relatada para o ambiente marinho (MASCHEK; BAKER, 2008). Esses compostos podem ser utilizados como suplementos alimentares e como constituintes ativos de produtos farmacêuticos e cosméticos, como exemplo os protetores solares (ANDRADE et al., 2013; CARDOZO et al., 2007; PANGESTUTI; SIAHAAN; KIM, 2018; PLAZA; CIFUENTES; IBÁÑEZ, 2008; SINGH et al., 2017). Além disso, os extratos de algas podem apresentar propriedades antioxidantes, anti-inflamatório, antibacteriana, antiviral, anticâncer, entre outras (AYYAD et al., 2011; BRITO et al., 2013; IBTISSAM et al., 2009; SAFAFAR et al., 2015; STAHL; SIES, 2003; WANG et al., 2017).

Os produtos ou compostos naturais são aqueles produzidos como respostas adaptativas, que permitem a sobrevivência dos organismos em condições adversas. O termo “produto natural” é utilizado por muitos autores como sinônimo de metabólito secundário que se refere a compostos que não estão envolvidos no desenvolvimento ou manutenção dos organismos, diferente dos metabólitos primários que compreendem compostos essenciais para o funcionamento celular como aminoácidos, cofatores e lipídios, por exemplo. Os metabólitos secundários são classificados de acordo com sua via de biossíntese. A Figura 7 apresenta as principais vias para produção da maioria dos produtos naturais, tendo como grupos principais os terpenóides, policetídeos, alcaloides e aqueles produzidos pela via do ácido chiquímico como fenilalanina, tirosina, triptofano e seus derivados (MASCHEK; BAKER, 2008).

Figura 7 - Principais vias de biossíntese dos produtos naturais.

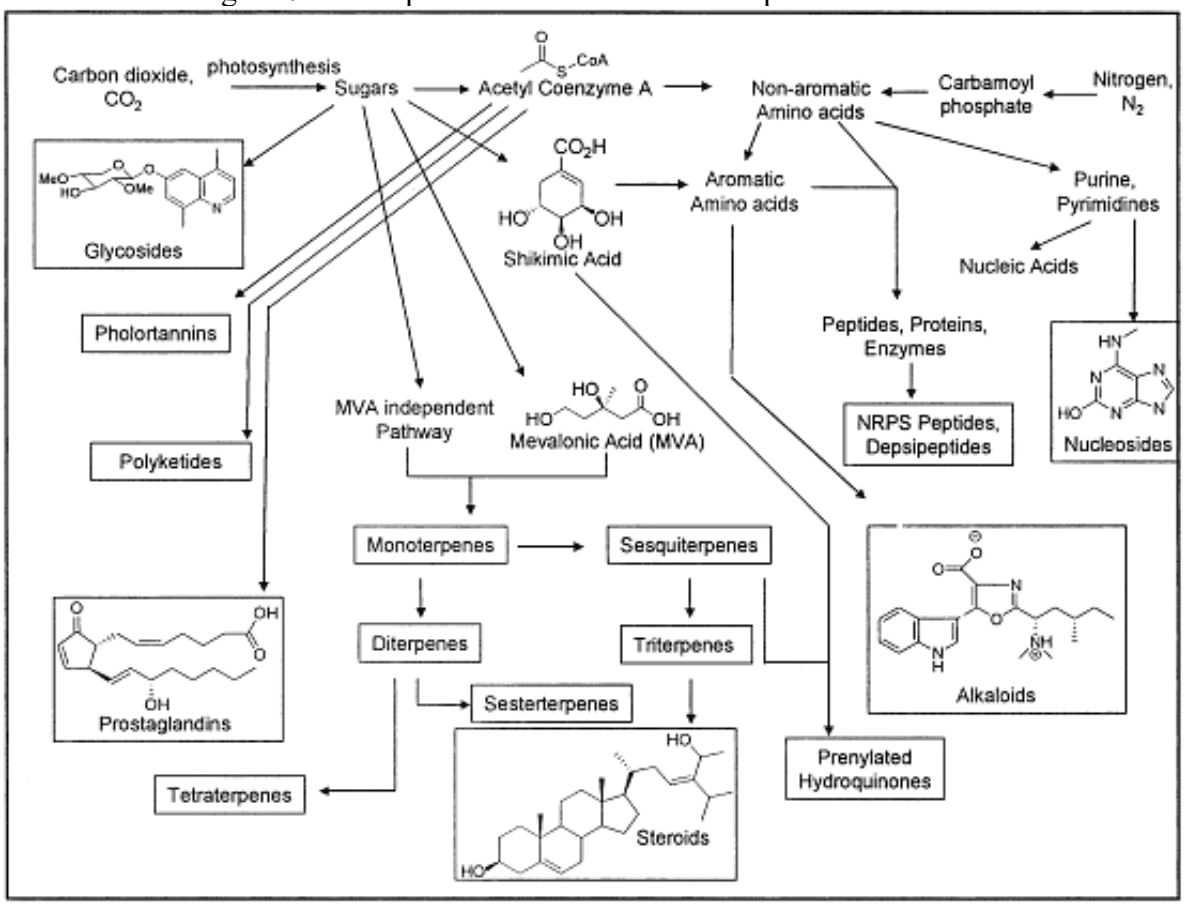

Fonte: (MASCHEK; BAKER, 2008).

As macroalgas vermelhas produzem mais de 1500 compostos no seu metabolismo, seus metabólitos secundários são ricos tanto em diversidade quanto em abundância quando comparado com outras macroalgas. As algas vermelhas se destacam principalmente pela produção de compostos halogenados, em torno de 90%, enquanto as algas verdes com 7% e as pardas ou marrons com 1%. As macroalgas pardas produzem mais que 1140 metabólitos secundários, incluindo diterpenos, florotaninos e acetogeninas. Esse grupo se destaca principalmente na produção de florotaninos. Já as macroalgas verdes possuem menos que 300 compostos conhecidos, sendo poucos descobertos a cada ano. Esse grupo é conhecido por produzir compostos semelhantes aos das algas vermelhas, porém menos halogenados (MASCHEK; BAKER, 2008).

1.2.1 Relação entre a radiação UV-Visível e a produção de compostos

As algas produzem naturalmente uma ampla variedade de substâncias químicas em resposta a interações com o ambiente e outros organismos. A luz pode ser um fator regulador

na produção de compostos especialmente quando se trata de fotoproteção. Para entender melhor, a absorção de radiação UV-visível pelas células faz com que as moléculas saiam do estado basal para o estado excitado. A energia presente nas moléculas excitadas pode seguir os seguintes caminhos principais: o primeiro é o retorno da molécula ao estado basal pela perda de energia na forma de calor, o segundo é a perda de energia na forma de fluorescência (emissão de fótons com comprimento de onda maior do que aqueles que foram absorvidos), o terceiro é o "*estado excitado triplet*". Essas moléculas *triplet* podem colidir com outras moléculas transferindo a energia e retornando ao estado basal, como ocorre na fotossíntese. Entretanto, pode ocorrer da energia ser transferida para o oxigênio, formando o oxigênio singlet ($^1O_2$), o qual pode reagir com muitas moléculas, incluindo os aminoácidos das proteínas. Além da transferência de energia pode ocorrer a transferência de elétrons, ocasionando fotooxidações e fotorreduções, podendo formar espécies reativas de oxigênio (EROS). Um caso especial é a formação do ânion radical superóxido $O_2^{\bullet -}$, o qual é um poderoso nucleófilo com capacidade de deslocar o grupo éster de algumas membranas lipídicas, formando o peróxido de hidrogênio (H_2O_2). O H_2O_2 pode reagir com os metais traços reduzindo, por exemplo, os complexos formados pelo ferro (Fe) e dando origem ao radical hidroxila ($HO^{\bullet}$), extremamente reativo. A hidroxila reage rapidamente com a maior parte dos compostos orgânicos e muitos íons inorgânicos. Os produtos formados podem reagir com moléculas orgânicas próximas ou com o oxigênio e formar substâncias potencialmente nocivas (LARSON; BEREBAUM, 1988).

A radiação UV pode ser ainda absorvida diretamente por componentes celulares importantes, tais como: o DNA (ácido desoxirribonucleico), RNA (ácido ribonucleico), proteínas, moléculas associadas às membranas, entre outras (LARSON; BEREBAUM, 1988). O DNA, assim como as proteínas, absorve radiação UV principalmente nas regiões do UV-B e UV-C, com absorção máxima próxima aos 280 nm (DIFFEY, 1991). Os danos causados pela radiação UV ao DNA podem comprometer a replicação e transcrição dos ácidos nucleicos, aumentando o número de mutações. A alta taxa de mutações pode levar a redução da expressão de um gene que debilita sua função ou aumenta a morte celular (KARSTEN, 2008). As proteínas são formadas por 20 tipos diferentes de aminoácidos, destes a tirosina, fenilalanina, triptofano e histidina contêm resíduos aromáticos capazes de absorver as radiações UV-B. As proteínas D1 do fotossistema II e a enzima Rubisco do ciclo de Calvin também são alvos típicos da radiação UV (BISCHOF; HANELT; WIENCKE, 2000). Os danos às proteínas podem comprometer suas funções, além disso, os processos de degradação e substituição de proteínas

requerem energia, o que poderia comprometer processos importantes como a reparação do DNA (KARSTEN, 2008).

Assim, se por um lado, a radiação UV-visível é essencial para sobrevivência dos organismos, principalmente os fotossintetizantes, por outro lado, ela também pode ser nociva. Por isso, os organismos desenvolveram estratégias para mitigar os seus efeitos. Uma delas é a produção de compostos fotoprotetores, tais como: carotenoides, aminoácidos tipo micosporinas (MAAs), compostos fenólicos e outros. Esses compostos apresentam o potencial de dissipar energia, anular ou amenizar os efeitos dos radicais livres ou ainda absorver os comprimentos de ondas mais energéticos (UV), como é o caso das MAAs (LA BARRE; ROULLIER; BOUSTIE, 2014).

1.2.1.1 Carotenoides

Como já comentado anteriormente neste trabalho, os carotenoides são pigmentos que auxiliam na coleta de luz para fotossíntese. Além disso, atuam na dissipação de energia e na neutralização de espécies reativas de oxigênio, apresentando atividade antioxidante e importante papel fotoprotetor (STAHL; SIES, 2003). Os carotenoides são onipresentes no ambiente marinho. Os mais comuns são a fucoxantina, astaxantina, zeaxantina, luteína, violaxantina, anteraxantina e β-caroteno, embora ainda exista outros (YE et al., 2019). Na Figura 8 é possível verificar a estrutura dos principais carotenoides.

Figura 8 - Estrutura química dos carotenoides.

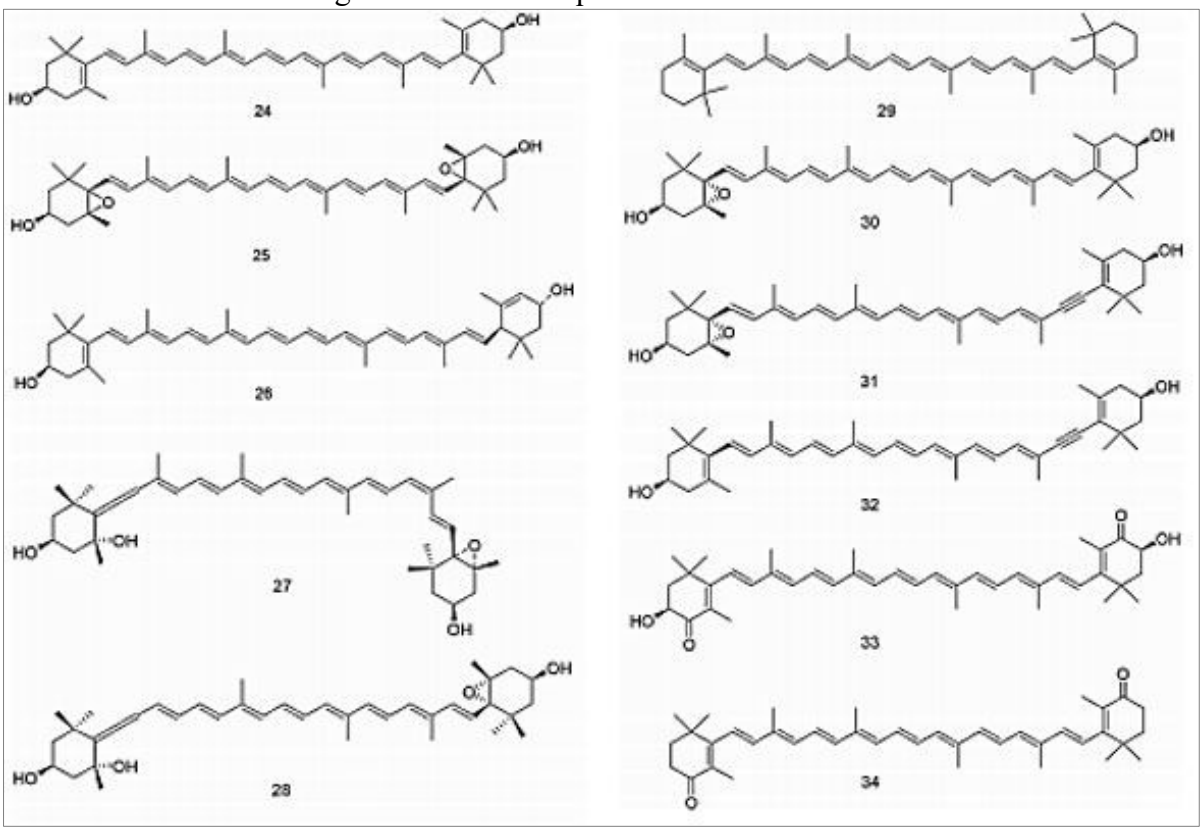

Zeaxantina (24), violaxantina (25), luteína (26), neoxantinas (*all-trans neoxanthin* e 9'-*cis neoxanthin*, 27-28), β-caroteno (29), anteraxantina (30), diadinoxantina (31), diatoxantina (32), astaxantina (33) e canthaxanthin (34). Fonte: (YE et al., 2019).

1.2.1.2 Aminoácidos tipo micosporinas (MAAs)

Os MAAs podem ser encontrados em diferentes organismos, tais como: cianobactérias fungos, liquens, corais, algas e outros (LA BARRE; ROULLIER; BOUSTIE, 2014). Dentre as macroalgas, as vermelhas (Rhodophyta) geralmente apresentam maior quantidade de MAAs, enquanto as algas verdes (Chlorophyta) e marrons (Phaeophyceae) produzem quantidades menores ou apenas traços desses compostos (LA BARRE; ROULLIER; BOUSTIE, 2014; SUN et al., 2020). Os MAAs apresentam alta atividade antioxidante e estão envolvidos em respostas de fotoproteção, com picos de absorção na região ultravioleta (UV) do espectro. Além disso, desempenham papéis como dissipadores de calor e podem contribuir com o equilíbrio osmótico sob estresse iônico (LA BARRE; ROULLIER; BOUSTIE, 2014; PANGESTUTI; SIAHAAN; KIM, 2018). Os principais MAAs encontradas em algas são shinorine (λ_{max} 334 nm), palitina (λ_{max} 320 nm), porfira-334 (λ_{max} 334 nm), asterina-330 (λ_{max} 330 nm), micosporina-glicina

(λ_{max} 310 nm) e palitinol (λ_{max} 332 nm), todas citadas como substâncias potenciais para produtos de proteção solar (COCKELL; KNOWLAND, 1999; MERCURIO et al., 2015; PANGESTUTI; SIAHAAN; KIM, 2018; SCHMID; SCHÜRCH; ZÜLLI, 2004, 2006; SINGH et al., 2017; TORRES et al., 2006; VEGA et al., 2021). Na Figura 9, é possível visualizar a estrutura de alguns dos principais MAAs encontrados na natureza.

Figura 9 - Estrutura de alguns dos principais aminoácidos tipo micosporinas (MAAs) encontrados na natureza, incluindo o comprimento de onda de máxima absorção.

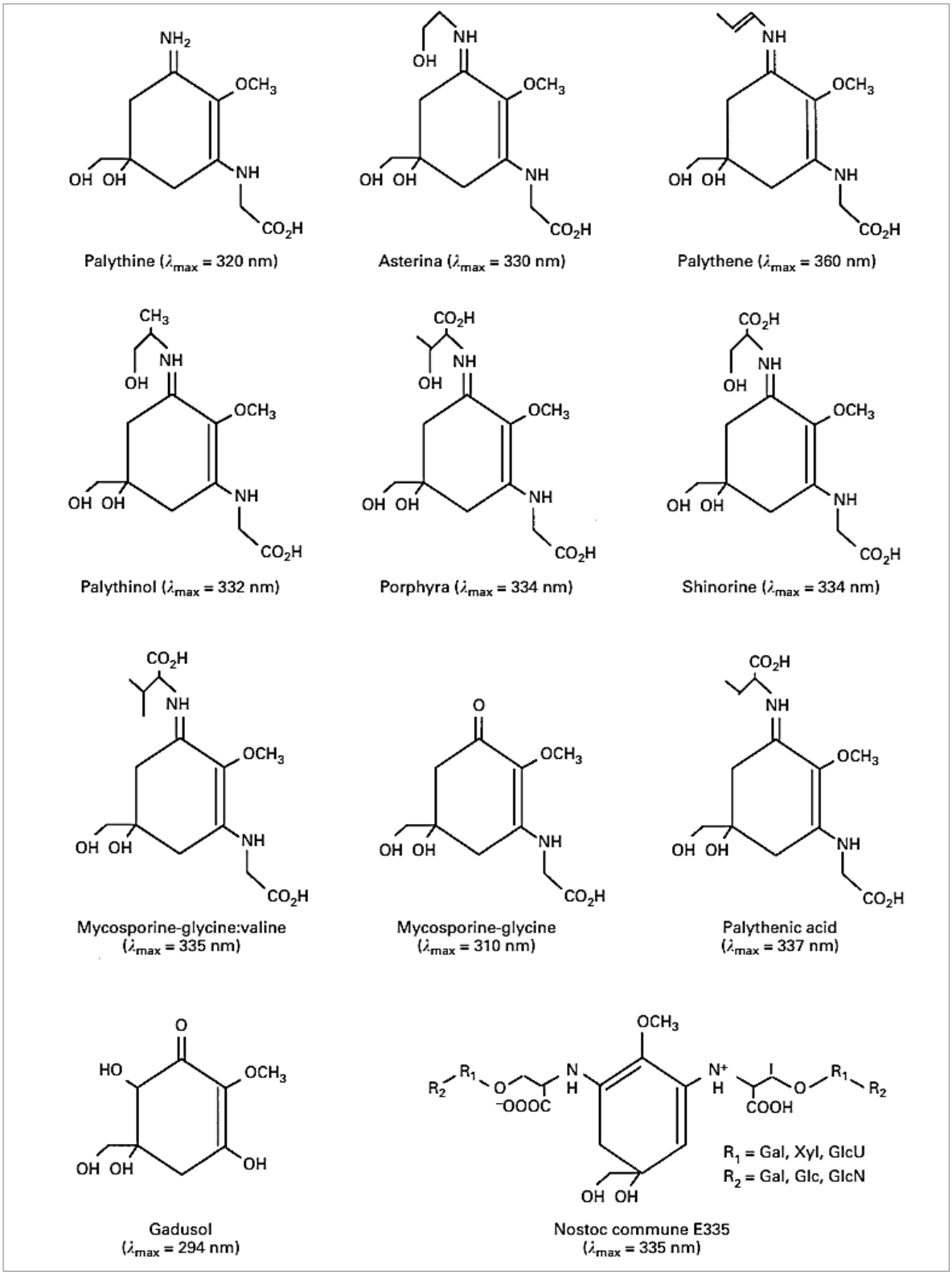

Fonte: (COCKELL; KNOWLAND, 1999)

1.2.1.3 Compostos Fenólicos

Os compostos fenólicos são produzidos pelo metabolismo secundário e apresentam diversas funções biológicas, dentre as quais forte atividade antioxidante e papel fotoprotetor (ABDALA-DÍAZ et al., 2014; MACHU et al., 2015; MASCHEK; BAKER, 2008; PANGESTUTI; SIAHAAN; KIM, 2018). Os fenólicos podem ser divididos em quatro principais grupos: ácidos fenólicos, flavonoides, taninos e ligninas (SINGH et al., 2017). Esses compostos são caracterizados pela presença de um anel aromático ligado a grupos hidroxila (PANGESTUTI; SIAHAAN; KIM, 2018; SINGH et al., 2017; WANG et al., 2017). A estrutura destes compostos pode ter relação direta com a capacidade de eliminar radicais livres e fotoproteger os sistemas biológicos, já que os grupos hidroxilas ligados aos anéis aromáticos podem atuar como doadores de elétrons neutralizando as EROS (PANGESTUTI; SIAHAAN; KIM, 2018). Na Figura 10, é possível visualizar a estrutura dos polifenóis e algumas funções e/ou bioatividades atribuídas a esses compostos, tais como: antioxidante, resistência (respostas de defesa), anticarcinogênico, antiviral, antifúngico, anti-inflamatório, antibacteriano e antitumoral.

Figura 10 - Características dos polifenóis.

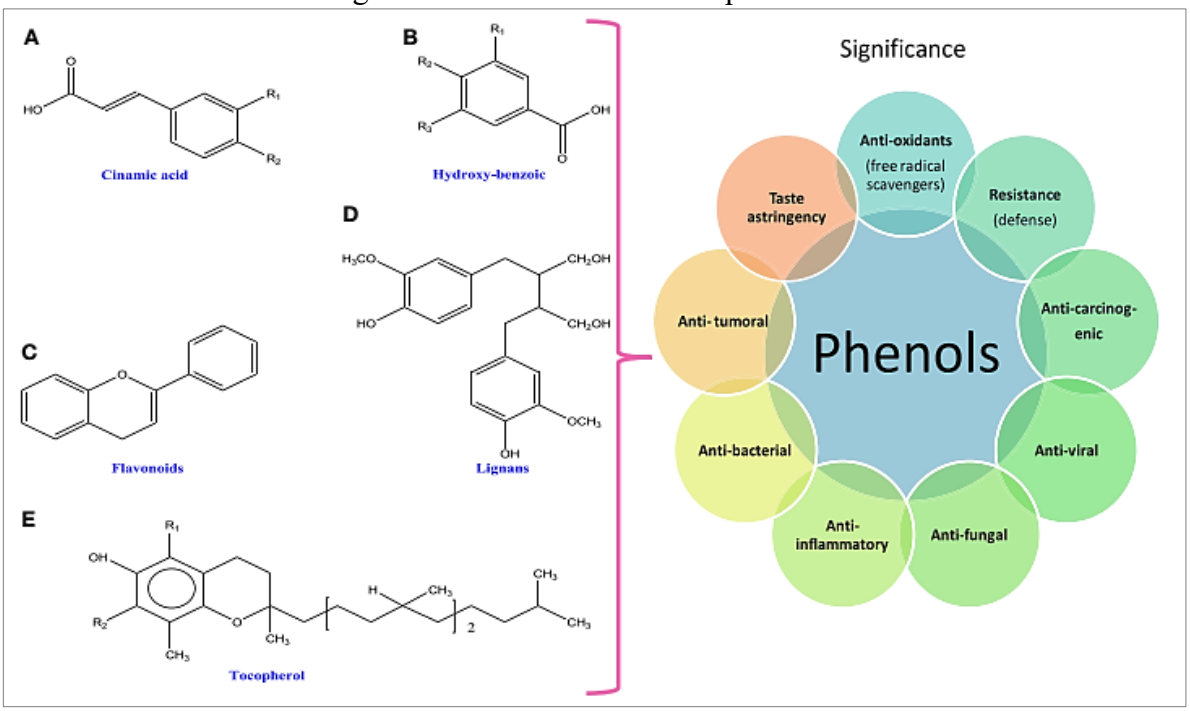

Nas imagens é possível visualizar a estrutura química dos polifenóis e algumas funções e/ou bioatividades atribuídas a esses compostos, tais como: antioxidante, resistência (respostas de defesa), anticarcinogênico, antiviral, antifúngico, anti-inflamatório, antibacteriano e antitumoral. A) ácido cinâmico, B) ácido hidroxibenzóico, C) flavonóides, D) lignanos e E) tocoferóis. Fonte: (SINGH et al., 2017).

Nas algas marrons, os principais compostos fenólicos são os florotaninos que chegam a constituir 14% da biomassa seca nessas algas. Os florotaninos são compostos hidrofílicos, formados por meio da polimerização do floroglucinol (CHAROENSIDDHI et al., 2017a). Os florotaninos apresentam propriedades antioxidantes e de fotoproteção, por isso são citados como compostos potenciais para serem utilizados em cremes e fotoprotetores (PANGESTUTI; SIAHAAN; KIM, 2018).

1.3 APLICAÇÕES E IMPACTO ECONÔMICO DAS ALGAS

As algas são um importante componente da aquicultura global. Segundo relatório da FAO, em 2019, o cultivo de alga contribuiu com aproximadamente 30 % das 120 milhões de toneladas da produção aquícola mundial. As algas marinhas vermelhas (Rhodophyta) e marrons (Phaeophyceae) foram o segundo e o terceiro maior grupo aquícola em nível global. Embora seja uma *commodity* de baixo valor, as algas foram responsáveis por 5,4 % dos 275 bilhões de dólares da produção mundial aquícola, em 2019. Esta porcentagem foi maior que os valores atribuídos, por exemplo, à produção de tilápias e outros ciclídeos (CAI et al., 2021; FAO, 2021a, 2021b).

Nos últimos anos, a quantidade de algas cultivadas aumentou, especialmente espécies tropicais (*Kappaphycus alvarezii*, *Eucheuma* spp. e *Gracilaria* spp.). Em 2018, as algas cultivadas representaram 97,1 % das 32,4 milhões de toneladas de algas produzidas/comercializadas. O aumento das algas cultivadas foi impulsionado pela necessidade de matéria prima para extração da carragenana (CAI et al., 2021; FAO, 2020). Assim, além de fonte de vários compostos bioativos e fotoprotetores, as algas são produtoras potenciais de polissacarídeos, principalmente carragenanas, agaranas de alginatos (CARDOZO et al., 2007; SINGH et al., 2017).

As algas são utilizadas em diferentes setores da indústria como aditivos alimentares, rações animais, produtos farmacêuticos, nutracêuticos, cosméticos, têxteis, biofertilizante/ bioestimulante, bioembalagem, biocombustível, entre outros (MCHUGH, 2003). Como alimento humano, elas são produzidas e consumidas principalmente no Leste e Sudeste Asiático, destacando-se as espécies *Undaria pinnatifida*, *Porphyra* spp. e *Caulerpa* spp. (FAO, 2020).

1.4 LIMITAÇÕES PARA O USO DE MACROALGAS

Há vários entraves conhecidos para o uso e/ou obtenção de macroalgas para fins comerciais, seja para extração de compostos químicos ou outros fins. As algas têm um papel vital na manutenção dos ecossistemas, formando a base energética da cadeia alimentar para todos os organismos aquáticos. Além disso, elas providenciam benefícios ambientais e serviços ecossistêmicos, tais como mitigação da eutrofização, sequestro de carbono, amenizando os efeitos das mudanças climáticas, também providenciam habitat e proteção das áreas costeiras (CAI et al., 2021). Assim, a exploração das algas no ambiente natural pode causar impactos negativos irreversíveis aos ecossistemas e, consequentemente, a saúde e bem-estar humano.

Com relação a extração de compostos bioativos (MAAs, carotenoides, fenólicos e outros), um dos grandes entraves é a obtenção de biomassa em quantidade suficiente (VEGA et al., 2021). Uma alternativa seria o cultivo em grande escala. Para algumas espécies (*Kappaphycus alvarezii*, *Eucheuma* spp. e *Gracilaria* spp.) isso já é possível (CAI et al., 2021), embora para outras o domínio do ciclo de vida e o cultivo em biorreatores ou fazendas marinhas precisa ser estudado e aperfeiçoado (SINGH et al., 2017). Os cultivos multitróficos integrados (IMTA) são uma alternativa interessante (BEDOUX et al., 2020; NAVARRO et al., 2018), embora ainda apresentem muitas restrições associadas à legislação e por serem sistemas complexos para operar e manter (KLEITOU; KLETOU; DAVID, 2018).

Existe ainda a possibilidade de utilizar biomassa de florações que ocorrem com algumas espécies de macroalgas dos gêneros *Sargassum* spp., *Ulva* spp., entre outros. Esta poderia ser uma alternativa também de biorremediação, já que estas florações geralmente impactam negativamente os ecossistemas devido a eutrofização e/ou produção de substâncias tóxicas. Entretanto, também apresenta limitações, pois as florações são fenômenos complexos e geralmente imprevisíveis, ocorrendo em épocas e locais diferentes.

A indução de compostos específicos, utilizando fatores abióticos em cultivos também pode ajudar a aumentar a razão composto/biomassa, entretanto essas técnicas também precisam ser estudadas, pois são muito espécie-específicas (SINGH et al., 2008). Melhorias no processo de extração e purificação dos compostos também podem ajudar a aumentar a razão composto/biomassa e ainda baratear custos (VEGA et al., 2021).

Mesmo com as limitações existentes, o uso de algas nos diversos setores da indústria é promissor, e a tendência é aumentar com a evolução das pesquisas biotecnológicas, incluindo

a engenharia genética e outras inovações nas áreas de cultivo e processamento (CARDOZO et al., 2007; SINGH et al., 2017; VEGA et al., 2021).

1.5 JUSTIFICATIVA

As algas formam um grupo muito amplo de macro e microrganismos. As primeiras algas desempenharam papéis importantes na formação da atmosfera do planeta, contribuíram com níveis significativos de oxigênio e armazenaram carbono. Essas mudanças permitiram que a vida migrasse para fora dos oceanos. Atualmente, as algas continuam desempenhando funções ecológicas importantes nos diferentes ecossistemas, seja pequeno ou grande como a Terra, já que são responsáveis pela produção de cerca de metade do oxigênio da atmosfera (GRAHAM et al., 2016b).

Além disso, nas últimas décadas, as algas têm chamado a atenção pelas suas potencialidades no campo da biotecnologia, seja na área ambiental como biorremediadoras ou na área industrial associadas à produção de combustíveis, alimentos, remédios e cosméticos (CARDOZO et al., 2007; CHAROENSIDDHI et al., 2017b; PLAZA; CIFUENTES; IBÁÑEZ, 2008; SINGH et al., 2017).

Tendo em vista a importância desses organismos, é essencial conhecer a diversidade de espécies e o que produzem. Também compreender a fisiologia, como respondem às variáveis ambientais e de que forma processos como a fotossíntese, a respiração e a calcificação interagem entre si e com o ambiente. O entendimento da biologia desses organismos possibilitará que sejam explorados em proporções ou locais onde os impactos sejam menores. Ou ainda, possibilitará o cultivo onde fatores como a luz, nutriente, temperatura e outros possam ser utilizados para modular as respostas como reprodução, crescimento e produção de compostos de interesse, como já é feito com algumas espécies (AVILA et al., 2010; BUSCHMANN et al., 2004; HWANG; PARK; BAEK, 2006; QIAN et al., 1996). Assim, esta tese se justifica para incrementar o conhecimento sobre os tópicos apresentados. O trabalho foi dividido em quatro capítulos, onde foram estudadas diferentes espécies com importância econômica e ecológica, a fim de buscar preencher algumas lacunas, tanto em viés de conhecimento de sua biologia e fisiologia, quanto com respeito à presença e síntese de potenciais compostos de valor agregado.

1.6 OBJETIVOS E HIPÓTESES

Nas seções abaixo estão descritos as hipóteses, o objetivo geral e os objetivos específicos desta tese.

1.6.1 Hipóteses

- O potencial fotoprotetor dos extratos das algas está associado a presença de compostos com atividade antioxidante e/ou que absorvem na região UV do espectro. Assim, quanto maior a quantidade de substâncias como MAAs e fenólicos maior será a capacidade fotoprotetora do extrato.

- Algas vermelhas e pardas tem extratos com maior capacidade antioxidante e potencial fotoprotetor do que algas verdes, especialmente as algas vermelhas por apresentarem maior quantidade de MAAs, os quais absorvem na região UV do espectro.

- Diferentes qualidades e intensidades de radiação podem induzir diferentes respostas fisiológicas e bioquímicas nas algas (*Osmundea pinnatifida* e *Gracilaria cornea*), sendo possível modular a produção de alguns compostos, tais como pigmentos (clorofila *a*, ficobiliproteínas e carotenoides), MAAs e compostos fenólicos.

- As algas estudadas (*O. pinnatifida* e *G. cornea*) têm fotorreceptores mediando respostas fisiológicas e bioquímicas induzidas por diferentes qualidades de radiação.

- Fotossíntese e calcificação variam sob diferentes intensidades de luz. Esses processos, juntamente com a respiração, alteram os parâmetros do sistema carbonato na água de cultivo das algas.

1.6.2 Objetivo Geral

Identificar e avaliar espécies de macroalgas quanto ao potencial para produção de compostos antioxidantes e fotoprotetores, além de verificar respostas fisiológicas e bioquímicas associadas a diferentes intensidades e qualidades de radiação UV-visível.

1.6.3 Objetivos Específicos

- Realizar uma bioprospecção, avaliando as propriedades fotoprotetoras dos extratos de macroalgas e um líquen, a fim de identificar espécies potencialmente produtoras de

compostos antioxidantes e/ou fotoprotetores, tais como: pigmentos (clorofila *a*, ficobiliproteínas e carotenoides), MAAs e compostos fenólicos.

- Verificar respostas fisiológicas, bioquímicas e de crescimento induzidas por diferentes qualidades de radiação UV-Visível e mediadas por fotorreceptores em duas espécies de macroalgas (*Osmundea pinnatifida* e *Gracilaria cornea*).

- Verificar respostas bioquímicas e fisiológicas, incluindo fotossíntese, respiração e calcificação da macroalga *Lithophyllum hibernicum* quando exposta a diferentes intensidades de luz.

2 MATERIAIS E MÉTODOS

2.1 MATERIAL BIOLÓGICO

Para o Capítulo I, as algas foram coletadas em dois pontos do litoral da Espanha: em La Araña, Málaga, coordenadas (UTM) 381471.00 m E e 4063686.00 m N, no dia 07 de março de 2018; e em Cádiz, Tarifa, coordenadas (UTM) 266115.51 m E e 3988333.17 m N, no dia 22 de março de 2018. As algas ficam expostas durante a maré baixa em ambos os locais (Figuras 11 e 12).

Figura 11 - Imagens de La Araña, Málaga.

Fonte: a autora

Figura 12 - Imagens de Cádiz, Tarifa.

Fonte: a autora

Foram coletadas 22 espécies de macroalgas, distribuídas em três grupos: Chlorophyta (5 espécies), Ochrophyta (4 espécies) e Rhodophyta (13 espécies). Também foi coletada uma espécie de líquen (Figuras 13, 14 e 15).

Figura 13 - Espécies de algas verdes (Chlorophyta).

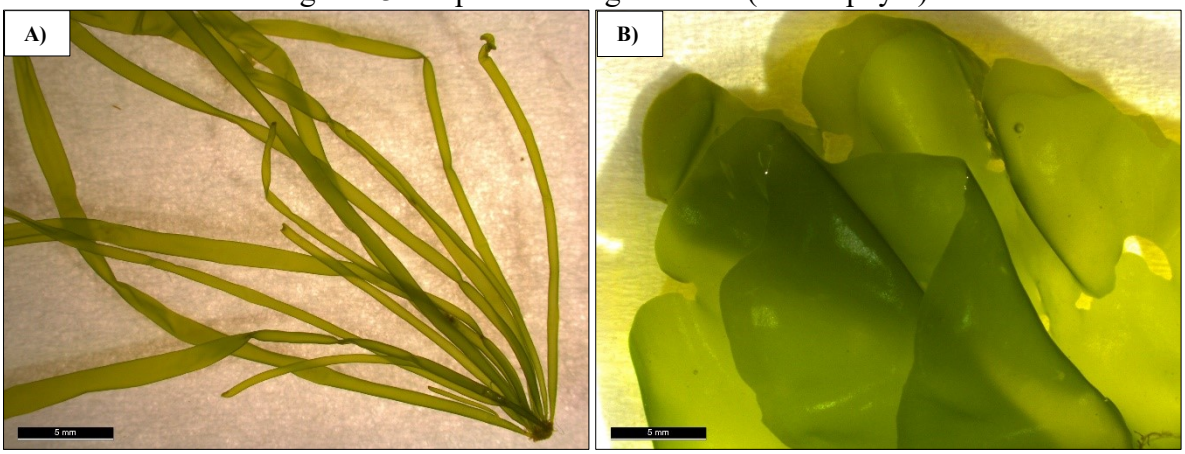

A) *Ulva intestinalis* Linnaeus, B) *Ulva linza* Linnaeus. Fonte: a autora.

Figura 14 - Espécies de algas vermelhas (Rhodophyta).

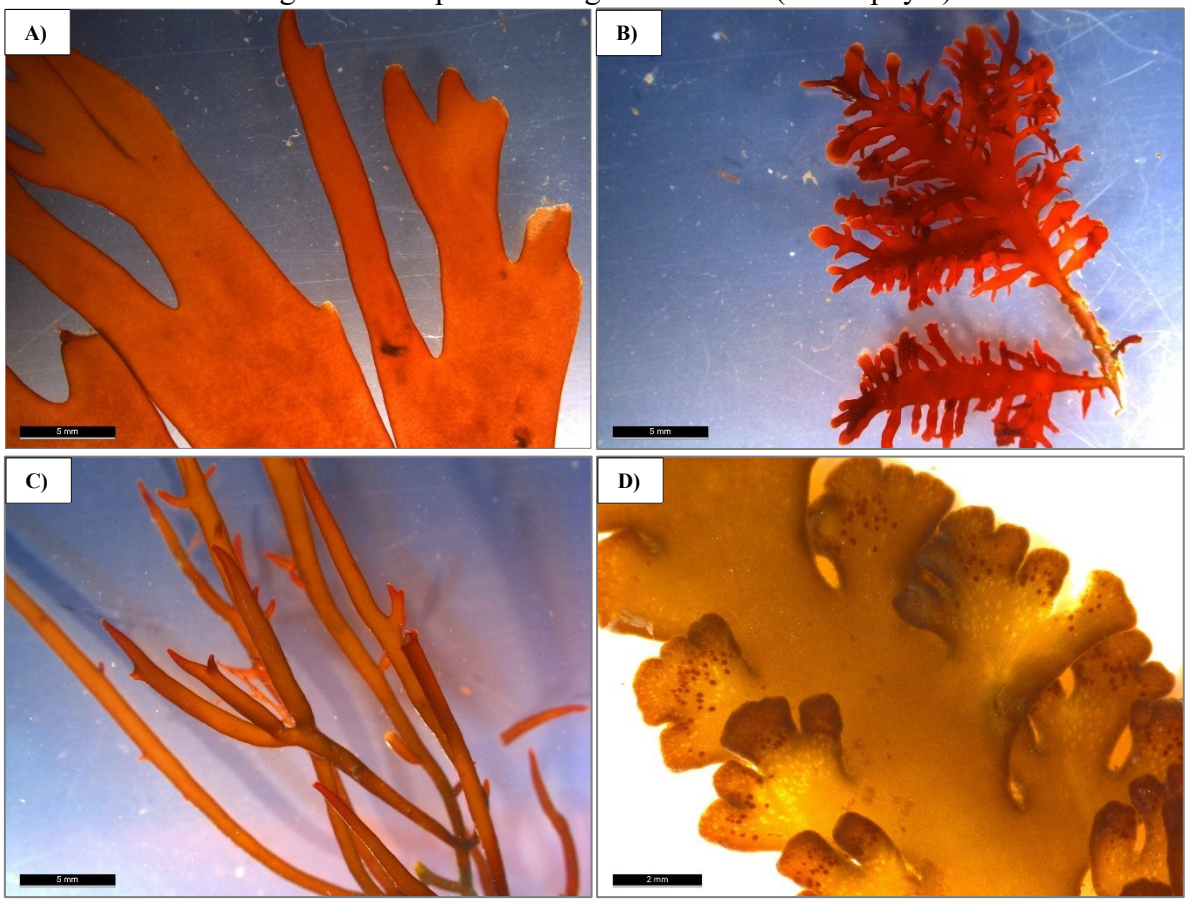

A) *Gracilaria multipartita* (Clemente) Harvey, B) *Gelidium spinosum* (S.G.Gmelin) P.C.Silva, C) *Chondracanthus acicularis* (Roth) Fredericq, D) *Osmundea pinnatifida* (Hudson) Stackhouse, E) *Porphyra umbilicalis* Kützing, F) *Gelidium* sp. Stackhouse, G) *Ceramium virgatum* Roth, H) *Gracilaria cornea* J.Agardh 1852. Fonte: a autora.

Figura 15 - Espécies de algas pardas ou marrons (Ochrophyta).

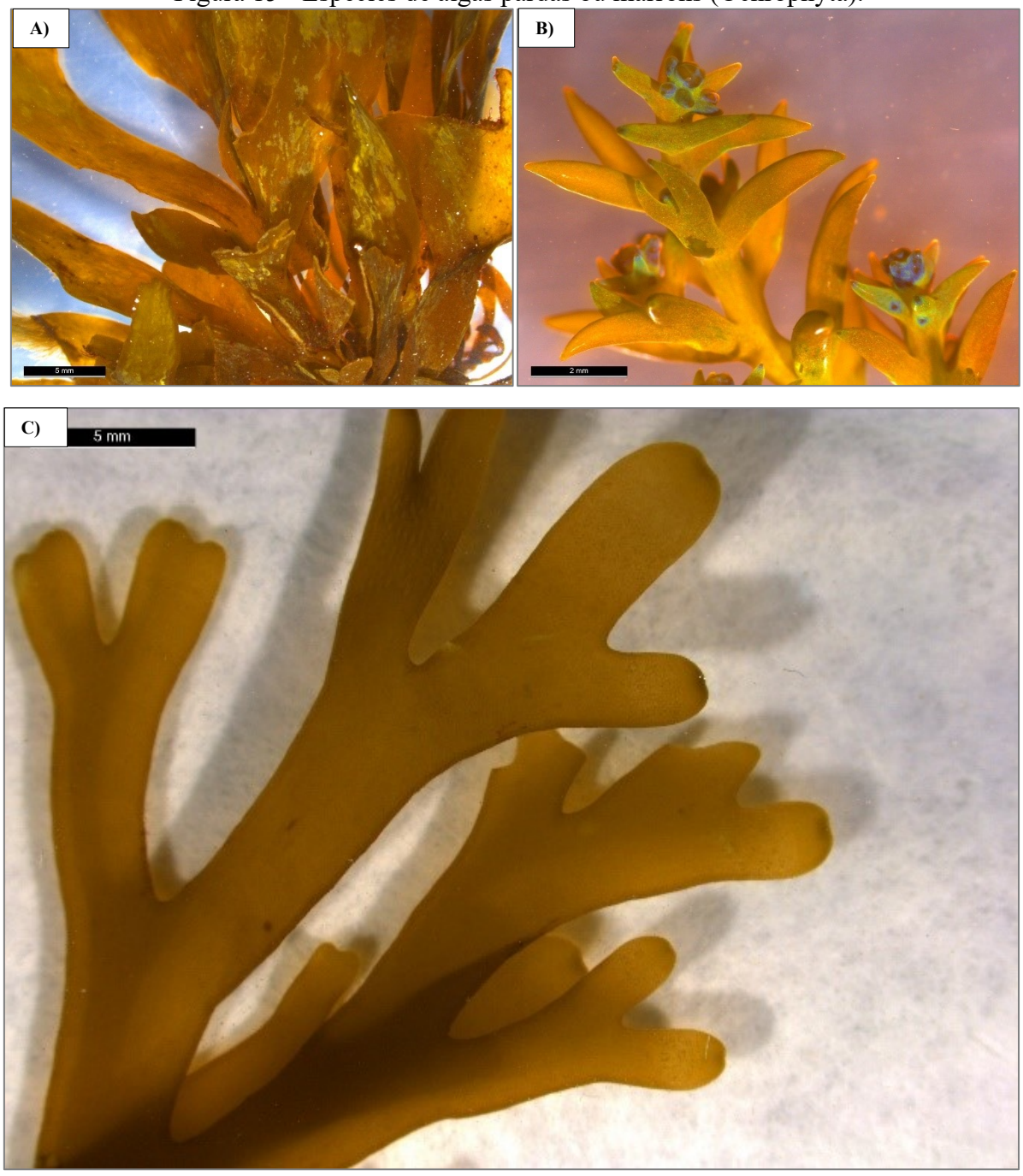

A) *Sargassum vulgare* C.Agardh, nom. illeg., B) *Carpodesmia tamariscifolia* (Hudson) Orellana & Sansón, C) *Rugulopteryx okamurae* (E.Y.Dawson) I.K.Hwang, W.J.Lee & H.S.Kim. Fonte: a autora.

Para o Capítulo II, espécimes da alga vermelha *Osmundea pinnatifida* (Hudson) Stackhouse 1809 foram coletados na praia de La Araña, Málaga, Espanha, nas seguintes coordenadas (UTM): 381411.37 m E e 4063748.42 m N, no dia 07 de março de 2018 (Figura 16).

Figura 16 - Alga vermelha *Osmundea pinnatifida* (Hudson) Stackhouse 1809, utilizada no experimento (Capítulo II).

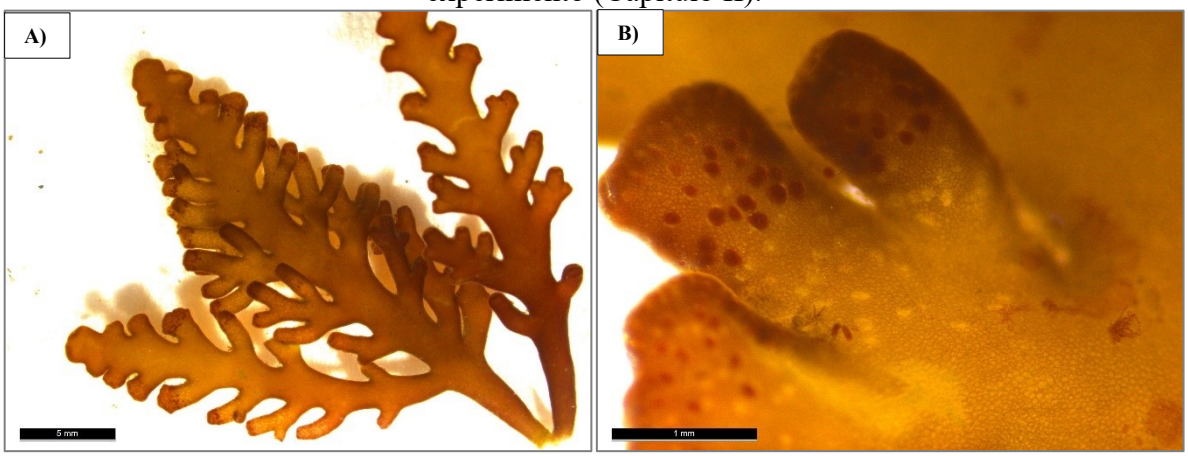

A) talo da alga *O. pinnatifida* e B) detalhe do talo. Fonte: a autora.

Para o Capítulo III, espécimes da alga vermelha *Gracilaria cornea* J.Agardh 1852 (conhecida anteriormente como *Crassiphycus corneus*) foram obtidos no centro de experimentação Grice-Hutchinson, da Universidade de Málaga, nas seguintes coordenadas (UTM): 367921.68 m E e 4059212.13 m N, no dia 16 de fevereiro de 2018 (Figura 17).

Figura 17 - Alga vermelha *Gracilaria cornea* J.Agardh 1852 , utilizada no experimento (Capítulo III).

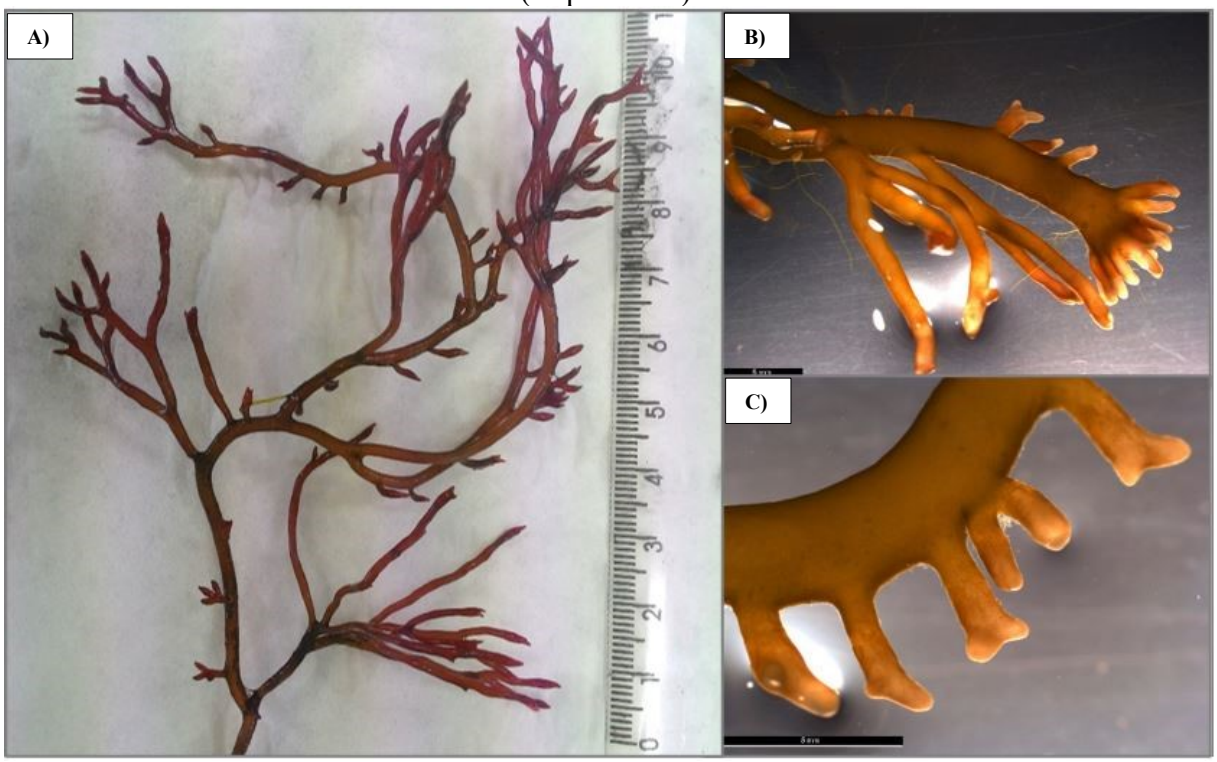

A) talo inteiro da alga *G. cornea*, B) e C) detalhes do talo. Fonte: a autora.

Para o Capítulo IV, espécimes da alga coralina vermelha *Lithophyllum hibernicum* Foslie 1906 foram coletados na Laguna Ria Formosa, Faro, Sul de Portugal, nas seguintes coordenadas (UTM): 604722.63 m E/4096663.20 m N e 604655.61 m E/ 4096591.12 m N. A coleta ocorreu no dia 14 de maio de 2018 (Figura 18).

Figura 18 - Alga coralina vermelha *Lithophyllum hibernicum* Foslie 1906, utilizada no experimento (Capítulo IV).

A) banco de rodolitos e gramas marinhas, B) banco de rodolitos e C) detalhes dos rodolitos. Fonte: a autora.

Os detalhes sobre os procedimentos de coleta, transporte para o laboratório, assim como os designs experimentais estão descritos na seção 3, Resultados, Capítulos I, II, III e IV.

2.2 ANÁLISES FISIOLÓGICAS E BIOQUÍMICAS

Esta seção apresenta as análises bioquímicas e fisiológicas realizadas nos diferentes experimentos. Trata-se de uma descrição geral, sendo que detalhes mais aprofundados como, por exemplo, quantidade de biomassa, volume de extrator e entre outras especificações devem ser consultadas nos diferentes Capítulos I, II, III e IV desta tese.

2.2.1 Porcentagem de água nos talos das algas

Nos Capítulos II e III, a porcentagem de biomassa (massa seca) presente nos talos das algas foi determinada para que os resultados das análises fossem expressos em µg ou mg por g de massa seca. Para isso, 20 amostras de algas com massa de aproximadamente 200 mg cada foram secas na estufa a 60 °C. A massa fresca (MF, em mg) e a massa seca (MS, em mg) foram obtidas em uma balança com quatro casas decimais de precisão. Os cálculos foram realizados de acordo com a seguinte fórmula:

$$\%biomassa = [(MF - MS) \div BF] \times 100$$

2.2.2Taxa de crescimento (TC)

Nos Capítulos II e III, a taxa de crescimento (TC) foi determinada com base na biomassa fresca das algas obtidas em diferentes momentos dos experimentos. A biomassa foi obtida em uma balança de precisão com quatro casas decimais. Antes da pesagem, o excesso de água das algas foi removido com auxílio de um papel toalha. Os cálculos das taxas de crescimento foram realizados de acordo com Lignell e Pedersén (LIGNELL; PEDERSÉN, 1989), conforme segue:

$$TC\%\ dia^{-1} = \left[\left(\frac{MF_{final}}{MF_{inicial}}\right)^{\frac{1}{t}} - 1\right] \times 100$$

Onde, TC% é a taxa de crescimento expressa em porcentagem por dia, MF_{final} é a massa fresca (em mg) obtida após transcorrido um determinado tempo (t, dias) do experimento, $MF_{inicial}$ é a massa inicial. Valores foram expressos em porcentagem de massa fresca por dia (%MF d^{-1}).

2.2.3 Fotossíntese a partir da fluorescência da clorofila *a*

Nos Capítulos II e III, a fotossíntese das algas pode ser monitorada por meio da medição de parâmetros da fluorescência da Chl*a* *in vivo*, utilizando um fluorímetro de amplitude modulada, o Diving PAM (Walz, Effeltrich, Alemanha). Para entender melhor, a Chl*a* é o principal pigmento fotossintetizante. A energia luminosa (fótons) absorvida pela Chl*a* pode seguir três destinos possíveis (MAXWELL; JOHNSON, 2000):

1ª Dissipação fotoquímica: é quando a energia luminosa é utilizada para o processo fotossintético;

2ª Fluorescência: emissão de radiação na região do visível (vermelho);

3ª Dissipação não-fotoquímica: é a produção de calor na forma de radiação infravermelha.

Essas três vias são competitivas, assim alterações nas taxas fotossintéticas (dissipação fotoquímica) causaram mudanças nas outras duas vias (fluorescência e dissipação não-fotoquímica). Portanto, as medidas de fluorescência permitem identificar alterações no processo fotossintético. Sob condições normais, praticamente toda a fluorescência é emitida pelas moléculas de clorofilas associadas ao fotossistema II (PSII). Essa fluorescência pode ser captada por um fluorímetro de amplitude modulada, permitindo o cálculo de diferentes parâmetros(MAXWELL; JOHNSON, 2000). A Figura 19 mostra a fluorescência emitida por um organismo fotossintetizante exposto em condições de escuro e a estímulos luminosos durante certo tempo (BONOMI-BARUFI, 2010).

Figura 19 - Fluorescência emitida por um organismo fotossintetizante exposto a diferentes estímulos (escuro e luz) durante certo tempo.

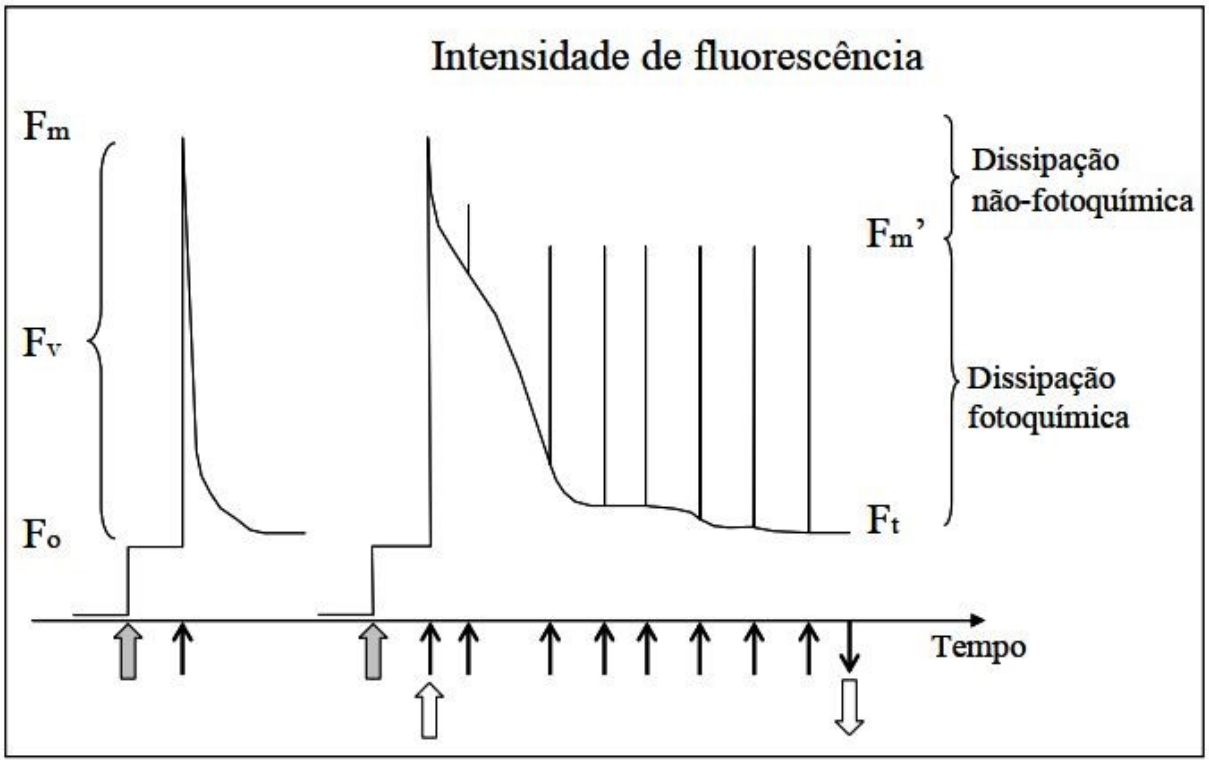

A seta cinza indica o momento em que a luz de medida do equipamento foi ligada. A seta preta indica a aplicação de um pulso saturante. A seta branca indica quando a luz actínica foi ativada (para cima) ou desativada (para baixo). F_0 é a fluorescência basal de um organismo adaptado ao escuro, tal fluorescência é emitida naturalmente independe da fotossíntese. F_m é a fluorescência máxima emitida após um organismo adaptado ao escuro ser iluminado com um pulso saturante. F_m' é a fluorescência máxima medida após um organismo adaptado à luz ser iluminado com um pulso saturante. F_t é a fluorescência emitida quando um organismo está sob luz actínica, fluorescência emitida em uma situação normal de fotossíntese. Fonte: (BONOMI-BARUFI, 2010).

O rendimento quântico máximo do PSII (F_v/F_m) foi obtido por meio da aplicação de um pulso saturante sobre a porção mediana do talo da alga (n=3), no período noturno (Figura 20 A). O rendimento quântico efetivo do PSII (Φ_{PSII}) foi obtido por meio de um pulso saturante aplicado no período diurno, após as algas terem recebido em torno de três horas de iluminação (MAXWELL; JOHNSON, 2000). O Φ_{PSII} foi utilizado para calcular as taxas de transporte de elétrons (ETR, µmol elétrons m^{-2} s^{-1}), (FIGUEROA; CONDE-ÁLVAREZ; GÓMEZ, 2003; GRZYMSKI; JOHNSEN; SAKSHAUG, 1997), conforme equação a seguir:

$$ETR = \Phi_{PSII} \times I \times 0{,}15 \times A$$

Onde, "I" é a irradiância na qual as algas foram aclimatadas durante 10 segundos antes e durante a aplicação do pulso de saturação. O valor de I foi ajustado no fluorímetro para que fosse apresentada um total similar àquele utilizado nas condições experimentais. O fator 0,15 é

utilizado para ajustar a irradiância captada e aproveitada pelo PSII, considerando a fração de Chl*a* associada a esse fotossistema. "A" é a absortância, que foi obtida por meio da seguinte equação:

$$A = 1 - (I_t \div I)$$

Onde, "I_t" é a irradiância transmitida através do talo da alga e "I" é a irradiância total ou inicial medida com o radiômetro (LI-COR, LI-250A). As medidas de irradiância foram obtidas antes (I) e após (I_t) o posicionamento do talo da alga sob uma lâmpada, mantendo a distância entre a fonte de luz e o sensor de medição. Foram realizadas três medidas em cada réplica de cada tratamento (n=3). Na Figura 20 B é possível observar a estrutura montada para realização das medidas de irradiância.

Figura 20 - Procedimentos para medição da atividade fotossintetizante a partir da fluorescência da clorofila *a*.

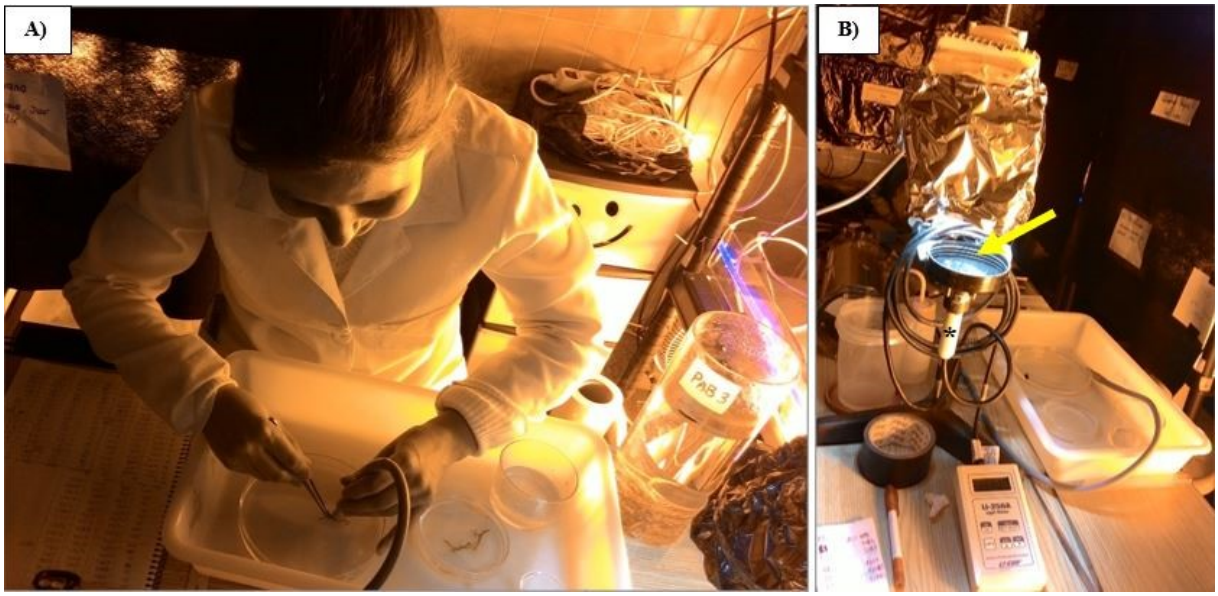

A) Aplicação do pulso saturante sobre a alga, utilizando o Diving PAM. B) Estrutura utilizada para medir as irradiâncias utilizadas no cálculo da absortância. A seta indica a plataforma na qual as algas foram posicionadas. Abaixo da plataforma foi instalado o sensor do radiômetro (*).

As curvas rápidas de luz foram realizadas utilizando a opção "Rapid Light Curve" (RLC). As RLCs foram obtidas com aclimatação prévia das algas em 20 minutos de escuro. Foram aplicados uma série de onze pulsos de luz saturante, cada um deles seguidos de uma luz actínica crescente que variou entre 0 e 1.580 µmol de fótons m^2 s^{-1}. Realizou-se uma curva em cada réplica de cada tratamento (n=3), sempre na posição mediana do talo das algas. As curvas

foram ajustadas (PLATT; GALLEGOS; HARRISON, 1980) para obtenção dos seguintes parâmetros: taxa máxima de transporte de elétrons (ETR_{max}, µmol elétrons m^{-2} s^{-1}), eficiência fotossintética (α_{ETR}) e irradiância de saturação ($I_{k\ ETR}$, µmol fótons m^{-2} s^{-1}). As seguintes fórmulas foram utilizadas:

$$\mathrm{ETR} = ETRs \times \left(1 - e^{\left(\frac{-\alpha \times \mathrm{I}}{\mathrm{ETRs}}\right)}\right) \times e^{\left(\frac{-\beta \times \mathrm{I}}{\mathrm{ETRs}}\right)}$$

$$ETR_{max} = \mathrm{ETRs} \times \left(\frac{\alpha}{\alpha + \beta}\right) \times \left(\frac{\beta}{\beta + \alpha}\right)^{\frac{\beta}{\alpha}}$$

$$I_{k\ ETR} = \frac{ETR_{max}}{\alpha_{ETR}}$$

Onde, ETRmax é o valor máximo determinado para o cálculo do parâmetro, ou seja, o ETR na ausência de fotoinibição. O α é o "slope" da curva (estimativa da eficiência fotossintética) e β é coeficiente de fotoinibição. O ajuste das curvas foi realizado em uma planilha do Excel (Microsoft 365).

2.2.4 Fotossíntese a partir da produção de O_2, respiração e calcificação

No Capítulo IV, foi realizada a estimativa das taxas de fotossíntese, respiração e calcificação por meio de medidas de oxigênio, pH e alcalinidade. Para isso, as algas foram incubadas em frascos Erlenmeyer de 100 ml, preenchidos com água e vedados com uma rolha de borracha. As incubações foram realizadas com intervalos de 30 minutos, iniciando com 30 minutos de escuro, seguidos de 30 min em cada uma das seguintes irradiâncias: 10, 25, 82, 154, 360, 650, 1000, 1400 (µmol photons m^{-2} s^{-1}). Durante as incubações, os frascos foram posicionados sobre um agitador shaker (Edmund Bühler, Kreisschüttler KL-2) para homogeneização da água. A luz artificial foi fornecida por lâmpadas LED (Lexman E27, 20kwh). As medições de luz foram realizadas com um quantômetro (LI-COR, LI-250-Lightmeter, U.S.A e sensor Q49612, made in USA).

Entre cada incubação foram realizadas medidas de oxigênio, pH e coletada amostras para cálculo de alcalinidade e taxas de calcificação. As medidas de oxigênio foram realizadas com um oxímetro (Microx 4, PreSens, Precision Sensing GmbH, Regensburg, Germany), acoplado a uma fibra (Oxygen Sensitive optode), ver Figura 21. As medidas de pH foram

realizadas com o pH meter (Thermo scientific, Orion Star A221, Denver, Colorado). As amostras de água para alcalinidade total (AT) foram armazenadas em frascos com capacidade para 12 mL e fixadas com 20µL de cloreto de mercúrio saturado.

Figura 21 - Equipamentos utilizados para medir a curva de luz.

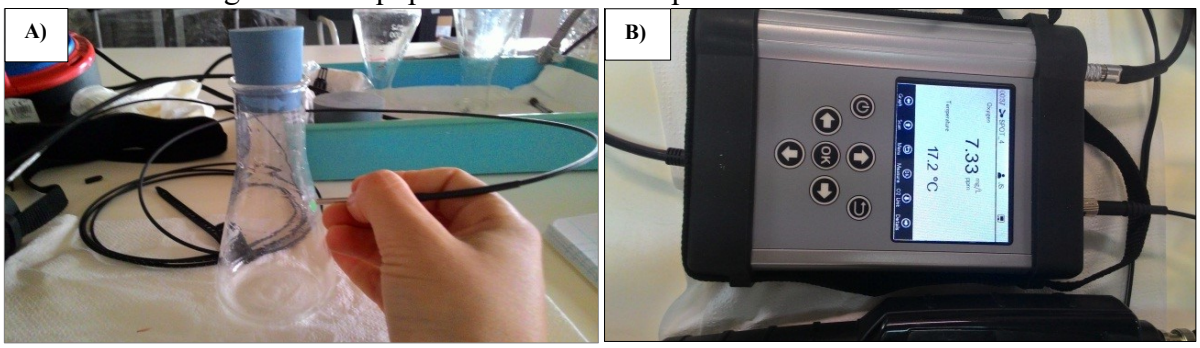

A) Frasco utilizado para as incubações. B) Oxímetro utilizado para as medidas de oxigênio. Fonte: a autora.

A fotossíntese líquida (incubação na luz) e as taxas de respiração (incubação no escuro) foram calculadas a partir das diferenças entre as concentrações iniciais e finais de oxigênio de cada incubação, normalizadas pelo tempo, quantidade de água presente nos frascos de incubação e superfície fotossintetizante das algas. Segue a fórmula utilizada nos cálculos (SORDO et al., 2018):

$$NP\ ou\ R = \frac{\Delta O_2 \times V}{A \times \Delta T}$$

Onde, NP é a fotossíntese líquida (em mg O_2 cm^{-2} h^{-1}), R é a respiração, ΔO_2 (oxigênio final menos oxigênio inicial mg L^{-1} ou µmol L^{-1}), V (volume da câmara de incubação em L), A (área fotossintetizante da alga em cm^2), ΔT (tempo final das incubações menos o inicial em horas).

As taxas de calcificação foram determinadas por meio da alcalinidade total (AT). A técnica de anomalia de alcalinidade é baseada no princípio de que cada mol de $CaCO_3$ precipitado resulta no decréscimo da alcalinidade total (AT) na razão de 1:2 (SMITH; KEY, 1975; WOLF-GLADROW et al., 2007). As medidas de alcalinidade foram realizadas conforme os procedimentos espectrofotométricos modificados de Yao e Byrne (YAO; BYRNE, 1998). Esta técnica consiste em monitorar a amostra com um espectroradiômetro enquanto uma solução ácida é adicionada. A concentração do ácido é quantificada utilizando um indicador a sulfoneftaleína, que pode ser o bromocresol green (BCG) ou o bromocresol purple, conforme a

solução ácida vai sendo liberada na amostra ocorre uma mudança na coloração que é detectada pelo equipamento (espectroradiômetro). Para as análises realizadas, optou-se por utilizar o bromocresol green (BCG 3 mM) e ácido clorídrico (HCl 0,3N).

As amostras de alcalinidade (frascos de 12 mL) foram divididas em três alíquotas de 4 mL, as quais foram borbulhadas com N_2 para retirada do CO_2 (aproximadamente 10 min). Após, 3 mL de cada alíquota e 10 µL do BCG foram adicionados em cubetas plásticas. As amostras foram pesadas em uma balança com quatro casas decimais de precisão e homogeneizadas em um agitador magnético (Agitador Magnético BIG SQUID, Ika, 3672000). Durante as medidas, a cubeta ficou posicionada sobre o agitador e alinhada com o sensor (fibra) do espectroradiômetro (Ocean Optics, USB2000+) (Figura 22). Uma seringa de vidro (Hamilton Company, Reno, USA) acoplada a um microtitulador liberava o ácido por aproximadamente 5 minutos (velocidade de 480 µL.h^{-1}). As mudanças na coloração das amostras foram detectadas pelas medidas de absorbância realizadas em 444 nm, 616 nm e 750 nm. A temperatura da água foi registrada com o termômetro digital Hanna (CHECKTEMP® 1 HI98509) de alta precisão. Os cálculos da alcalinidade total foram realizados conforme as equações descritas no trabalho de Yao e Byrne (YAO; BYRNE, 1998).

Figura 22 - Equipamentos utilizado para medir a alcalinidade.

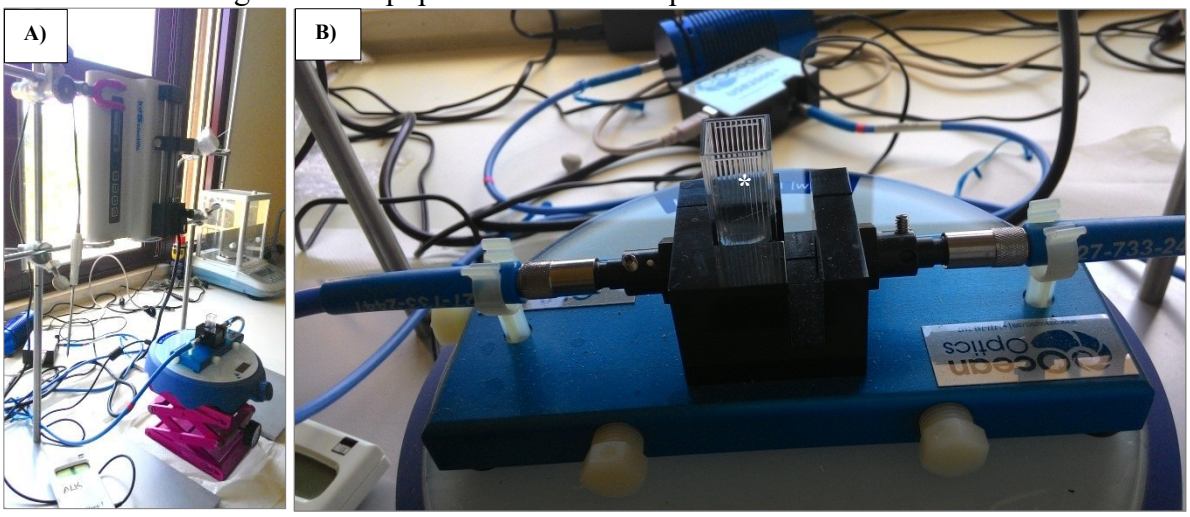

A) Microtitulador que faz a liberação do ácido (HCl) na amostra. B) Cubeta (*) posicionado sobre o agitador magnético.

Os valores de alcalinidade foram utilizados nos cálculos das taxas de calcificação (na luz e no escuro). A calcificação foi normalizada pelo tempo, volume das câmaras de incubação e a superfície fotossintetizante. Os cálculos foram realizados de acordo com a equação a seguir (STELLER et al., 2007):

$$GL\ ou\ GD = \left(\frac{\Delta AT \times V \times 0{,}5}{A}\right) \div \Delta t$$

Onde, GL é calcificação na luz (μmol $CaCO_3$ cm^{-2} h^{-1}), GD é a calcificação no escuro (μmol $CaCO_3$ cm^{-2} h^{-1}), ΔAT é a alcalinidade total inicial menos a final (em umol Kg^{-1}), V é o volume da câmara de incubação (em L), A é a área fotossintetizante da alga (em cm^2), ΔT é o tempo final das incubações menos o inicial (em horas).

2.2.4.1 Cálculo da superfície fotossintetizante das algas

No Capítulo IV, a superfície fotossintetizante das algas incubadas (em cm^2) foi estimada por meio de uma curva de calibração construída a partir de blocos com a área superficial conhecida e o peso desses depois de pintados. Assim, primeiramente blocos de tamanhos diferentes foram confeccionados com isopor. Esses blocos foram numerados, pesados (utilizando uma balança de precisão) e pintados. A primeira demão de tinta serviu para preencher imperfeiçoes superficiais, deste modo após a tinta seca os blocos foram pesados e pintados novamente. A diferença entre o peso da primeira e a segunda camada de tinta foi utilizada na curva de calibração (Figura 23).

Figura 23 - Blocos utilizados na curva de calibração.

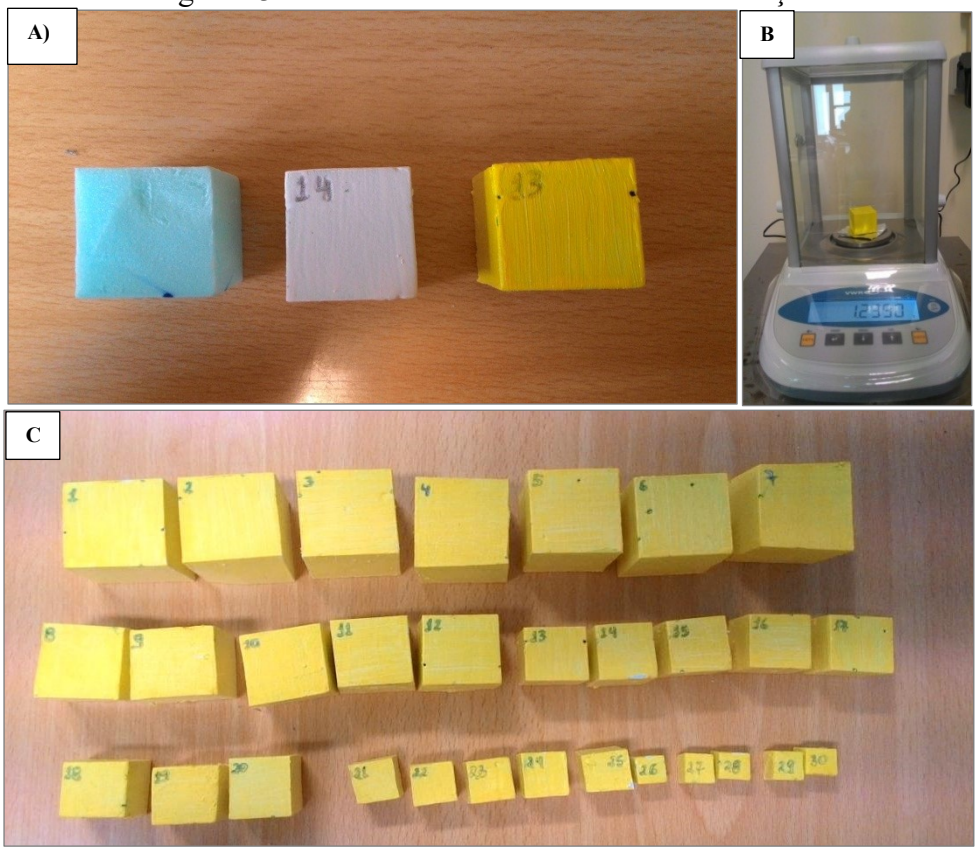

A) O bloco de isopor com a primeira demão de tinta branca e a segunda demão de tinta amarela. B) Os blocos foram pesados em uma balança de precisão. C) Blocos variando entre 1cm² a 3 cm² de lado.

Os mesmos procedimentos utilizados para a construção da curva de calibração foram também aplicados nas algas. Os espécimes utilizados na incubação foram secos na estufa (60 ºC), e em seguida foram pintados com duas camadas de tinta. A diferença entre o peso da primeira e a segunda camada foi utilizado para calcular a área superficial das algas (Figuras 24 e 25).

Figura 24 - Algas com a primeira e segunda demão de tinta.

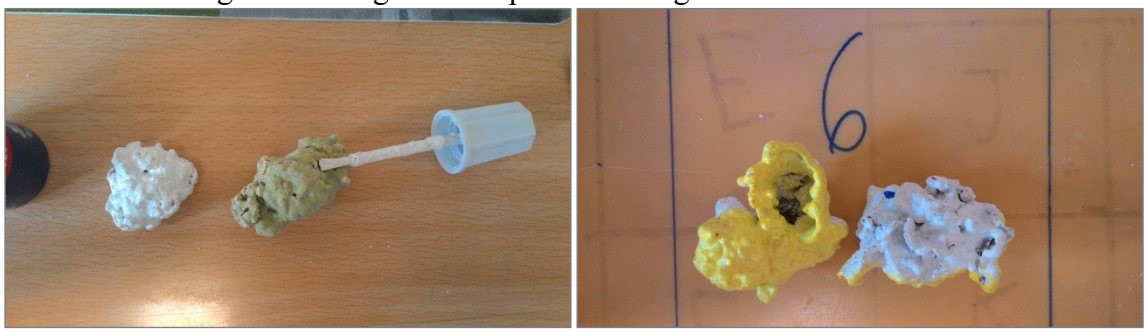

Fonte: a autora.

Figura 25 - Curva de calibração utilizada para cálculo da superfície fotossintetizante dos rodolitos.

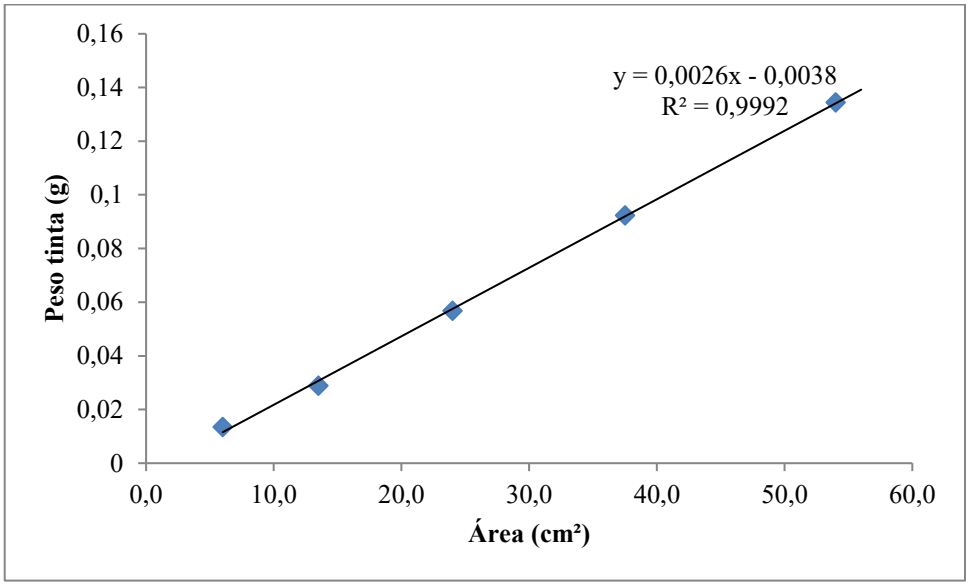

2.2.5Clorofila *a* e pigmentos carotenoides

Nos Capítulos II e III, foram determinados os carotenoides e a Chl*a* de acordo com Lubián e Montero (LUBIÁN; MONTERO, 1998). A biomassa das algas, juntamente com o extrator dimetilformamida (DMF), foram sonicados e posteriormente armazenados *overnight* (sob escuro e 4 °C). No dia seguinte, os extratos foram filtrados (filtro milipore 0,2 µm) e 80 µL de cada amostra foram injetados em um HPLC (High performance liquid chromatography), equipado com uma coluna cromatográfica (Symmetry® C18 of 5 µm 4,16x150mm column T91671L02). O fluxo das amostras foi de 1 mL minuto^{-1}. A varredura ocorreu durante 40 minutos em gradiente, com duas fases móveis: (a) água, par iônico e metanol (proporção 1:1:1), (b) acetona (HPLC) e metanol (HPLC) (proporção 1:1). O par iônico foi preparado com tetrabutilamônio (0,05 M) e acetato de amônio (1M). A varredura ocorreu entre 200 e 800 nm. As especificações do gradiente foram as seguintes:

a) 75% A+ 25% B (inicial)
b) (0-8 min) 25% A+ 75% B (lineal)
c) (8-10 min) isocrático
d) (10-18 min) convexo a 10% A+90% B
e) (18-23 min) côncavo a 100% B
f) (23-30 min) côncavo a 75% A + 25% B.

A identificação dos pigmentos foi realizada comparando o tempo de retenção e os picos com padrões comerciais de Chl*a*, violaxantina, diadinoxantina, anteraxantina, diatoxantina, zeaxantina, luteína, β-caroteno, neoxantina, cantaxantina, xantofila, echinenona e fucoxantina (DHI Water & Environment, DK-2970, Denmark).

A quantificação dos pigmentos foi realizada utilizando coeficientes de extinção molar disponíveis na literatura (DUNLAP; CHALKER; OLIVER, 1986; GLEASON, 1993; TAKANO; DAISUKE; YOSHIMASA, 1978; TAKANO; UEMURA; HIRATA, 1978; TSUJINO; YABE; SEKIKAWA, 1980) e a área dos picos cromatográficos de cada pigmento. Os resultados foram apresentados em µg de carotenoides e Chl*a* por g de massa seca (µg g^{-1}MS). Segue a fórmula utilizada para os cálculos (KORBEE-PEINADO, 2004):

$$\mu g\ g^{-1}MS = \frac{\acute{A}REA\ (\mu V.seg) \times Fluxo\ (mL.min^{-1})}{\varepsilon'(g^{-1}.L) \times V_{injeção}(mL) \times Peso(mg) \times 60}$$

Onde, ÁREA é área do pico presente no cromatograma (em µV microvolt, por segundo - unidade de absorbância - UA), Fluxo é a velocidade de injeção da amostra (em mL por min), Ɛ é o coeficiente de extinção molar (em g por L), $V_{injeção}$ é o volume de injeção (em mL), Peso é a biomassa seca (em mg).

2.2.6 Ficobiliproteínas

As ficobiliproteínas foram analisadas nos Capítulos II, III e IV. A extração foi realizada com tampão fosfato de sódio 0,1M, pH 6,5. A solução foi preparada com tampão fosfato de sódio monobásico (NaH_2PO_4) e dibásico (Na_2HPO_4), os tampões foram feitos separadamente e depois misturados. O volume utilizado é defino pelo pH que se deseja obter. O pH da solução foi definido com auxílio do medidor de pH (CRISON pH25$^+$). Os talos das algas foram macerados, posteriormente foi adicionado o tampão fosfato de sódio. As soluções foram agitadas no vórtex e permaneceram *overnight* a 4 ºC. Após as amostras foram centrifugadas (4000 rpm, 4 ºC, 10 min, 2.253 g) e os sobrenadantes foram coletados.

As leituras dos extratos foram realizadas no espectrofotômetro de UV-visível (Shimadzu UV Mini-1240) em 455 nm, 564 nm, 592 nm, 618 nm, 645 nm e 750 nm. As ficobiliproteínas foram quantificadas conforme equações de Beer e Eschel (BEER; ESCHEL, 1985). Os valores foram normalizados pelo volume do extrator (tampão fosfato) e pela

biomassa. Os resultados foram expressos em mg g^{-1} de massa seca. Seguem as equações para quantificação da ficocianina (PC) e ficoetrina (PE):

$$PC = \left[\left((A_{618} - A_{645}) - (A_{592} - A_{645}) \times 0{,}51\right) \times 0{,}15\right]$$

$$PE = \left[\left((A_{564} - A_{592}) - (A_{455} - A_{592}) \times 0{,}2\right) \times 0{,}12\right]$$

2.2.7Aminoácidos tipo micosporinas (MAAs)

Os aminoácidos tipo micosporinas (MAAs) foram analisados nos Capítulos I, II, III e IV, utilizando as metodologias de Karsten et al. (KARSTEN et al., 1998) e Korbee-Peinado et al. (KORBEE-PEINADO et al., 2004). As amostras secas em sílica foram colocadas em eppendorfs com metanol 20% e permaneceram em banho-maria a 45 ºC durante duas horas. Após os extratos foram centrifugadas (4000 rpm, 4 ºC, 10 min, 2.253 g) e em torno de 700 µL do sobrenadante foi coletado e transferido para outros eppendorfs.

Os eppendorfs com o sobrenadante foram levados para a centrifuga a vácuo, com a unidade de refrigeração sob temperatura de 45ºC, durante 7 a 8 horas para evaporação do extrator (metanol 20%). Passado o período, foram adicionados nas amostras 700 µL de metanol cromatográfico a 100%, com qualidade para ser utilizado no HPLC (High performance liquid chromatography). As amostras foram agitadas no vórtex e os sobrenadantes foram coletados e filtrados com auxílio de uma seringa contendo um filtro (milipore 0,2 µm).

No HPLC equipado como uma coluna (Symmetry® C18 of 5 µm 4,16x150mm column T91671L02) e uma pré-coluna (Phenomenex, Aschaffenburg, Germany) foram injetados 20 µL de cada amostra filtrada, com fluxo (1 mL min^{-1}) gradiente de duas fases móveis: A (metanol 1,5%) e B (ácido acético 0,15%). A varredura ocorreu de 280 a 400 nm. Os MAAs presentes nas amostras foram identificados comparando os picos das absorbâncias obtidos nas leituras e o tempo de retenção com padrões, conforme descrito por De La Coba et al. (DE LA COBA et al., 2019).

A quantificação dos MAAs foi realizada utilizando coeficientes de extinção molar presentes na literatura (DUNLAP; CHALKER; OLIVER, 1986; GLEASON, 1993; TAKANO; DAISUKE; YOSHIMASA, 1978; TAKANO; UEMURA; HIRATA, 1978; TSUJINO; YABE; SEKIKAWA, 1980) e a área do pico cromatográfico de cada MAAs. Os resultados foram

apresentados em mg de MAAs por g de massa seca (mg g^{-1} MS). Segue a fórmula utilizada para os cálculos (KORBEE-PEINADO, 2004):

$$mg.g^{-1}MS = \frac{ÁREA\ (\mu V.seg) \times Fluxo\ (mL.min^{-1})}{\varepsilon'(g^{-1}.L) \times V_{injeção}(mL) \times Peso(mg) \times 60} \times 0{,}001$$

Onde, ÁREA é a área do pico presente no cromatograma (em µV microvolt, por seg - unidade de absorbância - UA), Fluxo é a velocidade de injeção da amostra (em mL por min), Ɛ é o coeficiente de extinção molar (em L por g), $V_{injeção}$ é o volume de injeção (em mL), Peso é a massa seca (em mg).

2.2.8 Proteínas solúveis

Nos Capítulos II e III, as proteínas solúveis foram extraídas com tampão fosfato de sódio 0,1M, pH 6,5. A biomassa congelada (-80 ºC) de alga foi macerada no eppendorf com auxílio de N_2 líquido. Após a adição do tampão fosfato, as amostras foram agitadas no vórtex e permaneceram overnight a 4 ºC. No dia seguinte as amostras foram centrifugadas (4000 rpm, 4 ºC, 10 min, 2.253 g) e os sobrenadantes foram coletados.

A reação para detecção das proteínas foi realizada com 100 µL do sobrenadante, 700 µL de tampão fosfato de sódio (0,1M, pH 6,5) e 200 µL do reagente Biorad (BRADFORD, 1976). As soluções foram agitadas e após ficaram em repouso por 15 minutos, no escuro. As leituras de absorbância foram realizadas no espectrofotômetro de UV-visível (Shimadzu UV Mini-1240), em 595 nm. Foi lida também uma amostra somente com tampão fosfato e o Biorad, o branco.

A quantificação das proteínas foi realizada por meio de uma curva padrão com concentrações conhecidas de albumina sérica bovina (0, 1, 2, 4, 10, 15 e 20 µg mL^{-1}). Os valores foram normalizados pelo volume e pela biomassa. Os resultados foram expressos em mg de albumina sérica bovina por massa seca (mg_{BSA} g^{-1} MS).

2.2.9 Compostos fenólicos

Os compostos fenólicos foram analisados nos Capítulos I, II e III. A extração foi realizada com metanol 80%. Os talos das algas foram macerados em um almofariz com auxílio

de um pistilo. Após a adição do metanol, o conteúdo foi transferido para um tubo de 15 mL. As soluções foram agitadas em vórtex e permaneceram overnight a 4 ºC. No dia seguinte, os extratos foram centrifugados (4000 rpm, 4 ºC, 10 min, 2.253 g) e os sobrenadantes foram coletados.

A reação para identificação dos fenólicos nos extratos foi realizada conforme método de Folin-Ciocalteu (FOLIN; CIOCALTEU, 1927). Assim, em um tubo falcon de 15 mL foram adicionados 250 µL de sobrenadante, 1250 µL de água destilada e 125 µL do reagente Folin-Ciocalteu. As soluções foram agitadas e permaneceram 5 minutos em repouso, no escuro. Após 375 µL de carbonato de sódio anidro a 20% (Na_2CO_3) foi acrescentado, as soluções foram novamente agitadas e em seguida foi adicionado 500 µL de água destilada.

As leituras das amostras foram realizadas no espectrofotômetro de UV-visível (Shimadzu UV Mini-1240), em 760 nm. Foi realizada também a leitura do branco, incluindo todos os compostos, exceto o extrato que foi substituído por água destilada.

A quantificação dos fenólicos foi realizada por meio de uma curva padrão feita com concentrações conhecidas (0, 1, 2, 4, 8, 10, 8, 10, 16, 20, 40 e 80 µg mL^{-1}) de floroglucinol (Sigma P-3502). Os valores foram normalizados pelo volume e pela biomassa. Os resultados foram expressos em mg de equivalentes a floroglucinol por g massa seca (mg g^{-1} MS).

2.2.10 Determinação da atividade antioxidante

A determinação da atividade antioxidante dos extratos de algas foi realizada nos Capítulos I, II e III, utilizando dois métodos o DPPH (BLOIS, 1958) e o ABTS (RE et al., 1999). O primeiro consiste na redução do radical livre estável DPPH, 2,2-diphenyl-1-picrylhydrazyl, que é um receptor de íons de hidrogênio, assim quanto maior o poder redutor do extrato da alga também maior a sua atividade antioxidante. O segundo método se utiliza do mesmo princípio, o ABTS, 2,2'-azino-bis(3-ethylbenzothiazoline-6-sulphonic acid), também é um radical livre estável que pode ser capturado pelo extrato da alga.

A reação entre os radicais estáveis (ABTS e DPPH) e o extratos das algas é identificada por uma mudança na coloração que pode ser lida no espectrofotômetro. Os valores de absorbância obtidos e a posterior construção de uma curva padrão com um antioxidante conhecido possibilita quantificar os antioxidantes presentes nos extratos. Segue a descrição de cada método.

2.2.10.1 Método DPPH

A preparação do DPPH foi realizada com metanol 80%, com concentração de 1,27 mM (20 mg de DPPH e 40 mL de metanol 80%). A solução tem um tempo de vida ótimo de 4 horas, permanecendo resfriada e no escuro.

A biomassa foi previamente macerada, após foi adicionado metanol 80% e as amostras foram agitadas em vórtex e permaneceram *overnight* a 4ºC. No dia seguinte, os extratos foram centrifugados (4000 rpm, 4 ºC, 10 min, 2.253 g) e os sobrenadantes foram coletados.

A reação foi realizada com 1000 µL de metanol 80%, 150 µL de DPPH e 500 µL de sobrenadante. As amostras foram agitadas e lidas no espectrofotômetro de UV-visível (Shimadzu UV Mini-1240) em 517 nm. Após 30 minutos, as amostras foram lidas novamente. A ordem de leitura seguiu a ordem de preparação das soluções. O branco das amostras foi o metanol 80%. Segue a equação:

$$AA\% = \left[\left(abs_{inicial} - abs_{final}\right) \div abs_{inicial}\right] \times 100$$

Onde, AA% é a atividade antioxidante expressa em porcentagem, $abs_{inicial}$ é a absorbância inicial e abs_{final} é a absorbância das amostras após 30 minutos de reação ou adição da amostra.

A quantificação de compostos antioxidantes nos extratos foi realizada por meio da curva padrão feita com o antioxidante Trolox (6-hydroxy-2,5,7,8-tetramethylchroman-2-carboxylic acid), análogo a vitamina E. As concentrações utilizadas foram: 0, 20, 40, 60, 80 e 100 µM. Os valores foram normalizados pelo volume e pela biomassa. Os resultados foram expressos em µM de Trolox TE (trolox equivalentes) por massa seca ($\mu M_{TE}\ g^{-1}$ MS).

2.2.10.2 Método ABTS

A preparação do ABTS foi realizada com 10 mL de tampão fosfato de sódio (0,1M, pH 6,5), 38,41 mg de ABTS e 6,62 mg de persulfato de potássio ($K_2S_2O_8$). A solução foi mantida no escuro e na temperatura ambiente por 10 a 12 horas para formação completa do radical.

Para extração, os talos de algas foram previamente macerados e após foi adicionado o tampão fosfato. Os extratos foram agitados em vórtex e permaneceram *overnight* a 4 ºC. No dia

seguinte, as amostras foram centrifugadas (4000 rpm, 4 ºC, 10 min, 2.253 g) e os sobrenadantes foram coletados.

A reação entre o extrato e o radical ABTS foi realizada em cubetas de plástico de 2 mL. Adicionou-se nesta ordem: 890 µL de tampão fosfato, 10 µL de ABTS e 100 µL de sobrenadante. As amostras foram agitadas e lidas no espectrofotômetro de UV-visível (Shimadzu UV Mini-1240), em 727 nm. Passados 8 min, as amostras foram lidas novamente. O branco das amostras foi o tampão fosfato. As leituras iniciais ($abs_{inicial}$) e após 8 min (abs_{final}) foram utilizadas nos cálculos da atividade antioxidante (AA%), conforme a equação que segue:

$$AA\% = \left[\left(abs_{inicial} - abs_{final}\right) \div abs_{inicial}\right] \times 100$$

A quantificação de compostos antioxidantes nos extratos foi realizada por meio da curva padrão feita com o antioxidante Trolox (6-hydroxy-2,5,7,8-tetramethylchroman-2-carboxylic acid). As concentrações foram: 0, 5, 10, 15, 20, 25, 30 µM. Os valores foram normalizados pelo volume e pela biomassa. Os resultados foram expressos em µM de Trolox TE (trolox equivalentes) por massa seca ($\mu M_{TE}\ g^{-1}$ MS).

2.2.11 Carbono e nitrogênio elementar

Nos Capítulos II e III, um analisador elementar (CNHS LECO-932, Michigan, USA) foi utilizado para as análises de nitrogênio e carbono elementar. A combustão das amostras foi realizada a 1.100 ºC. A quantificação dos elementos foi realizada por espectroscopia de infravermelho (IR). EDTA foi usado como padrão. Os resultados foram expressos em mg de carbono ou nitrogênio por g de massa seca (mg g^{-1} MS).

2.2.12 Análises estatísticas

Os dados foram avaliados quanto a normalidade e homogeneidade pelos testes Kolmogorov-Smirnov e Cochran, respectivamente. A análise de variância (ANOVA), de uma via e/ou duas vias, foi utilizada para identificar as diferenças significativas. Após, o teste *post hoc* Student-Newman-Keuls (SNK) foi usado para identificar diferenças entre as médias, com nível de significância de $p<0,05$. No Capítulo IV, os dados foram ainda transformados, Log (x + 1), e uma matriz de similaridade foi calculada com Bray Curtis. Após, esta matriz foi usada

para realizar uma PCO (*Principal Coordinates Analysis*). Os softwares utilizados para realização das análises foram: Statistica 7.0 (StatSoft. Inc.), Excel (Microsoft 365) e Primer 6.

3 RESULTADOS

Os resultados foram divididos em diferentes Capítulos (I, II, III e IV). Cada capítulo corresponde a um artigo publicado, submetido ou a ser submetido em uma revista reconhecida internacionalmente. Cada artigo apresenta introdução, objetivos, materiais e métodos, resultados e discussão. Todas as referências são apresentadas no final desta tese.

O Capítulo I foi intitulado como: “Photoprotection properties of marine photosynthetic organisms grown in high ultraviolet exposure areas: cosmeceutical applications”. Neste capítulo, foi realizada uma bioprospecção com vinte e duas espécies de macroalgas e um líquen, coletados em zonas entremarés com alta exposição UV-visível. Os extratos hidroalcoólicos obtidos a partir desses organismos marinhos foram caracterizados bioquimicamente e avaliados quanto ao potencial de fotoproteção. Os resultados possibilitaram identificar espécies com potencial para serem utilizadas como fontes de compostos antioxidantes e fotoprotetores.

Os Capítulos II e III foram intitulados como: “Physiological and biochemical responses driven by different UV-visible radiation in *Osmundea pinnatifida* (Hudson) Stackhouse (Rhodophyta)” e “Effects of UV-visible radiation on growth, photosynthesis, pigment accumulation and UV-absorbing compounds in the red macroalga *Gracilaria cornea* (Gracilariales, Rhodophyta)”. Nestes capítulos, as espécies *O. pinnatifida e G. cornea* foram cultivadas sob diferentes tratamentos de radiação UV-visível. O delineamento experimental foi pensado com objetivo de avaliar respostas fisiológicas, bioquímicas e de crescimento induzidas por diferentes qualidades de radiação e mediadas por fotorreceptores não fotossintéticos.

O Capítulo IV foi intitulado como: “Photosynthesis, respiration, and calcification in the coralline alga *Lithophyllum hibernicum* Foslie 1906 (Corallinales, Rhodophyta) exposed to different irradiances”. Neste capítulo, foi investigada a fotossíntese, respiração e a calcificação da alga coralina vermelha *L. hibernicum* exposta a diferentes intensidades de luz. Variáveis como os diferentes ecossistemas onde a alga foi coletada e a existência de faces diferentemente pigmentadas foram consideradas. Os resultados possibilitaram entender melhor como esses processos interagem um com o outro e como são afetados pela luz.

4 CAPÍTULO I

Photoprotection properties of marine photosynthetic organisms grown in high ultraviolet exposure areas: cosmeceutical applications

Geniane Schneider[a*], Félix L. Figueroa[b], Julia Vega[b], Patricia Chaves[b], Félix Álvarez-Gómez[b], Nathalie Korbee[b], José Bonomi-Barufi[c]

[a] Phycology Laboratory, Postgraduate Program of Biotechnology and Biosciences, Department of Microbiology, Immunology and Parasitology, Federal University of Santa Catarina, 88040-900, Florianopolis, SC, Brazil

[b] Universidad de Málaga. Instituto Universitario de Biotecnología y Desarrollo Azul (IBYDA). Departamento de Ecología, Universidad de Málaga, Campus Universitario de Teatinos s/n, 29071, Málaga, España

[c] Phycology Laboratory, Botany Department, Federal University of Santa Catarina, 88049-900, Florianopolis, SC, Brazil

***Corresponding Author Address**
Geniane Schneider
E-mail: geniane.tega@gmail.com

Publicado em: *Algal Research 49 (2020) 101956.*
DOI: https://doi.org/10.1016/j.algal.2020.101956

4.1 ABSTRACT

Seaweeds have been identified as promising sources of bioactive substances for the cosmeceutical industry, especially by their photoprotection capacity. Accordingly, this study aimed to evaluate the photoprotective properties of extracts from macroalgae and one marine lichen. Samples of 22 species of macroalgae and one marine lichen, were collected along the southern Iberian Peninsula. Hydroethanolic extracts were prepared from algal and marine lichen lyophilized biomass. Ultraviolet (UV) and visible absorption spectra, polyphenol content, antioxidant activity, mycosporine-like amino acid content and composition were analyzed. In order to quantify the photoprotection capacity of the extracts against different biological effects, two new indices were used, i.e., effective solar absorption radiation (%ESAR) and extract photoprotection index (EPI), considering the radiation absorbed and transmitted by the extract, respectively. In the ultraviolet spectrum, *Porphyra umbilicalis* and *Pyropia elongata* presented the highest absorbance values at 330 nm, while *Ulva lactuca* showed a prominent peak at 290 nm. In the visible spectrum, a fucoxanthin peak (450 nm) was strongly evident in extracts from the brown algal species, while green algal extracts presented characteristic chlorophyll *a* and *b* peaks at 447, 620 and 664 nm. Polyphenol content and antioxidant activity were much higher in *Sargassum vulgare*, *Carpodesmia tamariscifolia*, *P. umbilicalis* and *Lichina pygmaea* in comparison to the other species. *P. umbilicalis* and *Bangia atropurpurea* showed the highest amount of mycosporine-like amino acids. *S. vulgare* and *P. umbilicalis* extracts presented the highest values of potential photoprotection against all analyzed biological response according to the different action spectra. *S. vulgare* and *P. umbilicalis* showed an increase in %ESAR values associated with an increase in the concentration of their extracts. Considering the analyzed species, our results suggest that *S. vulgare* and *P. umbilicalis* could be potential sources of photoprotective extracts. The potential use of these species in cosmeceutical products is discussed.

Keywords: action spectra, antioxidant activity, effective solar absorption radiation, extract photoprotection index, mycosporine-like amino acids, UV–visible absorption spectra.

4.2 INTRODUCTION

Ultraviolet (UV) radiation that reaches the Earth´s surface is divided into UV-B (290-320 nm), UV-AII (320-340 nm) and UV-AI (340-400 nm) (DIFFEY et al., 2000). In algae and other photosynthetic organisms, UV radiation may play important roles, influencing photoperiodic responses and aspects of metabolic development (DRING, 1988). On the other hand, UV radiation is easily absorbed by molecules, such as DNA and proteins, and can present harmful effects, such as the generation of reactive oxygen species (ROS) (DIFFEY, 1991; LARSON; BEREBAUM, 1988).

Both UV-A and UV-B can be absorbed by biomolecules of the human skin. UV-B radiation is fully retained by the stratum corneum and upper layers of the epidermis, while UV-A penetrates more deeply (ANTONIOU et al., 2008). UV-B radiation is also absorbed by DNA, causing direct damage such as mutations and the formation of toxic byproducts. UV-A radiation is strongly related to the formation of ROS, altering and inducing the expression of a series of collagen and elastin degrading enzymes, resulting in photoaging responses. In general, both UV-A and UV-B radiation induce mutations that can result in carcinomas (ANTONIOU et al., 2008; SCHMID; SCHÜRCH; ZÜLLI, 2004).

Exposure of human skin to UV radiation can produce short-term effects, such as erythema (skin redness), sunburn and pigmentation, as well as long-term effects, such as photoaging responses, carcinomas, dermal elastosis, and interference with the immune system, among others (DE GRUIJL, 2000; HORNECK, 1995; MORLIERE; MOYSAN; TIRACHE, 1995). UV radiation appears to interfere with a variety of immune responses involving cellular immunity, that is, immune reactions mediated by cell-cell contact (DE GRUIJL, 2000). UV-B and UV-A radiation also promotes lipid peroxidation, which is associated with the formation of ROS, and dermal elastosis, which is characterized by visible wrinkles and laxity caused by degenerative processes induced by sunlight (MORLIERE; MOYSAN; TIRACHE, 1995; POULSEN et al., 1984). On the other hand, UV radiation can induce positive effects, e.g., production of vitamin D, which is induced by sunlight. UV wavelengths penetrate the skin and photochemically convert precursors to vitamin D3, regulating the cutaneous production of vitamin D3 for humans (WEBB; DECOSTA; HOLICK, 1989).

Sunscreens composed of organic and inorganic filters have been developed to reduce the harmful effects of UV radiation on the skin. The first protects by absorbing UV rays, and the second protects mainly by reflecting and scattering UV radiation (ANTONIOU et al., 2008;

COCKELL; KNOWLAND, 1999). The performance of sunscreens can be measured by their sun protection factor (SPF), which is defined according to the efficiency in preventing erythema caused by UV rays, mainly UV-B. It is calculated utilizing the erythema action spectrum. Thus, a high SPF does not indicate protection against long UV-A rays (340-400 nm)(ANTONIOU et al., 2008; DIFFEY et al., 2000). Colipa's method proposes the UV-A protection factor (UVAPF) as an indicator of protection against UV-A radiation (COLIPA, 2011). UVAPF is calculated based on the action spectrum of persistent pigment darkening (PPD). However, the responses induced by UV radiation in humans are not restricted to the action spectra covered by these two photoprotection indicators. According to the different biological effects of UV-B and UV-A, De la Coba et al. (2019) suggested evaluating the capabilities of topical formulations through different biological effective protection factors (BEPFs) in addition to erythema and persistent pigmentation action spectra.

Action spectra are important tools. They contain information about biological responses versus wavelengths (UV-visible) (GORTON, 2010), i.e., action spectra clearly identify the wavelengths that most effectively induce a biological response and quantify the relative impacts from various wavelength regions (DE GRUIJL, 2000). Several action spectra have been published since the precursor study of Engelmann (ENGELMANN, 1882; GATES, 1929a, 1929b, 1930). Some spectra have been produced for very specific responses, such as the production of erythema on human skin, vitamin D3 synthesis, immunosuppression, lipid peroxidation, photoaging and others (BISSETT; HANNON; ORR, 1989; FABO; KRIPKE, 1980; MCKINLEY; DIFFEY, 1987; MORLIERE; MOYSAN; TIRACHE, 1995; WEBB; DECOSTA; HOLICK, 1989). Also, action spectra of growth and photosynthesis in plants and algae have been obtained (FLINT; CALDWELL, 2003; HAXO; BLINKS, 1950; LÜNING; DRING, 1985).

Algae form a diverse group and are present in a wide variety of marine habitats, including areas subjected to abiotic stresses, such as desiccation, high temperatures and high levels of UV radiation. Among other responses, UV radiation can induce the production of photoprotection compounds in algae, such as carotenoids, mycosporine-like amino acids (MAAs) and/or polyphenols like phlorotannins (FIGUEROA et al., 2003; GÓMEZ; HUOVINEN, 2010; KARSTEN et al., 1999a; LALEGERIE et al., 2019). These compounds have the potential to be used as alternative substances to replace compounds and/or improve the efficiency of sunscreens and other cosmetics. The actual formulations can have some limitations and/or adverse effects, for example, damage to skin cells and coral bleaching

(CORINALDESI et al., 2018; DANOVARO et al., 2008; PAN et al., 2009; REINOSA et al., 2018; WAKEFIELD et al., 2004). In addition, some data show that organic filters can bioaccumulate in trophic levels of the food web, causing long-term adverse effects (HE et al., 2019; SCHNEIDER; LIM, 2019).

Thus, this study aimed to evaluate photoprotective properties of marine photosynthetic organisms, including macroalgae and one marine lichen, collected in the intertidal areas along the southern Iberian Peninsula. Biochemical characteristics of the studied organisms were evaluated. In addition, photoprotection properties were verified using a newly proposed approach, effective solar absorption radiation (ESAR in %), which indicates the potential of extracts to absorb different UV wavelengths that can induce correspondingly different biological responses, and the extract photoprotection index (EPI), which is calculated in a manner analogous to that of SPF and BEPFs, applying different action spectra, as reported by De la Coba et al. (2019).

4.3 MATERIAL AND METHODS

4.3.1 Samples and species identification

Macroalgae samples and one marine lichen were employed in the present study; they were collected in different areas along the southern Iberian Peninsula: La Araña, Málaga (UTM 381471.00 m E/4063686.00 m N) and Tarifa, Cádiz (UTM 266115.51 m E/3988333.17 m N). Algae and the marine lichen were collected in the intertidal zone, during low tide. The algal species were selected according to criteria of available biomass as common species in the collection areas, and several of them were selected based on their culture potential. The intertidal marine lichen was also collected because it contains high levels of mycosporine glycine and mycosporine serinol, an UV-B absorbing MAA (DE LA COBA et al., 2009, 2019; LA BARRE; ROULLIER; BOUSTIE, 2014). The collection sites have high UV radiation exposure (HÄDER et al., 2001; WIENCKE et al., 2000). Only *Crassiphycus corneus* was obtained from cultures conducted in the Grice-Hutchinson Experimental Center, Málaga (UTM 367921.68 m E/4059212.13 m N). *C. corneus* was grown at a temperature between 20 and 25 ºC with constant and vigorous aeration under solar radiation. The water was renewed once a week with the addition of nutrients every two days (400 µM of NH_4Cl and 40 µL of KH_2PO_4). Original apices of *C. corneus* were supplied by the Spanish Bank of Algae of Las Palmas de GC University (Canary Islands, Spain) and wet-transported to the experimental center.

Samples collected along the southern Iberian Peninsula were transferred to plastic bags containing seawater and transported in iceboxes to the laboratory at the Sciences Faculty of Malaga University. The algae were then cleaned by removing epiphytes and stored at -80 ºC. Identification was performed with keys and guides available in the literature (CARRILLO; ACEDO, 1999; PÉREZ-LLORÉNS et al., 2012; RODRÍGUEZ-PRIETO et al., 2013).

4.3.2 Extractions

Frozen samples of algae and one marine lichen were lyophilized and ground into a fine powder with mortar and pestle. Afterwards, extracts were prepared for different analyses. Considering low availability of biomass, *Bangia atropurpurea* extracts were evaluated only to antioxidant activity (ABTS) and MAAs. All procedures performed with the algal biomass and extracts are summarized in Figure 26.

Figura 26 - Summary of all evaluated variables.

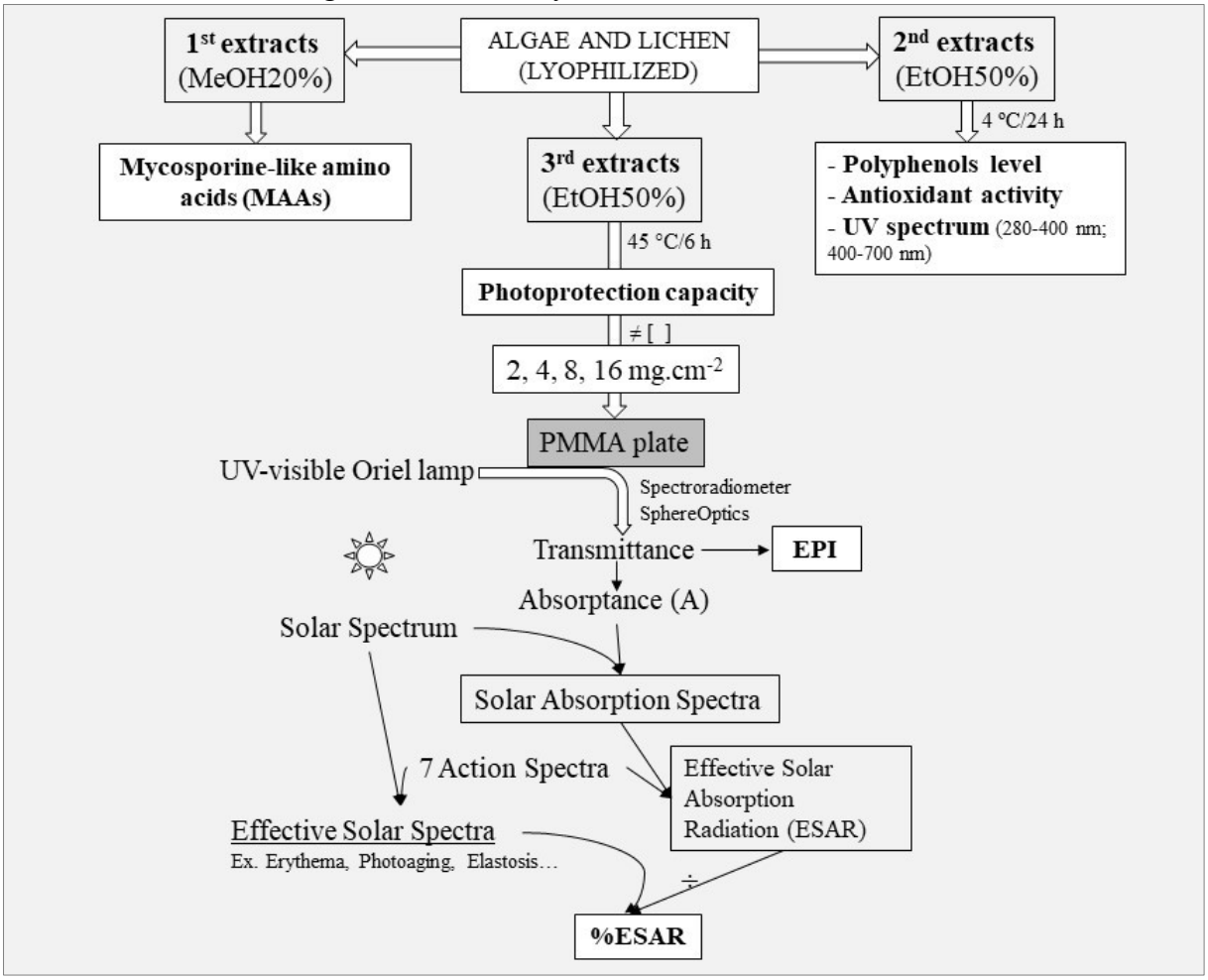

The biomass of algae and one marine lichen was lyophilized. Afterwards, different extracts were prepared (1st, 2nd, 3rd), hydromethanolic (methanol:water, v/v; MeOH20%) and hydroethanolic extracts (ethanol:water, v/v; EtOH50%). The 1st, 2nd, 3rd extracts were used for: evaluation of mycosporine-like amino acids (MAAs); absorption spectrum (UV-visible), phenolic compounds level and antioxidant activity (ABTS); and photoprotection capacity (%ESAR and EPI), respectively. To evaluate photoprotection capacity, the extracts were distributed on a PMMA (polymethylmethacrylate) plate, which was placed under a UV-visible Oriel Lamp. Transmittance measurements were performed with a spectroradiometer, and the values obtained were used to calculate the effective solar absorption radiation (%ESAR) and the extract photoprotection index (EPI) parameters.

The first extracts were prepared for evaluation of MAAs as described by Karsten et al. (KARSTEN et al., 1998) and Korbee-Peinado et al. (KORBEE-PEINADO et al., 2004), using 20 mg lyophilized biomass of algae and marine lichen and 1 mL of 20% aqueous methanol (v/v). Extracts were maintained for 2 h at 45ºC, followed by centrifugation (2500 g at 4ºC for 10 min). The supernatant (700 µL) was evaporated in a vacuum centrifuge for 24 h. After, the extract was resuspended in 700 µL of 100% chromatographic methanol and filtered using a syringe coupled to a filter (0.22 µm). Then, the filtered samples followed for determination by HPLC (high-performance liquid chromatography). The extractions were performed with three different samples for each species evaluated (n=3).

The second extracts were prepared for analysis of absorption spectrum (UV-visible), phenolic compounds level and ABTS). For this, 0.2 g of dry biomass (powder) was inserted in 10 mL of 50% ethanol (ethanol: distilled water, 1:1). The extracts were vortexed and remained in darkness at 4ºC and 24 h. After this period, the extracts were centrifuged (2500 g, 15 min) and supernatants were collected and separated for analyses. The extractions were performed with three different samples for each species evaluated (n=3).

The third extracts for evaluation of photoprotection capacity (%ESAR and EPI) were prepared in accordance with Álvarez-Gómez et al. (ÁLVAREZ-GÓMEZ; KORBEE-PEINADO; FIGUEROA, 2016), who specified that 2 g of lyophilized biomass (powder) from selected macroalgae were inserted into 40 mL of 50% ethanol (ethanol: distilled water, 1:1). The solutions were incubated for 6 h at 45 °C under constant stirring. After this period, the extracts were centrifuged (2500 g at 4ºC for 10 min). The supernatant was concentrated in a rotary evaporator up to 500 mg mL^{-1}.

4.3.3 Detailed extract analyses

4.3.3.1 Mycosporine-like amino acids (MAAs) composition and level

MAAs were detected by HPLC using an isocratic flow (1mL. min^{-1}) containing 1.5 % aqueous methanol (v/v) and 0.15% acetic acid (v/v). Twenty µL of the filtrate were injected into a Sphereclone C8 column (5 µm particle size; 250 x 4.6 mm) and a precolumn (Phenomenex, Aschaffenburg, Germany) coupled to a Waters (Barcelona, Spain) HPLC system. MAAs were detected with a Waters Photodiode Array Detector (996; Barcelona, Spain). The absorption spectra were recorded from 280 to 400 nm. Quantification was performed using published extinction coefficients (DUNLAP; CHALKER; OLIVER, 1986; GLEASON, 1993; TAKANO; DAISUKE; YOSHIMASA, 1978; TAKANO; UEMURA; HIRATA, 1978; TSUJINO; YABE; SEKIKAWA, 1980) and extracting chromatographic peak areas of the wavelength with maximum absorption of each MAA. The MAAs were identified using the same secondary standards as those used by De la Coba et al.(DE LA COBA et al., 2019).

4.3.3.2 Absorption spectrum

The absorbance of hydroethanolic extracts from macroalgae and one marine lichen was measured using a UV-visible spectrophotometer (Shimadzu UV Mini-1240), with a spectral window from 250 to 750 nm and resolution of 1 nm.

4.3.3.3 Phenolic compounds level

Quantification of phenolic compounds in the crude extract from macroalgae and one marine lichen was performed according to the Folin-Ciocalteu method (FOLIN; CIOCALTEU, 1927). Reaction was performed by adding 250 µL of crude extract, 1250 µL of distilled water and 125 µL of the Folin-Ciocalteu reagent. The solution was stirred and incubated at room temperature in darkness for 5 min. Following this, 375 µL of 20% anhydrous sodium carbonate (Na_2CO_3) and 500 µL of distilled water were added, and the solution was stirred again. The absorbance was measured at 760 nm using a UV-visible spectrophotometer (Shimadzu UV Mini-1240). The blank included all reagents, except the crude extract that was replaced by distilled water. Phenolic contents were determined by constructing a standard curve using different phloroglucinol (Sigma P-3502) concentrations. Results were expressed in mg equivalent of phloroglucinol per g of algal dry weight (DW).

4.3.3.4 Antioxidant activity

Antioxidant activity of macroalgae and marine lichen crude extract was measured using the ABTS method (RE et al., 1999). ABTS reagent was prepared in sodium phosphate buffer (0.1M, pH 6.5), ABTS (2,2'-azino-bis (3-ethylbenzothiazoline-6-sulphonic acid,7mM) and potassium persulfate ($K_2S_2O_8$, 2.45 mM). The reagent was incubated in darkness at room temperature for 12 to 16 h, allowing a complete formation of the radical. After this period, reaction was performed by adding 940 µL of sodium phosphate buffer (0.1M, pH 6.5), 10 µL of ABTS and 50 µL of algal extract. The samples were agitated, and absorbance was recorded by a UV-visible spectrophotometer (Shimadzu UV Mini-1240) at 727 nm (abs_{727}) immediately at the beginning of the reaction (T_0) and after 8 min of incubation (T_8). The blank was phosphate buffer. The antioxidant activity (AA) of free radicals was calculated as

$$AA\% = \left(\frac{Abs_{727}\, T_0 - abs_{727} T_8}{abs_{727} T_0}\right) \times 100$$

Quantification of antioxidant compounds was determined using a standard curve with Trolox (6-hydroxy-2,5,7,8-tetramethylchroman-2-carboxylic acid) concentrations. The results were expressed in mg g^{-1} of TE (Trolox equivalents) per g of algal or lichen dry weight (DW).

4.3.3.5 Photoprotection capacity

Photoprotective capacity was evaluated by calculating the effective solar absorption radiation (%ESAR) ratio and extract photoprotection index (EPI) by algal extracts. The %ESAR and EPI determination were performed for extracts of species that presented the most prominent results in previous analyses, such as polyphenols content, ABTS assay and MAA content and composition. Species selected were *Carpodesmia tamariscifolia*, *Porphyra umbilicalis*, *Sargassum vulgare*, and *Ulva lactuca*. *Lichina pygmaea* was also highlighted in the analyses, but %ESAR and EPI parameters were not evaluated because the cultivation of this species is not easy, and the available biomass in the environment is low.

The parameter %ESAR was calculated using the solar radiation retained and/or absorbed by algal extracts; this radiation, in turn, could effectively cause different types of biological responses in human beings. EPI was calculated using the radiation transmitted through algal extracts. EPI is analogous to BEPFs (biological effective protection factors), as proposed by De la Coba et al. (DE LA COBA et al., 2019). However, we chose to name our parameter as EPI, instead of BEPF, because we use algal extracts and De la Coba et al. did calculations with sunscreen lotions. In summary, %ESAR and EPI are proposed as indicators of photoprotective properties, thus, high values of %ESAR and EPI indicate greater effectiveness of the extracts to retain/absorb wavelengths associated with different biological responses.

EPI and %ESAR were calculated by applying 800 µL of different dilutions of the concentrated extracts on the rough side of polymethylmethacrylate (PMMA) plates (roughness Ra, 4.5-5.2 µm; dimension: 5 cm * 5 cm * 0.25 cm, 25 cm^2; Schönberg GmbH & Co. KG, Germany), which yielded final concentrations per plate area of 2, 4, 8 and 16 mg of algal dry weight per cm^2 (mg cm^{-2} DW). PMMA plates used in this study had a rough side, imitating the skin's surface, as recommended in the Colipa method. The extract was evenly distributed on

the plates with the tips of the fingers covered by nitrile gloves, following the recommendations of Colipa (COLIPA, 2011). The plates were incubated in darkness at room temperature for 15 min. After this period, they were positioned in the trajectory of the radiation emitted by the solar simulator (Spectra-Physics Model 66902) equipped with a mercury xenon lamp (Lamp Power 50-500 W). Below the plate, the transmittance was recorded by a spectroradiometer (Sphere Optics SMS-500, Contoocook, New Hampshire U.S.A.) between 200 and 800 nm (resolution of 1 nm). Eight plates (n=8) were measured for each concentration from the four selected macroalgae.

Transmittance values were converted to absorptance values (A(λ)) as

$$A(\lambda) = 1 - \left(\frac{T_0(\lambda)}{T_t(\lambda)}\right)$$

where $T_o(\lambda)$ is the transmittance by each sample at wavelength λ, and $T_t(\lambda)$ is the blank transmittance at wavelength λ. The blank was a PMMA plate containing water instead of algal extract.

Absorptance was utilized to calculate Solar Absorptance (SA) values, to each nm from a Solar Spectrum (SS). Solar Spectrum was obtained on July 6, 2010, a summer day in Malaga (UTM 368412.22 m E, 4064373.82 m N), without clouds, at 12:30 GMT, with a spectroradiometer (Sphere Optics SMS-500, Contoocook, New Hampshire U.S.A.).

$$SA(\lambda) = A(\lambda) \times SS(\lambda)$$

where A(λ) stands for the values of absorptance at each wavelength λ, and SS(λ) stands for the solar spectrum intensities at each wavelength λ. The unit of this parameter was $W.m^{-2}$. With the same solar spectrum, we also calculated the effective solar radiation (eSS) of each action spectrum analyzed (Act.Sp.):

$$eSS(\lambda) = SS(\lambda) \times Act.Sp.(\lambda)$$

ESAR was calculated by applying action spectra (Act.Sp.) to different biological responses driven by UV (see Table 1 and Figure 27), by the following formula (unit: $W.m^{-2}$):

$$ESAR = SA(\lambda) \times Act.Sp.(\lambda)$$

Proportion of ESAR with respect to solar radiation available was calculated as

$$\%ESAR = \frac{\sum_{(280-420\ nm)} ESAR(\lambda)}{\sum_{280-420\ nm} eSS(\lambda)}$$

The calculation of EPI was done with transmittance $T_o(\lambda)$ values, obtained as explained above, and also the effective solar radiation (eSS):

$$EPI = \frac{\sum_{(280-420\ nm)} eSS(\lambda)}{\sum_{(280-420\ nm)} \left(eSS(\lambda) \times T_0(\lambda)\right)}$$

Finally, %ESAR was plotted against EPI, and EPI_{50} was calculated by using the Quest Graph™ EC50 Calculator. In this case, this parameter represented the EPI value where %ESAR reached half of its maximal response.

Tabela 1 - Action spectra of biological responses driven by UV utilized to calculate effective solar absorption radiation (%ESAR) and extract photoprotection index (EPI) in this study.

Action spectra biological responses	**UV-B**	**UV-A-II**	**UV-A-I**	**Blue**	**Reference**
Vitamin D3 synthesis	100.0	0.0	0.0	0.0	(WEBB; DECOSTA; HOLICK, 1989)
Erythema	99.5	0.3	0.2	0.0	(MCKINLEY; DIFFEY, 1987)
Immunosuppression	96.9	3.1	0.0	0.0	(FABO; KRIPKE, 1980)
Lipid peroxidation	80.6	8.6	9.7	1.1	(MORLIERE; MOYSAN; TIRACHE, 1995)
Elastosis	63.4	12.4	24.1	0.0	(WULF et al., 1989)
Photoaging	3.6	34.8	61.6	0.0	(BISSETT; HANNON; ORR, 1989)
Persistent Pigment Darkening (PPD)	2.9	42.3	54.9	0.0	(MOYAL; CHARDON; KOLLIAS, 2000)

Action spectra were divided according to their influence in different spectral regions, such as UV-B (280-320 nm), UVA-I (320-340 nm), UVA-II (340-400 nm), and short-blue (400-420 nm).

Figura 27 - Action spectra of biological responses driven by UV radiation.

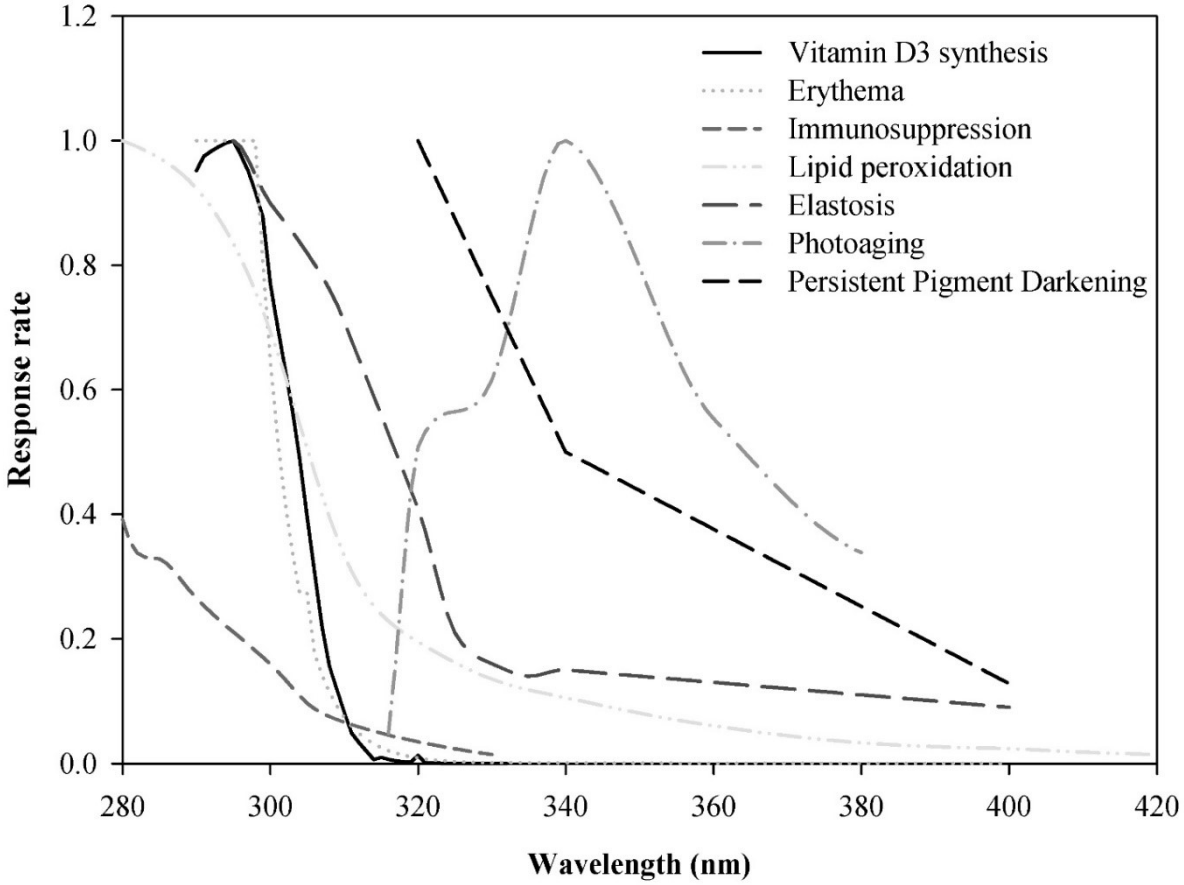

Action spectra were applied to calculate the percentage of effective solar absorption radiation (%ESAR) and extract photoprotection index (EPI) from algal extracts. Data from (BISSETT; HANNON; ORR, 1989; FABO; KRIPKE, 1980; MCKINLEY; DIFFEY, 1987; MORLIERE; MOYSAN; TIRACHE, 1995; MOYAL; CHARDON; KOLLIAS, 2000; WEBB; DECOSTA; HOLICK, 1989). See Table 1 for a more precise referencing.

4.3.4 Statistical analysis

Tests of normality (Kolmogorov-Smirnov) and homogeneity of variances (Cochran) were conducted. Analyses of variance (one-way ANOVA) were performed to verify significant differences with "species and concentrations", as the predicted variable, and biochemical analyses and UV driven biological responses, as dependent variables. The values obtained from %ESAR calculations were compared among the different extract concentrations for each species, and among the species for each concentration by one-way ANOVA. Student-Newman-Keuls (SNK) post-hoc test was used to identify significant differences between means with significance level of $p < 0.05$. Analyses were conducted with the Statistica 7.0 (StatSoft, Inc.) and Excel 2016 software.

4.4 RESULTS

In this study, 22 species of algae were collected and distributed into three groups: Chlorophyta with 5 species, Ochrophyta with 4 species, and Rhodophyta with 13 species. *Ellisolandia elongata* was the unique species found and collected at two sites. The lichen collected, *Lichina pygmaea*, belongs to the phylum Ascomycota (Table 2).

Tabela 2 - Collection sites and species evaluated in our study. The table contains 22 algae and one marine lichen. It is worth noting that

Phylum	**Species**	**Collection place**
Ascomycota	*Lichina pygmaea* (Lightfoot) C.Agardh	Tarifa, Cádiz
Chlorophyta	*Codium adhaerens* C.Agardh	Tarifa, Cádiz
	Ulva lactuca Linnaeus	Tarifa, Cádiz
	Ulva intestinalis Linnaeus	La Araña, Málaga
	Ulva linza Linnaeus	La Araña, Málaga
	Valonia utricularis (Roth) C.Agardh	Tarifa, Cádiz
Ochrophyta	*Carpodesmia tamariscifolia* (Hudson) Orellana & Sansón	La Araña, Málaga
	Rugulopteryx okamurae (E.Y.Dawson) I.K.Hwang, W.J.Lee & H.S.Kim	Tarifa, Cádiz
	Sargassum vulgare C.Agardh, nom. illeg.	La Araña, Málaga
	Scytosiphon lomentaria (Lyngbye) Link, nom. cons.	Tarifa, Cádiz
Rhodophyta	*Bangia atropurpurea* (Mertens ex Roth) C.Agardh	Tarifa, Cádiz
	Ceramium virgatum Roth	Tarifa, Cádiz
	Chondracanthus acicularis (Roth) Fredericq	La Araña, Málaga
	Crassiphycus corneus (J.Agardh) Gurgel, J.N.Norris & Fredericq	Grice Hutchinson, Málaga
	Ellisolandia elongata (J.Ellis & Solander) K.R.Hind & G.W.Saunders	La Araña, Málaga; Tarifa, Cádiz
	Feldmannophycus rayssiae (Feldmann & G.Feldmann) H.Augier & Boudouresque	La Araña, Málaga
	Gelidium microdon Kützing	Tarifa, Cádiz
	Gelidium spinosum (S.G.Gmelin) P.C.Silva	La Araña, Málaga
	Gracilaria multipartita (Clemente) Harvey	La Araña, Málaga
	Osmundea pinnatifida (Hudson) Stackhouse	La Araña, Málaga
	Porphyra umbilicalis Kützing	Tarifa, Cádiz
	Pyropia elongata (Kylin) Neefus & J.Brodie	La Araña, Málaga
	Sphaerococcus sp. Stackhouse	Tarifa, Cádiz

Ellisolandia elongata was collected at two sites, La Araña (LA) and Tarifa (TA).

Tarifa, Cádiz (UTM - 265902.89 m E/3988370.31 m N); La Araña, Málaga (UTM - 381471.00 m E/4063686.00 m N); Grice-Hutchinson Experimental Center, Málaga (UTM - 367921.68 m E/4059212.13 m N)

One-way ANOVA showed significant variation for all analyses and biological responses evaluated, with species and concentrations as predictive variables (see supplementary material, ANEXO A, Table S. 1 and S. 2).

MAAs were detected mainly in red algae, highlighting *P. umbilicalis*, *Bangia atropurpurea*, *Feldmannophycus rayssiae* and *Pyropia elongata*, all with more than 3 mg g^{-1} DW. *P. umbilicalis* reached more than 10 mg g^{-1} DW. *Lichina pygmaea* showed less than 1 mg g^{-1} DW of MAAs, but this content was higher than all green and brown algae, and the red alga *Sphaerococcus* sp., which showed amounts less than 0.008 mg of MAAs per g algal DW (Figure 28). Consequently, seven different MAAs were identified only in red algae (except *Sphaerococcus* sp.) and the marine lichen. Palythinol was predominant in all species, except of *B. atropurpurea*, *Gracilaria multipartita* and *P. umbilicalis*. For *B. atropurpurea* and *P. umbilicalis*, the main MAAs were porphyra-334 and asterina-330, representing 67% and 72% of total MAAs, respectively (Figure 28 B).

Figura 28 - Mycosporine-like amino acids (MAAs) detected in 20% methanolic extracts (methanol:water, v/v) from 23 algal and marine lichen species collected along the southern Iberian Peninsula .

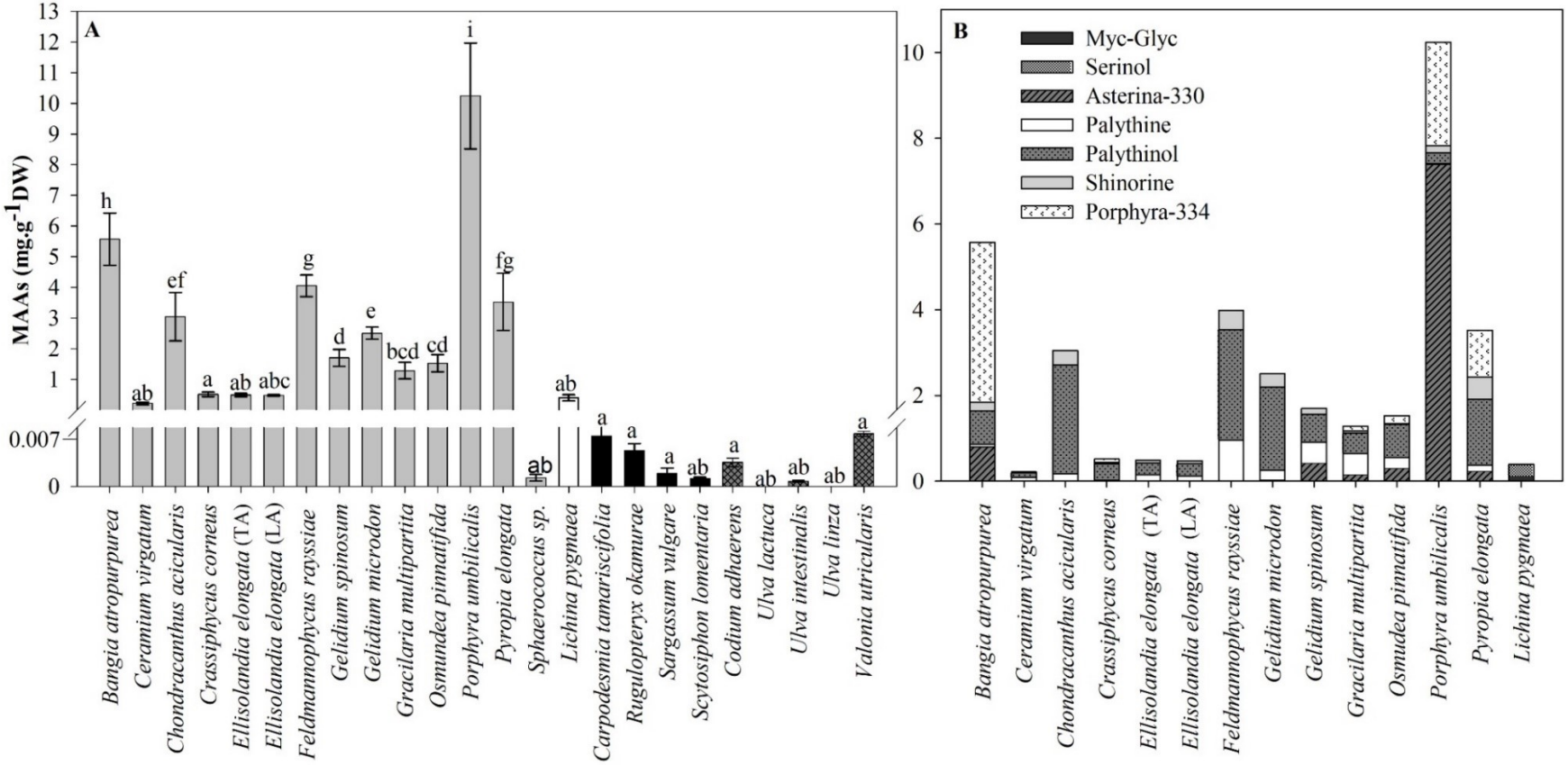

A) MAA concentration expressed in mg of MAAs by g of algal or lichen dry weight (DW). Grey bars: red algae, white bar: marine lichen, black bar: brown algae, hatched bars: green algae. Different letters above the bars indicate significant differences according to a posteriori Newman-Keuls test ($p<0.05$). Mean ± standard-deviation (n=3). B) MAA composition observed in extracts from red algae and one marine lichen. Two sites for *Ellisolandia elongata*: La Araña (LA) and Tarifa (TA).

The UV absorption spectra of brown algal extracts showed no clear formation of absorption zone (Figure 29 A), while they were found at 290 nm for the green alga *Ulva lactuca* (Figure 29 B) and between 320 and 340 nm for the red algae, with special attention to *Porphyra umbilicalis* and *Pyropia elongata* (Figure 29 C). The marine lichen showed a very small peak at 310 nm (Figure 29 D).

Figura 29 - UV absorption spectrum results (λ = 280-400 nm) performed with ethanol-water extracts (1:1 v/v) from the 23 species collected along the southern Iberian Peninsula (see details in Table 2).

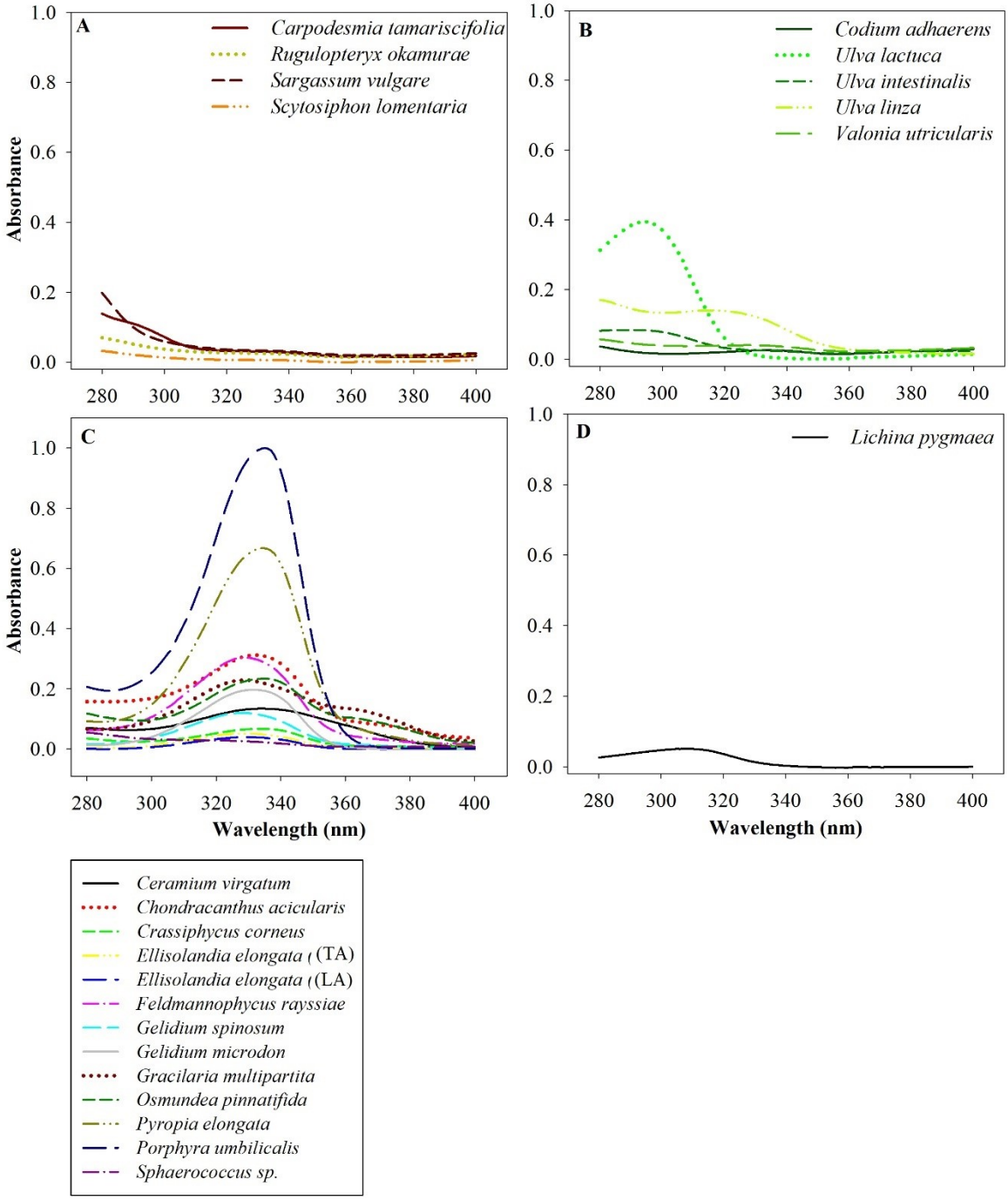

The graph shows the mean values (n=3). The data were classified according to taxonomic groups: A) Ochrophyta (brown algae), B) Chlorophyta (green algae), C) Rhodophyta (red algae) and D) Ascomycota (lichen). Two sites for *Ellisolandia elongata:* La Araña (LA) and Tarifa (TA).

Figure 30 presents the absorption spectra of algae and marine lichen extracts in the visible spectrum, highlighting brown and green algae (Figure 30 A and B). The former showed prominent peaks in the region of 450 nm, especially *Sargassum vulgare.* Subsequently, green

algae presented three peaks between 400 and 500 nm and others between 600 and 700 nm, mainly for *Codium adhaerens* and *Ulva intestinalis*. Red algae also showed peaks in the same regions as those of the green algae, but smaller (Figure 30 C).

Figura 30 - Visible absorption spectrum results (λ = 400-700 nm) were performed with ethanol-water extracts (1: 1 v / v) from 23 species along the southern Iberian Peninsula (see details in Table 2).

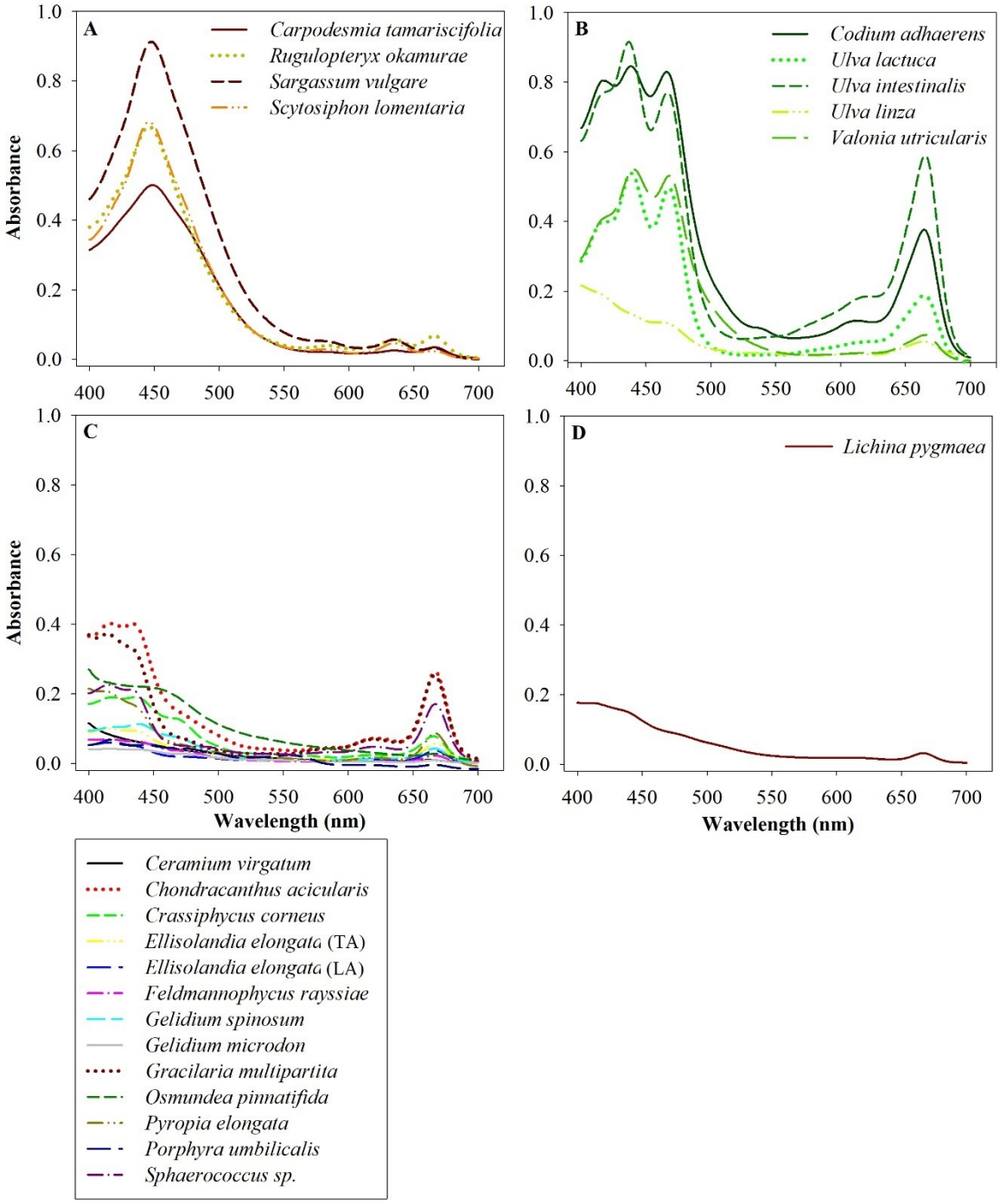

The graph shows the mean values (n=3). The data were classified according to taxonomic groups: A) Ochrophyta (brown algae), B) Chlorophyta (green algae), C) Rhodophyta (red algae) and D) Ascomycota (lichen). Two sites for *Ellisolandia elongata*: La Araña (LA) and Tarifa (TA).

Sargassum vulgare, Carpodesmia tamariscifolia, L. pygmaea, and *P. umbilicalis* showed prominent quantified phenolic compounds, with amounts greater than 15 mg of eq. phloroglucinol per g of algal or lichen dry weight (mg g^{-1} DW) (Figure 31).

Figura 31 - Level of phenolic compounds in hydroethanolic extracts (ethanol:water, v/v) from algae and marine lichen species collected along the southern Iberian Peninsula , as expressed in mg per g of algal or lichen dry weight (DW).

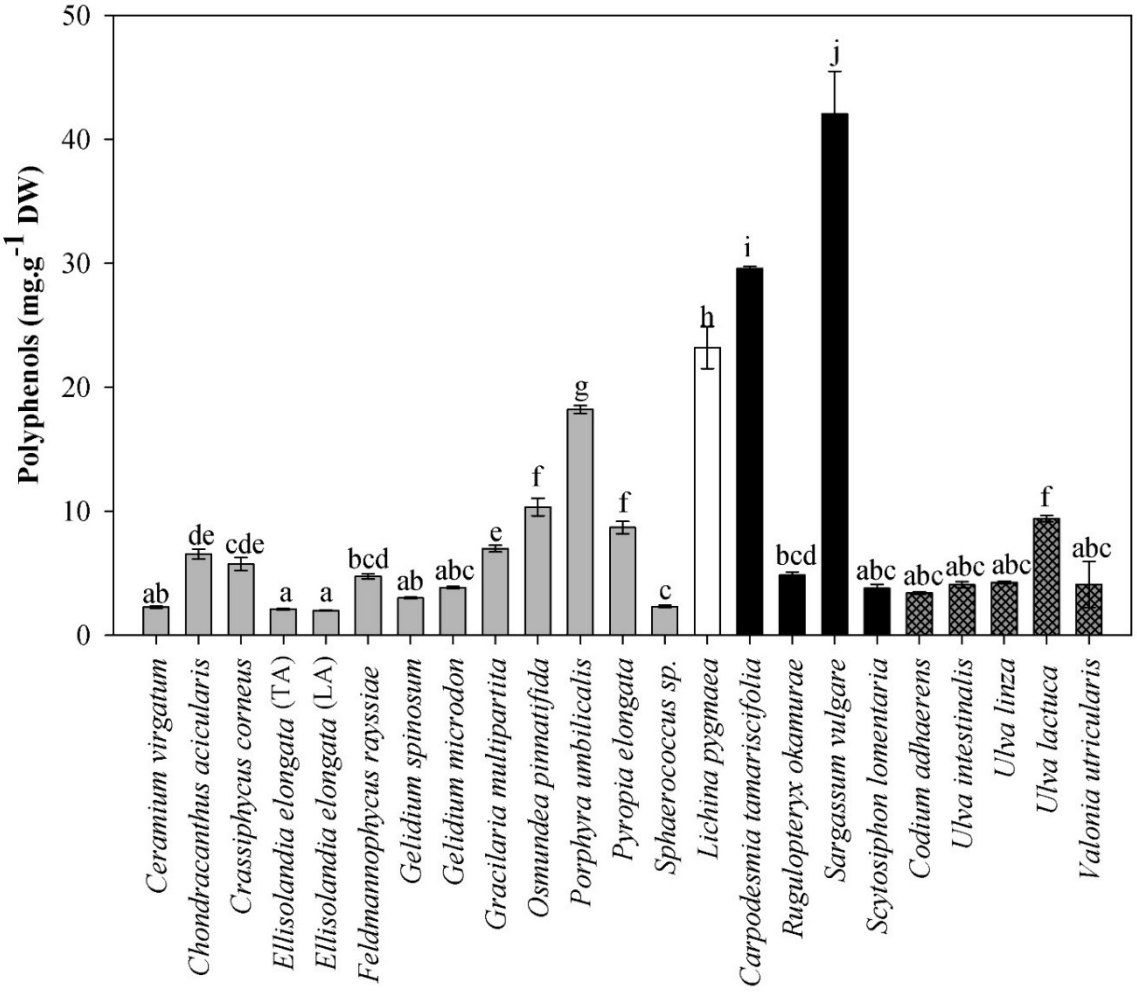

Grey bars: red algae, white bar: marine lichen, black bar: brown algae, hatched bars: green algae. Different letters above the bars indicate significant differences observed with a posteriori Newman-Keuls test ($p<0.05$). Mean ± standard-deviation (n=3). Two sites for *Ellisolandia elongata*: La Araña (LA) and Tarifa (TA).

Antioxidant activity obtained by the ABTS method was markedly high in extracts of the brown algae *C. tamariscifolia* and *S. vulgare,* as well as the marine lichen *L. pygmaea* (Figure 32). These three species showed values greater than 60 mg_{TE} g^{-1} DW. Red and green algae were best represented by *P. umbilicalis* and *Ulva lactuca* with 12 and 9 mg g^{-1} DW of TE, respectively (Figure 32).

Figura 32 - Antioxidant activity of hydroethanolic extracts (ethanol:water, v/v) from 23 algal and marine lichen species collected along the southern Iberian Peninsula evaluated by ABTS, as expressed in mg of Trolox Equivalents (TE) per g of algae or lichen dry weight (DW).

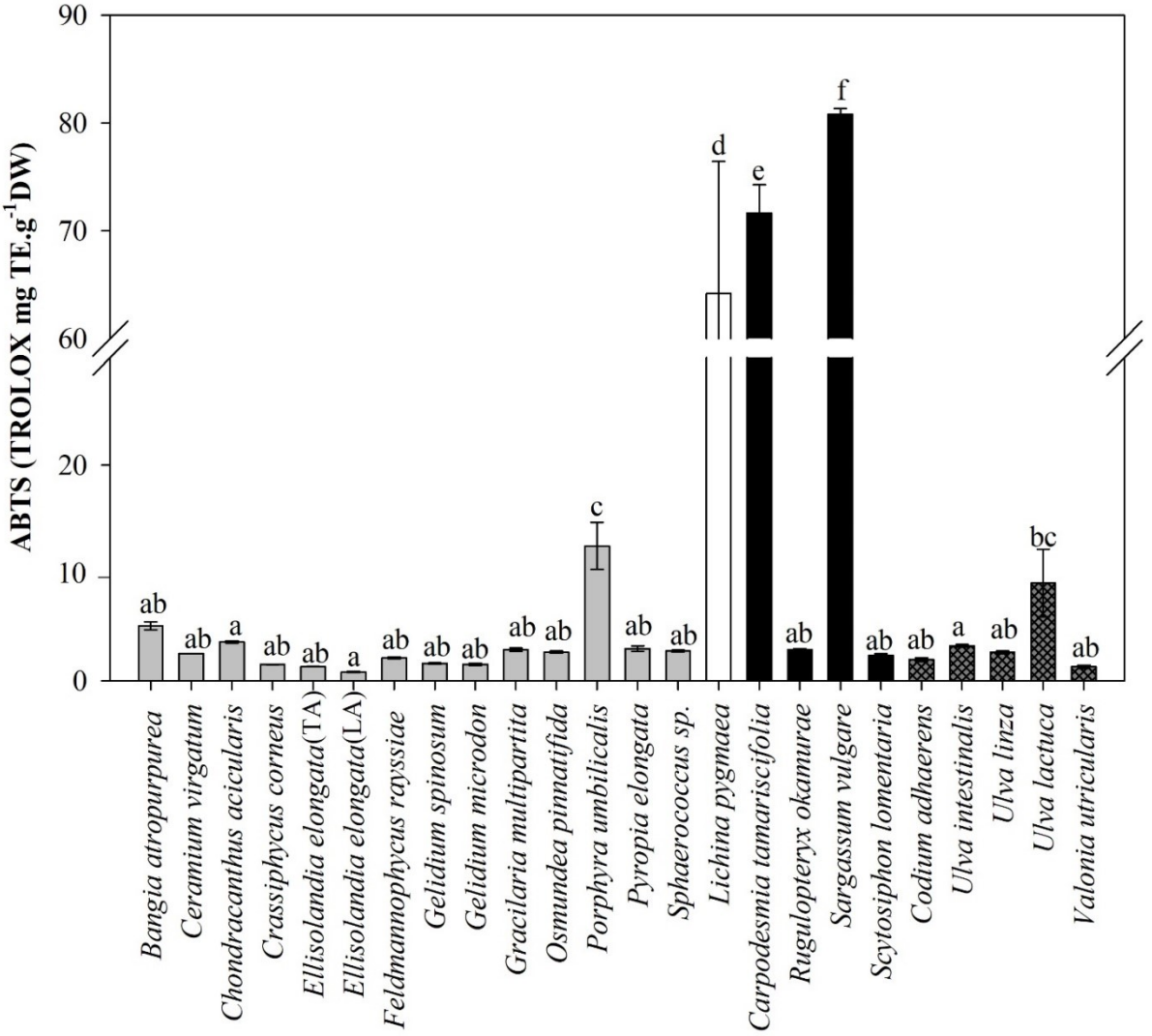

Grey bars: red algae, white bar: marine lichen, black bar: brown algae, hatched bars: green algae. Different letters above the bars indicate significant differences according to a posteriori Newman-Keuls test ($p<0.05$). Mean ± standard-deviation (n=3). Two sites for *Ellisolandia elongata*: La Araña (LA) and Tarifa (TA).

Table 3 shows the values of %ESAR calculated for four algal species using action spectra of different human skin biological responses driven by UV radiation. *P. umbilicalis* and *S. vulgare* were highlighted, exhibiting the highest values in all evaluated extract concentrations. For elastosis, at concentration 16 (mg cm^{-2} DW), *C. tamariscifolia* and *P. umbilicalis* showed similar values. In the highest algal concentration (16 mg cm^{-2} DW), *P. umbilicalis* and *S. vulgare* species showed %ESAR values greater than 90% for immunosuppression, erythema and vitamin D3 synthesis. In the last response and in the same concentration, *U. lactuca* also showed a value of 90% (Table 3). In the lowest concentration (2

mg cm^{-2} DW), *P. umbilicalis* was highlighted, exhibiting values between 30% and 50% (Table 3).

In general, %ESAR increased with extract concentrations for each species evaluated. For red and brown algal species (ANEXO A, Figure S. 1 A, B and C), %ESAR values increased almost linearly with increasing concentration, especially *C. tamariscifolia* (ANEXO A, Figure S. 1 A). In the case of *U. lactuca*, %ESAR was similar between concentrations 2 and 4 (mg cm^{-2} DW) for persistent pigment darkening (PPD), elastosis, photoaging and lipid peroxidation (ANEXO A, Figure S. 1 D).

Tabela 3 - Effective solar absorption radiation (ESAR, in %) by hydroethanolic algal extracts.

Species	[ ]	Vitamin D3 synthesis	Erythema	Immunosuppression	Lipid peroxidation	Elastosis	Photoaging	Persistent Pigment Darkening
Carpodesmia tamariscifolia	2	7.36±3.19^{b}	5.58±2.47^{c}	3.58±1.77^{c}	1.02±0.53^{c}	0.99±0.53^{c}	0.25±0.23^{c}	0.34±0.29^{c}
Porphyra umbilicalis	2	32.14±15.38^{a}	36.15±14.45^{a}	50.14±14.86^{a}	33.82±9.04^{a}	29.36±8.34^{a}	37.29±9.55^{a}	33.01±8.10^{a}
Sargassum vulgare	2	34.87±3.56^{a}	31.72±3.54^{ab}	31.03±3.60^{b}	17.80±3.21^{b}	17.12±3.28^{b}	16.83±3.30^{b}	15.89±3.25^{b}
Ulva lactuca	2	29.82±9.00^{a}	22.17±6.96^{b}	12.46±4.82^{c}	3.21±1.13^{c}	3.36±1.41^{c}	0.19±0.10^{c}	0.20±0.12^{c}
Carpodesmia tamariscifolia	4	29.51±10.06^{c}	25.70±9.17^{c}	22.99±9.45^{c}	12.52±5.44^{b}	11.65±5.39^{b}	11.91±5.71^{c}	10.81±5.18^{b}
Porphyra umbilicalis	4	65.88±10.18^{a}	66.96±8.94^{a}	79.37±7.53^{a}	52.33±4.98^{a}	46.51±4.77^{a}	57.47±5.65^{a}	50.01±4.66^{a}
Sargassum vulgare	4	70.92±2.81^{a}	67.13±2.91^{a}	66.76±2.99^{b}	49.22±3.20^{a}	48.31±3.20^{a}	48.92±3.32^{b}	47.21±3.27^{a}
Ulva lactuca	4	49.78±6.36^{b}	38.26±5.56^{b}	25.08±5.54^{c}	6.73±1.99^{c}	7.12±1.90^{c}	0.76±0.51^{d}	1.11±0.97^{c}
Carpodesmia tamariscifolia	8	58.32±11.73^{b}	53.39±11.76^{c}	50.64±12.37^{c}	34.96±10.85^{b}	33.99±10.97^{b}	34.84±11.94^{b}	33.03±11.24^{b}
Porphyra umbilicalis	8	83.37±4.18^{a}	82.12±3.59^{a}	90.92±2.49^{a}	60.78±2.15^{a}	54.89±2.31^{a}	67.57±2.88^{a}	58.24±2.33^{a}
Sargassum vulgare	8	79.49±7.00^{a}	76.33±7.38^{ab}	76.42±7.60^{b}	60.73±8.75^{a}	59.94±8.80^{a}	60.96±9.12^{a}	59.17±9.03^{a}
Ulva lactuca	8	81.83±6.65^{a}	69.15±7.61^{b}	59.07±9.23^{c}	27.90±9.42^{b}	28.23±9.31^{b}	16.08±9.20^{c}	19.04±9.43^{c}
Carpodesmia tamariscifolia	16	82.74±5.81^{c}	79.19±6.58^{b}	78.10±7.28^{b}	63.73±8.66^{c}	62.99±8.90^{b}	64.97±9.46^{c}	62.62±9.24^{c}
Porphyra umbilicalis	16	94.82±0.74^{a}	92.62±0.94^{a}	96.94±0.50^{a}	71.58±2.08^{b}	67.61±3.10^{b}	80.63±2.83^{b}	70.85±3.07^{b}
Sargassum vulgare	16	96.96±1.33^{a}	95.85±1.60^{a}	96.50±1.53^{a}	89.00±2.99^{a}	88.69±3.08^{a}	90.25±3.00^{a}	88.80±3.16^{a}
Ulva lactuca	16	90.94±1.32^{b}	80.50±1.73^{b}	73.84±2.30^{c}	43.86±2.78^{d}	43.93±2.76^{c}	32.32±2.91^{d}	35.47±2.94^{d}

Different extract concentrations were tested, and %ESAR was calculated to a solar spectrum on a summer day in Málaga and applying action spectra for diverse UV-driven responses, such as erythematic responses, vitamin D synthesis, immunosuppression, persistent pigment darkening (PPD), elastosis, photoaging, and lipid peroxidation. Table shows the mean values (n=8) ± standard deviations. Concentrations [ ] evaluated were 2, 4, 8, and 16 mg cm^{-2} DW. Different letters indicate significant differences among species in concentrations evaluated, which were detected with a posteriori Newman-Keuls test ($p<0.05$).

The results of EPI versus %ESAR, of the different algal extracts concentrations, showed hyperbolic trend responses with application of different action spectra (Figure 33). The increasing of EPI did not result in a corresponding increment to %ESAR. Both parameters followed a direct relationship with lower values of EPI achieving higher values of %ESAR. As the %ESAR was already high, the increment of EPI was not followed by the same order of magnitude as that of %ESAR. When analyzing vitamin D3 synthesis (Figure 33 A), erythema (Figure 33 B) and immunosuppression (Figure 33 C) responses, extracts of the four species could reach a saturation pattern, conferring values close to %ESAR 100% with *S. vulgare* extracts and EPI values higher than 30. EPI values close to 5 conferred effective absorption of more than 80% of effective solar radiation in the case of these three biological responses. *Sargassum vulgare* presented lower values of EPI_{50}, followed by *P. umbilicalis*, then *U. lactuca*, and, last, *C. tamariscifolia* for D3 synthesis, erythema and immunosuppression (Table 4). In the case of the other four biological responses, a different pattern was observed, although still hyperbolic. The pattern observed were not so acute, it means, the highest concentration of *S. vulgare* allowed EPI values as maximum as 10-15, reaching very high %ESAR, close to 90% (Figures 33 D-G). The figures evidenced a pattern of EPI vs. %ESAR responses, indicating that some species could still be more concentrated to confer higher %ESAR. In the case of lipid peroxidation, elastosis, PPD and photoaging, the best results were found with *S. vulgare* extracts, presenting lower EPI_{50} values (Table 4). *P. umbilicalis* and *U. lactuca* presented a similar EPI_{50} pattern, and *C. tamariscifolia* showed the highest values, indicating that the extract of this last species did not efficiently confer photoprotection against effective radiation to these four responses.

Figura 33 - Extraction photoprotection index (EPI) versus effective solar absorption Radiation (ESAR, in %) of different algal extract concentrations.

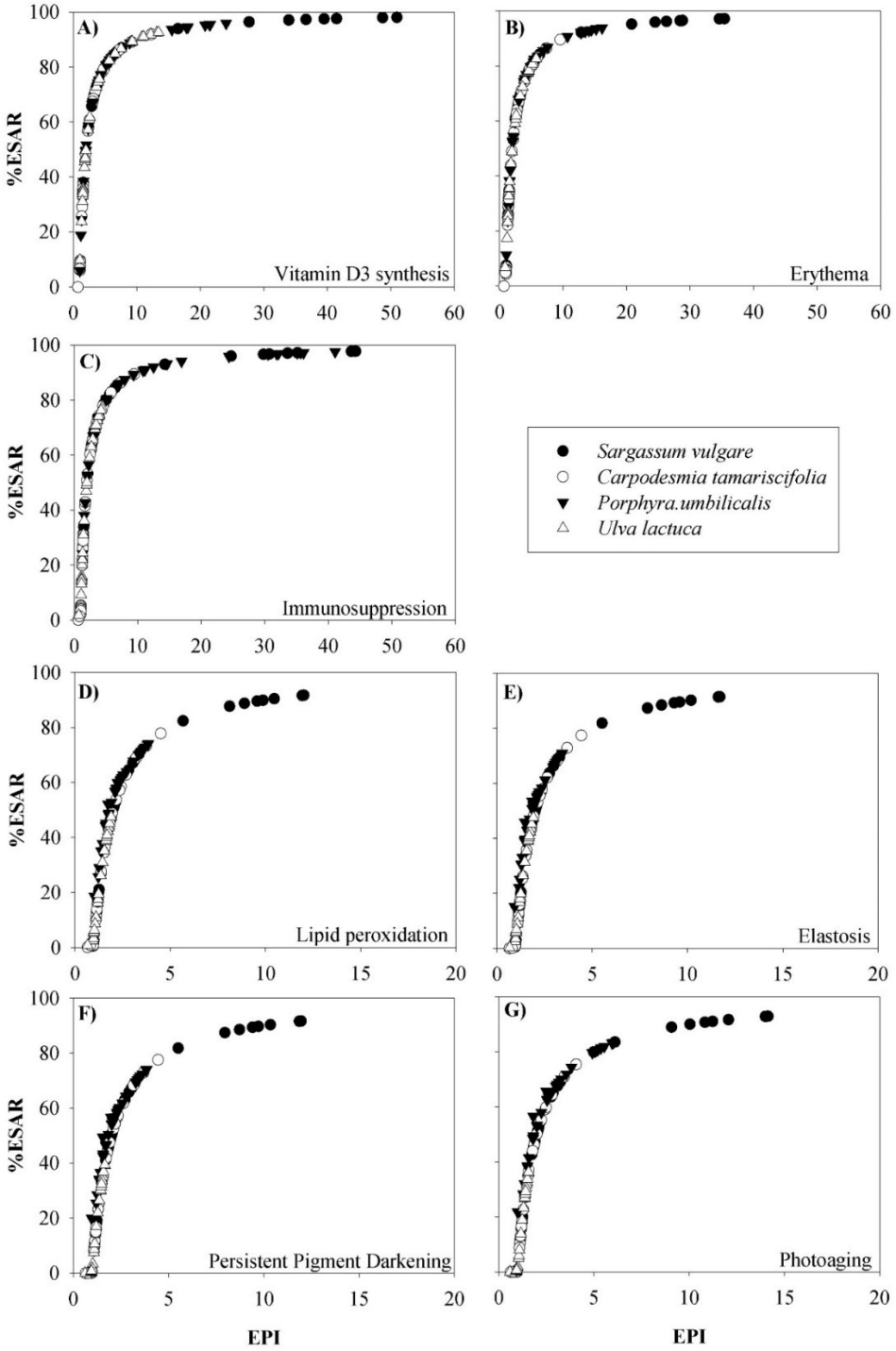

Four species were utilized: *Sargassum vulgare*, *Carpodesmia tamariscifolia*, *Porphyra umbilicalis* and *Ulva lactuca*. Seven action spectra of biological responses were applied. (A) vitamin D3 synthesis, (B) erythema, (C) immunosuppression, (D) lipid peroxidation, (E) elastosis, (F) persistent pigment darkening (PPD), and (G) photoaging. Data were plotted considering eight replicates per each extract concentration of 2, 4, 8, and 16 mg DW.cm^{-2}.

Tabela 4 - Extract photoprotection index (EPI_{50}) calculated for different biological responses between effective solar absorption radiation (%ESAR) versus EPI, applying different algal extract concentrations (2, 4, 8, and 16 mg $DW.cm^{-2}$).

Species / EPI_{50}	Vitamin D3 synthesis	Erythema	Immunosuppression	Lipid peroxidation	Elastosis	Photoaging	PPD
C. tamariscifolia	1.468	1.545	1.768	1.619	1.530	1.557	1.53
P. umbilicalis	0.319	0.433	0.259	1.201	1.198	1.375	1.32
S. vulgare	0.295	0.297	0.315	0.337	0.384	0.324	0.34
U. lactuca	0.667	1.479	1.605	1.347	1.349	1.245	1.26

Four species were utilized: *Sargassum vulgare*, *Carpodesmia tamariscifolia*, *Porphyra umbilicalis* and *Ulva lactuca*. Seven action spectra of biological responses were applied: vitamin D3 synthesis, erythema, immunosuppression, lipid peroxidation, elastosis, photoaging, and persistent pigment darkening (PPD).

4.5 DISCUSSION

In this study, biochemical characteristics, antioxidant activity and photoprotection properties of hydroethanolic and methanolic extracts from algae and one marine lichen were evaluated. MAAs were more abundant in *Lichina pygmaea* and red algae, except *Sphaerococcus* sp. (Figure 28). MAAs are small water-soluble molecules with absorption peaks in the UV region of the spectrum, mainly between 310 and 360 nm (LA BARRE; ROULLIER; BOUSTIE, 2014; PANGESTUTI; SIAHAAN; KIM, 2018). MAAs exhibit antioxidant properties, participate in osmotic balance, and can be isolated in various marine organisms, such as cyanobacteria, red algae and many marine invertebrates (LA BARRE; ROULLIER; BOUSTIE, 2014; SCHMID; SCHÜRCH; ZÜLLI, 2004). MAAs are potential molecules for UV protection, especially against UV-A (ÁLVAREZ-GÓMEZ et al., 2019; COCKELL; KNOWLAND, 1999; DE LA COBA et al., 2009; MERCURIO et al., 2015; PANGESTUTI; SIAHAAN; KIM, 2018; SCHMID; SCHÜRCH; ZÜLLI, 2004, 2006; SINGH et al., 2017; TORRES et al., 2006).

Schmid et al. (SCHMID; SCHÜRCH; ZÜLLI, 2004, 2006) evaluated a sunscreen filter lotion containing *Porphyra umbilicalis* extract. The extract contained MAAs, such as porphyra-334, with absorption peak at 334 nm and potential UV-A protection. Schmid et al. (SCHMID; SCHÜRCH; ZÜLLI, 2004) also evaluated parameters, such as skin lipid peroxidation and skin aging (elasticity, wrinkle depth and roughness), and found excellent results because the filter lotion containing 0.005% MAAs neutralized the effects of UV-A. A formulation (Helioguard^{TM} 365) containing unpurified MAAs was evaluated for prevention of photoaging, as well as

avoidance of DNA damage and loss of cell viability. The formulation showed positive responses, reducing the effects of UV-A on the skin (SCHMID; SCHÜRCH; ZÜLLI, 2006).

In our study, *P. umbilicalis* showed the highest amount of MAAs (> 10 mg g^{-1}DW) and exhibited five MAAs (asterina-330, palythine, palythinol, shinorine and porphyra-334). Among them, porphyra-334 (2.41 mg g^{-1}DW) and asterina-330 (7.39 mg g^{-1}DW) represented 23% and 72% of the total MAAs, respectively. In another study, *P. umbilicalis* extract exhibited three main MAAs, identified as shinorine, palythine and porphyra-334. Porphyra-334 was quantitatively dominant in all samples (KARSTEN; ESCOUBEYROU; CHARLES, 2009). *Porphyra leucosticta* presented MAAs, such as shinorine, asterina-330, palythine and porphyra-334, the latter in greater quantity, regardless of the treatment (KORBEE; FIGUEROA; AGUILERA, 2005). *Porphyra dioica* also presented porphyra-334 as quantitatively predominant MAAs (GUIHÉNEUF; GIETL; STENGEL, 2018; LALEGERIE et al., 2019).

Recently, both isolated and purified MAAs were tested for stability against stressors, such as pH and temperature. All MAAs, such as porphyra-334, mycosporine-serinol, shinorine, asterina-330 and palythine, showed stability over a wide range of pH and temperature (DE LA COBA et al., 2019). These same MAAs were found in some organisms evaluated in our study. Mycosporine-serinol was found only in *L. pygmaea* (0.26 mg g^{-1}DW). This MAA shows an absorption peak at 310 nm and was identified and extracted from *L. pygmaea* at higher concentrations (0.52 mg g^{-1}DW) in another study (LA BARRE; ROULLIER; BOUSTIE, 2014). MAAs from species grown in high UV-exposure areas have already been proposed as UV screen substances in cosmeceutical creams (NAVARRO et al., 2018).

UV absorption spectra results showed prominent peaks for green and red algae (Figure 29). As previously mentioned, the red algae have MAAs that absorb in the UV region. *P. umbilicalis* and *Pyropia elongata* excelled in the UV absorption spectrum with prominent peaks between 320 and 340 nm in accordance with the presence of MAAs absorbing in this range (RASTOGI et al., 2010; SINGH et al., 2008), such as: palythinol (peak absorption at 332 nm), asterina-330 (absorption peak at 330 nm), porphyra-334 (peak absorption at 334 nm) and others. UV spectra and MAAs assay were performed using two different extraction methods, applying two solvents ethanol and methanol, respectively. In some references (ÁLVAREZ-GÓMEZ; KORBEE-PEINADO; FIGUEROA, 2016; TORRES et al., 2015), MAAs were also extracted with ethanol, therefore, it is possible to assume that the peaks observed between 320 and 340 nm may be due to the presence of MAAs in the hydroethanolic extracts.

In the visible spectra (Figure 30), peaks between 400 and 500 nm and 600 and 700 nm were observed in all algal groups and in the marine lichen, coinciding with the absorption peaks of photosynthetic and protective pigments, such as chlorophyll *a*, *b* and *c*, phycobiliproteins and carotenoids (GRAHAM et al., 2016a). The prominent peak of brown algae (close to 450 nm) can be attributed to fucoxanthin, an accessory carotenoid pigment that shows antioxidant activity and exhibits an important role in photoprotection (JASWIR et al., 2013; PANGESTUTI; SIAHAAN; KIM, 2018).

Polyphenol concentration was high for *Lichina pygmaea* and brown algae, mainly *Sargassum vulgare* and *Carpodesmia tamariscifolia* (Figure 31). Polyphenols are a class of secondary metabolites with diverse biological functions. They can be divided into three main groups: phenolic acids, flavonoids and tannins (PANGESTUTI; SIAHAAN; KIM, 2018). Brown algae exhibit a large amount of polyphenols, mainly phlorotannins, only observed in brown seaweeds and formed by the polymerization of phloroglucinol (1,3,5-trihydroxybenzene), representing about 14% of their dry biomass. Red and green algae also contain polyphenols, but not phlorotannins, in a smaller amount than that of brown algae (ABDALA-DÍAZ et al., 2014; CHAROENSIDDHI et al., 2017a; MACHU et al., 2015). The green alga *Dasycladus vermicularis* produces 3,6,7-trihydroxycoumarin (THC), a phenolic compound with peak absorption in the UV region (346 nm), which can function as natural sunscreen according to the authors (PÉREZ-RODRÍGUEZ; AGUILERA; FIGUEROA, 2003). Polyphenols have various functions in algae, including protection against UV radiation. Photoprotection is strongly related to polyphenol structure, as characterized by the ability to scavenge free radicals. This ability is partially related to the structure of the polyphenols, which are characterized by an aromatic ring with hydroxyl groups. The hydroxyl group (-OH) acts as an electron donor for the reactive oxygen species (ROS), causing their neutralization (ABDALA-DÍAZ et al., 2014; MACHU et al., 2015; PANGESTUTI; SIAHAAN; KIM, 2018; WANG et al., 2017).

Polyphenols are mentioned in several studies as compounds containing high antioxidant activity (ABDALA-DÍAZ et al., 2014; CHAROENSIDDHI et al., 2017a; MACHU et al., 2015; PANGESTUTI; SIAHAAN; KIM, 2018; RAJAURIA; FOLEY; ABU-GHANNAM, 2016; SANJEEWA et al., 2016). In the present study, species with high amounts of polyphenols also showed higher antioxidant activity (Figure 32). Extracts from *C. tamariscifolia* and *S. vulgare* were investigated, and we found that antioxidant activity could be associated with polyphenols, especially phlorotannins (ABDALA-DÍAZ et al., 2014;

ANDRADE et al., 2013; CELIS-PLÁ et al., 2016; NURJANAH et al., 2017), as well as other compounds, such as fucoxanthin (AYYAD et al., 2011). These extracts were also studied for their antioxidant potential and UV protection (PANGESTUTI; SIAHAAN; KIM, 2018). The antioxidant activity of *L. pygmaea* was tested in other studies (ÁLVAREZ-GÓMEZ; KORBEE-PEINADO; FIGUEROA, 2016; DE LA COBA et al., 2009) and may be associated not only with polyphenolic compounds, but also with the presence of MAAs.

Species that showed high antioxidant activity and high amounts of phenolics and MAAs were selected to calculate effective solar absorption radiation (%ESAR, Table 3) and extract photoprotection index (EPI, Figure 33, Table 4). *C. tamariscifolia*, *S. vulgare*, *P. umbilicalis* and *Ulva lactuca* were the chosen species. The %ESAR was proposed in this study as an indicator of extract photoprotection properties, considering the retained radiation (avoidance of the occurrence of biological response), while EPI was calculated considering the transmitted radiation, which would cause biological responses in the skin. %ESAR shows the action of extracts from algae on UV wavelengths that induce different biological responses. Thus, higher %ESAR values indicate greater potential of the extracts to absorb certain wavelengths, preventing and / or reducing the induction of the biological response associated with the absorbed wavelength. *P. umbilicalis* and *S. vulgare* were highlighted in the %ESAR evaluation, showing the highest values in all extract concentrations and in all biological responses evaluated.

Induction of vitamin D3 synthesis occurs mainly between wavelengths 290 and 300 nm (WEBB; DECOSTA; HOLICK, 1989), indicating a beneficial effect associated with UV radiation. However, the wavelengths responsible for vitamin D3 induction also cause erythema (MCKINLEY; DIFFEY, 1987; WEBB; DECOSTA; HOLICK, 1989). In this study, high %ESAR values for vitamin D3 synthesis were presented by *P. umbilicalis* (94%), *S. vulgare* (96%) and *U. lactuca* (90%) in greater concentration (16 mg cm^{-2} DW). Very similar values of %ESAR were presented for erythema in the same concentration, except for *U. lactuca,* which exhibited a higher %ESAR for vitamin D3 synthesis than that for erythema induction (80%) (Table 3). Thus, in some cases, the extract has the potential to reduce erythema induction, but at the same time, it can also reduce vitamin D3 production.

P. umbilicalis showed a peak of absorption between 315 and 350 nm (Figure 29 C). In this range are found the wavelengths that induce photoaging, around 337 to 346 nm (BISSETT; HANNON; ORR, 1989). Thus, *P. umbilicalis* showed a high %ESAR value for photoaging (37%), even at the lowest concentration (2 mg cm-² DW). However, at the highest tested

concentration (16 mg cm^{-2} DW), *S. vulgare* showed the highest value (90%), while *P. umbilicalis* 80% (Table 3). %ESAR for immunosuppression was also high for *P. umbilicalis* and *S. vulgare* in both the lowest (2 mg cm^{-2} DW) and the highest concentration (16 mg cm^{-2} DW), about 50% and 31%, and about 96%, respectively (Table 3). The stimulus for immunosuppression occurs mainly between 280 and 310 nm (FABO; KRIPKE, 1980).

A clear pattern of hyperbolic responses between %ESAR and EPI was observed for *S. vulgare* and *P. umbilicalis*. Other algal extracts with the highest concentration did not show the highest possible %ESAR, indicating that the species *U. lactuca* and *C. tamariscifolia* could still be used, but applying higher concentrations, which could follow the trend of *S. vulgare*, reaching high %ESAR to the different action spectra evaluated in this study. In the case of *U. lactuca*, the biomass availability could be provided, as the species of *Ulva* can be successfully cultured in tanks under high nutrient levels as in integrated multitrophic aquaculture systems (IMTA) (NEORI et al., 2003). Thus, high levels of biomass to get cosmeceuticals products or animal feed can be produced at a lower cost than other non-cultivable species (BIKKER et al., 2016; VALENTE et al., 2016). In addition, *U. lactuca* can reduce the effluents spilled to sea and consequently the eutrophication risks (FIGUEROA et al., 2009; NEORI, 2007).

EPI is analogous to SPF (Solar Protection Factor) and BEPFs (biological effective protection factors), as proposed by De la Coba et al. (DE LA COBA et al., 2019). Unlike EPI, the BEPFs are calculated based on a cream containing isolated and purified MAAs. The results of BEPFs were good for almost all biological responses evaluated, including erythema and immunosuppression, especially when the MAAs were combined. In this study, *P. umbilicalis*, which has MAAs in its extract, also showed good EPI results for erythema, vitamin D3 synthesis and, mainly, for immunosuppression (Table 4).

In conclusion, *S. vulgare*, *C. tamariscifolia*, *P. umbilicalis* and *L. pygmaea* were distinguished by the significantly higher content of polyphenols and antioxidant activity. Considering %ESAR, *S. vulgare* and *P. umbilicalis* showed excellent results. *S. vulgare* also presented the best results for EPI. Its extract has practically no MAAs, so its photoprotection potential may be associated with the high amount of polyphenols, mainly phlorotannins, and carotenoids, such as fucoxanthin. Fucoxanthin was not extracted in this study, but its presence in extracts can be evidenced by the peaks in the visible region of the spectrum. The highlight of *S. vulgare* and *P. umbilicalis* in %ESAR showed that the extract of these species has potential for photoprotection for different biological responses driven by UV. %ESAR and EPI are interesting indicators, since they allow to evaluate the photoprotection properties of organisms

for different biological responses. These parameters provide a preliminary analysis, since the crude extracts from algae and marine lichen were used in the analyzes, without a creamy formulation as is usually done in other studies. The data presented in this study may provide important inputs for future studies, especially research aimed at improving the performance of sunscreens and other cosmetics.

5 CAPÍTULO II

Physiological and biochemical responses driven by different UV-visible radiation in *Osmundea pinnatifida* (Hudson) Stackhouse (Rhodophyta)

Geniane Schneider[*a], Félix L. Figueroa[b], Julia Vega[b], Antonio Avilés [b], Patricia Chaves [b], Paulo Antunes Horta [c], Nathalie Korbee[b], and José Bonomi-Barufi [c]

[a] Phycology Laboratory, Postgraduate Program of Biotechnology and Biosciences, Department of Microbiology, Immunology and Parasitology, Federal University of Santa Catarina, 88040-900, Florianopolis, SC, Brazil.

[b] Universidad de Málaga. Instituto Universitario de Biotecnología y Desarrollo Azul (IBYDA). Departamento de Ecología, Universidad de Málaga, Campus Universitario de Teatinos s/n, 29071, Málaga, España.

[c] Phycology Laboratory, Botany Department, Federal University of Santa Catarina, 88049-900, Florianopolis, SC, Brazil.

***Corresponding Author Address**
Geniane Schneider
E-mail: geniane.tega@gmail.com

Publicado em: *Photochem. Photobiol. Sci*., 2020, 19, 1650–1664
DOI: 10.1039/d0pp00135j

5.1 ABSTRACT

Light, or visible radiation, serves as a source of energy for photosynthesis of plants and most algae. In addition, light and ultraviolet radiation (UV-A and UV-B) act as a biological signal, triggering several cellular processes that are mediated by photoreceptors. The aim of this study was to evaluate the physiological and biochemical responses of *Osmundea pinnatifida* driven by different radiations through putative photoreceptors. For this, *O. pinnatifida* was grown under different radiation treatments composed by high intensity of light emitted by a low pressure sodium lamp (SOX), aiming to saturate photosynthesis, which was supplemented by low intensities of visible (red, green and blue) and ultraviolet radiation (UV-A and UV-B), in order to activate photoreceptors. Growth rates, photosynthesis, antioxidant activity, polyphenols, soluble proteins, phycobiliproteins, mycosporine-like amino acids (MAAs) and carotenoids were evaluated during the experiment. Complementary UV-A radiation positively influenced growth rates after 15 days of experiment, although the presence of a peak of blue light in this treatment can also have contributed. UV-B radiation increased the concentration of zeaxanthin and chlorophyll *a*. The blue light caused the accumulation of chlorophyll *a*, violaxanthin, phycoerythrin and polyphenols on different days of the experiment. Phycoerythrin also increased under green and red light conditions. Our results showed that some compounds can be modulated by different radiation, and the involvement of photoreceptors is suggested. In red algae, photoreceptors sensitive to red, green and blue light have been identified, however little is known about UV photoreceptors. The presence of photoreceptors sensitive to UV radiation in *O. pinnatifida* is discussed.

5.2 INTRODUCTION

Solar radiation is mainly composed of infrared, visible and ultraviolet radiation (UV-A, UV-B and UV-C). The visible portion of the electromagnetic spectrum, which is also known as light, includes the wavelengths that activate photosynthesis, i.e., the photosynthetically active radiation (PAR, 400-700 nm) (BJÖRN, 2008; KIRK, 2010). PAR is used as an energy source for photosynthesis in plants and most algae. In addition, visible and UV radiation, which reaches the Earth's surface (UV-A and UV-B), are used as a biological signal, triggering several cellular processes that are mediated by photoreceptors.

Photoreceptors are light sensitive protein-chromophores that are linked to different signalling pathways to continuously monitor light, acclimating the physiological activities of organisms to environmental changes (KIANIANMOMENI; HALLMANN, 2014). There are different families of photoreceptors, as phytochromes, cryptochromes, phototropins, UVR8, and others (FERNÁNDEZ et al., 2016; JIAO; LAU; DENG, 2007). In plants, photoreceptors are responsible for multiple processes, such as seed germination, seedling photomorphogenesis, phototropism, gravitropism, chloroplast movement, shade avoidance, circadian rhythms and flower induction (JIAO; LAU; DENG, 2007). In algae, the photoreceptors and the physiological processes driven by them are still poorly understood, although in recent decades, studies have sought to identify and understand the role of light sensors in these organisms (FERNÁNDEZ et al., 2016; HEGEMANN, 2008; KIANIANMOMENI; HALLMANN, 2014).

Phytochrome-like photoreceptors were found in several algae, including Rhodophyta, using monoclonal antibodies (FIGUEROA et al., 1990). In *Chondrus crispus*, a cryptochrome photoreceptor was sequenced (COLLÉN et al., 2013). *Cyanidioschyzon merolae* has three types of cryptochromes (KIANIANMOMENI; HALLMANN, 2014). Different phytochromes not limited to red/far-red responses were detected in brown and green algae (ROCKWELL et al., 2014). Photoreceptor UVR8 sensitive to UV-B radiation was identified in green algae (FERNÁNDEZ et al., 2016). Furthermore, other light-sensitive proteins, such as BLUF-proteins, photolyases and cryptochromes, have been detected in algae (HEGEMANN, 2008; OLIVERI et al., 2014a).

Photoreceptors can perceive the quantity (fluence), quality (wavelength), direction and duration of different radiations (visible, UV) in the environment (JIAO; LAU; DENG, 2007), driving various physiological processes in algae. Through photoreceptors, monochromatic radiation (purple, blue, green, yellow, orange, red) can provide signals to regulate growth, metabolism, and reproduction (DRING, 1988). *Pyropia haitanensis* growth rates were higher under blue and green radiation (WU, 2016). *Porphyra umbilicalis* showed higher growth rates under red light (FIGUEROA; AGUILERA; NIELL, 1995). This monochromatic radiation also induced reproduction in *Gracilaria birdiae* (BARUFI et al., 2015). Phytochrome and cryptochrome have been proposed to control chlorophyll and biliproteins synthesis in algae (FIGUEROA; NIELL, 1990; LÓPEZ-FIGUEROA, 1991). Induction of soluble proteins and photosynthetic pigments, such as chlorophyll, phycocyanin and phycoerythrin, occurred when the algae were grown under blue light (BARUFI et al., 2015; FIGUEROA; AGUILERA; NIELL, 1995; KORBEE; FIGUEROA; AGUILERA, 2005). Blue light also favored the

accumulation of mycosporine-like amino acids (MAAs), such as porphyra-334, palythine and asterina-330 in *Porphyra leucosticta* (KORBEE; FIGUEROA; AGUILERA, 2005).

Photoreceptors can also mediate photoprotective responses, for example, the orange carotenoid protein (OCP), sensitive to blue-green light, which triggers a photoprotective mechanism in cyanobacteria (KIRILOVSKY; KERFELD, 2013). In green algae, energy dissipation appears to be controlled by a photoreceptor sensitive to blue light and UV-B radiation (ALLORENT; PETROUTSOS, 2017). Blue light sensitive PHOT protein (phototropin) controls energy dissipation processes in the green alga *Chlamydomonas reinhardtii* (PETROUTSOS et al., 2016).

Considering the studies presented, we hypothesize that pigments and other compounds can be regulated by different wavelengths in *Osmundea pinnatifida* through photoreceptors and other light-sensitive molecules. Understanding how ambient light modulates responses in these organisms is important not only as a basic science, but also because the algae have shown an interesting biotechnological potential recently, since they produce a wide variety of bioactive compounds (PANGESTUTI; SIAHAAN; KIM, 2018; SINGH et al., 2017; WANG et al., 2017).

Aiming to study the radiation effects on physiological and biochemical responses through possible photoreceptors in *O. pinnatifida*, we use a high fluence PAR source provided by low pressure sodium lamp (SOX), which was complemented with low intensity of monochromatic radiations (red, blue, green, UV-A and UV-B). The light from SOX lamp was used to ensure photosynthesis saturation. This lamp has an emission spectrum with a narrow yellow peak (590 nm), so, there is no interference with the other monochromatic radiations used. To avoid the interference of complementary radiations in photosynthesis, a low fluence rate was applied, since photoreception occurs in many light intensities, varying below and above the photosynthetic threshold (PETROUTSOS et al., 2016). Intensities from 1 to 20 µmol photons m^{-2} s^{-1} are sufficient to induce photoreceptor-mediated responses (PETROUTSOS et al., 2016; SEGOVIA; GORDILLO; FIGUEROA, 2003). The experimental strategy used in this study has also been used in other studies, in order to verify the performance of photoreceptors (BRITZ; SAGER, 1990; PAGELS et al., 2020; SEGOVIA; GORDILLO; FIGUEROA, 2003; THOMAS; DICKINSON, 1979).

The alga object of this study was *O. pinnatifida*, a red macroalga of the family Rhodomelaceae (GUIRY; GUIRY, 2019), which grows during the year on rocks in the intertidal zones of the coast of Portugal, Spain and, mainly, in the Macaronesia region, including

Azores, Madeira, Selvagens, and Canary Islands. This alga is abundant and has traditionally been consumed in several European countries as a spice and for other purposes, as it has a peppery taste (MACHÍN-SÁNCHEZ et al., 2016; MACHÍN-SÁNCHEZ; GIL-RODRÍGUEZ, 2018; SILVA et al., 2019).

5.3 MATERIAL AND METHODS

5.3.1 Algal material and experimental design

Osmundea. pinnatifida samples for the experiment were collected in La Araña, Malaga, UTM 381471.00 m E/4063686.00 m N, in an intertidal zone. The specimens were placed in bags containing sea water and transported to the laboratory at Faculty of Sciences in Malaga University. In the laboratory, the algae were cleaned, and the epiphytes removed. Eighteen methacrylate flasks containing 1200 mL of filtered sea water were prepared, and 10 g of algal thalli were added to each one. The flasks were maintained during the acclimation in a culture chamber at 25 °C, with constant and vigorous aeration, and photoperiod of 12 h light: 12h darkness. During light period, low pressure sodium lamp - SOX (PHILIPS 135W BY22d T65) was used. This lamp presents amber coloration (yellow/orange mix) and spectrum with a narrow peak at 590 nm. In addition, the heat production in this lamp is low and the energy conversion efficiency to light is very high (DARKO et al., 2014).

The *O. pinnatifida* thalli remained in acclimation period for 7 days, when the water of the flasks was renewed every two days. After acclimation, the experiment was conducted for 15 days. In this case, 10 g biomass was sorted into new flasks containing renewed water, constant aeration and under the following radiation treatments: SOX-only light (SOX), SOX plus red light (SOX+R), SOX plus green light (SOX+G), SOX plus blue light (SOX+B), SOX plus UV-A radiation (SOX+UVA), and SOX plus UV-A and UV-B radiation (SOX+UVA+UVB). Three flask replicates (n = 3) per treatment were used. The coloured lights (red, green, and blue) were provided by RGB light emitting diode (LED), and ultraviolet radiation (UV-A and UV-B) by fluorescent lamps (Q-Panel UVA 340 LAMP H5B8, Canada). The SOX+UVA treatment was obtained covering the acrylic flasks with UV-B filter foil (Lee-130). Spectra for the different radiation sources used are shown in Figure 34. Both SOX+UVA and SOX+UVA+UVB treatments showed a peak in the blue region of the spectrum (436 nm, Figure 34). The photoperiod during the experiment was of 12 h, and during the daytime the

SOX lamps were switched on for 11 h 30 min while the coloured LEDs and UV lamps were switched on for the entire 12 h period, meaning that the last 30 min of photoperiod was composed by monochromatic light radiation. The radiation spectrum in $W.m^{-2}$ was measured with the Multidiode Spectroradiometer (Spectrometer Ocean Optics, USA, serial number: U5B2G13398). Photosynthetic active radiation (PAR, λ=400 -700 nm) in µmol photons m^{-2} s^{-1} was measured by using a spherical PAR light sensor US-SQS (Walz GmbH, Germany) connected to LI-COR radiometer (LI-1000-Data Logger, LDL209 serial number, Licor Ltd, USA). Table 5 shows radiation data and daily doses provided during the experiment in different treatments.

Figura 34 - Relative spectral radiation emitted by low pressure sodium lamp (SOX), ultraviolet (UV) lamp and coloured light emitting diodes (LEDs) (blue, green and red).

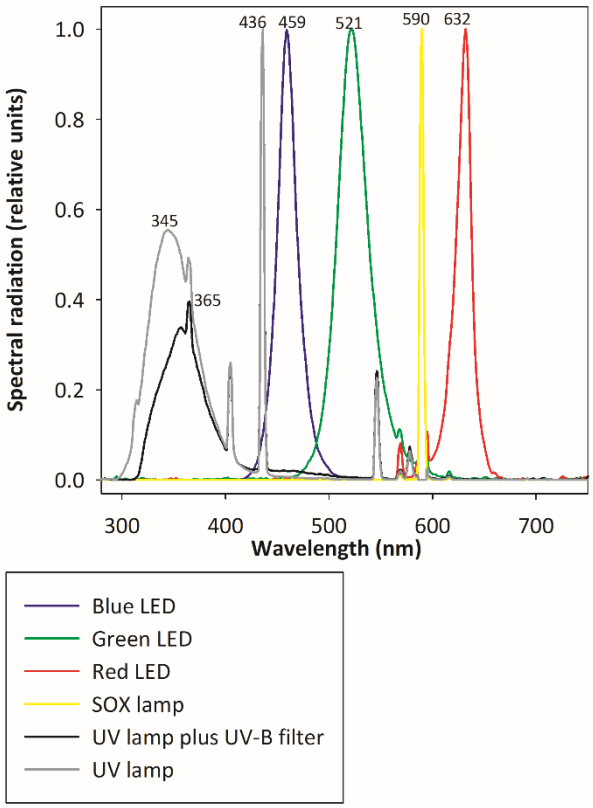

The radiation was measured by a Spectroradiometer (Spectrometer Ocean Optics, SMS 500, USA).

Tabela 5 - Radiation data and daily doses provided for *O. pinnatifida* during the experiment in different treatments.

Radiation UV-visible was emitted by low pressure sodium lamp (SOX) lamp, light emitting diode (LEDs) and ultraviolet (UV) fluorescent lamp (UV-A and UV-B). The light

Treatment	Radiation				Daily doses of radiation				Photosynthetic effective radiation (PER)		PER/total radiation ratio	
	SOX	LED	UV-A	UV-B	SOX	LED	UV-A	UV-B	SOX	LED	SOX	LED
	µmol photons m^{-2} s^{-1}		W.m^{-2}		mol.m^{-2}		KJ.m^{-2}		W.m^{-2}		Relative units	
SOX+R	455.22	18.22	-	-	18.85	0.79	-	-	9.66	0.43	0.59	0.53
SOX+G	466.22	20.55	-	-	19.30	0.89	-	-	10.70	0.80	0.59	0.65
SOX+B	497.22	21.33	-	-	20.59	0.92	-	-	13.71	0.43	0.59	0.32
SOX	442.56	-	-	-	18.32	-	-	-	14.57	-	0.59	-
SOX+UVA	428.22	-	6.44	0.16	17.73	-	278.19	6.75	13.75	-	0.59	-
SOX+UVA+UVB	418.33	-	8.07	0.73	17.32	-	348.59	31.60	12.07	-	0.59	-

photoperiod was of 12 h; SOX lamps were switched on for 11 h 30 min; LEDs and UV lamps were switched on for 12 h. Photosynthetic effective radiation (PER) was calculated according to the photosynthetic action spectra reported for *Pyropia perforata* (HAXO; BLINKS, 1950). Data are expressed as mean values (n=3). SOX+R (SOX lamp plus red LED); SOX+G (SOX lamp plus green LED); SOX+B (SOX lamp plus blue LED); SOX light (only lamp SOX); SOX+UVA (SOX lamp plus UV lamp plus filter of UV-B); SOX+UVA+UVB (SOX lamp plus UV lamp).

During the experiment, the water was renewed every two days with addition of nutrients (0.66 mM of $NaNO_3$; 50 µM of $C_3H_7Na_2O_6P$; 14.6 µM of Na_2HPO_4). The following parameters were monitored: temperature (HOBO sensor); salinity, conductivity meter (CRISON CM35$^+$, Shilu Instruments COLTD); and pH meter (CRISON pH25$^+$, Hach Longe Spain S.L.U). Nutritional composition of the water (nitrate and phosphate) was evaluated every two days. Nutrients were analysed by segmented flow analyser (SFA) using a Seal Analytical autoanalyzer QuAAtro following the methods described by Grashoff et al. (GRASSHOFF; EHRHARDT; KREMLING, 1983). The detection limits of the inorganic nutrients were 0.05 µM for nitrates, and phosphates.

In vivo chlorophyll *a* fluorescence was measured on different experimental days (1st, 5th, 8th, 12th and 15th). At the beginning (initial), after seven days of acclimation under SOX light, middle (8th day) and at the end (15th day) of the experiment, algae samples were collected and frozen (-80 ℃) for biochemical analyses, such as phycobiliproteins, soluble proteins, phenolic compounds, mycosporine-like amino acids (whole thallus) and antioxidant activity (ABTS).

For carotenoid, chlorophyll, carbon, nitrogen, and MAAs of the apices, the samples were collected and frozen or dried in silica only on the 15th day. Aiming to express the results in dry weight (DW), the percentage of water in the algal tissues was previously verified. All analyses were performed in triplicates (n=3).

5.3.2 Algal growth rates

Growth rate was determined using the fresh weight of the algae obtained at three moments of the experiment (initial, 8th and 15th days). The algal biomass was obtained on a precision analytical balance. The excess of water was removed with a paper towel before weighing. Growth rate calculations were performed to the periods from initial to 8th day and from 8th to 15th day, following the formula (LIGNELL; PEDERSÉN, 1989):

$$GR\% = \left[\left(\frac{FW_{final}}{FW_{initial}}\right)^{\frac{1}{t}} - 1\right] \times 100$$

where, GR% is percentage growth rate, FW_{final} is the final fresh weight (mg), $FW_{initial}$ is the initial fresh weight (mg) and t is time (days). Values were expressed as percent of fresh weight per day (% FW day^{-1}).

5.3.3 Photosynthesis activity measured from chlorophyll *a* fluorescence

Fluorescence parameters of chlorophyll *a* fluorescence were determined *in situ* in alga growing in the chambers by using a Diving-PAM (Walz, Effeltrich, Germany). The maximum quantum yield of photosystem II - PSII (Fv/Fm) and the effective quantum yield of PSII (Φ_{PSII}) were calculated in the thalli under cultivation after the application of saturation pulses in the median portion of the algae, during the night and in the daily period, respectively (MAXWELL; JOHNSON, 2000).

The Φ_{PSII} values were used to calculate the electron transport rate (ETR, µmol electrons m^{-2} s^{-1}) by the following formula:

$$ETR = \Phi_{PSII} \times E \times A \times 0.15$$

where E is the irradiance to which the alga has been acclimated and A is the absorptance. The factor 0.15 is used to adjust the irradiance captured and used by Photosystem II (PSII) (FIGUEROA; CONDE-ÁLVAREZ; GÓMEZ, 2003; GRZYMSKI; JOHNSEN; SAKSHAUG, 1997). Absorptance (A) was calculated by the formula:

$$A = 1 - \left(\frac{E_F}{E_0}\right)$$

where E_F is the irradiance transmitted through of the algae thalli and E_0 is the total irradiance, measured with the LI-COR radiometer.

In addition, rapid light curves were conducted in the middle (8^{th} day) and at the end (15^{th} day) of the experimental periods. The maximum electron transport rate (ETR_{max}, µmol electrons m^{-2} s^{-1}) and photosynthetic efficiency (α_{ETR}) were calculated by fitting of the curves with the formula of Platt et al. (PLATT; GALLEGOS; HARRISON, 1980). Saturation irradiance ($E_{k\ ETR}$, µmol photons m^{-2} s^{-1}) was also calculated by the formula:

$$E_{k\ ETR} = \frac{ETR_{max}}{\alpha_{ETR}}$$

5.3.4 Carotenoid and chlorophyll pigments

Extraction and quantification of carotenoids and chlorophyll *a* occurred by high performance liquid chromatography (HPLC), (LUBIÁN; MONTERO, 1998). For extraction, 1 mL of dimethylformamide (DMF) and 0.1 g of fresh biomass were used. The extracts were remaining in darkness overnight at 4℃ for 24 h. Next, the extracts were filtered (0.2 µm filters) and 80 µL of the solutions were injected into the HPLC. The C18 5-µm chromatographic column (Symmetry® C18 of 5-µm 4.16 x 150 mm column T91671L 02) was used in the HPLC to separate the pigments. Two mobile phase gradients were used: (A) distilled water, ionic pair and methanol (1: 1: 1 ratio) and (B) acetone and methanol (1: 1 ratio). The ionic pair was prepared with tetrabutylammonium (0.05 M) and ammonium acetate (1 M). The flow of the mobile phase was 1 $mL.min^{-1}$ for 40 min. The gradient specifications were as follows: (1) 75% A + 25% B (initial); (2) (0-8 min) 25% A + 75% B (linear); (3) (8-10 min) isocratic flow; (4) (10-18 min) convex at 10% A + 90% B; (5) (18-23 min) concave at 100% B; (6) (23-40 min) concave at 75% A + 25% B. The pigment peaks were determined with a Waters Photodiode Array Detector. The identification of the carotenoid and chlorophyll pigments was performed by comparing the absorption time and spectra with commercial standards for chlorophyll *a*, violaxanthin, antheraxanthin, zeaxanthin, lutein and β-carotene (DHI Water and Environment, Denmark). The quantification was performed according to Barufi et al. (BARUFI et al., 2011a). The results were expressed as µg per g of dry weight (µg g^{-1} DW).

5.3.5 Phycobiliproteins

Extraction of phycobiliproteins was performed with 1.2 mL of sodium phosphate buffer (0.1 M, pH 6.5) and 0.05 g of fresh biomass. Algal tissues were ground with liquid nitrogen. After addition of the buffer, the extracts were vortexed and in darkness and at 4℃ for 2 h. After, the samples were centrifuged at 4000 rpm for 10 min. The supernatants were collected and read by UV-visible Spectrophotometer (Shimadzu UV Mini-1240) at 455 nm, 564 nm, 592 nm, 618 nm, 645 nm and 750 nm. Quantification of phycobiliproteins, such as phycoerythrin (PE) and phycocyanin (PC), was performed following the calculations of Beer

and Eshel (BEER; ESCHEL, 1985). The results were expressed as mg of PE or PC per g of dry weight (mg g^{-1} DW).

5.3.6 Soluble proteins

Extract for soluble protein determination was prepared as described in the previous assay (phycobiliproteins). The protein detection reaction was performed with 100 µL of extract, 700 µL of sodium phosphate buffer (0.1 M, pH 6.5) and 200 µL of the Biorad reagent (BRADFORD, 1976). The solutions were stirred and rested for 15 minutes in darkness. Afterwards, the samples were read by UV-visible Spectrophotometer (Shimadzu UV Mini-1240) at 595 nm. Protein quantification was performed by a standard curve with bovine seric albumin (BSA). The results were expressed as mg of bovine albumin per g of dry weight (mg g^{-1} DW).

5.3.7 Quantification of phenolic compounds

Extraction of the phenolic compounds was performed with 0.2 g of fresh biomass. The algal tissue was ground with liquid nitrogen. After, 2.5 mL of 80% methanol was used to solubilize the algal powder. The extracts were vortexed and remained overnight in the dark at 4 ° C. Next day, the extracts were centrifuged at 4000 rpm for 15 min and the supernatants were collected. The reaction for detection of phenolics was performed according to Folin-Ciocalteu method (FOLIN; CIOCALTEU, 1927). 250 µL of supernatant, 1250 µL of distilled water and 125 µL of Folin-Ciocalteu reagent were added in a falcon tube. The solutions were stirred and rested for 5 minutes in darkness. After 375 µL of 20% anhydrous sodium carbonate (Na_2CO_3) and 500 µL of distilled water were added. The samples were stirred and read by UV-visible Spectrophotometer (Shimadzu UV Mini-1240) at 760 nm. Phenolic quantification was performed by preparation of a standard curve with phloroglucinol (Sigma P-3502). The results were expressed as mg of phloroglucinol per g of dry weight (mg g^{-1} DW).

5.3.8 Mycosporine-like amino acids (MAAs)

Mycosporine-like amino acids (MAAs) were determined according to Karsten et al. (KARSTEN et al., 1998) and Korbee-Peinado et al. (KORBEE-PEINADO et al., 2004). The

MAAs were extracted from whole thalli of *O. pinnatifida* on the 8th and 15th day, and of the apical portion only on the 15th day. Extraction was performed using samples dried in silica gel (20 mg DW) and 1 mL of 20% aqueous methanol (v/v) for 2 h at 45℃, followed by centrifugation (4000 rpm at 4℃ for 10 min). The supernatant (700 µL) was evaporated in a vacuum centrifuge and after drying, the extract was resuspended in 700 µL of 100% chromatographic methanol. Then, the samples were filtered using a syringe coupled to a filter (0.22 µm) and transferred to the vials. MAAs were detected by HPLC method (high performance liquid chromatography), using an isocratic flow gradient (1mL.min^{-1}) of mobile phase containing 1.5 % aqueous methanol (v/v) and 0.15% acetic acid (v/v). 20 µL of the filtrate was injected into a Sphereclone C8 column (5 µm particle size and 250 x 4.6 mm diameter) and a precolumn (Phenomenex, Aschaffenburg, Germany) coupled to Waters (Barcelona, Spain) HPLC system. MAAs were detected with a Waters Photodiode Array Detector (996; Barcelona, Spain). The range of the absorption spectrum was 280 to 400 nm. Quantification was performed using published extinction coefficients (DUNLAP; CHALKER; OLIVER, 1986; GLEASON, 1993; TAKANO; DAISUKE; YOSHIMASA, 1978; TAKANO; UEMURA; HIRATA, 1978; TSUJINO; YABE; SEKIKAWA, 1980), extracting chromatographic peak areas of the wavelength with maximum absorption of each MAA. The MAAs were identified using the same secondary standards used by De La Coba et al. (DE LA COBA et al., 2019). The results were expressed as mg of MAAs per g of dry weight (mg g^{-1} DW).

5.3.9 Antioxidant activity (ABTS)

ABTS, 2,2'-azino-bis (3-ethylbenzothiazoline-6-sulphonic acid), method was performed according to Re and collaborators (RE et al., 1999), with slight modifications. Extraction occurred with 0.05 g of fresh biomass, which was ground with liquid nitrogen, followed by the addition of 1.2 mL of sodium phosphate buffer (0.1 M, pH 6.5). The extracts were vortexed and remained overnight in darkness at 4 °C. Next day, the extracts were centrifuged at 4000 rpm for 15 min and the supernatants were collected. The reaction was performed in plastic cuvettes (2mL), in this order: 890 µL phosphate buffer, 10 µL ABTS and 100 µL supernatant. Immediately after addition of the supernatant, the samples were stirred and read (0 min), and the procedure was repeated after 8 min (8 min). Readings were performed by UV-visible Spectrophotometer (Shimadzu UV Mini-1240) at 727 nm. Calculations of the antioxidant activity followed the formula:

$$AA\% = [(A_{0\,min} - A_{8min}) \div A_{0\,min}] \times 100$$

where AA% is the antioxidant activity expressed as percentage, A_{0min} is the initial absorbance, A_{8min} is the absorbance after 8 min.

Quantification was performed by the standard TROLOX (6-hydroxy-2,5,7,8-tetramethylchroman-2-carboxylic acid) curve. The results were expressed as μM of Trolox Equivalents (TE) per g of dry weight (μM $_{TE}$. g^{-1} DW).

5.3.10 Carbon and nitrogen

Elemental analyser (CNHS LECO-932, Michigan, USA) was used for elemental carbon and nitrogen analysis. The complete and instantaneous oxidation of the sample in a combustion with pure oxygen was performed, at temperatures up to 1100 ºC, in a controlled atmosphere. Quantification was performed by infrared (IR) spectroscopy. EDTA was used as the standard. The results were expressed as mg of carbon or nitrogen per g of dry weight (mg g^{-1} DW).

5.3.11 Statistical analysis

Initially, the tests of normality (Kolmogorov-Smirnov) and homogeneity of variances (Cochran) were performed. Afterwards, the analyses of variance (one-way ANOVA and factorial ANOVA) were conducted. Factorial ANOVA (radiation treatment and time 8th and 15th day) was applied to growth rate, chlorophyll *a* fluorescence parameters (Fv/Fm, ETR, α_{ETR}, ETR_{max} and $E_{K\ ETR}$), phycobiliproteins, phenolic compounds, soluble proteins, mycosporine-like amino acids (MAAs) extracted from the whole thalli and antioxidant activity (ABTS). One-way ANOVA (radiation treatment) was performed for elemental carbon and nitrogen, carotenoid pigments and chlorophyll, and for MAAs extracted from the apices. The Student-Newman-Keuls (SNK) post-hoc test was applied to identify significant differences among the treatments, with significance level $p < 0.05$.

5.4 RESULTS AND DISCUSSION

Osmundea pinnatifida was acclimated for seven days under high intensity irradiance emitted by the SOX lamp. Afterwards, the alga was grown for fifteen days under different radiation treatments (experiment). The average temperature of the culture medium during the experiment was 23.8 ℃ ± 1.7. The maximum temperature value was observed during the daytime (30.5 ℃) and the minimum during the night-time (21.1 ℃). The mean pH and salinity (n = 84) were 8.17 ± 0.2 and 40.8 ± 1.4, respectively. The nutrients were consumed by the algal thalli during the experiment, especially nitrate and phosphate (data not shown).

The results of analysis of variance (ANOVA), factorial and one-way, are in the supplementary information (ANEXO B, Tables S. 3 and S. 4). Growth rates of *O. pinnatifida* were higher under SOX+R, SOX+UVA and SOX+UVA+UVB treatments compared to SOX-only after 8 days. From 8^{th} to 15^{th} day, the growth decreased in all the treatments, except in SOX+UVA (Figure 35). The SOX+UVA and SOX+UVA+UVB treatments had a peak in the blue region of the spectrum (436 nm), see Figure 34, this peak could influence the growth responses in these treatments. The algal growth under the treatment with complementary blue light (SOX+B) decreased in the second period of the experiment (8^{th} to 15^{th} day), as well as in SOX+UVA+UVB. In SOX+UVA, algae maintained their growth rates, so it is possible to evaluate the results from three hypotheses, (i) the blue peak in SOX+UVA may have positively interfered, which did not happen in the other treatments with blue light (SOX+B which contained a different blue light type, and SOX+UVA+UVB), (ii) UV-A radiation positively influenced growth, (iii) both UV-A and the blue peak (436 nm) act synergistically, maintaining growth rates.

Figura 35 - *O. pinnatifida* growth rates expressed as percentage of fresh weight per day (% FW day^{-1}).

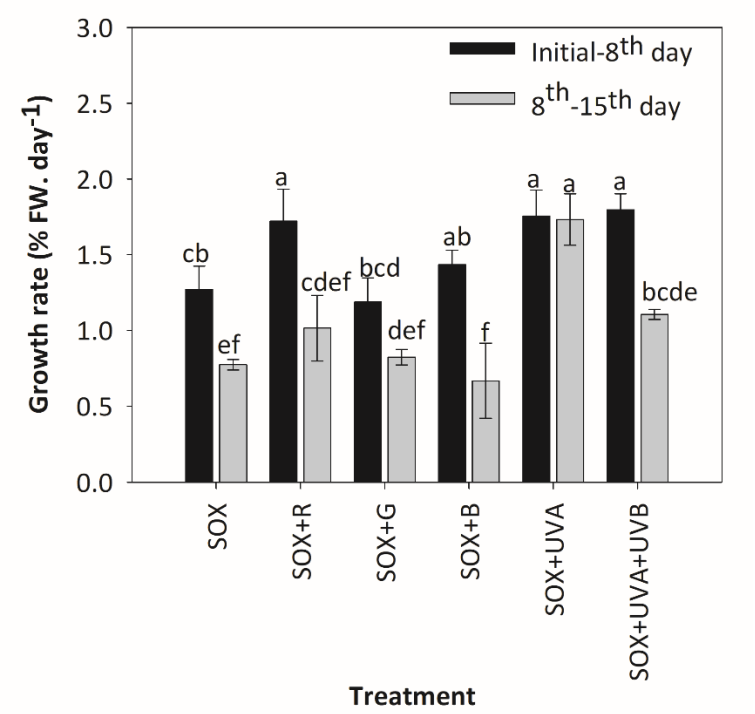

Growth rates were measured in different radiation treatments, over time (Factorial ANOVA), in two periods of the experiment, from the initial to the 8th day, and from 8th to 15th days. The letters indicate significant differences among the mean values, according to Newman-Keuls test ($p < 0.05$). The graph shows the mean values (n = 3) ± standard deviations.

UV-A radiation has positively influenced algae growth in other studies (ALTAMIRANO; FLORES-MOYA; FIGUEROA, 2000; GAO; XU, 2008; HENRY; ALSTYNE, 2004), while blue light appears to be associated with growth inhibition (BRIGGS, 2006; COSGROVE, 1994; KORBEE; FIGUEROA; AGUILERA, 2005; THOMAS; DICKINSON, 1979). On the other hand, blue light can participate in photoprotection processes, serving as a signal to dissipate energy excess (PETROUTSOS et al., 2016). Both UV-A and blue light are detected by a photoreceptor, the cryptochrome (JIANG; LI, 2015). This photoreceptor is associated with photolyases, which are photoenzymes known to repair some DNA damage (BJÖRN, 2015b; OLIVERI et al., 2014a). Thus, the maintenance of the growth rates in SOX+UVA can be an indirect result of the activation of repair and/or photoprotection mechanisms. That is, these mechanisms do not induce growth, but prevent their inhibition under the high intensity light from SOX lamp (about 450 µmol photons m^{-2} s^{1}), used to saturate photosynthesis. Excessive light can cause oxidative damage and cell death (PETROUTSOS et al., 2016). Although the alga have been acclimated for seven days under SOX light, it is possible that the prolonged exposure and accumulated SOX light doses have triggered some negative

effect, leading to reduced growth in SOX-only and other treatments, after 15 days of experiment, except in SOX+UVA condition.

Another photoreceptor sensitive to blue light is phytochrome, which seems to act synergistically with the cryptochrome by controlling growth in some plants (COSGROVE, 1994; JIANG; LI, 2015). Phytochrome is also sensitive to red light and can be interconverted in its active (Pr) or inactive (Pfr) form, absorbing red (peak around 660 nm) and far-red (peak around 730 nm) lights, respectively. Pfr form inhibited growth in *Lactuca sativa* (COSGROVE, 1994). In the present study, the red light complementary had a peak at 632 nm, which could have resulted in the conversion of Pr to Pfr, resulting in *O. pinnatifida* growth inhibition. However, the observed inhibition in SOX+R does not seems to be related to the performance of phytochrome, since the inhibition also occurred when red light was absent (SOX-only) and under green light (SOX+G). In an opposite way, in *Arabidopsis thaliana*, green light promoted growth and caused morphological changes similar to shaded plants, possibly associated with cryptochrome and another unknown photoreceptor (ZHANG; MARUHNICH; FOLTA, 2011).

Table 6 shows the photosynthetic parameters obtained through *in vivo* chlorophyll *a* fluorescence evaluation. The maximum quantum yield (Fv/Fm) of photosystem II (PSII) and photosynthetic efficiency (α_{ETR}) exhibited similar values among the treatments and the SOX-only on the 15th day. The values of Fv/Fm reduced around 15% in SOX-only during the experiment, but this reduction was accompanied by other treatments. SOX+UVA treatment was greater than SOX in electron transport rate (ETR and ETR_{max}) and saturation irradiance ($E_{K\,ETR}$) on the 15th day, about 35% and 30%, respectively. SOX and SOX+G decreased about 30% in ETR during experiment, although on the 15th day, both presented values statistically similar to the other treatments, except SOX+UVA. This treatment increased around 17% in ETR over experiment.

Tabela 6 - *In vivo* chlorophyll *a* fluorescence parameters were measured in *O. pinnatifida* during the culture under different radiation treatments.

	Times	Treatments					
		SOX	**SOX+R**	**SOX+G**	**SOX+B**	**SOX+UVA**	**SOX+UVA+UVB**
ETR	1st day	7.0 ± 0.36^{def}	5.7 ± 0.31^{abcde}	7.1 ± 0.66^{def}	5.8 ± 1.27^{abcde}	6.2 ± 0.28^{abcdef}	6.1 ± 0.54^{abcdef}
	5th day	5.9 ± 1.04^{abcdef}	4.2 ± 0.66^{ab}	5.5 ± 0.57^{abcde}	6.0 ± 0.52^{abcdef}	7.9 ± 0.46^{f}	6.7 ± 0.14^{abcde}
	8th day	4.9 ± 0.11^{abcd}	4.1 ± 0.40^{a}	4.6 ± 0.32^{abc}	4.8 ± 0.67^{abc}	6.1 ± 0.94^{abcdef}	5.5 ± 0.80^{cdef}
	12th day	5.5 ± 0.31^{abcde}	4.7 ± 1.00^{abc}	4.6 ± 0.93^{abc}	4.7 ± 0.57^{abc}	6.4 ± 0.86^{dcdef}	5.5 ± 0.54^{abcde}
	15th day	4.8 ± 1.29^{abc}	5.2 ± 0.79^{abcd}	4.7 ± 0.06^{abc}	5.6 ± 0.85^{abcde}	7.5 ± 1.18^{ef}	6.0 ± 1.22^{abcdef}
Fv/Fm	1st day	0.6 ± 0.02^{d}	0.6 ± 0.01^{abcd}	0.6 ± 0.03^{cd}	0.6 ± 0.04^{abcd}	0.6 ± 0.04^{cd}	0.6 ± 0.04^{abcd}
	5th day	0.5 ± 0.02^{ab}	0.6 ± 0.02^{abcd}	0.6 ± 0.03^{abcd}	0.6 ± 0.03^{d}	0.6 ± 0.01^{abcd}	0.5 ± 0.02^{abc}
	8th day	0.5 ± 0.03^{ab}	0.6 ± 0.07^{abcd}	0.5 ± 0.02^{abc}	0.6 ± 0.03^{bcd}	0.5 ± 0.03^{abc}	0.5 ± 0.01^{abc}
	12th day	0.5 ± 0.01^{ab}	0.5 ± 0.01^{ab}	0.5 ± 0.02^{abc}	0.6 ± 0.01^{abcd}	0.6 ± 0.04^{abcd}	0.6 ± 0.00^{abcd}
	15th day	0.5 ± 0.01^{a}	0.5 ± 0.02^{ab}	0.5 ± 0.03^{abc}	0.5 ± 0.02^{abc}	0.5 ± 0.02^{ab}	0.6 ± 0.01^{abcd}
α_{ETR}	8th day	0.086 ± 0.015^{ab}	0.047 ± 0.014^{b}	0.095 ± 0.018^{a}	0.095 ± 0.001^{a}	0.079 ± 0.026^{ab}	0.088 ± 0.003^{ab}
	15th day	0.067 ± 0.012^{ab}	0.080 ± 0.010^{ab}	0.096 ± 0.012^{a}	0.058 ± 0.016^{ab}	0.081 ± 0.026^{ab}	0.080 ± 0.018^{ab}
ETR_{max}	8th day	23.2 ± 3.4^{ac}	12.4 ± 3.4^{b}	23.3 ± 3.7^{ac}	21.9 ± 1.5^{ac}	28.5 ± 5.3^{c}	22.8 ± 1.0^{ac}
	15th day	13.4 ± 2.1^{b}	18.6 ± 1.8^{ab}	17.8 ± 3.3^{ab}	14.1 ± 4.2^{b}	23.5 ± 3.7^{ac}	17.1 ± 2.0^{ab}
$E_{K\ ETR}$	8th day	270.7 ± 18.1^{a}	268.7 ± 31.7^{a}	247.0 ± 8.4^{ab}	229.7 ± 15.3^{abcd}	226.5 ± 28.8^{abcd}	259.1 ± 9.9^{a}
	15th day	174.4 ± 38.5^{c}	233.3 ± 30.3^{abcd}	183.6 ± 14.4^{cd}	243.4 ± 3.8^{abd}	252.0 ± 37.2^{ab}	193.1 ± 3.2^{bcd}

Factorial ANOVA (see supplementary information, ANEXO B, Table S. 3) and Newman-Keuls test ($p<0.05$) were performed. Mean values (n=3) and standard deviation are shown. Distinct letters indicate significant differences. ETR (electron transport rate, µmol electrons m^{-2}. s^{-1}), Fv/Fm (maximum quantum yield of PSII), α_{ETR} (photosynthetic efficiency), ETR_{max} (maximum electron transport rate, µmol electrons m^{-2} s^{-1}) and $E_{k\ ETR}$ (saturation irradiance, µmol photons m^{-2} s^{-1}).

Photosynthetic parameters did not decrease significantly in SOX+R, SOX+B and SOX+UVA+UVB during the experiment to explain the reduction in growth rates in these treatments (Table 6). There was a slight reduction (around 15%) in Fv/Fm in SOX-only and other treatments. The decline of this parameter can be interpreted as photoinhibition, i.e., a decrease in photosynthesis in response to excess light (ADAMS III et al., 2008; LONG; HUMPHRIES; FALKOWSKI, 1994). Photoinhibition does not mean that there was in fact photodamage to PSII (LONG; HUMPHRIES; FALKOWSKI, 1994), since a down-regulation of photosynthesis can be reversible. The reversibility of photosynthetic rates depends on the organism's ability to repair the damage caused by excess light (GREER; BERRY; BJÖRKMAN, 1986). The decrease in ETR could also be indicative of photosynthetic reduction, although some studies have shown that under high irradiance this parameter increases or decreases, while the evolution of oxygen remains constant. This means that electrons transported in the electron transport chain at photosynthetic apparatus can be used to regulate other internal pathways (photoprotection, antioxidant reactions, Calvin cycle enzymes, and others).Thus, under saturating irradiance, ETR appears to be limited to explain photosynthesis (CARR; BJORK, 2003; FRANKLIN; BADGER, 2001).

Finally, the photosynthetic parameters seem to have little relation with the growth rates. In fact, few changes in photosynthesis were expected for our study, since photosynthesis saturation was promoted by the high intensity SOX lamp, and complementary radiations were applied in very low fluence, almost insignificant compared to SOX light intensity. This photobiological treatment is precisely used to verify responses associated with photomorphogenic photoreceptors, regardless of photosynthesis. In other studies, using other experimental designs and light sources, UV-B radiation and blue light caused reduction of photosynthetic parameters in red algae (AGUILERA; FIGUEROA; NIELL, 1997; GAO; XU, 2008; KORBEE; FIGUEROA; AGUILERA, 2005). Haxo and Blinks' pioneering action spectra study showed low photosynthetic efficiency under blue light in red algae (HAXO; BLINKS, 1950). In consequence, the red alga *Porphyra umbilicalis* exhibited higher growth rate and photosynthetic efficiency under red light compared to blue light (FIGUEROA; AGUILERA; NIELL, 1995). However, *O. pinnatifida* showed a different pattern, probably related to the experimental design strategy.

Carotenoid pigments and chlorophyll showed significant variation among the treatments (Supplementary information, ANEXO B, Table S. 4). β-carotene was significantly smaller in SOX+UVA and SOX+UVA+UVB (<10 μg g^{-1} DW) compared to SOX-only and

coloured treatments (SOX+R, SOX+G and SOX+B). SOX, SOX+R and SOX+G exhibited β-carotene values above 15 µg g^{-1} DW, and the SOX+B treatment showed values around 20 µg g^{-1} DW for the same carotenoid (Figure 36 A). Antheraxanthin showed no significant variation (Figure 36 B), exhibiting values above of 9 µg g^{-1} DW. Zeaxanthin and lutein were produced in greater amounts under SOX+UVA+UVB, showing values greater than 100 and 2 µg g^{-1} DW, respectively (Figure 36 C and D). In comparison to SOX-only, SOX+UVA+UVB exhibited 35% and 23% higher concentrations of zeaxanthin and lutein, respectively. Violaxanthin exhibited the highest values under SOX+UVA+UVB and SOX+B (Figure 36 E). Violaxanthin reaches values above 4 (µg g^{-1} DW) in SOX+B, i.e., 30% higher compared to SOX-only. Chlorophyll *a* values were higher in SOX+R, SOX+B and SOX+UVA+UVB than in the other treatments, especially when compared to SOX-only. SOX+R, SOX+B and SOX+UVA+UVB reached chlorophyll *a* values close to 200 µg g^{-1} DW. The lowest amounts of chlorophyll *a* were observed in SOX+UVA and SOX-only (<150 µg g^{-1} DW) (Figure 36 F).

Figura 36 - Carotenoid pigments and chlorophyll a of *O. pinnatifida* cultivated under different radiation treatments, on the 15th day.

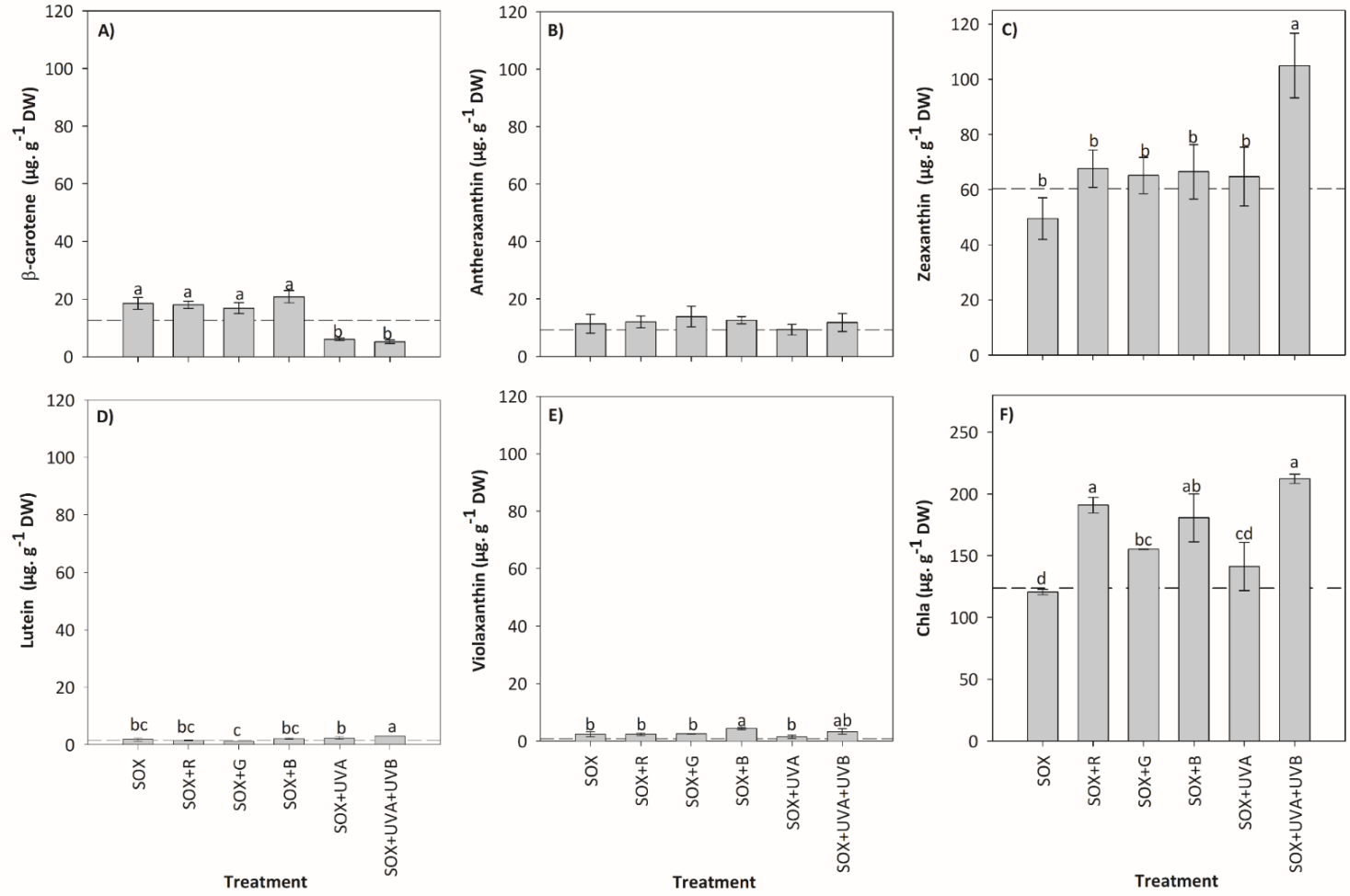

One-way ANOVA and Newman-Keuls test ($p<0.05$) were performed. The dashed line shows the mean of initial value, such as A) β-carotene 12.6 ± 0.4 µg g^{-1} DW, B) Antheraxanthin 9.1 ± 0.3 µg g^{-1} DW, C) Zeaxanthin 60.3 ± 8.7 µg g^{-1} DW, D) Lutein 1.4 ± 0.3 µg g^{-1} DW, E) Violaxanthin 0.72 ± 0.1 µg g^{-1} DW, and F) Chl*a* (chlorophyll *a*) 123.6 ± 17.4 µg g^{-1} DW. Distinct letters indicate significant differences. Data are expressed as mean values (n=3) ± standard deviations.

Zeaxanthin was the dominant carotenoid in this and other studies conducted with *O. pinnatifida* (ESTEBAN et al., 2009; LALEGERIE et al., 2019). Quantities of zeaxanthin less than 0.2 mg g^{-1} DW were obtained when *O. pinnatifida* was collected in winter. In summer, this carotenoid was not detected (LALEGERIE et al., 2019). Another species, *Osmundea spectabilis*, showed β-carotene as the dominant carotenoid, followed by zeaxanthin, β-cryptoxanthin, and antheraxanthin; violaxanthin was absent. Other red algae showed lutein in higher concentration (SCHUBERT; GARCÍA-MENDOZA; PACHECO-RUIZ, 2006). We found lutein and violaxanthin in quantities of less than 4 μg g^{-1} DW.

Violaxanthin, antheraxanthin and zeaxanthin are part of the xanthophyll cycle (XC), in which violaxanthin is converted to zeaxanthin with antheraxanthin as an intermediate. This conversion occurs under conditions of light stress and the reverse process (zeaxanthin to violaxanthin) occurs under dark or low light (BJÖRN, 2015a). XC has an important role in photoprotection in plants, although in red algae the presence of this cycle and its interconversion reactions have been discussed (BJÖRN, 2015a; DAUTERMANN; LOHR, 2017; SCHUBERT; GARCÍA-MENDOZA; PACHECO-RUIZ, 2006). The presence of XC carotenoids in this study and in others may be indicative of a photoprotection mechanism. Zeaxanthin accumulation in algae may be related to acclimation under stressful light conditions (SCHUBERT; GARCÍA-MENDOZA, 2008; SCHUBERT; GARCÍA-MENDOZA; PACHECO-RUIZ, 2006). This carotenoid has the lowest energy level at 704 nm, that is, zeaxanthin can receive excess energy from any antenna chlorophyll *a* and degrade in small amounts of quanta (heat) (BJÖRN, 2015a). Our results showed a high concentration of zeaxanthin in all treatments (Figure 36 C), mainly SOX+UVA+UVB. This may be the result of the acclimation of *O. pinnatifida* under saturating light. SOX+UVA+UVB plus blue peak showed amounts greater than 0.1 mg g^{-1} DW of zeaxanthin. We believe that the increase of this carotenoid was induced by UV-B, since UV-A radiation plus blue peak (SOX+UVA) did not affect zeaxanthin concentration. According to Björn (BJÖRN, 2015a), UV-B may inhibit the enzyme violaxanthin de-epoxidase, which performs the XC conversion reaction (from violaxanthin to zeaxanthin). Assuming that XC conversion reactions, if present, were responsible for the increase in zeaxanthin, then UV-B radiation should have inhibited and not increased the concentration of this carotenoid. Thus, it is possible that *O. pinnatifida* has other photoprotection mechanism that increase specific carotenoids, such as zeaxanthin, involving photoreceptors sensitive to visible light and UV radiation. Photoreceptors for UV radiation have been identified in green algae, for example, UVR8 sensitive to UV-B radiation (FERNÁNDEZ et al., 2016), although this photoreceptor

appears to be absent in red algae. UV-B radiation also induced carotenoid accumulation in another red alga, *Pterocladiella capillacea* (LEE; SHIU, 2009).

Blue light (SOX+B) caused the accumulation of violaxanthin and chlorophyll in this study. The increase of chlorophyll and other photosynthetic pigments under blue light was previously verified (BARUFI et al., 2015; FIGUEROA et al., 1995; FIGUEROA; AGUILERA; NIELL, 1995; FIGUEROA; NIELL, 1990; KORBEE; FIGUEROA; AGUILERA, 2005). Blue light can influence photoreceptors, such as phototropin which is involved in chlorophyll and carotenoid biosynthesis (KIANIANMOMENI; HALLMANN, 2014).

Phycocyanin (PC) was not influenced by time and treatment variables, showing average values below of 0.5 (mg g^{-1} DW). Phycoerythrin (PE) exhibited higher concentrations under SOX+B (8^{th} day) and SOX+G (15^{th} day) treatments (> 0.8 mg g^{-1} DW). Compared to SOX-only, PE was 83% and 72% higher in SOX+B and SOX+G, respectively. In addition, PE in SOX+R and SOX+UVA was about 63% and 59% greater than PE in SOX-only on the 15^{th} day, respectively. SOX-only treatment resulted PE values below 0.2 mg g^{-1} DW in both periods, 8^{th} and 15^{th} days (Figure 37). In another study, *O. pinnatifida* exhibited amounts of PE lower than 5 mg g^{-1} DW when collected in winter, and values below the limit of quantification when collected in summer (LALEGERIE et al., 2019), evidencing that the PE quantity in this species is subjected to seasonal oscillations, responding to environmental characteristics, for example, light quality and intensity.

Figura 37 - Phycoerythrin (mg g^{-1} DW) of *O. pinnatifida* cultivated under different radiation treatments, on the 8th and 15th day (Factorial ANOVA).

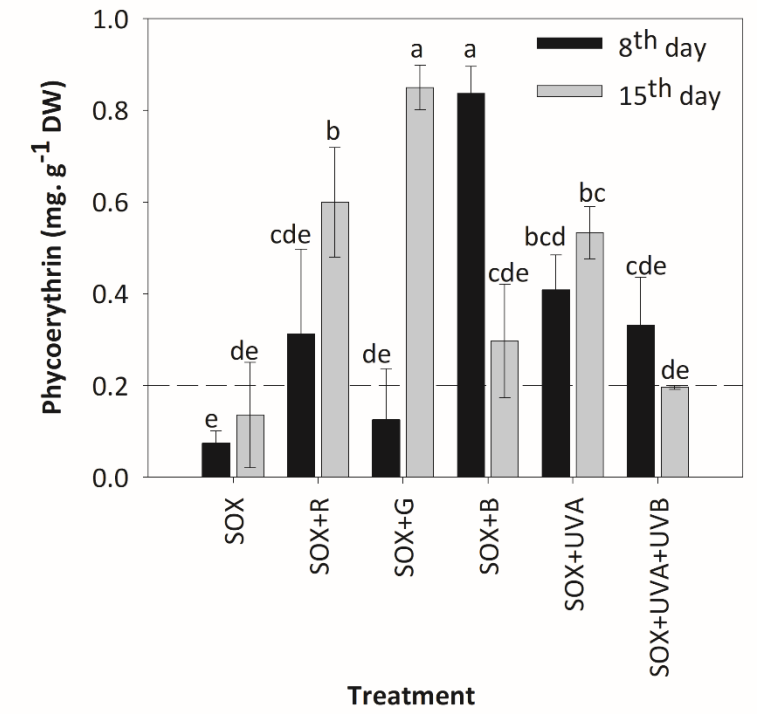

The dashed line shows the mean of initial value, as 0.23 ± 0.008 mg g^{-1} DW. The letters indicate significant differences, according to Newman-Keuls test ($p < 0.05$). The graph shows the mean values (n = 3) ± standard deviations.

Phycobiliproteins are accessory pigments composed of a protein and chromophore called phycobilin and are present in organisms, as red algae and cyanobacteria. Phycobilin, as allophycocyanin (APC), PC and PE, occur organized in phycobilisomes. PE is present in the periphery, followed by PC and after APC. The energy transference occurs in the same order, that is, light is captured first by PE and then transferred to other phycobiliproteins until the chlorophyll in the PSII antenna complex. The absorption peaks are around 560 nm for PE, 620 nm for PC and 650 nm for APC, allowing the absorption of different qualities of light, such as blue-green, green, yellow, or orange (GRAHAM et al., 2016c; GROSSMAN et al., 1993; KIRK, 2011a). Red algae can change the composition of their pigments in response to the spectral quality to which they are being exposed. This process is called chromatic adaptation and depends on both quality and intensity of light (KIRK, 2011c). Under low irradiance, a microalgae *Porphyridium cruentum* showed a higher PE/chlorophyll ratio in green light than in blue light. The opposite was observed when the algae was exposed to high irradiance, that is, the PE/chlorophyll ratio was greater under blue light (BRODY; EMERSON, 1959). In 1980, it was suggested that chromatic adaptation occurs under a general principle, in which

photosystems need to be similarly excited to maintain photosynthetic efficiency. Thus, considering that in red algae, light can be absorbed by phycobilisomes in PSII and directly by chlorophyll in photosystem I (PSI), then, high intensity of red light can excite mainly chlorophyll in PSI, causing an imbalance between the photosystems. Photosynthetic efficiency can be restored by decreasing the amount of chlorophyll in the PSI or increasing the chlorophyll and PE in the PSII. However, if the high intensity of light mainly excites PE in the PSII, then this pigment can be reduced to restore balance. But, if the light is of low fluence and captured mainly by phycoerythrin, the cell increases this pigment, because now the problem is the low amount of energy and not the imbalance between the photosystems (KIRK, 2011c; LEY; BUTLER, 1980).

In our study, *O. pinnatifida* received a high intensity of SOX light (peak at 590 nm, yellow/orange light), which was complemented by different qualities of low intensity radiation. The spectral quality of SOX is mainly absorbed by phycobilisomes associated with PSII, when the algae was exposed to SOX-only there was a reduction in both chlorophyll *a* and phycoerythrin (Figures 36 F and 37), possibly to reduce the amount of light absorbed in the PSII The lowest concentration of chlorophyll in SOX-only was observed previously (BRITZ; SAGER, 1990). When we added the complementary lights (low fluency), the responses did not follow a pattern, since the algae received at the same time a signal of high and low intensity from different regions of the spectrum. By the principle of chromatic adaptation, low-intensity lights induce pigments that can improve their absorption, so PE was induced under green light (SOX+G). However, PE and chlorophyll *a* were also induced under the complementary red and blue lights (SOX+R and SOX+B, in Figures 36 F and 37), as if there was a need to balance the energy absorption between the photosystems, these responses are expected when the red and blue lights are provided in high intensity, disproportionately exciting the PSI. PE also increased in SOX+UVA (Figure 37), possibly because this treatment has a peak in the blue region of the spectrum (Figure 34). PE production in *Chondrus crispus* was also affected by the low fluence rate of green, red, and blue lights (6 µmol photons m^{-2} s^{-1}) (LÓPEZ-FIGUEROA, 1991). PE was stimulated mainly by the green light; this increase was reversed by different fluences of the far-red (6 and 100 µmol photons m^{-2} s^{-1}). According to the authors, these results were modulated by light qualities through photoreceptors. Our results also suggest the performance of photoreceptors in the PE control, mainly under complementary low fluence lights.

Mycosporine-like amino acids (MAAs) were analysed in the whole thalli of the alga at the beginning (initial), after seven days of acclimation under SOX light, on the 8th and 15th

day of the experiment. MAAs from apices were evaluated only on the 15th day and were not affected by treatments (ANEXO B, Table S. 4), showing mean values of 0.15 ± 0.05 mg g^{-1} DW for asterina-330, 0.07 ± 0.03 mg g^{-1} DW for palythine, 0.04 ± 0.03 mg g^{-1} DW for palythinol, 0.04 ± 0.02 mg g^{-1} DW for shinorine, 0.09 ± 0.03 mg g^{-1} DW for porphyra-334 and 0.39 ± 0.13 mg g^{-1} DW for total MAAs. Asterina-330 was quantitatively superior. Apices of *O. pinnatifida* grown under SOX-only and other treatments showed similar colour and appearance (Figure 38).

Figura 38 - Images of thalli apex of *Osmundea pinnatifida* cultivated under SOX light conditions, over time.

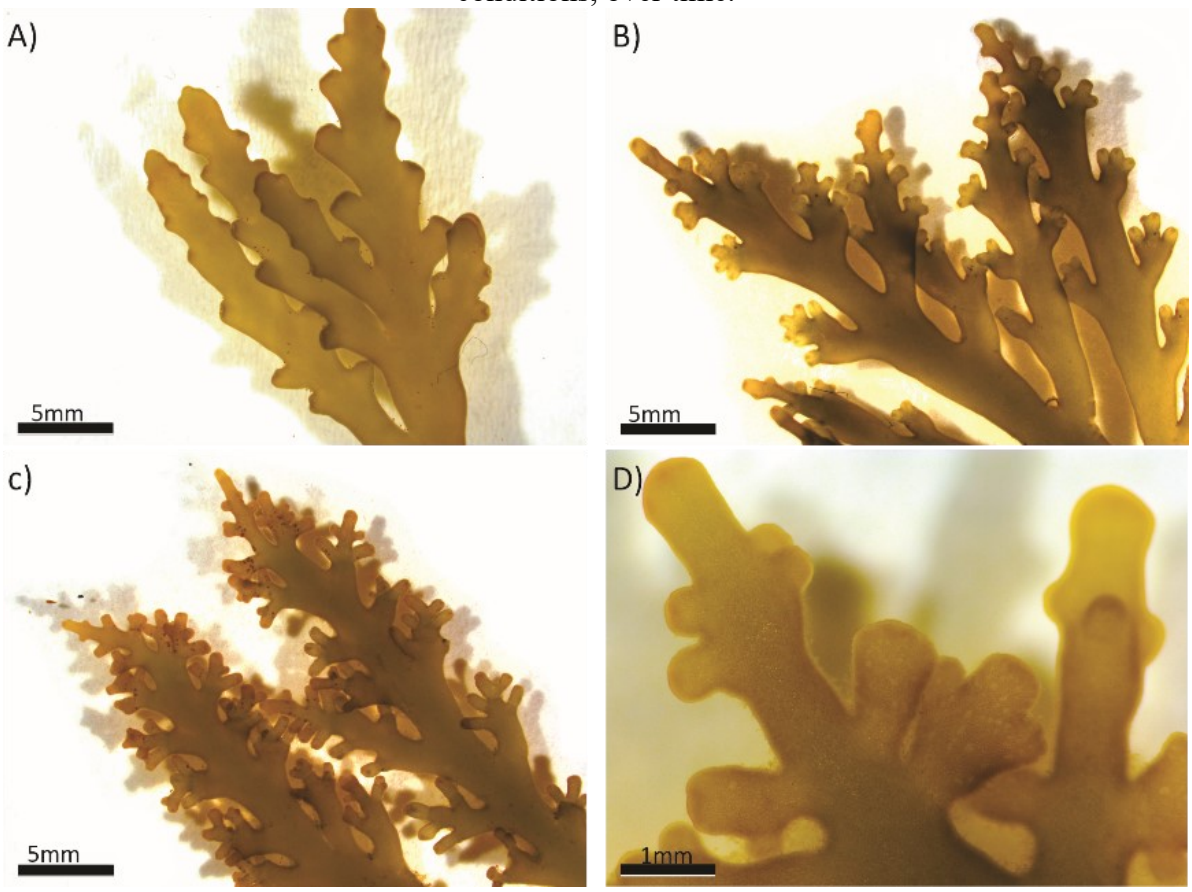

The apices showed differences in size and shape during the experiment, however, no visible differences were observed among different treatments. A) Start of experiment, B) 8th day, C) 15th day, and D) 15th apex detail.

MAAs extracted from whole algae thalli responded to the sources of variation (time and treatment), according to the factorial ANOVA (Supplementary information, ANEXO B, Table S. 3). The MAAs found were asterina-330, palythine, palythinol, shinorine and porphyra-334. Asterina-330 and palythinol were quantitatively dominant in all treatments (Figure 39),

although they decreased in SOX+R, SOX+G and SOX+B after 15 days (Figure 39 A and D). Palythinol concentration was above 0.5 mg g^{-1} DW in SOX+R (Figure 39 D).

Figura 39 - Concentrations of different types of mycosporine-like amino acids (MAAs) from whole thalli of *O. pinnatifida* cultivated under different radiation treatments, on the 8th and 15th day.

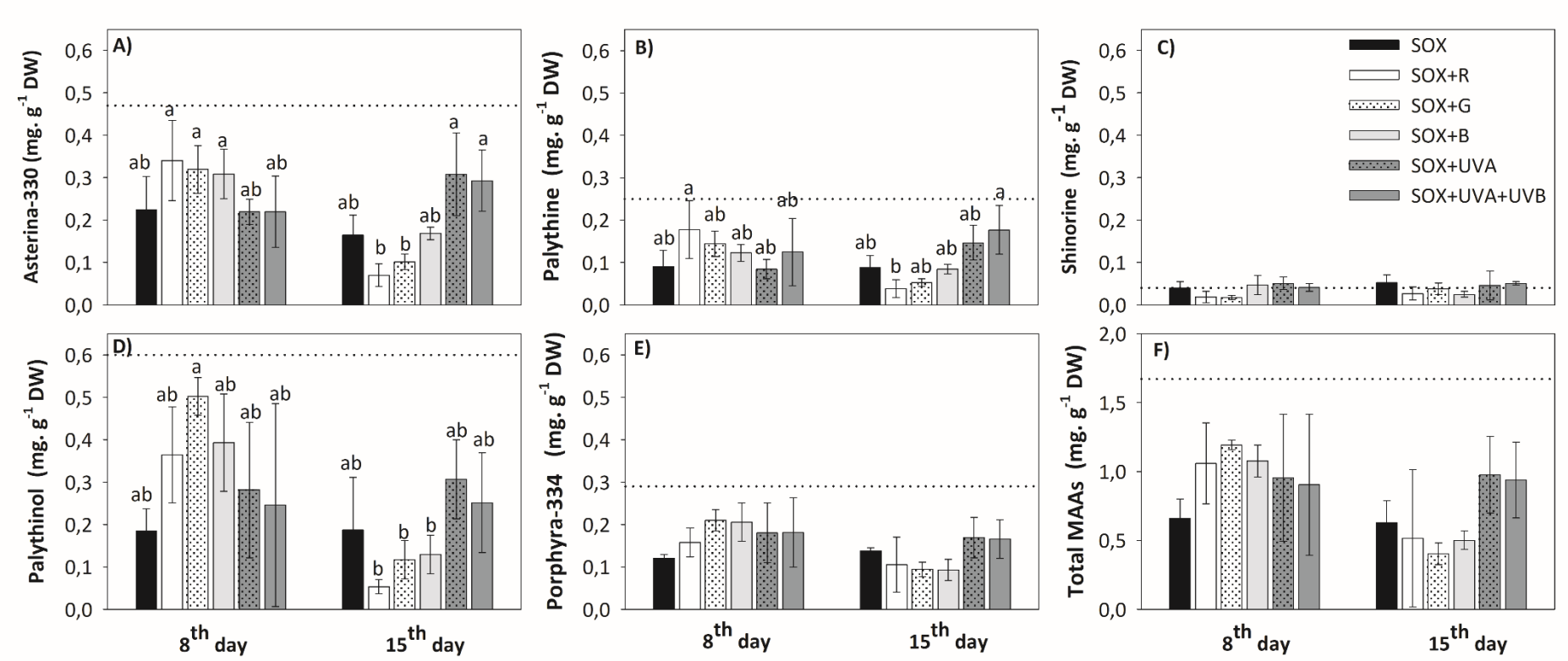

Factorial ANOVA and Newman-Keuls test ($p<0.05$) were performed. Data are expressed as mean values (n=3) ± standard deviation. Different letters indicate significant differences. The dashed line shows the mean of initial value, such as A) Asterina-330 0.47 ± 0.11 mg g^{-1} DW, B) Palythine 0.25 ± 0.05 mg g^{-1} DW, C) Shinorine 0.04 ± 0.02 mg g^{-1} DW, D) Palythinol 0.60 ± 0.06 mg g^{-1} DW, E) Porphyra-334 0.29 ± 0.06 mg g^{-1} DW and F) Total MAAs 1.67 ± 0.27 mg g^{-1} DW.

In a recent study (LALEGERIE et al., 2019), *O. pinnatifida* presented around seven types of MAAs, including usujirene and palythene (both not found in our case). Among the MAAs observed, Porphyra-334 was quantitatively dominant, while in the present study asterina-330 and palythinol were found in greater quantity. Lalegerie et al. (LALEGERIE et al., 2019) collected algae in estuarine areas and intertidal pools, where exposure to sunlight is high. Depending on the irradiance conditions, the quality and quantity of MAAs may vary even in the same species, as noted by Karsten et al. (KARSTEN et al., 1999a).

These authors performed an experiment transplanting algae 2 m deep to the surface (where they received more UV radiation), and after one week, the algae doubled the total amount of MAAs, especially of mycosporine-glycine and palythine. In this same study, the red alga *Devaleraea ramentacea*, collected from 1m depth, had 5-fold more MAAs at the apex than at the base of the thallus. Among the MAAs found at the apex, palythine was quantitatively dominant. In the present study, total MAAs from apices of *O. pinnatifida* was lower compared to the total MAAs from thalli.

Possibly, the irradiance conditions offered during the experiment were not adequate or stressful enough to induce the production of MAAs by photoreceptors. Since, except shinorine, the other MAAs showed a significant decrease during the experiment in all treatments, according to initial values (dashed line, Figure 39, initial values were collected after seven days of acclimation). Shinorine was the only MAA to maintain levels during the experiment (dashed line, Figure 39 C), although no differences were found between SOX-only and other treatments. The reduction in levels of MAAs was observed even in UV treatments, although slightly higher amounts of MAAs (asterina-330 and palythine) were observed in SOX+UVA and SOX+UVA+UVB compared to SOX after 15 days (Figure 39 A and B).

MAAs production by algae in response to UV radiation was well documented in reviews (COCKELL; KNOWLAND, 1999; LA BARRE; ROULLIER; BOUSTIE, 2014; RASTOGI et al., 2010), although activation mechanisms and production pathways are still unclear. In the red alga *C. crispus*, UV-B radiation had a negative effect in the accumulation of shinorine (λmax=334 nm) and palythine (λmax=320 nm), while short UV-A wavelengths exhibited the highest quantum efficiency on their biosynthesis. On the other hand, UV-B radiation was the main inducer of the synthesis of asterina-330 (λmax=330 nm), palythinol (λmax=332 nm) and palythene (λmax=360 nm) (KRÄBS et al., 2002). In 2001, Franklin et al. suggested the existence of two photoreceptors for the synthesis of MAAs in *C. crispus*, one for UV-A and one for blue light, both controlling the synthesis of shinorine (FRANKLIN; KRÄBS;

KUHLENKAMP, 2001a). Later, UV-A-type photoreceptor with peaks at 320, 340 and 400 nm was suggested, also related to the synthesis of the shinorine in *C. crispus* (KRÄBS; WATANABE; WIENCKE, 2004). Finally, in 2013, the genome of *C. crispus* was sequenced and only one photoreceptor was found, a cryptochrome.

The concentration of phenolic compounds and the antioxidant activity (ABTS) were influenced by the treatments during the experiment (Factorial ANOVA, ANEXO B, Table S. 3). Phenolics content in SOX+G (27.05 ± 1.6 mg g $^{-1}$ DW) and SOX+B (27.43 ± 2.0 mg g $^{-1}$ DW) was about 32% higher than in SOX-only (18.28 ± 0.7 mg g $^{-1}$ DW) after 8 days. SOX+R exhibited amounts of phenolics greater than 20 mg g^{-1} DW in both periods, values around 20% (8th day) and 25% (15th day) higher than SOX-only values. The antioxidant activity, assessed using the ABTS test, was similar in all treatments in both evaluated periods (8th and 15th day), except for SOX+B and SOX+UVA+UVB, which showed values about 50% and 40% lower than the other treatments on the 8th and 15th day, respectively. Antioxidant potential is generally correlated to substances, such as carotenoids, phycobiliproteins, phenolic compounds, MAAs and others (ÁLVAREZ-GÓMEZ et al., 2017; CHAROENSIDDHI et al., 2017b; LA BARRE; ROULLIER; BOUSTIE, 2014; PANGESTUTI; SIAHAAN; KIM, 2018). In this study, SOX+B showed high levels of PE and polyphenols on the 8th day. SOX+UVA+UVB stood out to produce of zeaxanthin carotenoid on the 15th day. However, both treatments (SOX+B and SOX+UVA+UVB) showed low antioxidant activity on the same days. These results could be related to the substances used in the extraction of the compounds. Phenols and carotenoids were extracted with methanol, while ABTS assay was performed with phosphate buffer. However, phycobiliproteins were also extracted with phosphate buffer and did not show any correlation with antioxidant activity.

Soluble proteins were also evaluated, but no significant statistical differences were detected by the Student-Newman-Keuls test, although the ANOVA indicated significant interaction (time and treatment), ANEXO B, Table S. 3. The concentration of the proteins was between 5 and 10 mg g^{-1} DW. SOX+B treatment (8th day) showed the highest average value of 9.08 ± 1.06 mg g^{-1} DW. The treatments, such as SOX+G (8th day) and SOX+UVA (15th day) with the lowest average values of 6.48 ± 0.53 mg g $^{-1}$ DW and 6.45 ± 0.93 mg g $^{-1}$ DW, respectively.

Carbon and elemental nitrogen were evaluated after 15 days of experiment. These elements did not show significant variation among the SOX and other treatments (ANEXO B, Table S. 4). The mean value of carbon content was 279.60 ± 11.63 mg g^{-1} DW, and nitrogen

was 16.73 ± 1.84 mg g^{-1} DW, and carbon and nitrogen ratio (C: N) was 16.85 ± 1.51 mg g^{-1} DW, including all treatments.

Table 7 summarizes all the results of the physiological and biochemical analyses performed with *O. pinnatifida* during the experiment. Complementary radiation treatments were compared with SOX-only light.

Tabela 7 - Responses of *O. pinnatifida* grown under different radiation treatments on the 8th and 15th day of the experiment.

Variable	Treatment									
	SOX+R		SOX+G		SOX+B		SOX+UVA		SOX+UVA+UVB	
	8th day	15th day	8th day	15th day	8th day	15th day	8th day	15th day	8th day	15th day
Growth rate	↑	↑	↓	↑	↑	↓	↑	↑↑	↑	↑
Fv/Fm	↑	–	–	↑	↑	↑	≈↑	≈↑	≈↑	↑
ETR	↓	↑	↓	↓	↓	↑	↑	↑	↑	↑
α_{ETR}	↓	↑	↑	↑	↑	↓	↓	↑	↑	↑
ETR_{max}	↓	↑	≈↑	↑	↓	↑	↑	↑	↓	↑
E_k	≈↓	↑	↓	↑	↓	↑	↓	↑	↓	↑
Chlorophyll *a*	n	↑	n	↑	n	↑	n	↑	n	↑
Violaxanthin	n	↑	n	↑	n	↑	n	↓	n	↑
Antheraxanthin	n	↑	n	↑	n	↑	n	↓	n	↑
Zeaxanthin	n	↑	n	↑	n	↑	n	↑	n	↑↑
Lutein	n	↓	n	↓	n	↑	n	↑	n	↑
β-carotene	n	↓	n	↓	n	↑	n	↓↓↓	n	↓↓↓
Phycocyanin	↑	↑	≈↓	↑	↑	↑	≈↑	↑	≈↓	↑
Phycoerythrin	>↑↑↑	>↑↑↑	↑	>↑↑↑	>↑↑↑	↑↑	>↑↑↑	↑↑↑	>↑↑↑	↑
Phenolic compounds	↑	↑	↑	↓	↑	↓	↑	↑	↓	↑
Soluble proteins	↑	↑	↓	↑	↑	↑	↑	↓	↓	↑
Total MAAs whole thallus	↑	↓	↑	↓	↑	↓	↑	↑	↑	↑
Asterina-330 whole thallus	↑	↓↓	↑	↓	↑	–	≈↓	↑	≈↓	↑
Palythine whole thallus	↑	≈↑	↑	↓	↑	–	≈↓	↑	↑	↑↑
Palythinol whole thallus	↑	↑	↑↑	↓	↑↑	↓	↑	↑	↑	↑
Shinorine whole thallus	↓↓	↓	↓↓	↓	–	↓↓	≈↑	≈↓	–	–
Porphyra-334 whole thallus	↑	↓	↑	↓	↑	↓	↑	↑	↑	↑
Total MAAs apex thallus	n	↑	n	↓	n	↓	n	↑	n	↑
Asterina-330 apex thallus	n	↑	n	↓	n	≈↓	n	↑	n	↑
Palythine apex thallus	n	↑	n	–	n	≈↓	n	–	n	↑
Palythinol apex thallus	n	≈↓	n	-	n	-	n	↑	n	↑↑
Shinorine apex thallus	n	≈↓	n	≈↓	n	↓	n	≈↑	n	↓
Porphyra-334 apex thallus	n	↑	n	≈↑	n	-	n	↑	n	↑
ABTS assay	↓	↓	↑	↓	↓	↓	↓	↓	↓	↓
Carbon (C)	n	↑	n	↑	n	↑	n	↑	n	↑
Nitrogen (N)	n	↑	n	↑	n	↑	n	≈↑	n	↑
C:N ratio	n	↓	n	↓	n	↓	n	≈↑	n	–

Complementary radiation treatments (SOX+R, SOX+G, SOX+B, SOX+UVA, SOX+UVA+UVB) versus SOX-only light.Higher (↑), lower (↓), slightly higher (≈↑), slightly lower (≈↓), twice higher (↑↑), twice lower (↓↓), three times higher (↑↑↑), three times lower (↓↓↓), four times higher or more (>↑↑↑), four times lower or more (>↓↓↓), no effect (-), not evaluated (n).

5.5 CONCLUSIONS

In summary, we found a higher growth rate in algae under UV-A radiation on the 15th day of the experiment. Under UV-B radiation (SOX+UVA+UVB), we observed higher content of carotenoids (zeaxanthin, lutein and violaxanthin) and chlorophyll *a*. Under blue and green light (SOX+B and SOX+G), we found higher content of pigments (chlorophyll *a* and phycoerythrin) and phenolic compounds (8th day).

Our results showed that different wavelengths can influence the growth rates and production of pigments and other compounds in *O. pinnatifida*. This physiological acclimation of the alga to light involves several regulatory mechanisms, including the action of photoreceptors. As some compounds vary under UV radiation in *O. pinnatifida*, we suggest the presence of a UV photoreceptor or another molecule capable of perceiving this quality of radiation, triggering processes, especially those that result in increased production of photoprotection compounds.

6 CAPÍTULO III

Effects of UV-visible radiation on growth, photosynthesis, pigment accumulation and UV-absorbing compounds in the red macroalga *Gracilaria cornea* (Gracilariales, Rhodophyta)

Geniane Schneider*[a], Félix L. Figueroa[b], Julia Vega[b], Antonio Avilés [b], Paulo Antunes Horta [c], Nathalie Korbee[b], and José Bonomi-Barufi [c]

[a] Phycology Laboratory, Postgraduate Program of Biotechnology and Biosciences, Department of Microbiology, Immunology and Parasitology, Federal University of Santa Catarina, 88040-900, Florianopolis, SC, Brazil.

[b] Universidad de Málaga. Instituto Universitario de Biotecnología y Desarrollo Azul (IBYDA). Departamento de Ecología, Universidad de Málaga, Campus Universitario de Teatinos s/n, 29071, Málaga, España.

[c] Phycology Laboratory, Botany Department, Federal University of Santa Catarina, 88049-900, Florianopolis, SC, Brazil.

***Corresponding Author Address**
Geniane Schneider
E-mail: geniane.tega@gmail.com

Submitted in: *Algal Research*

6.1 ABSTRACT

Radiation induces different processes in photosynthetic organisms through photosynthetic pigments and photoreceptors. This study evaluated the performance of the red algae *Gracilaria cornea* cultivated under different radiation treatments. The objective was to identify responses associated with the treatments and mediated by photoreceptors. For this, *G. cornea* was exposed for 15 days to low fluence radiation of the ultraviolet (UV)-visible spectrum (red, green and blue light, and UV-A and UV-B radiation) combined with a high fluence radiation provided by a low pressure sodium lamp (SOX), in order to saturate the photosynthesis. We measure the growth rate and other variables, such as photosynthesis estimated as chlorophyll *a* fluorescence, chlorophyll *a*, phycobiliproteins, carotenoids, mycosporine-like amino acids (MAAs), phenolic compounds, antioxidant activity, soluble proteins, and internal carbon and nitrogen content. The results showed that the UV radiation influenced the growth rates, as well as the accumulation of internal compounds (carotenoids: violaxanthin, antheraxanthin and zeaxanthin; and MAA palythine; and phenolic compounds). As the treatments with UV radiation also had a peak of blue light, the presence of photoreceptors sensitive to these qualities of radiation (UV-A, UV-B and blue light) is suggested. In general, UV-A appears to induce some compounds without affecting growth, while UV-B seems to cause the accumulation of compounds at the expense of growth. The effect of light quality on growth and metabolism in *G. cornea* is compared to that in other species following similar experimental design.

Keywords: photoreceptors, photosynthesis, UV-visible radiation, MAAs, and carotenoids.

6.2 INTRODUCTION

Light is a basic resource for photosynthetic organisms, so, throughout the evolutionary process, they have developed mechanisms of acclimation to the ambient light conditions. In addition to the photosynthetic pigments that collect light for photosynthesis, there are also photoreceptors, which are light-sensitive proteins linked to different signaling pathways that allow to acclimate the physiological activities of organisms to changes in environmental light (KIANIANMOMENI; HALLMANN, 2014).

Photoreceptors are like photosensory switches and light can modulate their functioning. The quality (wavelength), quantity (fluence), direction and duration of the different radiations (ultraviolet and visible) present in the environment are perceived by the photoreceptors, which trigger a cascade of biological reactions that in plants control developmental processes, such as: circadian rhythms, shade avoidance, seed germination, chloroplast movement, seedling photomorphogenesis and phototropism (JIAO; LAU; DENG, 2007).

In algae, photoreceptors are less understood, although in the last decade these light-sensitive molecules have been identified for controlling different processes in these organisms, such as photo-orientation, growth, reproduction, photoprotection, and even the photosynthetic process. Photoreceptors from different families (e.g., phytochromes, cryptochromes, phototropins, UVR8 and others) have been identified in algae (ALLORENT; PETROUTSOS, 2017; COLLÉN et al., 2013; DRING, 1988; FERNÁNDEZ et al., 2016; HEGEMANN, 2008; KIANIANMOMENI; HALLMANN, 2014; LÓPEZ-FIGUEROA et al., 1989; OLIVERI et al., 2014b; ROCKWELL et al., 2014).

Algae have great biotechnological potential, since they have a wide chemical composition, being source of pigments, polysaccharides, vitamins, proteins, fibers, lipids, antioxidant substances, phenolic compounds and mycosporine-like amino acids (MAAs). Many of these compounds have their production modulated by different types of radiation, including ultraviolet (UV-A and UV-B) and visible (purple, blue, green, yellow, orange, red and other lights). For example, blue and white light stimulated the synthesis of the MAA palythine in *Chondrus crispus* (FRANKLIN; BADGER, 2001). In *Porphyra leucosticta*, MAAs as porphyra-334, palythine and asterina-330 were accumulated under blue light, and shinorine was accumulated under white, yellow, green, and red lights (KORBEE; FIGUEROA; AGUILERA, 2005). MAAs are also accumulated in response to UV radiation. UV-B radiation induced the accumulation of asterina-330, palythinol and palythene, while UV-A radiation induced the synthesis of shinorine and palythine in *Chondrus crispus* (KRÄBS et al., 2002). UV radiation stimulated MAAs in *Gracilaria tenuistipitata* (BONOMI-BARUFI et al., 2020). Photosynthetic pigments, such as chlorophyll, phycocyanin and phycoerythrin, were accumulated in algae under blue light (BARUFI et al., 2015; FIGUEROA; AGUILERA; NIELL, 1995; KORBEE; FIGUEROA; AGUILERA, 2005).

If the content of compounds is increased by specific wavelengths under saturation of photosynthesis by photosynthetic active radioation (PAR), photoreceptors could be involved in

these biological processes. The participation of photoreceptors in the modulation of compounds by light was previously suggested (FIGUEROA; NIELL, 1990; FRANKLIN; KRÄBS; KUHLENKAMP, 2001b; KRÄBS; WATANABE; WIENCKE, 2004; LÓPEZ-FIGUEROA, 1991). For example, the synthesis of the MAA shinorine in *C. crispus* was possibly controlled by photoreceptors sensitive to blue light and UV-A radiation (FRANKLIN; KRÄBS; KUHLENKAMP, 2001b; KRÄBS; WATANABE; WIENCKE, 2004). The synthesis of chlorophyll and biliproteins were mediated by phytochrome and cryptochrome (FIGUEROA; NIELL, 1990; LÓPEZ-FIGUEROA, 1991).

In a biotechnological perspective, understanding how changes in light or different radiations affect algae is essential for successful cultivation and the production of compounds of interest. Sunlight contains different types of radiation that interact with photosynthetic organisms through photoreceptors and photosynthetic pigments. These interactions trigger different processes that in practice are difficult to separate. Thus, to evaluate the performance of possible photoreceptors, we use an experimental strategy used by Thomas and Dickinson (THOMAS; DICKINSON, 1979) and repeated by other authors (BRITZ; SAGER, 1990; CASTRO-VARELA et al., 2021; GHEDIFA et al., 2021; PAGELS et al., 2020; SCHNEIDER et al., 2020b; SEGOVIA; GORDILLO; FIGUEROA, 2003). We grew algae under a high-fluence light source to saturate photosynthesis, and we complemented this light source with different low-fluence monochromatic radiations to activate responses from possible photoreceptors. To better understand this, the high fluence light was provided by the low pressure sodium lamp (SOX), which had a narrow peak of emission in the yellow/orange region of the spectrum (590 nm). Thus, this quality of light could not interfere with photoreceptors sensitive to complementary monochromatic radiations (red, blue, green, UV-A and UV-B). To avoid the interference of monochromatic radiation in the photosynthetic process, we applied radiations with low fluence, enough to activate photoreceptors, but insufficient for relevant change in photosynthetic rate. Photoreception can occur above and below the photosynthetic threshold (PETROUTSOS et al., 2016). Low intensities from 1 to 20 µmol photons m^{-2} s^{-1} are enough to activate photoreceptors (PETROUTSOS et al., 2016; SEGOVIA; GORDILLO; FIGUEROA, 2003). Following this experimental design, Pagels et al. (PAGELS et al., 2020) showed in the cyanobacterium *Cyanobium* sp. that SOX emitting enough light to sature photosynthesis and suplemeted with red light stimulated the accumulation of phycocyanin, lipids, carotenoids and produced an incraese of antioxidant activity, and when supplemeted with green light, this species presented an increase in the level of chlorophyll *a* and carbohydrates.

Schneider et al. (SCHNEIDER et al., 2020b) showed that UV-B radiation and blue, green and red light influenced the accumulation of pigments, such as chlorophyll *a*, carotenoids and phycobiliproteins in the alga *Osmundea pinnatifida*.

The alga selected for this study was *Gracilaria cornea* J.Agardh 1852, a red alga from the family Gracilariaceae, formerly known as *Hydropuntia cornea* (J.Agardh) M.J.Wynne 1989 and *Crassiphycus corneus* (J.Agardh) Gurgel, J.N.Norris & Fredericq 2018 (GUIRY; GUIRY, 2021). *G. cornea* can be found in the Western Atlantic Ocean from Bermuda, across the Gulf of Mexico, the Caribbean Sea, to the North of Cabo Frio, in Brazil (BIRD; DEOLIVEIRA; MCLACHLAN, 1986). Usually, this species occurs in clear and troubled waters, in places temporarily exposed (intertidal zone) up to 38 meters deep (PEREIRA et al., 1981). *G. cornea* thalli have different sizes from 6 to 45 cm, with irregular branching pattern, fleshy-cartilaginous texture, purple color, but may vary depending on the lighting conditions (BIRD; DEOLIVEIRA; MCLACHLAN, 1986). This species is economically important because it is a source of a polysaccharide (agar) with high quality and yields (FREILE-PELEGRÍN; ROBLEDO, 1997; JOFRE; NAVARRO; PLASTINO, 2020) and it is also source of MAAs and presenting high antioxidant activity (ÁLVAREZ-GÓMEZ; KORBEE-PEINADO; FIGUEROA, 2016; ÁLVAREZ-GÓMEZ; KORBEE; FIGUEROA, 2019).

Based on the previous information, the aim of this study was to evaluate physiological and biochemical changes in *Gracilaria cornea* grown under different radiation treatments and the possible participation of photoreceptors in the responses of this alga. This study also sought to identify a general pattern of responses among red algae, since this study uses an experimental design similar to another recently published study with another red alga *O. pinnatifida* (SCHNEIDER et al., 2020b).

6.3 MATERIAL AND METHODS

6.3.1 Algal samples

Gracilaria cornea J.Agardh samples were obtained from cultivation in the Grice Hutchinson Experimental Center, of Málaga University (WGS84 Huso30 UTM X: 367.921 Y: 4.059.212). There, the species was grown in water with the addition of nutrients every two days (400 μM of NH_4Cl and 40 μM of KH_2PO_4), at a temperature between 20 and 25℃ and under

constant and vigorous aeration. The water was renewed once a week and the cultivation tanks were exposed to solar radiation (≈800 to 1000 μmol photons m^{-2} s^{-1}).

G. cornea samples grown at the Grice Hutchinson Experimental Center of Malaga University were placed in plastic bags with water and transported in iceboxes to the laboratory of the Faculty of Sciences located 7 km far. In the laboratory, the algae were cleaned and selected for the experiment.

6.3.2 Experimental design

Before the experiment, the algae were acclimated for seven (7) days to laboratorial culture conditions. During this period, 10 g of algae were placed in methacrylate flasks with 1200 mL of sea water. The flasks were maintained in the culture chamber at a temperature ≈25℃, receiving constant and vigorous aeration. Photoperiod was 12 h light and 12 h dark, being light period provided by low pressure sodium (SOX) lamps (PHILIPS 135W BY22d T65). The cultivation water was renewed once during the acclimation and there was no addition of nutrients.

During the experimental period (15 days), the algae were maintained in the culture chamber under similar conditions of temperature and aeration. The renewal of water and addition of nutrients (0.66 mM of $NaNO_3$; 50 μM of $C_3H_7Na_2O_6P$; 14.6 μM of Na_2HPO_4) occurred four times during experiment (1^{st}, 4^{th}, 8^{th}, and 11^{th} days). Photoperiod was also 12 h light and 12 h dark. In the light period, the algae were exposed to different radiation treatments, such as SOX-only light (SOX), SOX plus red light (SOX+R), SOX plus green light (SOX+G), SOX plus blue light (SOX+B), SOX plus UV-A radiation (SOX+UVA), and SOX plus UV-A and UV-B radiation (SOX+UVA+UVB). The coloured lights (red, green, and blue) were provided by RGB light emitting diodes (LEDs), and ultraviolet radiation (UV-A and UV-B) by fluorescent lamps (Q-Panel UVA 340 LAMP H5B8, Canada). A UV-B filter foil (Lee-130) was used for SOX+UVA treatment. The radiation spectra of the lamps and LEDs are shown in Figure 40. SOX+UVA and SOX+UVA+UVB treatments showed a peak in the blue region of the spectrum (436 nm, Figure 40). Three flasks with algae were used for each treatment (three replicates, n=3).

Figura 40 - Spectra from different radiation sources, such as low pressure sodium (SOX) lamp, colored light (blue, green and red) emitting diodes (LEDs), and ultraviolet (UV) lamp.

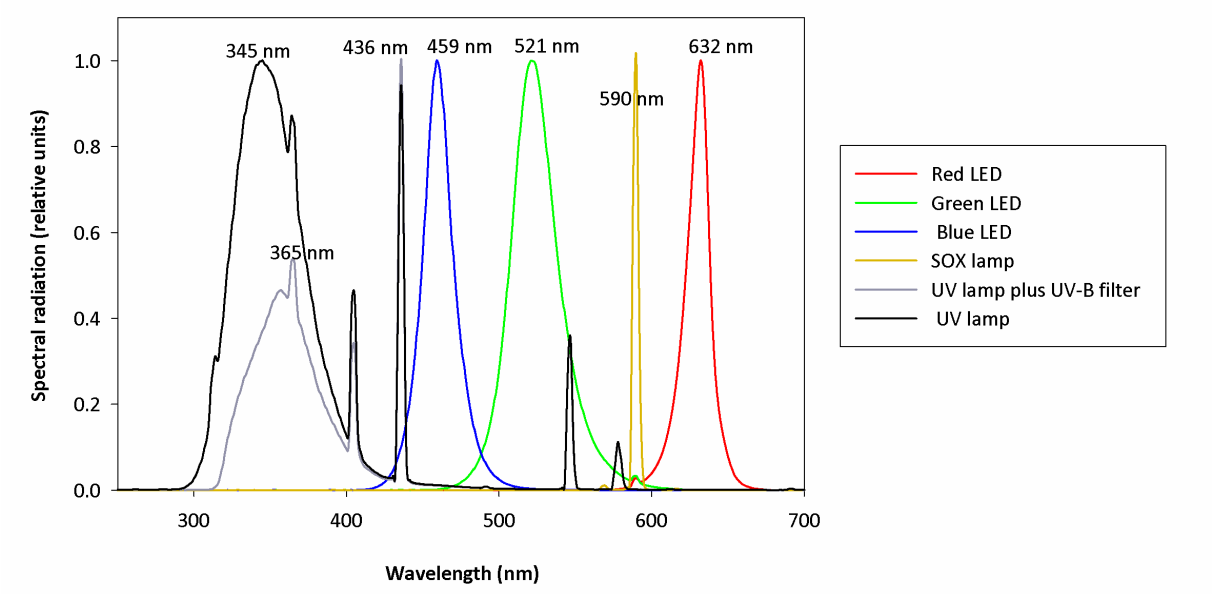

Radiation spectra (W m^{-2}) were measured with the Multidiode Spectroradiometer (Spectrometer Ocean Optics, USA, serial number: U5B2G13398), being normalized to the maximal value (relative units between 0-1). The main peaks are indicated for each radiation quality.

Radiation spectra in W m^{-2} were obtained with the Multidiode Spectroradiometer (Spectrometer Ocean Optics, USA, serial number: U5B2G13398). Photosynthetic active radiation (PAR, $\lambda = 400 - 700$ nm) in µmol photons m^{-2} s^{-1} was measured using a spherical PAR light sensor US-SQS (Walz GmbH, Germany) and LI-COR radiometer (LI-1000-Data Logger, LDL209 serial number, Licor Ltd, USA). The radiation data and the daily doses provided during the experiment in the different treatments are provided in the Table 8. During the experiment, the temperature (HOBO sensor), salinity (conductivity meter CRISON CM35+, Shilu Instruments COLTD) and pH (pH meter CRISON pH25+, Hach Longe Spain S.L.U) were also measured. Nutrients were analyzed by segmented flow analyser (SFA) using a Seal Analytical autoanalyzer QuAAtro following the methods described by Grasshoff et al. (GRASSHOFF; EHRHARDT; KREMLING, 1983). The detection limits of the inorganic nutrients were 0.05 µM for nitrates and phosphates.

Tabela 8 - Radiation data and daily doses provided for *G. cornea* during the experiment in different treatments.

Treatment	Irradiance						Daily doses of irradiance			
	SOX	LED	SOX	LED	UV-A	UV-B	PAR-SOX	PAR-LED	UV-A	UV-B
	µmol photons $m^{-2} s^{-1}$		W m^{-2}		W m^{-2}		Mol m^{-2}		KJ m^{-2}	
SOX	529 ± 71		29.6 ± 2.9				22.7 ± 2.6			
SOX+R	590 ± 66	17.6 ± 1.4	28.1 ± 3.5	0.77 ± 0.02			25.2 ± 2.6	0.76 ± 0.06		
SOX+G	606 ± 63	21.8 ± 2.3	32.2 ± 1.0	1.18 ± 0.15			26.1 ± 2.7	0.95 ± 0.10		
SOX+B	647 ± 69	25.5 ± 2.1	31.1 ± 6.6	3.71 ± 0.11			27.9 ± 2.2	1.12 ± 0.10		
SOX+UVA	597 ± 68		28.2 ± 4.5		3.4 ± 0.3	0.042 ± 0.004	25.6 ± 2.3		148 ± 13.8	1.84 ± 0.19
SOX+UVA +UVB	632 ± 71		30.7 ± 4.4		6.2 ± 0.2	0.507 ± 0.026	27.3 ± 2.6		269 ± 12.3	21.9 ± 1.13

Radiation UV-visible was emitted by low pressure sodium lamp (SOX) lamp, light emitting diode (LEDs) and ultraviolet (UV) fluorescent lamp (UV-A and UV-B). Photoperiod was of 12 h of light and 12 h of darkness. Data are mean ± standard deviation (n = 3). Treatments: SOX light (only lamp SOX); SOX+R (SOX lamp plus red LED); SOX+G (SOX lamp plus green LED); SOX+B (SOX lamp plus blue LED); SOX+UVA (SOX lamp plus UV lamp plus filter of UV-B); SOX+UVA+UVB (SOX lamp plus UV lamp).

Physiological and biochemical analyses were performed during the experiment. Algae growth rates were calculated from 1st to 8th day and from 8th to 15th day. In vivo chlorophyll *a* fluorescence was measured on the 1st, 4th, 8th, 11th, and 15th days of the experiment. The analyses of chlorophyll *a*, carotenoids, phycobiliproteins, mycosporine-like amino acids (MAAs), phenolic compounds, antioxidant activity (ABTS and DPPH assays) and soluble proteins were carried out with frozen algal biomass (-80℃) on the 1st, 8th, and 15th days of the experiment, except for MAAs that were evaluated with samples dried in silica gel on the same days. Nitrogen and carbon were evaluated on the 1st and 15th of the experiment. All analyses were performed in triplicates (n=3). To express the results in dry weight (DW), the percentage of water present in the algae tissues was previously calculated (≈87,50% of water and ≈12,49% dry biomass). The extraction of phycobiliproteins, phenolic compounds and proteins from algae tissues was performed as described in Schneider et al. (SCHNEIDER et al., 2020b).

6.3.3 Algae growth rates

To calculate the growth rates, the fresh algae tissue was dried with a paper towel to remove excess water and weighed in a precision analytical balance (Sartorius, Practum-1S). The values obtained were applied in the following equation (LIGNELL; PEDERSÉN, 1989):

$$GR\% = \left(\left(\frac{Fw_{\text{final}}}{Fw_{\text{initial}}} \right)^{\frac{1}{t}} - 1 \right) \times 100$$

where, GR% is percentage growth rate, FW_{final} is the final fresh weight (g), $FW_{initial}$ is the initial fresh weight (g) and t is time (days). Values were expressed as percent of fresh weight per day (% FW day^{-1}).

6.3.4 In vivo chlorophyll *a* fluorescence

Chlorophyll *a* fluorescence was measured using a Diving-PAM (Walz, Effeltrich, Germany). Saturation pulses were applied on the median portion of the algal thalli, during the experimental night and the day (after ≈ 4 h with the lamps on), to obtain maximal (F_m and F_m') and basal (F_o) or steady-state (F_t) fluorescence values. With these values, the maximum quantum yield of photosystem II - PSII (Fv/Fm) and the effective quantum yield of PSII (ΦPSII or Y(II)) were calculated (MAXWELL; JOHNSON, 2000). Φ_{PSII} values were applied in the following equation to calculate the electron transport rate (ETR, µmol electrons m^{-2} s^{-1}):

$$ETR = \Phi_{PSII} \times E \times A \times 0.15$$

Where, E is the irradiance to which the alga has been acclimated and A is the absorptance. The factor 0.15 is used to adjust the irradiance captured and used by Photosystem II (PSII) (FIGUEROA; CONDE-ÁLVAREZ; GÓMEZ, 2003; GRZYMSKI; JOHNSEN; SAKSHAUG, 1997). Absorptance (A) was calculated by the following equation:

$$A = 1 - \frac{E_F}{E_T}$$

Where, E_F is the irradiance transmitted through of the algae thalli and E_T is the total irradiance, measured with the LI-COR radiometer.

Maximum electron transport rate (ETR_{max}, µmol electrons m^{-2} s^{-1}), photosynthetic efficiency (α_{ETR}) and saturation irradiance (Ek_{ETR}, µmol photons m^{-2} s^{-1}) were calculated by fitting of the rapid light curves (RLC) according to Platt et al. (PLATT; GALLEGOS; HARRISON, 1980). The RLC were also obtained with saturation pulses combined with increasing actinic lights applied on the median portion of the algae thalli on the 8th and 15th days. To obtain the RLCs, the algae were previously maintained for 10 min in darkness.

6.3.5 Chlorophyll *a* and carotenoids

For extraction of chlorophyll *a* and carotenoids, extracts with 0.1 g of fresh biomass and 1 mL of dimethylformamide (DMF) were prepared, remaining in darkness overnight at 4 ℃ for 24 h. Later, the extracts were filtered (0.2 µm filters) and injected (80 µL) in the HPLC (high performance liquid chromatography) for analysis. The HPLC was equipped with a chromatographic column (Symmetry® C18 of 5-µm 4.16 x 150 mm column T91671L 02) and two mobile phases with flow of 1 mL min^{-1} for 40 min were used: (A) distilled water, ionic pair and methanol (1: 1: 1 ratio) and (B) acetone and methanol (1: 1 ratio). The ionic pair was prepared with tetrabutylammonium (0.05 M) and ammonium acetate (1 M). The gradient specifications are as described by Schneider et al. (SCHNEIDER et al., 2020b). The scan was between 350 and 800 nm and the pigment peaks were determined with a Waters Photodiode Array Detector. The identification of chlorophyll *a* and carotenoids (violaxanthin, antheraxanthin, zeaxanthin and β-carotene) was carried out comparing with commercial standards (DHI Water and Environment, Denmark). The quantification was performed according to Barufi et al. (BARUFI et al., 2011b). The results were expressed as µg per g of dry weight (µg g^{-1} DW).

6.3.6 Phycobiliproteins

Phycobiliproteins were extracted from algal thalli ground in liquid nitrogen with mortar and pestle, with addition of phosphate buffer (0.1M, pH 6.5). After the centrifugation of algal extracts (4000 rpm for 15 min), the supernatants obtained were read by UV-visible Spectrophotometer (Shimadzu UV Mini-1240) at 455 nm, 564 nm, 592 nm, 618 nm, 645 nm and 750 nm. Phycoerythrin (PE) and phycocyanin (PC) quantifications were carried out according to Beer and Eshel (BEER; ESCHEL, 1985) and the results were expressed as mg per g of dry weight (mg g^{-1} DW).

6.3.7 Mycosporine-like amino acids (MAAs)

Mycosporine-like amino acids (MAAs) analyses occurred as described by Karsten et al. (KARSTEN et al., 1998) and Korbee-Peinado et al. (KORBEE-PEINADO et al., 2004), with modifications. MAAs were extracted using samples dried in silica gel (20 mg dry weight). The algal thalli were inserted in 1 mL of 20% aqueous methanol (v/v) for 2 h at 45 ℃. The extracts

were prepared and centrifugation (4000 rpm at 4℃ for 10 min). The supernatants (700 µL) were evaporated in a vacuum centrifuge. After, the samples were resuspended (700 µL of 100% chromatographic methanol) and filtered using a syringe with a filter (0.22 µm). Twenty µL of filtered samples were injected into a HPLC equipped with a Luna C8 column (5 µm particle size and 250 x 4.6 mm diameter) and a precolumn (Phenomenex, Aschaffenburg, Germany) coupled to Waters (Barcelona, Spain) HPLC system. MAAs detection was performed with a Waters Photodiode Array Detector (Waters 996; Barcelona, Spain), using an isocratic flow gradient (1mL min^{-1}) of mobile phase containing 1.5 % aqueous methanol (v/v) and 0.15% acetic acid (v/v). The scan was done from 280 to 400 nm. MAA quantification was calculated using published extinction coefficients (DUNLAP; CHALKER; OLIVER, 1986; GLEASON, 1993; TAKANO; DAISUKE; YOSHIMASA, 1978; TAKANO; UEMURA; HIRATA, 1978; TSUJINO; YABE; SEKIKAWA, 1980) and the areas of the chromatographic peaks of each MAA (DE LA COBA et al., 2019). MAAs were identified using secondary standards as described by (DE LA COBA et al., 2019). The results were expressed as mg of MAAs per g of dry weight (mg g^{-1} DW).

6.3.8 Phenolic compounds

Phenolic compounds extracted from algae thalli were detected according to Folin-Ciocalteu (FOLIN; CIOCALTEU, 1927). Samples were read by UV-visible Spectrophotometer (Shimadzu UV Mini-1240) at 760 nm. For the quantification of the phenolics, a standard curve with phloroglucinol (Sigma P-3502) was prepared. Results were expressed as mg of phloroglucinol per g of dry weight (mg g^{-1} DW).

6.3.9 Antioxidant activity (ABTS and DPPH assays)

DPPH (2,2-diphenyl-1-picrylhydrasyl) radical scavenging activity was determined according to Brand-Williams et al. (BRAND-WILLIAMS; CUVELIER; BERSET, 1995). Antioxidant compounds extraction was performed with 0.2 g of fresh biomass and 2.5 mL of 80% methanol. The biomass was previously homogenized by mortar and pistil in liquid nitrogen. The extracts were mixed by vortex and remained overnight in darkness and at 4 ° C. In the following day, the extracts were centrifuged at 4000 rpm for 15 min and the supernatants were collected. The reaction was performed with 1000 µL of 80% methanol, 150 µL of DPPH

and 500 µL of the supernatant. The samples were stirred and maintained to stand by 30 min at room temperature. Readings were performed by UV-visible Spectrophotometer (Shimadzu UV Mini-1240) at 517 nm. One of the samples was prepared by replacing the extract with 80% methanol (blank). The antioxidant activity (AA) was calculated by the following equation:

$$AA\% = \left((A_{\text{before}} - A_{\text{after}}) \div A_{\text{before}}\right) \times 100$$

Where, AA% is the antioxidant activities expressed as percentage, A_{before} is the absorbance of the sample prepared before adding the extract (blank), A_{after} is the absorbance obtained after the addition of extract.

ABTS (2.2'-azino-bis, 3-ethylbenzothiazoline-6-sulphonic acid) method was performed according to Re et al. (RE et al., 1999), with modifications. For the extraction of antioxidant compounds, 0.05 g of fresh biomass and 1.2 mL of sodium phosphate buffer (0.1 M, pH 6.5) were used. The biomass was previously homogenized by mortar and pistil in liquid nitrogen. The extracts were vortexed and remained overnight in darkness at 4 °C. After, the extracts were centrifuged at 4000 rpm for 15 min and the supernatants were collected. The reaction to determine the antioxidant compounds was carried out as described by Schneider et al. (SCHNEIDER et al., 2020b). The samples were read by a UV-visible Spectrophotometer (Shimadzu UV Mini-1240) at 727 nm. Antioxidant activity was calculated using the following equation:

$$AA\% = \left((A_{0\text{min}} - A_{8\text{min}}) \div A_{0\text{min}}\right) \times 100$$

Where, AA% is the antioxidant activity expressed as percentage, A_{0min} is the initial absorbance, A_{8min} is the absorbance after 8 min.

The quantification of antioxidant compounds for the DPPH and ABTS assays was performed using the standard TROLOX (6-hydroxy-2,5,7,8-tetramethylchroman-2-carboxylic acid) curve. Results were expressed as µM of Trolox Equivalents (TE) per g of dry weight (µM $_{TE}$ g^{-1} DW).

6.3.10 Soluble proteins

Soluble proteins were extracted from algal thalli and detected according to the Bradford methodology (BRADFORD, 1976). In plastic cuvettes (2mL), 100 µL of extract, 700 µL of sodium phosphate buffer (0.1 M, pH 6.5) and 200 µL of the Biorad reagent were added. The solutions were stirred, remaining in the dark for 15 min. After, the samples were read by UV-visible Spectrophotometer (Shimadzu UV Mini-1240) at 595 nm. A standard curve with bovine seric albumin (BSA) was performed to quantify proteins. Results were expressed as mg of BSA per g of dry weight (mg g^{-1} DW).

6.3.11 Nitrogen and carbon

Total internal Carbon and Nitrogen analysis were performed using an elemental analyser (CNHS LECO-932, Michigan, USA), as described by Schneider et al. (SCHNEIDER et al., 2020b). Results were expressed as mg of carbon or nitrogen per g of dry weight (mg g^{-1} DW).

6.3.12 Statistical analysis

Tests of normality (Kolmogorov-Smirnov) and homogeneity of variances (Cochran) were applied on the data obtained. After, the factorial ANOVA (analyses of variance) was applied for growth rate, fluorescence parameters of chlorophyll *a* (F_v/F_m, ETR, α_{ETR}, ETR_{max} and EK_{ETR}), chlorophyll *a*, carotenoids, phycobiliproteins, mycosporine-like amino acids (MAAs), phenolic compounds, antioxidant activity (ABTS and DPPH), and soluble proteins. Time and treatment were the predictor variables in the factorial ANOVA. One-way ANOVA was applied only to internal total Carbon and Nitrogen, with treatment being the predictor variable. To identify the differences between the means, Student-Newman-Keuls (SNK) post-hoc test was used, with significance level of $p < 0.05$.

6.4 RESULTS AND DISCUSSION

During the experiment (15 days), abiotic parameters of the cultivation water were the following: temperature 24.0 ℃ ± 0.84, salinity 40.3 ± 1.63, pH 8.1 ± 0.26, and conductivity 62.6

mS cm^{-1} ± 2.28 (mean values including all treatments ± standard-deviations). The concentration of nutrients varied during experiment (ANEXO C, Table S. 5). Phosphate and nitrate were consumed, reaching significantly low values every 3-4 days of experiment in the different treatments.

Growth rates of *G. cornea* were the highest in SOX+UVA treatment from 1st to 8th day of the experiment, above 6% FW day^{-1}. In the second period (from 8th to 15th), the growth of algal thalli decreased statistically in SOX-only, SOX+B, SOX+UVA, and mainly in SOX+UVA+UVB which exhibited values below 2 % FW day^{-1} (Figure 41).

Figura 41 - *G. cornea* growth rates expressed as percentage of fresh weight per day (% FW day^{-1}).

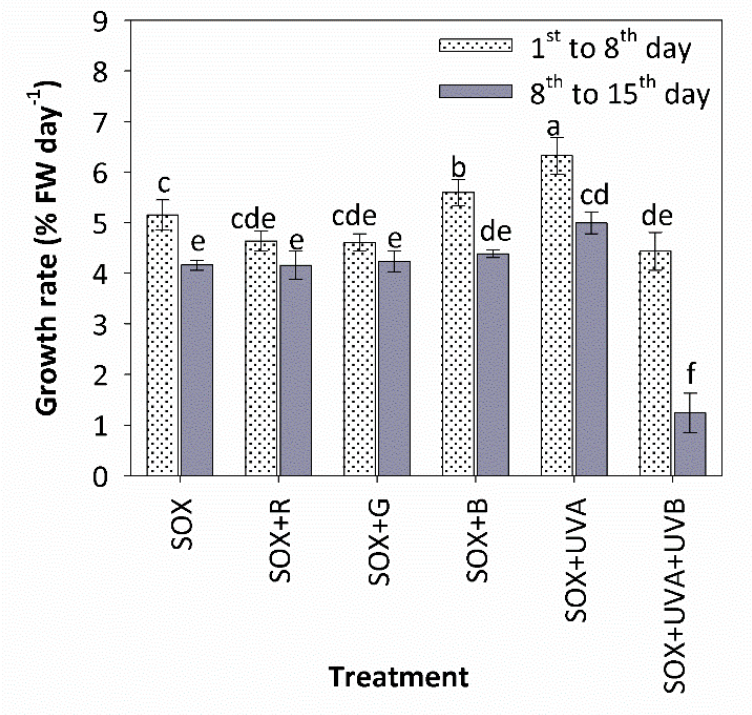

The growth rates were measured in different radiation treatments during the experiment (from 1st to 8th day and from 8th to 15th day). The letters indicate significant differences among the mean values, according to Newman-Keuls test ($p < 0.05$). Data are mean ± standard deviation (n = 3).

According to Cosgrove (COSGROVE, 1994), there are two ways by which light can influence plant growth. The first is through photosynthesis, which provides energy and assimilates that are basic resources for growth. The second is through photocontrol via photomorphogenic pigments. *Gracilaria gracilis* exhibited the highest growth rate under complementary red light (SOX+Red, 7.24% d^{-1}), followed by algae under blue light (SOX+Blue, 5.73% d^{-1}) and UV-A radiation (SOX+UVA, 5.25 day^{-1}) (GHEDIFA et al., 2021). In the study by Schneider et al. (SCHNEIDER et al., 2020b), *O. pinnatifida* showed the highest

growth rates under SOX+R, SOX+UVA and SOX+UVA+UVB from 1st to 8th day of experiment, and from 8th to 15th day all the treatments decreased, except SOX+UVA. In this study and Schneider et al. (SCHNEIDER et al., 2020b), the SOX+UVA and SOX+UVA+UVB treatments exhibited a peak in the blue region of the spectrum, which may have influenced the growth, since UV-A radiation and blue light are perceived by the cryptochrome photoreceptor (JIANG; LI, 2015). In the SOX+UVA treatment, the UV-A radiation or the synergy between UV-A and blue light seems to influence positively growth. The positive effect could be an indirect result of the activation pathways of photoprotection or DNA repair associated to cryptochrome or another photoreceptor, as discussed previously (SCHNEIDER et al., 2020b). To understand this, we supposed that one of the reasons for the reduction in the growth of *O. pinnatifida* and *G. cornea* from 8th to 15th day of experiment could be the excess light of the SOX lamp (present in all treatments). The presence of UV-A and/or blue light in SOX+UVA may have activated photoprotection pathways that favored the growth of algae under the SOX+UVA treatment in this study from 1st to 8th days and in Schneider et al. (SCHNEIDER et al., 2020b) throughout the experiment. Other studies suggest the involvement of UV-A radiation in mechanisms of DNA repair and growth enhancement (HENRY; ALSTYNE, 2004; PAKKER et al., 2000; PAKKER; BEEKMAN; BREEMAN, 2000). Pakker et al. (PAKKER et al., 2000; PAKKER; BEEKMAN; BREEMAN, 2000) showed the participation of UV-A and PAR (photosynthetically active radiation) in the repair of thymine dimmers and photoproducts after exposure to UV-B radiation in two red algae *Palmaria palmata* and *Rhodymenia pseudopalmata*. The formation of these dimmers can affect cell division and, therefore, growth rates (PAKKER; BEEKMAN; BREEMAN, 2000).

In the SOX+UVA+UVB treatment, the growth rates decreased significantly in the second period of the experiment in this study. This may be a result of the UV-B radiation, which has been associated with growth inhibition in algae, as described by Altamirano et al. (ALTAMIRANO; FLORES-MOYA; FIGUEROA, 2000) and Gao and Xu (GAO; XU, 2008). These authors had an improvement in growth rates when the UV-B radiation was cut, maintaining only UV-A and PAR. UV-B radiation was associated with the accumulation of photoprotective substances, such as MAAs and photosynthetic pigments (BONOMI-BARUFI et al., 2020; HOYER; KARSTEN; WIENCKE, 2002; KRÄBS et al., 2002). This accumulation can occur in detriment of growth. In other words, the algae driven energy to produce photoprotective substances instead of investing in growth when are under UV-B radiation.

Photosynthesis of *G. cornea* was evaluated through the *in vivo* chlorophyll *a* fluorescence (Table 9). The parameters examined showed greater variation over time than between treatments, since on the 15th day all treatments showed similar values. Electron transport rates (ETR) decreased in SOX+G and increased in SOX+UVA, comparing the 1st with the 15th day (Table 9). Maximum quantum yield of PSII (F_v/F_m) decreased significantly in all treatments during the experiment, whereas under SOX+UVA+UVB no significant variations were observed (Table 9). Changes in the F_v/F_m parameter can be interpreted as photoinhibition (ADAMS III et al., 2008; LONG; HUMPHRIES; FALKOWSKI, 1994), i.e., stress conditions for photosynthesis, such as excess of light or nutrient limitation. *G. cornea* was cultivated in the Grice Hutchinson Experimental Center of Malaga University under high solar radiation (from 800 to 1000 µmol photons m^{-2} s^{-1}). After collection for the experiment, the algae were previously acclimated for seven days under SOX light. Even so, they may have been photoinhibited during the experiment by the high intensity and/or emission quality (narrow peak at 590 nm) of SOX lamp. In relation to SOX+UVA+UVB, F_v/F_m showed no significant variations, therefore, changes in photosynthesis were not responsible for the sharp decline in growth in this treatment. As explained in Schneider et al. (SCHNEIDER et al., 2020b), we expected few changes in photosynthetic parameters, since photosynthesis was saturated with the high intensity light from the SOX lamp. The complementary radiations of low fluence aimed to promote photomorphogenic responses, regardless of photosynthesis.

Tabela 9 - Chlorophyll *a* fluorescence parameters measured in *G. cornea* during experiment with different radiation treatments.

Times		Treatments					
		SOX-only	**SOX+R**	**SOX+G**	**SOX+B**	**SOX+UVA**	**SOX+UVA+UVB**
ETR	1st day	6.10 ± 0.33^{bcd}	5.77 ± 0.98^{bcd}	8.23 ± 0.32^{a}	6.72 ± 1.28^{b}	2.20 ± 0.63^{e}	5.87 ± 1.30^{bcd}
	4th day	4.70 ± 0.98^{bcd}	2.26 ± 0.10^{e}	4.15 ± 0.31^{d}	4.18 ± 0.51^{d}	4.18 ± 0.67^{cd}	5.70 ± 1.30^{bcd}
	8th day	6.45 ± 0.47^{bcd}	6.34 ± 0.52^{bcd}	5.93 ± 0.42^{bcd}	6.22 ± 0.18^{bcd}	5.74 ± 0.72^{bcd}	5.88 ± 0.91^{bcd}
	11th day	4.20 ± 0.75^{d}	4.72 ± 0.10^{bcd}	4.70 ± 0.41^{bcd}	4.65 ± 0.86^{bcd}	4.43 ± 0.85^{bcd}	5.27 ± 0.15^{bcd}
	15th day	6.65 ± 0.54^{b}	5.87 ± 0.95^{bcd}	6.02 ± 0.79^{bcd}	6.54 ± 1.10^{bc}	5.61 ± 0.44^{bcd}	5.03 ± 0.70^{bcd}
Fv/Fm	1st day	0.53 ± 0.01^{ab}	0.56 ± 0.03^{a}	0.57 ± 0.01^{a}	0.57 ± 0.02^{a}	0.52 ± 0.02^{abcd}	0.48 ± 0.03^{abcdefg}
	4th day	0.47 ± 0.03^{abcdefg}	0.52 ± 0.01^{abc}	0.51 ± 0.03^{abcde}	0.49 ± 0.04^{abcdef}	0.40 ± 0.00^{fg}	0.37 ± 0.06^{g}
	8th day	0.45 ± 0.03^{bcdefg}	0.51 ± 0.02^{abcdef}	0.49 ± 0.03^{abcdef}	0.50 ± 0.03^{abcdef}	0.38 ± 0.01^{g}	0.41 ± 0.08^{cdefg}
	11th day	0.40 ± 0.03^{efg}	0.44 ± 0.02^{bcdefg}	0.44 ± 0.03^{bcdefg}	0.47 ± 0.04^{abcdefg}	0.37 ± 0.02^{g}	0.45 ± 0.06^{bcdefg}
	15th day	0.41 ± 0.06^{defg}	0.41 ± 0.04^{cdefg}	0.44 ± 0.01^{bcdefg}	0.44 ± 0.06^{bcdefg}	0.37 ± 0.06^{g}	0.44 ± 0.04^{bcdefg}
α_{ETR}	8th day	0.068 ± 0.010^{a}	0.072 ± 0.015^{a}	0.068 ± 0.002^{a}	0.075 ± 0.015^{a}	0.063 ± 0.011^{a}	0.071 ± 0.007^{a}
	15th day	0.057 ± 0.009^{a}	0.049 ± 0.008^{a}	0.063 ± 0.007^{a}	0.073 ± 0.011^{a}	0.072 ± 0.015^{a}	0.086 ± 0.009^{a}
ETR_{max}	8th day	23.6 ± 4.3^{ab}	16.4 ± 1.6^{b}	21.0 ± 3.2^{ab}	25.3 ± 3.6^{a}	27.7 ± 2.5^{a}	25.8 ± 3.8^{a}
	15th day	21.3 ± 1.5^{ab}	19.4 ± 1.9^{ab}	19.7 ± 2.6^{ab}	22.2 ± 2.2^{ab}	24.4 ± 1.9^{ab}	26.6 ± 2.5^{a}
EK_{ETR}	8th day	344.2 ± 21.1^{abc}	264.7 ± 37.7^{c}	307.3 ± 41.7^{abc}	338.9 ± 36.3^{abc}	404.8 ± 13.6^{ab}	364.8 ± 30.4^{abc}
	15th day	421.9 ± 45.7^{a}	401.9 ± 90.3^{ab}	314.3 ± 48.0^{abc}	304.8 ± 29.7^{abc}	388.4 ± 27.1^{abc}	275.0 ± 48.6^{bc}

Factorial ANOVA was performed (factors evaluated were time and treatments, ANEXO C, Table S. 6) and Newman-Keuls test ($p < 0.05$). Data are mean ± standard deviation ($n = 3$). Significant differences are indicated by different letters. ETR (electron transport rate, µmol electrons m^{-2} s^{-1}), F_v/F_m (maximum quantum yield of PSII), α_{ETR} (photosynthetic efficiency), ETR_{max} (maximum electron transport rate, µmol electrons m^{-2} s^{-1}) and Ek_{ETR} (saturation irradiance, µmol photons m^{-2} s^{-1}).

Chlorophyll *a* level in *G. cornea* decreased on the 8th (< 0.36 mg g^{-1} DW) and 15th days (< 0.26 mg g^{-1} DW) in relation to the 1st day (≈0.40 mg g^{-1} DW) of the experiment in all treatments. On the 15th day, the highest concentration of chlorophyll *a* was found in SOX+UVA+UVB (≈0.26 mg g^{-1} DW) and the lowest in SOX+UVA (≈0.15 mg g^{-1} DW) (Figure 42).

Figura 42 - Chlorophyll *a* concentration (mg g^{-1} DW) in *G. cornea* grown under different radiation treatments.

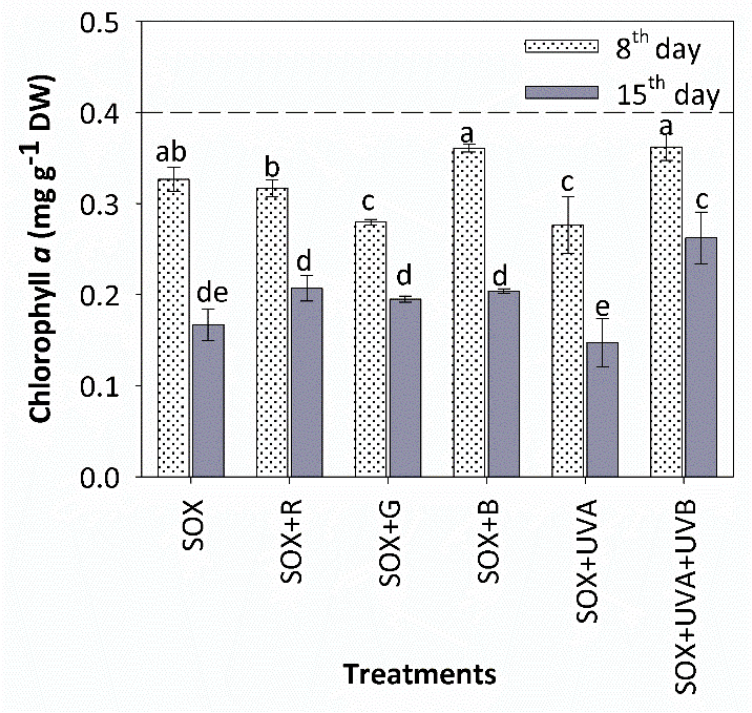

Chlorophyll concentration was analyzed on the 1st, 8th, and 15th day of the experiment. The dashed line shows the mean value of Chlorophyll *a* (0.40 µg g^{-1} DW) on the 1st day of the experiment. Factorial ANOVA was performed (factors evaluated were time and treatments, ANEXO C, Table S. 6) and Newman-Keuls test ($p < 0.05$). Data are mean ± standard deviation (n = 3). Significant differences are indicated by different letters.

Phycobiliprotein content in *G. cornea* also decreased during the experiment in all treatments. Initial values (1st day of the experiment) were about 0.35 mg g^{-1} DW for phycocyanin (PC) and 2.65 mg g^{-1} DW for phycoerythrin (PE), while on the 15th day, the algae showed values of PC and PE below 0.15 mg g^{-1} DW and 0.6 mg g^{-1} DW for all treatments, respectively (Figure 43 A and B). In the Figure 44, it is possible to verify the differences in the coloration of *G. cornea* thalli due to the decrease in PC and PE during the experiment. The thalli presented more reddish color on the collection date (Figure 44 A) compared to the 1st (Figure 44 B) and 15th days of the experiment (Figure 44 C, D, E, F, G and H).

Figura 43 - Phycobiliproteins concentration (mg g^{-1} DW) in *G. cornea* grown under different radiation treatments. Phycobiliproteins concentrations were analyzed on the 1st, 8th, and 15th day of the experiment.

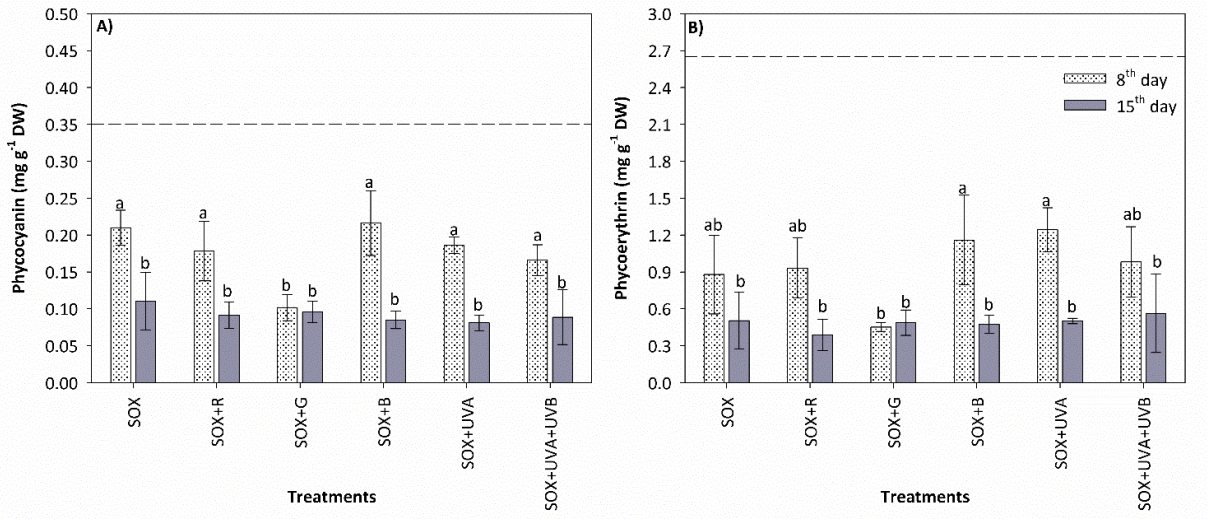

The dashed line shows the mean value of phycobiliproteins on the 1st day of the experiment, as follows: A) phycocyanin (0.35 ± 0.04 mg g^{-1} DW) and B) phycoerythrin (2.65 ± 0.76 mg g^{-1} DW). Factorial ANOVA was performed (factors evaluated were time and treatments, ANEXO C, Table S. 6) and Newman-Keuls test ($p < 0.05$). Data are mean ± standard deviation (n = 3). Significant differences are indicated by different letters.

Figura 44 - Coloration and morphology of *G. cornea* thalli in different times of the experiment.

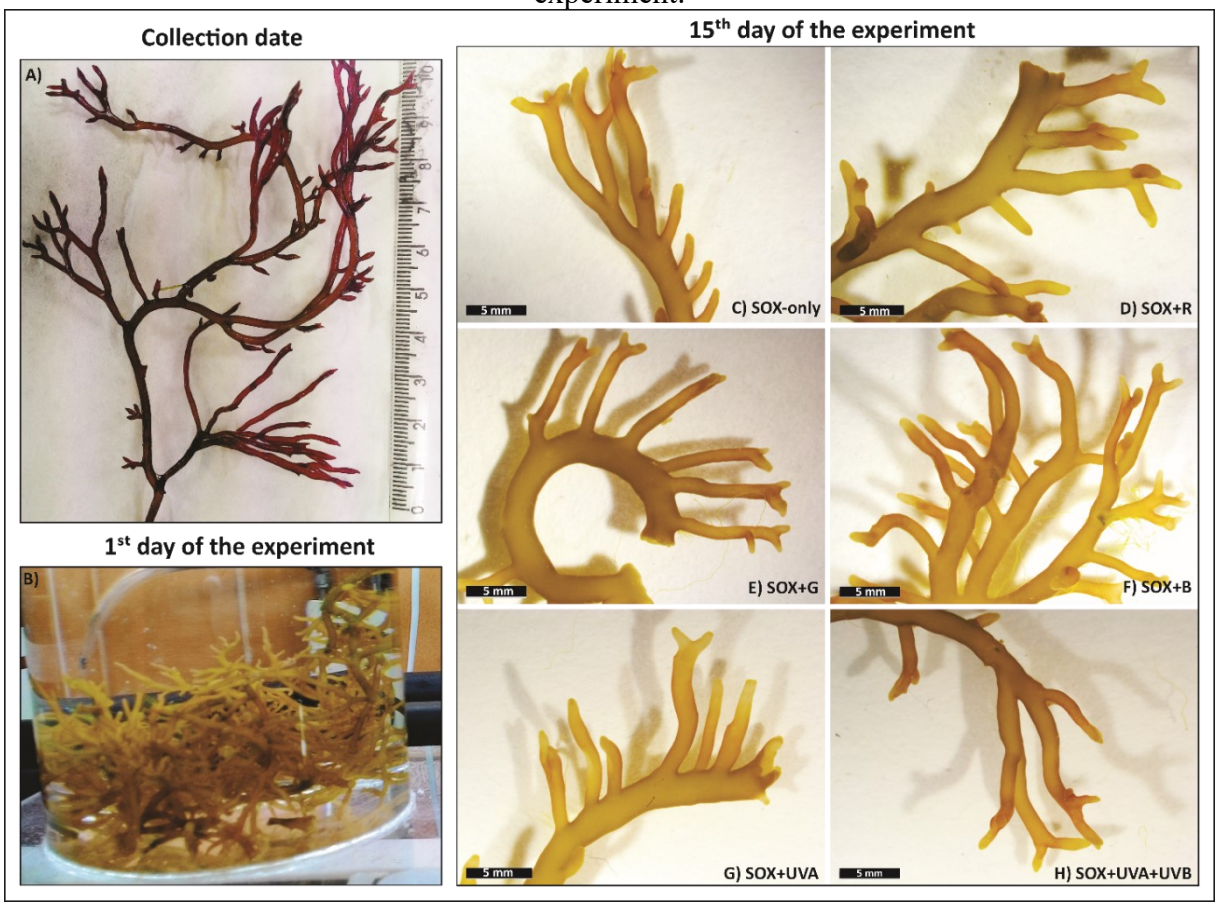

A) Collection date (from Grice Hutchinson Center); B) 1st day of the experiment, after acclimation period; C) 15th day, SOX-only; D) 15th day, SOX+R treatment; E) 15th day, SOX+G treatment; F) 15th day, SOX+B treatment; G) 15th day, SOX+UVA treatment; H) 15th day, SOX+UVA+UVB treatment.

Chlorophyll *a* is the main photosynthetic pigment, while phycobiliproteins are accessory pigments organized in phycobilisomes. These pigments have different light absorption peaks, such as chlorophyll *a* about 430 nm and 662 nm, PE about 560 nm, PC about 620 nm, and allophycocyanin (APC) about 650 nm (BJÖRN; GHIRADELLA, 2015; GROSSMAN et al., 1993). Although these absorption peaks can vary slightly, encompassing more nanometers, they are different from the narrow emission peak of the SOX lamp (590 nm, Figure 40), the light source for photosynthesis during experiment. Thus, algae would need to acclimate, allowing an improvement in the absorption of light available for photosynthesis. In Schneider et al. (SCHNEIDER et al., 2020b), *O. pinnatifida* showed a significant increase of PE in SOX+B (8th day) and SOX+G (15th day), which could be an attempt to improve the absorption of complementary light of low fluence, following one of the principles of chromatic adaptation. In this study, *G. cornea* did not follow the same principle, reducing the content of chlorophyll *a* and phycobiliproteins. Álvarez-Gómez et al. (ÁLVAREZ-GÓMEZ; KORBEE;

FIGUEROA, 2019) also carried out an experiment with *G. cornea* (at that time known as *Hydropuntia cornea*), which was collected in a greenhouse at the Spanish Bank of Algae. The initial values of PC (0.16 mg g^{-1} DW) and PE (0.79 mg g^{-1} DW) were lower than those obtained in this study. However, our values decreased considerably during the experiment, while in Álvarez-Gómez et al. (ÁLVAREZ-GÓMEZ; KORBEE; FIGUEROA, 2019) the content of PC and PE increased to 0.36 and 1.33 mg g^{-1} DW, after 14 days, under PAR radiation (provided by a fluorescent lamp) and receiving a high concentration of nutrients. Thus, in addition to light, the reduction and absence of nutrients can also have contributed to the reduction of pigments. Several studies indicate that the increase or decrease in pigment content is related to the availability of nutrients (BARUFI et al., 2011b, 2012; FIGUEROA et al., 2010). In this study, nutrients were quickly consumed by the algae, reaching significantly low values every 3-4 days of experiment (ANEXO C, Table S. 5).

Carotenoid concentration varied over time and radiation treatments (factorial ANOVA, ANEXO C, Table S. 6). Four types of carotenoids were detected in *G. cornea*, such as: violaxanthin, antheraxanthin, zeaxanthin and β-carotene (Figure 45 A, B, C and D). Violaxanthin, antheraxanthin and β-carotene were found in higher concentration in *G. cornea* in all treatments on the 8^{th} day compared to the 15^{th} day of the experiment, except β-carotene in SOX+UVA with low content in both periods (Figure 45 A, B and D). On the 8^{th} day, algae grown under SOX+UVA+UVB treatment showed the highest concentrations for the three carotenoids cited: violaxanthin (> 10 μg g^{-1} DW), antheraxanthin (> 60 μg g^{-1} DW) and β-carotene (> 5 μg g^{-1} DW), see Figure 45 A, B and D. Zeaxanthin content in algae was significantly higher on the 15^{th} day compared to the 8^{th} day in SOX-only and SOX+UVA. In SOX+UVA, zeaxanthin reached the highest values, above 50 μg g^{-1} DW (Figure 45 C). The concentration of this carotenoid was very high in all the treatments, comparing the values on the 15^{th} day with the initial value (1^{st} day).

Figura 45 - Carotenoid concentration (µg g^{-1} DW) in *G. cornea* grown under different radiation treatments.

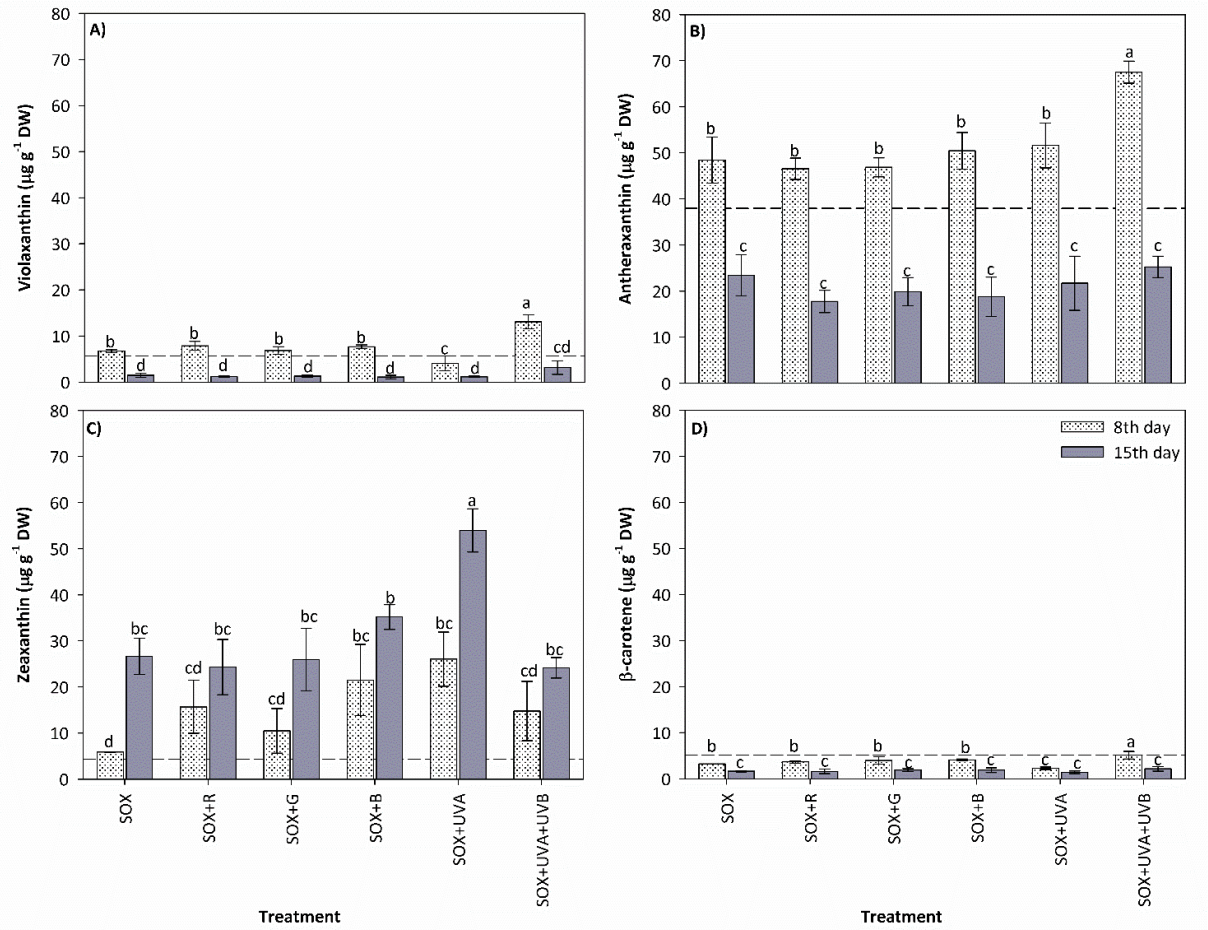

Carotenoid concentration was analyzed on the 1st, 8th, and 15th day of the experiment. The dashed line shows the mean value of carotenoids on the 1st day of the experiment, as follows: A) violaxanthin (8.32 ± 0.40 µg g^{-1} DW), B) antheraxanthin (37.96 ± 2.31 µg g^{-1} DW), C) zeaxanthin (4.33 ± 1.09 µg g^{-1} DW), and D) β-carotene (5.14 ± 0.61 µg g^{-1} DW). Factorial ANOVA was performed (factors evaluated were time and treatments, ANEXO C, Table S. 6) and Newman-Keuls test ($p < 0.05$). Data are mean ± standard deviation (n = 3). Significant differences are indicated by different letters.

In *Gracilaria* spp., carotenoids such as violaxanthin, antheraxanthin, zeaxanthin, β-cryptoxanthin and β-carotene were found, being antheraxanthin and zeaxanthin quantitatively superior (SCHUBERT; GARCÍA-MENDOZA; PACHECO-RUIZ, 2006). Except β-cryptoxanthin, the other carotenoids were also detected in this study. Carotenoids are also known as accessory pigments, which play important roles, such as light-harvesting and photoprotection (RASTOGI et al., 2010; SCHUBERT; GARCÍA-MENDOZA; PACHECO-RUIZ, 2006). Violaxanthin, antheraxanthin and zeaxanthin are especially important because they are part of the xanthophyll cycle (XC). In this cycle, under high light levels, violaxanthin is converted to zeaxanthin with antheraxanthin as an intermediate, process known as de-epoxidation. In the dark or under low light levels, the reverse process occurs (so-called

epoxidation). XC allows to dissipate the excess energy absorbed by the photosynthetic apparatus in plants (BJÖRN, 2015a). The presence of this cycle in red algae has been discussed (DAUTERMANN; LOHR, 2017; SCHUBERT; GARCÍA-MENDOZA; PACHECO-RUIZ, 2006), although the presence of the three XC carotenoids may be an indication of this cycle occurrence. In Figure 45, it is possible to verify that *G. cornea* exhibited a low content of violaxanthin during the experiment, but mainly on the 15th day for all treatments compared to the other periods (Figure 45 A). In addition, *G. cornea* showed the highest concentration of antheraxanthin on the 8th day and zeaxanthin on the 15th day in all treatments, but especially in SOX+UVA+UVB for antheraxanthin and SOX+UVA for zeaxanthin (Figure 45 B and C). These results are a strong indication that some photoprotection mechanism can be operating during the experiment, mainly in treatments with UV radiation, leading to zeaxanthin accumulation after 15 days of experiment. The accumulation of zeaxanthin under light stress in algae has been reported previously (SCHUBERT; GARCÍA-MENDOZA, 2008; SCHUBERT; GARCÍA-MENDOZA; PACHECO-RUIZ, 2006), although this accumulation is not always associated with XC.

MAAs content in *G. cornea* varied over time and treatments (ANOVA, ANEXO C, Table S. 6). Four types of MAAs were detected in *G. cornea*, such as: palythine, porphyra-334, palythinol and shinorine (Figure 46 A, B, C and D). Porphyra-334 and shinorine were the MAAs quantitatively superior in *G. cornea*, > 0.7 mg g^{-1} DW and > 0.4 mg g^{-1} DW, respectively (Figure 46 B and D). Palythine was found in higher concentration in algae grown under SOX+UVA and SOX+UVA+UVB. In the treatment with UV-B radiation, the concentration of palythine was above 0.04 mg g^{-1} DW (Figure 46 A). Total MAAs increased in all treatments on the 8th and 15th days compared to the initial value (1st day of the experiment), see Figure 46 A, B, C, D and E.

Figura 46 - Mycosporine-like amino acids (MAAs) concentration (mg g^{-1} DW) in *G. cornea* grown under different radiation treatments.

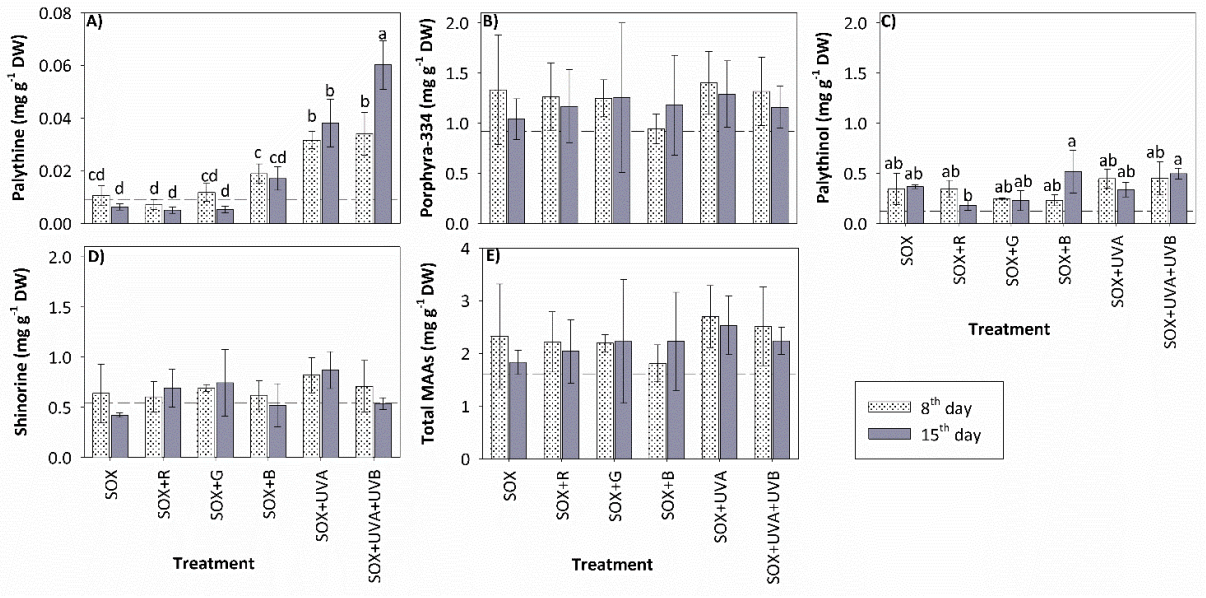

MAAs concentration was analyzed on the 1st, 8th, and 15th day of the experiment. The dashed line shows the mean value of MAAs on the 1st day of the experiment, as follows: A) palythine (0.009 mg g^{-1} DW), B) porphyra-334 (0.92 mg g^{-1} DW), C) palythinol (0.12 mg g^{-1} DW), D) shinorine (0.54 mg g^{-1} DW), and E) total MAAs (1.60 mg g^{-1} DW). Factorial ANOVA was performed (factors evaluated were time and treatments, ANEXO C, Table S. 6) and Newman-Keuls test ($p < 0.05$). Data are mean ± standard deviation (n = 3). Significant differences are indicated by different letters.

In previous studies, five types of MAAs were identified in *G. cornea*, such as palythine, porphyra-334, palythinol, shinorine and asterina-330 (ÁLVAREZ-GÓMEZ et al., 2019; ÁLVAREZ-GÓMEZ; KORBEE; FIGUEROA, 2019). We did not find asterina-330 in our study. The diversity and concentration of MAAs can vary in the same species depending on the radiation conditions (KARSTEN et al., 1999b). In this study, it was verified the accumulation of palythine in algae grown under UV radiation (SOX+UVA and SOX+UVA+UVB), as well as occurred in Álvarez-Gómez et al. (ÁLVAREZ-GÓMEZ; KORBEE; FIGUEROA, 2019). Production of MAAs in response to UV radiation has been verified in different species of algae (BONOMI-BARUFI et al., 2020; GHEDIFA et al., 2021; HOYER; KARSTEN; WIENCKE, 2002; KARSTEN et al., 1999b; KRÄBS et al., 2002). MAAs absorb certain wavelengths in the UV region of the spectrum, therefore, they appear to play a photoprotective role (LA BARRE; ROULLIER; BOUSTIE, 2014). In addition, PAR and UV radiation seem to have an important role in the interconversions of the different MAAs (BEDOUX et al., 2020; LA BARRE; ROULLIER; BOUSTIE, 2014; RASTOGI et al., 2010). The involvement of UV-A-type and blue light photoreceptors mediating the synthesis and/or accumulation of MAAs has been suggested in other studies (FRANKLIN; KRÄBS; KUHLENKAMP, 2001b; KRÄBS; WATANABE; WIENCKE, 2004). Interestingly in this

study, UV radiation (both UV-A and UV-B) promoted the accumulation of palythine, a MAA with high antioxidant activity and high capacity for photoprotection of DNA from human keratinocytes exposed to UV radiation, i.e., reduction of pyrimidine dimers (LAWRENCE et al., 2017). As these treatments also have a peak of blue light (Figure 40), it is possible that a photoreceptor sensitive to UV-A and blue light mediated this response, although palythine was the less abundant in comparison to the other three types found in *G. cornea*. In addition, the palythine variation by itself was not reflected in an increment of the total MAAs.

Phenolic compounds content increased in *G. cornea* in all treatments during experiment compared to the 1st day (Figure 47). The highest concentration of phenolics was found in algae grown under SOX+UVA+UVB on the 8th day. On the 15th day, phenolic value in SOX+UVA+UVB was similar to other treatments. Similar result occurred with *G. cornea* in Álvarez-Gómez et al. (ÁLVAREZ-GÓMEZ; KORBEE; FIGUEROA, 2019), i.e., an increase in the concentration of phenolics in the treatment with UV radiation on the 8th day followed by a decrease at the end of the experiment. In *G. gracilis* occurred accumulation of phenolic compounds under blue light (SOX+B) after two weeks (GHEDIFA et al., 2021). *O. pinnatifida* exhibited higher content of phenolics under complementary blue and green light (SOX+B and SOX+G) after eight days, and after fifteen days the values decreased, being similar to SOX-only (SCHNEIDER et al., 2020b). Phenolic compounds are a class of secondary compounds with several functions, including photoprotection (MACHU et al., 2015). The photoprotective role seems to have a strong relationship with the structure of these compounds, which are capable of donating electrons to neutralize reactive oxygen species (ROS) (PANGESTUTI; SIAHAAN; KIM, 2018; WANG et al., 2017). In this study, the phenolic levels in all treatments were higher during the experiment compared to 1st day. This may be a result of the stress caused by the quality and/or intensity of the light from SOX lamp (present in all treatments).

Figura 47 - Phenolic compounds concentration (mg g^{-1} DW) in *G. cornea* grown under different radiation treatments.

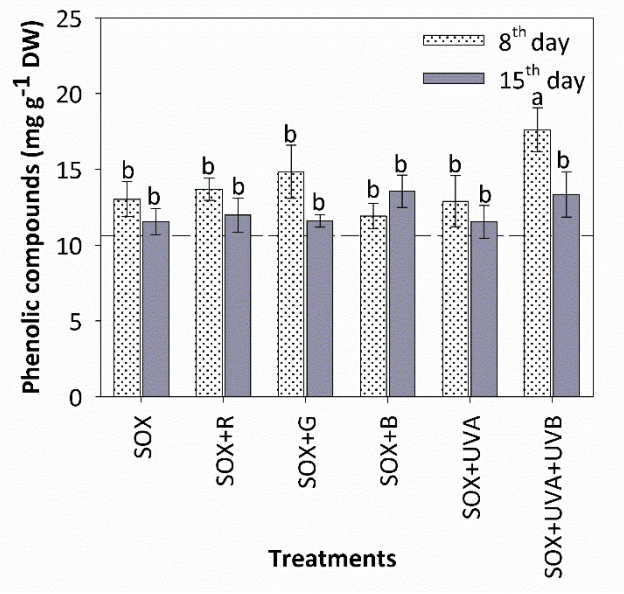

Phenolics concentration was analyzed on the 1st, 8th, and 15th day of the experiment. The dashed line shows the mean value of phenolics (10.62 mg g^{-1} DW) on the 1st day of the experiment. Factorial ANOVA was performed (factors evaluated were time and treatments, ANEXO C, Table S. 6) and Newman-Keuls test ($p < 0.05$). Data are mean ± standard deviation (n = 3). Significant differences are indicated by different letters.

DPPH assay showed that the antioxidant content in *G. cornea* was similar between treatments during experiment (1st, 8th, and 15th days, see Figure 48 A). ABTS assay detected a greater accumulation of antioxidant in algae under SOX-only on the 8th day, in SOX+UVA on the 8th and 15th days, and in SOX+UVA+UVB on the 15th day (Figure 48 B). Generally, antioxidant activity is associated with compounds that provide photoprotection to neutralize ROS. In Schneider et al. (SCHNEIDER et al., 2020a), algae species that showed the highest concentrations of phenolics and MAAs also showed the highest antioxidant activity. In another study also carried out with *G. cornea*, the antioxidant activity was correlated with the phenolics, proteins, and MAAs content (ÁLVAREZ-GÓMEZ; KORBEE; FIGUEROA, 2019). In the present study, antioxidant activity seems to have few relationships with phenolics, since SOX+UVA+UVB exhibited higher phenolic content on the 8th day and showed higher antioxidant activity on the 15th day. However, the antioxidant activity may be related to the concentration of MAAs (palythine) and carotenoids that were found in greater concentration in SOX+A and SOX+UVA+UVB during experiment.

Figura 48 - Antioxidant concentration (µMTE g^{-1} DW) evaluated by the DPPH and ABTS assays in *G. cornea* grown under different radiation treatments.

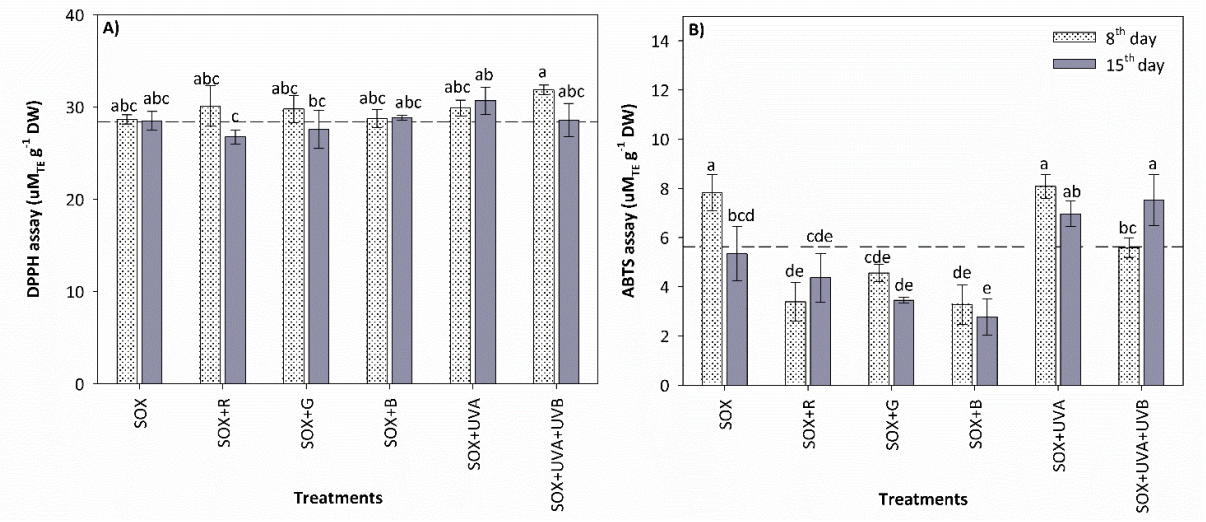

Antioxidant concentration was analyzed on the 1st, 8th, and 15th days. The dashed line shows the mean value of antioxidant on the 1st day of the experiment, as follows: A) DPPH assay (28.38 µMTE g^{-1} DW) and B) ABTS assay (5.63 µMTE g^{-1} DW). Factorial ANOVA was performed (factors evaluated were time and treatments, ANEXO C, Table S. 6) and Newman-Keuls test ($p < 0.05$). Data are mean ± standard deviation (n = 3). Significant differences are indicated by different letters.

Soluble proteins decreased in *G. cornea* in all treatments during the experiment compared to initial value (1st day). SOX+R, SOX+B and SOX+UVA remained slightly higher in relation to other treatments on the 8th day, although without statistical difference (Figure 49).

Figura 49 - Soluble proteins concentration (mg_{BSA} g^{-1} DW) in *G. cornea* grown under different radiation treatments.

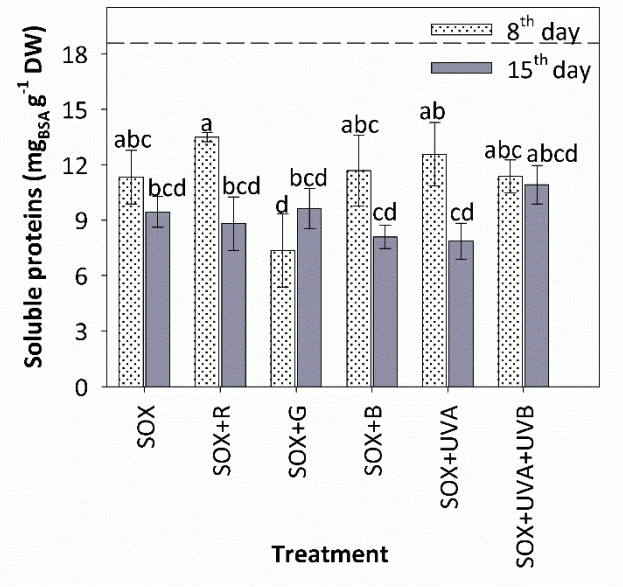

Protein concentrations was analyzed on the 1st, 8th, and 15th day of the experiment. The dashed line shows the mean value of proteins (18.58 mg_{BSA} g^{-1} DW) on the 1st day of the experiment. Factorial ANOVA was performed (factors evaluated were time and treatments, ANEXO C, Table S. 6) and Newman-Keuls test ($p < 0.05$). Data are mean ± standard deviation (n = 3). Significant differences are indicated by different letters.

Internal total Carbon and Nitrogen were evaluated on the 1st and 15th days of the experiment (Figure 50 A and B). The content of nitrogen in the algae was lower in all treatments on the 15th day compared to the 1st day (Figure 50 B). Carbon accumulation was higher in SOX-only and SOX+UVA+UVB compared to the other treatments on the 15th day (Figure 50 A). C:N ratio showed no significant differences between treatments. On the 15th day, the minimum and maximum average ratios were 14.02 ± 0.46 for SOX+G and 17.53 ± 1.66 for SOX+UVA, respectively. On the 1st day, the C:N ratio was 8.70 ± 0.43. The increase in the C:N ratio on the 15th day compared to the 1st day was due to a reduction in the N content. The decrease of internal N can be related to the decrease in soluble proteins. According to Figueroa et al. (FIGUEROA et al., 1995), proteins appear to constitute an internal nitrogen store to maintain growth during cultivation. Phycobiliproteins and chlorophyll were also proposed as proteins and nitrogen stores (LALEGERIE et al., 2019). In this study, there was a reduction in the content of chlorophyll, phycobiliproteins, soluble proteins and nitrogen in all treatments on the 8th and 15th day compared to the 1st day of the experiment. This may be associated with nutrients consumption, as the nitrate and phosphate were consumed after 3-4 days of experimental period. The nutrients have a strong relationship with the accumulation of pigments and proteins and with growth (ÁLVAREZ-GÓMEZ et al., 2017; KORBEE et al., 2005; NAVARRO et al.,

2014). C:N ratio is used to assess a possible limitation of algae growth by nitrogen (FIGUEROA et al., 1995). Ratios about 10 indicate an N-repleted state for macroalgae (DUARTE, 1992; FIGUEROA et al., 1995). We obtained high ratio (between 14 and 17) due to the decrease in nitrogen content. Thus, the decrease in algal growth during our experiment may be associated with a combination of different factors, such as: quality and/or high intensity of light from SOX lamp and depletion of nutrient storages.

Figura 50 - Carbon and elemental nitrogen (mg g^{-1} DW) in *G. cornea* grown under different radiation treatments.

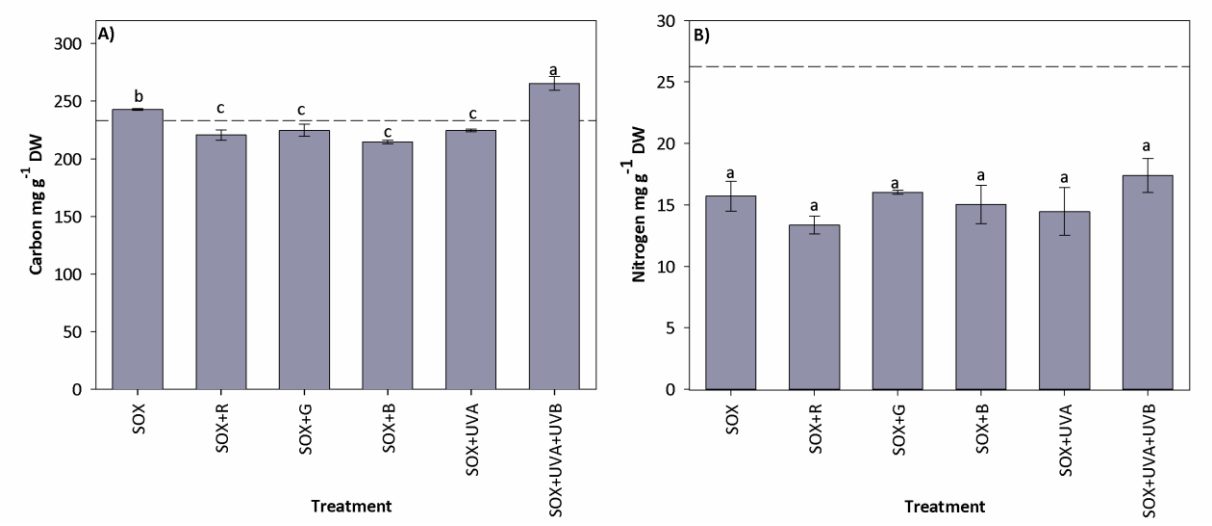

Carbon and nitrogen were analyzed on the 1st and 15th day of the experiment. The dashed line shows the mean value of carbon and nitrogen on the 1st day of the experiment, as follows: A) carbon (233.30 mg g^{-1} DW) and B) nitrogen (26.26 mg g^{-1} DW). One-way ANOVA was performed (factors evaluated was treatment, ANEXO C, Table S. 6) and Newman-Keuls test ($p < 0.05$). Data are mean ± standard deviation (n = 3). Significant differences are indicated by different letters.

Finally, in Table 10 it is possible to compare the results of analysis performed with *G. cornea* and *O. pinnatifida* (SCHNEIDER et al., 2020b) grown under different radiation treatments. *G. cornea* grew more than *O. pinnatifida* regardless of treatment, except on SOX+UVA+UVB (15th day). Chlorophyll *a* content was similar between species. *G. cornea* did not exhibit the carotenoid lutein. The concentration of antheraxanthin was higher in *G. cornea*, while zeaxanthin was much higher in *O. pinnatifida*. β-carotene was also higher in *O. pinnatifida*, except in the SOX+UVA+UVB treatment, in which the values were similar comparing the 8th day of *G. cornea* with the 15th day of *O. pinnatifida*. *G. cornea exhibited more total MAAs than O. pinnatifida*, mainly porphyra-334. The other MAAs showed similar values between species. Asterina-330 was found only in *O. pinnatifida*. Antioxidant activity was similar between species by the ABTS assay and higher in *G. cornea* by the DPPH assay.

Carbon content was greater in *O. pinnatifida* and nitrogen was similar between species. We did not observe a clear pattern of behaviour between the two species associated with different radiation treatments. Both species responded to UV radiation, UV-B associated with the accumulation of different compounds (depending on the species) in detriment of growth, and UV-A radiation inducing the accumulation of some compounds, but without severely affecting growth.

Tabela 10 - Results of physiological and biochemical analysis performed with *Osmundea pinnatifida* (SCHNEIDER et al., 2020b) and *Gracilaria cornea* (present study) grown under different radiation treatments.

	Treatment																							
	SOX				**SOX+R**				**SOX+G**				**SOX+B**				**SOX+UVA**				**SOX+UVA+UVB**			
	G. cornea		*O. pinnatifida*		*G. cornea*		*O. pinnatifida*		*G. cornea*		*O. pinnatifida*		*G. cornea*		*O. pinnatifida*		*G. cornea*		*O. pinnatifida*		*G. cornea*		*O. pinnatifida*	
	8th	**15th**	**8th**	**15th**	**8th**	**15th**	**8th**	**15th**	**8th**	**15th**	**8th**	**15th**	**8th**	**15th**	**8th**	**15th**	**8th**	**15th**	**8th**	**15th**	**8th**	**15th**	**8th**	**15th**
Growth rate (% FW day^{-1})	5.2	4.2	1.3	0.8	4.6	4.2	1.7	1.0	4.6	4.2	1.2	0.8	5.6	4.4	1.4	0.7	6.3	5.0	1.8	1.8	4.4	1.2	1.8	1.1
Chlorophyll *a* (mg g^{-1} DW)	0.3	0.2	-	0.1	0.3	0.2	-	0.2	0.3	0.2	-	0.2	0.4	0.2	-	0.2	0.3	0.1	-	0.1	0.4	0.3	-	0.2
Violaxanthin (µg g^{-1} DW)	6.7	1.5	-	2.3	7.9	1.2	-	2.4	6.9	1.3	-	2.4	7.6	1.1	-	4.4	4.0	1.2	-	1.5	13.1	3.1	-	3.3
Antheraxanthin (µg g^{-1} DW)	48.4	23.4	-	11.3	46.5	17.8	-	12.0	46.9	19.9	-	13.9	50.5	18.8	-	12.6	51.6	21.7	-	9.3	67.5	25.3	-	11.8
Zeaxanthin (µg g^{-1} DW)	15.9	26.6	-	49.5	7	24.3	-	67.6	10.5	26.0	-	65.1	21.5	35.2	-	66.5	26.0	54.0	-	64.7	14.8	24.2	-	105.0
Lutein (µg g^{-1} DW)	-	-	-	1.8	-	-	-	1.5	-	-	-	1.2	-	-	-	2.1	-	-	-	2.3	-	-	-	3.0
β-carotene (µg g^{-1} DW)	3.2	1.7	-	18.5	3.7	1.6	-	18.0	4.0	1.9	-	16.8	4.1	1.9	-	20.8	2.3	1.4	-	6.0	5.1	2.2	-	5.2
Phycocyanin (mg g^{-1} DW)	0.2	0.1	0.4	0.3	0.2	0.1	0.4	0.4	0.1	0.1	0.4	0.4	0.2	0.1	0.5	0.5	0.2	0.1	0.4	0.4	0.2	0.1	0.4	0.4
Phycoerythrin (mg g^{-1} DW)	0.9	0.5	0.1	0.1	0.9	0.4	0.3	0.6	0.5	0.5	0.1	0.8	1.2	0.5	0.8	0.3	1.2	0.5	0.4	0.5	1.0	0.6	0.3	0.2
Total MAAs *(mg g^{-1} DW)	2.3	1.8	0.7	0.6	2.2	2.0	1.1	0.5	2.2	2.2	1.2	0.4	1.8	2.2	1.1	0.5	2.7	2.5	1.0	1.0	2.5	2.2	0.9	0.9
Asterina-330 (mg g^{-1} DW)	-	-	0.2	0.2	-	-	0.3	0.1	-	-	0.3	0.1			0.3	0.2	-	-	0.2	0.3	-	-	0.2	0.3
Palythine (mg g^{-1} DW)	0.0	0.0	0.1	0.1	0.0	0.0	0.2	0.0	0.0	0.0	0.1	0.1	0.0	0.0	0.1	0.1	0.0	0.0	0.1	0.1	0.0	0.1	0.1	0.2
Palythinol (mg g^{-1} DW)	0.3	0.4	0.2	0.2	0.3	0.2	0.4	0.1	0.2	0.2	0.5	0.1	0.2	0.5	0.4	0.1	0.4	0.3	0.3	0.3	0.5	0.5	0.2	0.3
Shinorine (mg g^{-1} DW)	0.6	0.4	0.0	0.1	0.6	0.7	0.0	0.0	0.7	0.7	0.0	0.0	0.6	0.5	0.0	0.0	0.8	0.9	0.1	0.0	0.7	0.5	0.0	0.1
Porphyra-334 (mg g^{-1} DW)	1.3	1.0	0.1	0.1	1.3	1.2	0.2	0.1	1.2	1.3	0.2	0.1	0.9	1.2	0.2	0.1	1.4	1.3	0.2	0.2	1.3	1.2	0.2	0.2
Phenolic compounds (mg g^{-1} DW)	13.0	11.6	18.3	17.0	13.7	12.0	23.0	22.8	14.8	11.6	27.1	16.1	11.9	13.6	27.4	13.9	12.9	11.5	19.9	17.8	17.6	13.3	13.6	20.3
Soluble proteins (mg$_{BSA}$ g^{-1} DW)	11.3	9.4	7.5	7.3	13.5	8.8	7.7	8.7	7.4	9.6	6.5	8.3	11.7	8.1	9.1	7.5	12.6	7.9	7.9	6.5	11.4	10.9	7.0	7.7
ABTS assay (µM$_{TE}$ g^{-1} DW)	7.8	5.3	4.5	5.3	3.4	4.4	4.5	4.5	4.6	3.4	4.7	4.0	3.3	2.8	2.3	4.3	8.1	7.0	3.9	4.0	5.6	7.5	3.6	3.2
DPPH assay (µM$_{TE}$ g^{-1} DW)	28.6	28.5	14.2	13.7	30.1	26.7	11.1	12.8	29.8	27.6	11.0	14.2	28.7	28.9	12.1	14.0	29.9	30.7	12.5	16.2	31.9	28.6	10.8	14.2
Carbon (C) *(mg g^{-1} DW)	-	242.8	-	267.3	-	220.6	-	273.2	-	224.7	-	284.2	-	214.7	-	291.4	-	224.7	-	281.5	-	265.3	-	279.9
Nitrogen (N) *(mg g^{-1} DW)	-	15.7	-	15.5	-	13.4	-	17.6	-	16.0	-	17.8	-	15.0	-	17.4	-	14.5	-	15.9	-	17.4	-	16.2
C:N	-	16.1	-	17.4	-	16.5	-	15.5	-	14.0	-	16.2	-	15.3	-	16.8	-	17.5	-	17.7	-	14.9	-	17.4

* MAAs = Mycosporine-like amino acids.

6.5 CONCLUSIONS

This study aimed to verify physiological and biochemical changes mediated by photoreceptors in response to different radiation treatments in the red macroalga *Gracilaria cornea*. We observed generalized responses (in all treatments) that may have occurred due to factors, such as: quality and/or high intensity of light from SOX lamp and depletion of nutrient stores. These responses include decrease of growth, the F_v/F_m parameter associated with photosynthesis, photosynthetic pigments (chlorophyll and phycobiliproteins), soluble proteins, and elementary nitrogen levels. On the other hand, we observed specific responses that can be associated with the performance of photoreceptors, such as the highest growth in SOX+UVA (from 1st to 8th days) and the lowest in SOX+UVA+UVB (from 8th to 15th days), and the accumulation of carotenoids (violaxanthin, antheraxanthin, and zeaxanthin), MAAs (palythine), and phenolics in the same treatments. SOX+UVA and SOX+UVA+UVB had a peak of blue light. Thus, photoreceptors sensitive to UV-A and UV-B radiation and blue light may be involved in these responses. UV-A radiation and blue light appear to act positively on algae growth, but these radiations also induce the accumulation of compounds, such as carotenoids (zeaxanthin). In relation to UV-B radiation, it seems to act in the opposite direction to growth, i.e., directs the energies of algae to accumulation of compounds. Anyway, all these radiation qualities (UV-A, UV-B, and blue light) can be involved in photoprotection, either by accumulating pigments and/or by activating repair mechanisms. The SOX+B treatment did not show responses different of SOX-only in practically none of the analysis. This makes us suppose that UV radiation is essential and/or acts synergistically with blue light in the photoprotection responses. There are indications of the existence of photoreceptors sensitive to UV radiation in *G. cornea*. Sequencing molecular studies are needed to identify these photoreceptors. Comparing the responses of this study with those of the study carried out recently with the alga *O. pinnatifida*, we concluded that there was no clear pattern of behavior between species and associated with different radiation treatments. UV-radiation induces different compounds depending on the species, although for both species UV-A appears to induce compounds without affecting growth, while UV-B seems to cause the accumulation of compounds at the expense of growth.

7 CAPÍTULO IV

Photosynthesis, respiration, and calcification in the coralline alga *Lithophyllum hibernicum* Foslie 1906 (Corallinales, Rhodophyta) exposed to different irradiances

Geniane Schneider[*a], José Bonomi-Barufi[a], Félix L. Figueroa[b], Nathalie Korbee[b], João Silva[c], Rui Santos[c], Nadine Schubert[c], Paulo Antunes Horta[a]

[a] Phycology Laboratory, Botany Department, Federal University of Santa Catarina, 88049-900, Florianopolis, SC, Brazil.

[b] Universidad de Malaga, Instituto Universitario de Biotecnología y Desarrollo Azul (IBYDA). Departamento de Ecología, Campus Universitario de Teatinos s/n, 29071, Málaga, España.

[c] Marine Plant Ecology Research Group, Centre of Marine Sciences (CCMAR), University of Algarve, Faro, Portugal.

***Corresponding Author Address**
Geniane Schneider
E-mail: geniane.tega@gmail.com

Will be submitted in: *Marine Environmental Research*

7.1 ABSTRACT

Photosynthesis, respiration, and calcification are key processes in the physiology of some organisms, such as coralline red algae (CRA). In this work, we seek to understand these processes and their interactions under different levels of irradiances. For this, we performed photosynthetic light curves by measuring oxygen evolution in the alga *Lithophyllum hibernicum* (Rhodophyta), which collected inside and outside seagrass meadows in the Ria Formosa lagoon, South Portugal. As this alga had different pigmented sides or faces, we hypothesized that acclimation to the collection sites and different faces could also influence physiological responses. During the light curve, we measured oxygen, pH, temperature and collected samples to verify the carbonate chemistry and calculate calcification rates. These parameters translated chemical changes driven by photosynthesis, respiration, and calcification while the alga was exposed to increasing levels of light. We verified that parameters, such as temperature, pH, calcification, net O_2 flux, CO_3^{-2}, Ω calcite and Ω aragonite increased with increasing irradiance and were inversely related to AT, DIC, net CO_2 flux, HCO_3^-, CO_2 and pCO_2. O_2 production and CO_2 fixation (photosynthesis) were not influenced by faces or collection sites. Daily calcification rates were higher in rhodoliths collected inside seagrass meadows, although these results were strongly influenced by the dark calcification that is discussed. The presence of differently pigmented faces was confirmed by pigment analysis, i.e., chlorophyll *a*, carotenoids and MAAs were more concentrated on the face exposed to light (adaxial face) and phycobiliproteins, mainly phycoerythrin, were more concentrated on the face adjacent to the sediment (abaxial face) inside seagrass meadows.

Keywords: coralline algae, rhodoliths, calcification, photosynthesis, light curve

7.2 INTRODUCTION

The homeostasis of our biosphere, responsible to support of our biodiversity and humanity, is dependent of basic physiological process observed in microorganism and representatives of our fauna and flora, from cells to complex organisms (MONTGOMERY; TIPTON, 2019). Photosynthesis, respiration, and calcification are key biological processes observed in different ecosystems, in different groups and species, including peculiar group of marine primary producers, the coralline red algae (CRA). The interaction among these

processes and abiotic factors, in each different regions of thallus, drive the physiology of these algae, also resulting in changes in the surrounding environment. As already know, photosynthesis and respiration are complementary processes in relation to the fixation and release of carbon (carbon dioxide, CO_2), and release and consumption of oxygen (O_2). Photosynthesis standout as light dependent process, while the respiration as an uninterrupted process in all living tissue to support metabolic chemical demands. The primary metabolism of these organisms becomes more complex when we include calcification, which also consumes carbon ($CO_3^{-2} + Ca^{2+} \leftrightarrow CaCO_3$) and release hydrogen ions ($Ca^{2+} + HCO_3^- \leftrightarrow CaCO_3 + H^+$) and/or CO_2 ($Ca_2^+ + 2HCO_3^- \leftrightarrow CaCO_3 + CO_2 + H_2O$). The interaction of these processes alters carbonate system chemistry of the surrounding water. Variables, such as pH and the saturation state (Ω) of carbonate ion (CO_3^{-2}), increase when CO_2 is consumed by the photosynthesis, which favors calcification. Thus, theoretically, respiration and calcification act to reduce and photosynthesis to increase pH level. However, the result of these interactions is still dependent on other factors, as light and temperature (DE BEER; LARKUM, 2001; DONEY et al., 2009; HOFMANN; BISCHOF, 2014; HOFMANN; SCHOENROCK; DE BEER, 2018; MARTIN et al., 2013; MARTIN; CASTETS; CLAVIER, 2006; MARTIN; CHARNOZ; GATTUSO, 2013; MCCONNAUGHEY, 1991).

The relationship among photosynthesis, calcification and respiration have been investigated in several studies (DE BEER; LARKUM, 2001; EGILSDOTTIR; OLAFSSON; MARTIN, 2016; HOFMANN; SCHOENROCK; DE BEER, 2018; LEGRAND et al., 2019; MARTIN et al., 2013; MARTIN; CASTETS; CLAVIER, 2006; MARTIN; CHARNOZ; GATTUSO, 2013; MCCONNAUGHEY, 1991; NOISETTE et al., 2013; SEMESI; BEER; BJÖRK, 2009; SORDO et al., 2018). Beer and Larkum (DE BEER; LARKUM, 2001) and Hofmann et al. (HOFMANN; SCHOENROCK; DE BEER, 2018), using microsensors obtained oxygen, pH and CO_3^{-2} data from the algal surface under light–dark shifts. These studies showed a strong relationship between pH and calcification, and the pH was influenced by respiration and photosynthesis. Hofmann et al. (HOFMANN; SCHOENROCK; DE BEER, 2018) suggested mechanisms in arctic coralline algae that control surface chemistry, where active calcification occurs. Responses from photosynthesis, respiration and calcification to light were investigated by Martin et al. (MARTIN; CASTETS; CLAVIER, 2006) and Martin et al. (MARTIN et al., 2013). Calcification rates were strongly related to light in these studies. Semesi et al. (SEMESI; BEER; BJÖRK, 2009) showed that photosynthesis induced an increase in seawater pH in the seagrass meadows, and pH rise enhanced calcification rates of coralline algae growing within these meadows. This way, the interaction between photosynthesis and

calcification also occurs in an environmental scale, besides interaction described at the body plan.

In this study, we investigated the effects of different irradiances under the photosynthesis, respiration, and calcification of *Lithophyllum hibernicum* Foslie 1906, a non-geniculate CRA. These primary producers can grow on hard or soft substrates of organic or inorganic origin (AGUIRRE; BRAGA; BASSI, 2017). Growth can occur in all directions, completely covering the substrate and forming nodular structures called rhodoliths. Environmental particularities and ontogenetic characteristics result in different morphologies (subspherical, globular, or amoeboidal) and sizes (BOSELLINI; GINSBURG, 1971; BOSENCE, 1983). Rhodoliths are present in a wide variety of marine habitats, from arctic to tropical, ranging from shallow pools in intertidal areas to greater depths, limited to the photic zone because they are photosynthetic organisms (AGUIRRE; BRAGA; BASSI, 2017; BOSENCE, 1983). Rhodolith beds, formed by rhodolith groups or associations, are among the main benthic communities on Earth, with several ecological functions, as habitat and nursery for other taxa (CAVALCANTI et al., 2014; FOSTER, 2001). In addition, the rhodoliths act as bioengineering organisms, contributing significantly to primary production and deposition of carbon and carbonate (MARTIN et al., 2013; MARTIN; CASTETS; CLAVIER, 2006; MARTIN; CHARNOZ; GATTUSO, 2013; PEREIRA-FILHO et al., 2012b; TEICHERT; FREIWALD, 2014).

L. hibernicum was found in Ria Formosa lagoon, south of Portugal, forming rhodolith beds situated inside and outside the seagrass meadows. In addition, we observed that the rhodoliths had different sides, one facing the sediment, more pigmented, and the other facing sunlight, less pigmented or bleached. Thus, we hypothesized that the physiological responses of *L. hibernicum* vary in response to different irradiances and to different faces and collection sites, reinforcing the complementary perspective of the three basic physiological process in the thallus plan. In an environmental perspective, seagrass meadows canopy can provide environments with different intensities and qualities of light for *L. hibernicum*. In addition, seagrass primary production can induce variations in seawater pH, as verified by Semesi et al. (SEMESI; BEER; BJÖRK, 2009). Thus, it is possible that rhodoliths growing inside of seagrass meadows are acclimated to these variations (light and pH). Therefore, the physiological responses of rhodoliths inside meadows can vary in relation to rhodoliths growing outside seagrass meadows. We found no references in the literature about faces or sides in rhodoliths. The presence of faces in *L. hibernicum* due to differences in pigmentation

may be the result of the low energy of the waters of Ria Formosa, i.e., rhodoliths are not moved by water and remain in the same position for some time. This can result in differences in productivity, assuming that the faces are also physiologically different.

7.3 MATERIAL AND METHODS

7.3.1 Macroalgal and collection site

Specimens of *Lithophyllum hibernicum* Foslie 1906 (Rhodophyta) for this study were collected in Ria Formosa lagoon, located on the south coast of Portugal. *L. hibernicum* specimens were identified considering methods and characters described by Hernandez-Kantun et al. (HERNANDEZ-KANTUN et al., 2015). Ria Formosa is a large lagoon, formed by subtidal channels and tidal plains, with a total area of approximately 170 km^2. Tidal amplitude varies between 1.30 and 3.50 m. There are areas dominated by vascular plants, such as *Spartina maritima* (Curtis) Fernald and seagrasses, as *Cymodocea nodosa* (Ucria) Ascherson, *Zostera noltii* (Hornemann) and *Zostera marina* Linnaeus (RIBEIRO et al., 2006; SILVA et al., 2013; SILVA; SANTOS, 2003).

L. hibernicum was collected in May, in the spring, in different sites: inside (37°00'37.1"N 7°49'22.4"W) and outside (37°00'34.0"N 7°49'25.2"W) seagrass meadows (Figure 51). We identified the sites as: “rhodoliths/seagrass” and “rhodoliths”, respectively. In addition, the rhodoliths collected in different locations had different sides, the face adjacent to the sediment, more pigmented, which we identified as the abaxial face, and the face exposed to sunlight, less pigmented, which we identified as the adaxial face (Figure 51). In summary, the data were collected under four conditions: (I) rhodoliths/adaxial, (II) rhodoliths/abaxial, (III) rhodoliths/seagrass/adaxial and (IV) rhodoliths/seagrass/abaxial.

Figura 51 - Rhodolith collection site in Ria Formosa lagoon, Faro, Portugal.

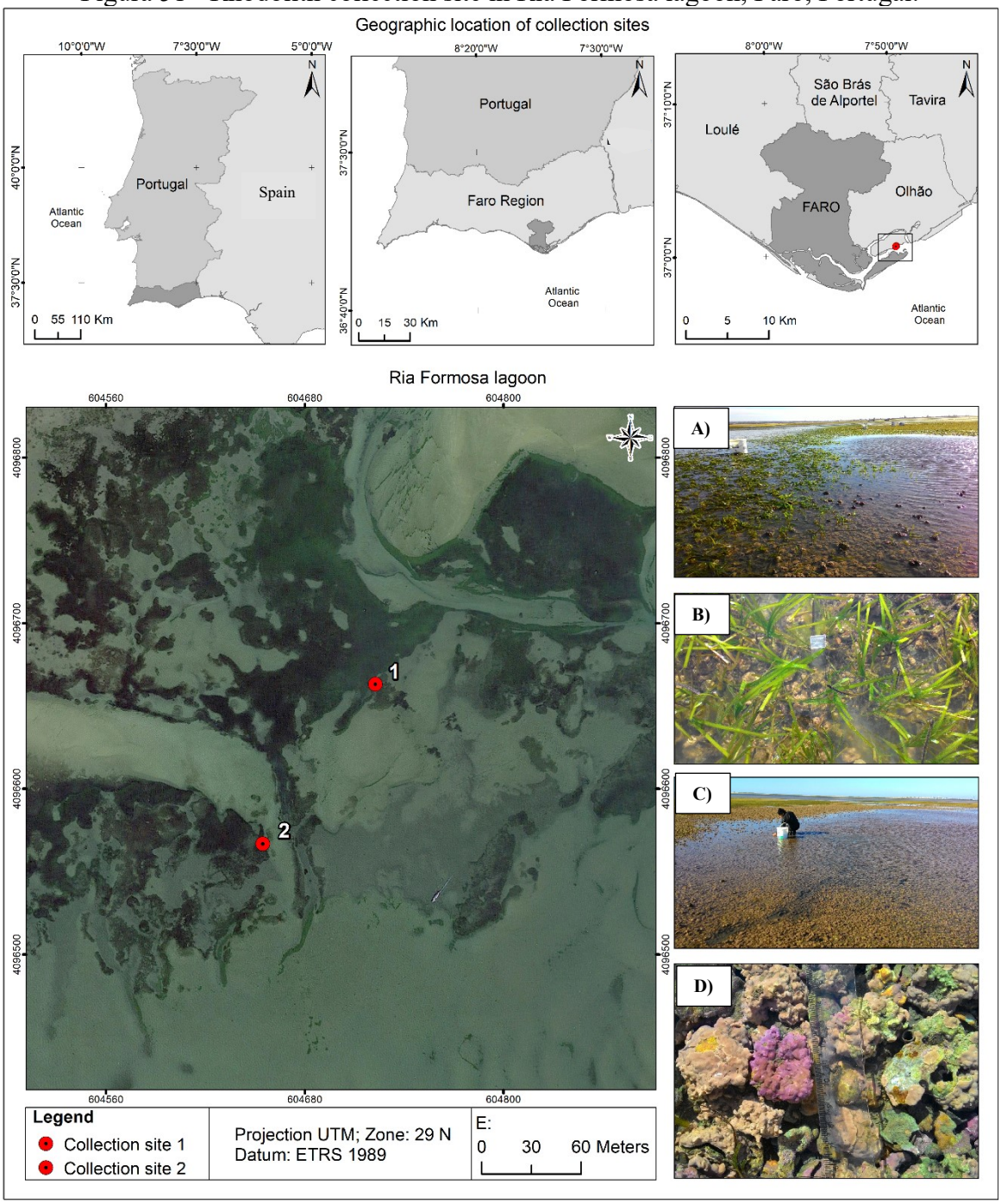

Collection sites 1: inside seagrass meadows (37°00'37.1"N 7°49'22.4"W), images A) and B) show the association between algae and seagrass. Collection sites 2: outside seagrass meadows (37°00'34.0"N 7°49'25.2"W), image C) showing rhodolith bed. In image D) it is possible to see different sides or face, differently pigmented.

The collected was carried out in natural pools formed during low tide, at 8 am. Environmental parameters were measured at different and random points near the collection sites, such as pH (Thermo scientific, Orion Star A221, Denver, Colorado), photosynthetic

active radiation (PAR) (LI-COR, LI-250-Lightmeter, U.S.A), and temperature (Pendant Temperature/Light 64K Data Logger). Measurements were performed in quintuplicates (n=5).

L. hibernicum (rhodoliths) samples, with similar sizes and shapes, were transported in boxes with local seawater from Ria Formosa to the laboratory located in the Centre of Marine Sciences (CCMAR), University of the Algarve. In the laboratory, the rhodoliths were cleaned with a brush to remove sediment and fauna. Afterwards, some rhodoliths were frozen at -80 °C and dried in silica gel to extract pigments and others were placed in aquariums. The aquariums were placed inside a culture chamber (Fotoclima 750E), for 24 h, under artificial irradiance around 25 μmol photons m^{-2} s^{-1} (Lexman LED lamp, E27) photoperiod of 12 h light: 12 h darkness, vigorous and constant aeration, and temperature around 19 °C.

7.3.2 Metabolic measurements

Metabolic rates of *Lithophyllum hibernicum* were measured through incubations performed in darkness and under different light intensities. Specimens of *L. hibernicum* were placed into transparent flasks filled with pre-filtered Ria Formosa water (about 140 mL) and sealed during incubation. Ten flasks were used with two rhodoliths each. Five flasks for rhodoliths collected outside seagrass meadows and five for rhodoliths collected inside of seagrass meadows (n=5). After 30 min in darkness, the rhodoliths were exposed to increasing levels of irradiances provided by LED lamps (Lexman LED, E27). Eight irradiances were obtained with shading screens, ranging from 10 to 1400 μmol photons m^{-2} s^{-1} (PAR). Irradiance measurements were performed with a quantometer (LI-COR, LI-250-Lightmeter, USA and sensor quantum, Q49612, USA). On the first day, a round of nine incubations with 30 min each was performed, positioning the adaxial face of the rhodoliths upwards (exposed to light from lamps). On the second day, the same process was repeated with rhodoliths abaxial face positioned upwards. During the incubations, the flasks were placed on a shaker (Edmund Bühler, Kreisschüttler KL-2) to provide constant movement, homogenizing the water. Measures of temperature, pH and dissolved oxygen were carried out before and after each incubation, using an oximeter (Microx 4, PreSens, Precision Sensing GmbH, Regensburg, Germany) and pH meter (Thermo scientific, Orion Star A221, Denver, Colorado). Between incubations, the water in the flasks was renewed by water from the original stock. Water samples from incubations were fixed with saturated mercuric chloride to measure total alkalinity (TA) and calcification rates.

Net photosynthesis (incubation in light) and respiration (incubation in darkness) were calculated from the differences between the final and initial concentrations of dissolved oxygen (O_2). We use the following formula (SORDO et al., 2018):

$$P_{net} \text{ or } R_d = \frac{\Delta O_2 \times V}{AB \times \Delta T}$$

where, P_{net} is net photosynthesis expressed by O_2 production and R_d is respiration rates in darkness expressed by O_2 uptake (µmol O_2 cm^{-2} h^{-1} or µmol O_2 g DW h^{-1}), ΔO_2 is the final concentration of dissolved oxygen minus the initial one (mg L^{-1} or µmol L^{-1}), V is water volume of incubation flasks (liters, L), AB is photosynthetic area or dry biomass of the algae (cm^2 or g), ΔT is the time of incubation (hours, h).

Calcification rates were determined using the alkalinity anomaly, this technique is based on the principle that each mole of precipitated $CaCO_3$ (calcium carbonate) results in a decrease of two moles in TA, 1:2 ratio (Smith, Kinsey 1975, Wolf-Gladrow et al. 2007). Alkalinity measurements were performed according to the modified spectrophotometric method of Yao and Byrne (YAO; BYRNE, 1998) and as described by Enríquez and Schubert (ENRÍQUEZ; SCHUBERT, 2014). For this, each sample (12mL) previously fixed with mercury chloride was divided into three aliquots of 4 mL (n=3). The aliquots were bubbled with N_2 from 5 to 10 min to remove CO_2. Afterwards, 3 mL of each aliquot and 10 µl of the bromocresol green indicator (3 mM; BCG; Sigma Aldrich, Steinheim, Germany) were added in plastic cuvettes (1cm length) positioned on a scale. The weight of the solution was recorded, with four digits of precision. The introduction of the acid solution (HCl 0.3N) into the sample was carried out at a rate of 480 µL.h^{-1}, for around 5 min, using a glass syringe (Hamilton Company, Reno, USA) fitted to a syringe pump (Kd Scientific Inc., Holliston, USA). During the microtitration, the cuvette was placed on a magnetic stirrer (BIG SQUID, IKA, 3672000) to homogenize the sample. Changes in sample color were continuously recorded by a spectroradiometer (Ocean Optics, USB2000+, Dunedin, USA) and using a xenon light source (PX-2, Ocean Optics, Dunedin, USA), at absorbances 444, 616 and 750 nm. Samples temperature was recorded high precision digital thermometer (Hanna, CHECKTEMP® 1 HI98509). Certified reference samples, with known AT, from the Marine Physical Laboratory (Scripps Institution of Oceanography, USA), were used to ensure the accuracy of the alkalinity values. AT calculations were performed according to Yao and Byrne (YAO; BYRNE, 1998).

The AT values were used to determine calcification rates. Calcification was calculated for light and dark incubations, according to Steller et al. (STELLER et al., 2007) equation, with modifications:

$$G \text{ or } G_d = \left(\frac{\Delta AT \times V \times 0.5}{AB}\right) \div \Delta T$$

where, G is the calcification in the light and G_d is the calcification in darkness (μmol $CaCO_3$ cm^{-2} h^{-1} or μmol $CaCO_3$ g^{-1} DW h^{-1}), ΔAT is the change in the total alkalinity during the incubation (μmol.Kg^{-1}).

Temperature, AT, pH and salinity data were plotted in the CO_2Sys software, version 2.1 (PIERROT; LEWIS; WALLACE, 2006), to calculate the dissolved inorganic carbon (DIC) in μmol kg^{-1} (see Table 11), as follows:

$$DIC = HCO_3^- + CO_3^{-2} + CO_2$$

The DIC was used to determinate the fixation or uptake of CO_2 (carbon dioxide) or C (carbon) for light and dark incubations, according to Martin et al. (MARTIN et al., 2013) and Egilsdottir et al. (EGILSDOTTIR; OLAFSSON; MARTIN, 2016):

$$FCO_{2\,net} \text{ or } R_{dCO2} = -\left(\frac{\Delta DIC \times V}{AB \times \Delta T} - G \text{ or } G_d\right)$$

where, $FCO_{2\,net}$ is the net fixation of CO_2 and R_{dCO2} is the respiration in darkness expressed by CO_2 release (μmol CO_2 cm^{-2} h^{-1} or μmol CO_2 g^{-1} DW h^{-1}), ΔDIC is the change in the concentration of dissolved inorganic carbon during the incubation (μmol kg^{-1}).

Graphs with the response curves or light curves were constructed using irradiance (E, μmol photons m^{-2} s^{-1}) versus photosynthesis (O_2), CO_2 fixation and calcification. Response curves were fitted by the equation of Platt et al. (PLATT; GALLEGOS; HARRISON, 1980), modified by addition of the respiration or calcification in darkness (R_d, R_{dCO2} or G_d), according to the following equation:

$$P_{net} \text{ or } FCO_{2\,net} \text{ or } G = Ps \times \left(1 - e^{\left(\frac{-\alpha \times E}{Ps}\right)}\right) \times e^{\left(\frac{-\beta \times E}{Ps}\right)} + R_d, R_{dCO2} \text{ or } G_d$$

where, Ps is the maximum value determined for the calculated parameter, i.e., P_{net} or $FCO_{2\,net}$ or G, in the absence of photoinhibition; α is the slope of the response curves; β is the photoinhibition coefficient.

The maximum estimated rate of net photosynthesis (P_{net}^{max}), or net CO_2 fixation (FCO_{2net}^{max}), or calcification (G^{max}), was performed using the equation:

$$P_{net}^{max} \text{ or } FCO_{2net}^{max} \text{ or } G^{max} = Ps \times \left(\frac{\alpha}{\alpha + \beta}\right) \times \left(\frac{\beta}{\beta + \alpha}\right)^{\frac{\beta}{\alpha}} + R_d, \text{ or } R_{dCO2} \text{ or } G_d$$

The maximum estimated rate of gross photosynthesis (P_{gross}^{max}) or gross CO_2 fixation (FCO_{2gross}^{max}) was performed using the equation:

$$P_{gross}^{max} = -R_d + P_{net}^{max}$$

$$FCO_{2gross}^{max} = -R_{dCO2} + FCO_{2net}^{max}$$

Saturation irradiance (E_k, μmol photons m^{-2} s^{-1}) and compensation irradiance (E_c, μmol photons m^{-2} s^{-1}) were calculated using the following equations (negative results were multiplied by -1):

$$E_k = \frac{P_{gross}^{max}}{\alpha} \text{ or } \frac{FCO_{2gross}^{max}}{\alpha} \text{ or } \frac{G^{max}}{\alpha}$$

$$E_c = \frac{R_d}{\alpha} \text{ or } \frac{R_{dCO2}}{-\alpha} \text{ or } \frac{G_d}{\alpha}$$

Daily primary productivity (DPP) and daily calcification rates (DGR) were estimated, considering a daily cycle with 12h light and 12h of dark. The following equations were used:

$$DPP(O_2) = (P_{net}^{max} \times 12) + (-R_d \times 12)$$

$$DPP(CO_2) = (-FCO_2^{max}_{net} \times 12) + (R_{dCO2} \times 12)$$

$$DGR(CaCO_3) = (G^{max} \times 12) + (G_d \times 12)$$

7.3.3 Dry biomass and photosynthetic area determination

To allow comparison with other studies, the data were normalized per dry biomass and photosynthetic area. Photosynthetic area estimation of *Lithophyllum hibernicum* was performed according to Hoegh-Guldberg (1988), with modifications. The rhodoliths from the incubations were dried at 60 ºC and weighed to obtain the dry biomass. After, a uniform layer of ink (water-based and quick-drying) was applied over the rhodoliths, correcting surface imperfections and porosity. After approximately 60 min, a second layer of ink was applied. The difference between the initial (after 1st layer ink) and final weight (after 2nd layer) was recorded. The same procedure was performed with Styrofoam blocks (n=30) of different sizes (between 1 cm^3 and 3 cm^3) and known surface area. Thus, the linear relationship between rhodoliths weight and Styrofoam blocks surface area was used to calculate the photosynthetic area of rhodoliths ($y = 0.0026x - 0.0038$; $R^2 = 0.9992$).

7.3.4 Photosynthetic Pigment and MAAs

Lithophyllum hibernicum samples collected in the field and stored at -80 ºC were used to extract pigments, such as: chlorophyll, total carotenoids and phycobiliproteins. Dry samples in silica gel were used to evaluate mycosporine-like amino acids (MAAs). Pigments were determined in five replicates (n=5) for each collection site (rhodoliths/seagrass and rhodoliths) and each face (abaxial and adaxial). To extract the pigments, the photosynthetic surface layer of the rhodoliths was scraped and photographed to determine the extraction area with the software ImageJ (ImageJ 1.52, National Institutes of Health, USA).

Chlorophylls (Chl*a*) and carotenoids were extracted with 1.5 mL of acetone 90% saturated with $CaCO_3$. Algae samples were ground with liquid nitrogen and homogenized with acetone. The extracts were maintained at 4 ºC in darkness for 3 h. After, they were centrifuged at 4000 rpm for 10 min. The supernatants were collected and read by a spectrophotometer (Beckman Coulter DU-650) at 480 nm, 647 nm, 664 nm e 750 nm. The quantification of chlorophylls and carotenoids was performed according to Ritchie (RITCHIE, 2006, 2008) and

Parsons and Strickland (PARSONS; STRICKLAND, 1963), respectively. The results were expressed as µg/cm², obtained by the following equations:

$$\text{Chl}a = 11.4711 \times (\text{A}_{664} - \text{A}_{750}) - 1.6841 \times (\text{A}_{647} - \text{A}_{750})$$

$$\text{Carotenoids} = 10 \times (\text{A}_{480} - \text{A}_{750})$$

where, A is absorbance and subscribed value is the wavelength (nm).

Phycobiliproteins extraction was performed with 1.2 mL of sodium phosphate buffer (0.1 M, pH 6.5) and algae samples previously ground with liquid nitrogen. The extracts were homogenized and maintained *overnight* at 4ºC. After this period, the extracts were centrifuged at 4500 rpm for 20 min. The supernatants were collected and read by a spectrophotometer at 498nm, 614nm, 651 nm and 750 nm. To quantify phycobiliproteins, calculations were performed according to Kursar et al. (KURSAR; VAN DER MEER; ALBERTE, 1983). The results expressed as µg/cm². Following equations used:

$$\text{Allophycocyanin (APC)} = 181.3 \times \text{A}_{651} - 22.3 \times \text{A}_{614}$$

$$\text{Phycocyanin (PC)} = 151.1 \times \text{A}_{614} - 99.1 \times \text{A}_{651}$$

$$\text{Phycoerythrin (PE)} = 155.8 \times \text{A}_{498} - 40.0 \times \text{A}_{614} - 10.5 \times \text{A}_{651}$$

Mycosporine-like amino acids (MAAs) were evaluated as described by Karsten et al. (KARSTEN et al., 1998) and Korbee-Peinado et al. (KORBEE-PEINADO et al., 2004). Extraction was performed with about 20 mg of dry biomass and 1 mL of 20% aqueous methanol (v/v), for 2 h at 45ºC, followed by centrifugation (4000 rpm at 4ºC for 10 min). The supernatant (700 µL) was evaporated in a vacuum centrifuge. After, the extract was resuspended in 700 µL of 100% chromatographic methanol. The samples were filtered using a syringe coupled to a filter (0.22 µm) and transferred to vials of HPLC (high-performance liquid chromatography). MAAs were detected by HPLC using an isocratic flow (0.5 mL. min^{-1}) containing 1.5 % aqueous methanol (v/v) and 0.15% acetic acid (v/v). Twenty µL of the filtrate were injected into a Sphereclone C8 column (5 µm particle size; 250 x 4.6 mm) and a precolumn

(Phenomenex, Aschaffenburg, Germany) coupled to a Waters (Barcelona, Spain) HPLC system. MAAs were detected with a Waters Photodiode Array Detector (996; Barcelona, Spain). The absorption spectra were recorded from 280 to 400 nm. MAAs were quantified and identified as described by De La Coba et al. (DE LA COBA et al., 2019).

7.3.5 Statistics

Firstly, the homogeneity of variances (Cochran) and normality (Kolmogorov-Smirnov) of the data were evaluated. After, the analyses of variance (factorial ANOVA) were performed with independent variables, such as sites (rhodoliths and rhodoliths/seagrass) and faces (adaxial and abaxial). Dependent variables included pigments (chlorophyll, total carotenoids and phycobiliproteins) and mycosporine-like amino acids (MAAs), and parameters calculated from response curves or light curves, such as photosynthesis (O_2), CO_2 fixation, and calcification ($CaCO_3$). The Student-Newman-Keuls (SNK) post-hoc test comparisons were applied to identify significant differences ($p < 0.05$). In addition, Permutational Multivariate Analysis of Variance (Permanova) was performed to test the factors, such as site, sides or faces, and irradiances. For this, the data were transformed, Log (x + 1), and a similarity matrix was calculated with Bray Curtis. After, the matrix was used in Principal Coordinates Analysis (PCO). The PCO included variables, such as temperature, pH, total alkalinity (AT), pCO_2, HCO_3^-, CO_3^{-2}, CO_2, DIC (dissolved inorganic carbon), calcite and aragonite saturation (Ω), Net fluxes (µmol CO_2 and O_2 cm^2 h^{-1}) and calcification (µmol $CaCO_3$ cm^{-2} h^{-1}), under different irradiances (darkness, 10, 25, 82, 154, 360, 651, 1002 and 1417 µmol photons m^{-2} s^{-1}). Pearson coefficient correlation among these variables and PCO axis were calculated. The softwares Statistica 7.0 (StatSoft. Inc.), Excel (Microsoft 365) and Primer 6 were used in above-described analyses.

7.4 RESULTS

During the collection of rhodoliths (*Lithophyllum hibernicum*) in Ria Formosa lagoon, some environmental parameters were measured. In places with seagrass and rhodoliths, the pH and water temperature were 8.16 ± 0.006 and 15.7 ºC ± 0.15, respectively. Where there were only rhodoliths, the pH was 8.09 ± 0.007 and the temperature was 16.3 ºC ± 0.30. Mean irradiance measured near the water surface was 1043 µmol photons m^{-2} s^{-1} ± 66.4.

Table 11 shows the physicochemical characteristics of the water used in the incubations performed with *L. hibernicum* in the dark and under different light intensities, and in the different conditions evaluated, such as rhodoliths/adaxial, rhodoliths/abaxial, rhodoliths/seagrass/adaxial and rhodoliths/seagrass/abaxial. It is possible to observe that the pH values remains equal or increase in relation to the initial value from 360 µmol photons m^{-2} s^{-1} for rhodoliths/adaxial, 82 µmol photons m^{-2} s^{-1} for rhodoliths/abaxial, 154 µmol photons m^{-2} s^{-1} for rhodoliths/seagrass/adaxial and 82 µmol photons m^{-2} s^{-1} for rhodoliths/seagrass/abaxial. Only rhodoliths/abaxial and rhodoliths/seagrass/abaxial reached pH (8.3) higher than initial values (8.2) (Table 11). Carbonate ion (CO_3^{-2}) values and the saturation state (Ω) of calcite and aragonite become higher than initial values from 360 µmol photons m^{-2} s^{-1} for all conditions (Table 11).

Tabela 11 - Temperature and carbonate chemistry from the original stock (initial values) and incubation water after 30 min exposed to darkness and different irradiances.

Conditions	Irradiance (µmol photons m^{-2} s^{-1})	Time	pH	Temperature (°C)	AT (µmol Kg^{-1})	pCO_2 (µatm)	HCO_3^- (µmol kg^{-1})	CO_3^{-2} (µmol kg^{-1})	CO_2 (µmol kg^{-1})	DIC (µmol kg^{-1})	Ω calcite	Ω aragonite
Stock water		**Initial value**	**8.2 ± 0.0**	**19.1 ± 0.0**	**2508.0 ± 4.0**	**303.1 ± 0.5**	**1904.2 ± 3.2**	**248.3 ± 0.4**	**10.0 ± 0.0**	**2162.5 ± 3.6**	**5.7 ± 0.0**	**3.7 ± 0.0**
Rhodoliths/ adaxial	Darkness	After 30 min	>8.0 ± 0.0	19.1 ± 0.4	<2532.2 ± 29.8	<472.5 ± 41.1	<2071.7 ± 26.6	>189.8 ± 13.3	<15.6 ± 1.3	<2277.1 ± 23.8	>4.4 ± 0.3	>2.8 ± 0.2
	10		>8.0 ± 0.0	18.7 ± 0.1	>2494.9 ± 26.8	<465.3 ± 18.4	<2047.5 ± 18.9	>183.8 ± 7.2	<15.6 ± 0.6	<2246.9 ± 21.2	>4.2 ± 0.2	>2.7 ± 0.1
	25		>8.0 ± 0.0	18.7 ± 0.2	>2505.7 ± 26.4	<451.6 ± 38.9	<2044.4 ± 37.5	>189.7 ± 10.8	<15.1 ± 1.3	<2249.1 ± 32.0	>4.4 ± 0.2	>2.8 ± 0.2
	82		>8.1 ± 0.0	18.7 ± 0.1	>2436.5 ± 27.7	<370.2 ± 23.6	<1932.7 ± 26.7	>206.0 ± 10.8	<12.4 ± 0.8	>2151.1 ± 24.7	>4.7 ± 0.2	>3.1 ± 0.2
	154		>8.1 ± 0.0	18.7 ± 0.1	>2410.9 ± 22.2	<318.5 ± 12.6	>1864.3 ± 20.4	>223.0 ± 6.4	<10.7 ± 0.4	>2098.0 ± 20.3	>5.1 ± 0.1	>3.3 ± 0.1
	360		>8.1 ± 0.0	19.2 ± 0.1	>2408.2 ± 65.7	<304.1 ± 13.6	>1838.7 ± 52.8	>232.4 ± 9.6	=10.0 ± 0.5	>2081.2 ± 59.0	>5.3 ± 0.2	>3.5 ± 0.1
	651		=8.2 ± 0.0	19.8 ± 0.2	>2320.1 ± 28.5	>251.3 ± 17.4	>1707.0 ± 41.1	<248.4 ± 9.1	>8.2 ± 0.6	>1963.6 ± 35.9	=5.7 ± 0.2	=3.7 ± 0.1
	1002		=8.2 ± 0.0	20.6 ± 0.2	>2282.7 ± 35.2	>227.4 ± 14.4	>1635.8 ± 38.5	<261.3 ± 8.8	>7.2 ± 0.5	>1904.4 ± 36.8	<6.0 ± 0.2	<3.9 ± 0.1
	1417		=8.2 ± 0.0	21.7 ± 0.3	>2282.3 ± 27.1	>233.3 ± 27.0	>1626.2 ± 53.2	<265.2 ± 14.6	>7.2 ± 0.8	>1898.6 ± 42.1	<6.1 ± 0.3	<4.0 ± 0.2
Stock water		**Initial value**	**8.2 ± 0.0**	**20.3 ± 0.3**	**2532.5 ± 4.8**	**283.6 ± 1.8**	**1874.8 ± 5.8**	**271.1 ± 1.1**	**9.1 ± 0.0**	**2155.1 ± 5.4**	**6.2 ± 0.0**	**4.1 ± 0.0**
Rhodoliths/ abaxial	Darkness	After 30 min	>8.1 ± 0.1	18.6 ± 0.2	>2496.5 ± 34.9	<380.3 ± 49.3	<1980.2 ± 37.8	>212.1 ± 22.5	<12.8 ± 1.7	<2205.1 ± 26.2	>4.9 ± 0.5	>3.2 ± 0.3
	10		>8.0 ± 0.0	18.7 ± 0.1	>2528.2 ± 26.2	<437.4 ± 35.0	<2050.0 ± 25.5	>197.0 ± 14.0	<14.7 ± 1.2	<2261.6 ± 20.6	>4.5 ± 0.3	>2.9 ± 0.2
	25		>8.0 ± 0.0	18.7 ± 0.1	>2476.7 ± 26.7	<418.3 ± 32.6	<1999.4 ± 26.4	>195.8 ± 13.1	<14.0 ± 1.1	<2209.2 ± 22.3	>4.5 ± 0.3	>2.9 ± 0.2
	82		>8.1 ± 0.0	18.7 ± 0.3	>2439.8 ± 31.7	<327.5 ± 16.0	<1892.4 ± 18.8	>223.9 ± 11.0	<11.0 ± 0.6	>2127.3 ± 21.9	>5.1 ± 0.3	>3.3 ± 0.2
	154		=8.2 ± 0.0	18.6 ± 0.2	>2437.5 ± 39.8	>264.4 ± 10.4	>1816.3 ± 32.4	>253.9 ± 6.6	>8.9 ± 0.3	>2079.1 ± 5.9	>5.8 ± 0.2	>3.8 ± 0.1
	360		=8.2 ± 0.0	18.9 ± 0.2	>2378.8 ± 38.7	>229.6 ± 12.7	>1723.1 ± 33.6	>266.8 ± 9.7	>7.6 ± 0.4	>1997.6 ± 35.0	>6.1 ± 0.2	>4.0 ± 0.1
	651		<8.3 ± 0.0	19.4 ± 0.3	>2363.6 ± 38.6	>209.4 ± 19.6	>1670.0 ± 49.4	<281.9 ± 12.0	>6.9 ± 0.6	>1958.8 ± 44.3	<6.5 ± 0.3	<4.2 ± 0.2
	1002		<8.3 ± 0.0	20.2 ± 0.2	>2376.1 ± 35.5	>203.9 ± 16.5	>1655.4 ± 44.5	<293.3 ± 9.5	>6.6 ± 0.5	>1955.2 ± 40.7	<6.8 ± 0.2	<4.4 ± 0.1
	1417		<8.3 ± 0.0	21.3 ±0.2	>2365.2 ± 43.4	>202.3 ± 21.7	>1626.1 ± 63.9	<300.7 ± 13.3	>6.3 ±0.7	>1933.1 ± 55.7	<6.9 ± 0.3	<4.5 ± 0.2
Stock water		**Initial value**	**8.2 ± 0.0**	**19.1 ± 0.0**	**2508.0 ± 4.0**	**303.1 ± 0.5**	**1904.2 ± 3.2**	**248.3 ± 0.4**	**10.0 ± 0.0**	**2162.5 ± 3.6**	**5.7 ± 0.0**	**3.7 ± 0.0**
Rhodoliths/ seagrass /adaxial	Darkness	After 30 min	>8.0 ± 0.0	18.9 ± 0.1	>2459.6 ± 15.7	<464.2 ± 47.5	<2016.3 ± 29.4	>181.7 ± 14.0	<15.4 ± 1.6	<2213.4 ± 19.6	>4.2 ± 0.3	>2.7 ± 0.2
	10		>8.0 ± 0.0	18.9 ± 0.1	>2450.9 ± 11.7	<478.4 ± 35.9	<2020.4 ± 22.3	>176.3 ± 10.8	<15.9 ± 1.2	<2212.7 ± 14.6	>4.1 ± 0.2	>2.6 ± 0.2

Conditions	Irradiance (µmol photons m^{-2} s^{-1})	Time	pH	Temperature (°C)	AT (µmol Kg^{-1})	pCO_2 (µatm)	HCO_3^- (µmol kg^{-1})	CO_3^{-2} (µmol kg^{-1})	CO_2 (µmol kg^{-1})	DIC (µmol kg^{-1})	Ω calcite	Ω aragonite
	25		>8.0 ± 0.0	19.0 ± 0.1	>2420.4 ± 23.9	<416.2 ± 30.5	<1954.9 ± 15.9	>190.2 ± 11.5	<13.8 ± 1.0	>2159.0 ± 14.4	>4.4 ± 0.3	>2.8 ± 0.2
	82		>8.1 ± 0.0	18.9 ± 0.1	>2382.2 ±23.9	<348.5 ± 13.1	>1872.9 ± 24.9	>207.4 ± 4.5	<11.6 ± 0.4	>2091.9 ± 24.6	>4.8 ± 0.1	>3.1 ± 0.1
	154		>8.1 ± 0.0	18.9 ± 0.1	>2370.4 ± 24.2	<322.8 ± 16.4	>1840.0 ± 24.3	>215.8 ± 7.9	<10.8 ± 0.6	>2066.6 ± 23.1	>5.0 ± 0.2	>3.2 ± 0.1
	360		=8.2 ± 0.0	19.2 ± 0.2	>2319.9 ± 30.3	>278.1 ± 14.0	>1751.2 ± 32.2	>230.4 ± 7.9	>9.2 ± 0.5	>1990.7 ± 30.8	>5.3 ± 0.2	>3.4 ± 0.1
	651		=8.2 ± 0.0	20.0 ± 0.1	>2275.4 ± 24.0	>227.7 ± 16.6	>1641.3 ± 35.4	<255.9 ± 9.4	>7.4 ± 0.5	>1904.6 ± 30.1	<5.9 ± 0.2	<3.8 ± 0.1
	1002		=8.2 ± 0.0	20.8 ± 0.2	>2267.3 ± 29.7	>229.8 ± 26.2	>1625.4 ± 44.9	<259.0 ± 18.1	>7.3 ± 0.8	>1891.7 ± 34.0	<6.0 ± 0.4	<3.9 ± 0.3
	1417		=8.2 ± 0.0	22.4 ± 0.1	>2310.5 ± 34.6	>223.2 ± 25.5	>1615.3 ± 50.8	<281.8 ± 17.1	>6.8 ± 0.8	>1903.8 ± 41.3	<6.5 ± 0.4	<4.3 ± 0.3
Stock water		**Initial value**	**8.2 ± 0.0**	**20.3 ± 0.3**	**2532.5 ± 4.8**	**283.6 ± 1.8**	**1874.8 ± 5.8**	**271.1 ± 1.1**	**9.1 ± 0.0**	**2155.1 ± 5.4**	**6.2 ± 0.0**	**4.1 ± 0.0**
Rhodoliths/ seagrass/ abaxial	Darkness	After 30 min	>8.0 ± 0.0	18.6 ± 0.2	>2432.3 ± 23.3	<438.8 ± 42.3	<1983.4 ± 19.6	>183.5 ± 15.1	<14.7 ± 1.4	<2181.6 ± 12.0	>4.2 ± 0.3	>2.7 ± 0.2
	10		>8.0 ± 0.0	18.9 ± 0.1	>2424.6 ± 21.4	<466.4 ± 42.8	<1979.3 ± 27.7	>182.0 ± 13.2	<14.28 ± 1.4	<2176.2 ± 20.8	>4.1 ± 0.3	>2.7 ± 0.2
	25		>8.0 ± 0.0	19.0 ± 0.1	>2412.2 ± 19.5	<403.8 ± 30.5	<1939.3 ± 23.0	>193.1 ± 11.3	<13.4 ± 1.0	>2145.8 ± 17.7	>4.4 ± 0.3	>2.9 ± 0.2
	82		>8.1 ± 0.0	19.0 ± 0.2	>2398.7 ± 26.9	<328.0 ± 17.0	>1861.9 ± 13.2	>218.9 ± 10.5	<10.9 ± 0.6	>2091.7 ± 16.0	>5.0 ± 0.2	>3.3 ± 0.2
	154		=8.2 ± 0.0	18.7 ± 0.2	>2374.1 ± 19.0	>267.3 ± 10.9	>1779.2 ± 15.2	>242.0 ± 7.2	>8.9 ± 0.3	>2030.1 ± 15.0	>5.6 ± 0.2	>3.6 ± 0.1
	360		=8.2 ± 0.0	18.9 ± 0.1	>2374.1 ± 25.2	>236.6 ± 10.8	>1732.2 ± 26.7	>261.0 ± 7.0	>7.8 ± 0.4	>2001.2 ± 25.5	>6.0 ± 0.2	>3.9 ± 0.1
	651		<8.3 ± 0.0	19.4 ± 0.1	>2337.3 ± 35.7	>201.0 ± 15.6	>1640.9 ± 41.6	<282.4 ± 10.4	>6.6 ± 0.5	>1929.9 ± 38.5	<6.5 ± 0.2	<4.2 ± 0.2
	1002		<8.3 ± 0.0	20.4 ± 0.2	>2325.2 ± 28.5	>203.4 ± 19.9	>1622.0 ± 47.5	<285.0 ± 9.9	>6.5 ± 0.6	>1913.5 ± 40.2	<6.6 ± 0.2	<4.3 ± 0.1
	1417		<8.3 ± 0.0	22.4 ± 0.4	>2322.4 ± 22.3	>211.9 ± 24.1	>1602.2 ± 43.5	<292.1 ± 15.7	>6.4 ± 0.7	>1900.7 ± 32.1	<6.8 ± 0.4	<4.4 ± 0.2

The incubations were performed with rhodoliths collected outside and within seagrass meadows, and both faces: adaxial (exposed to sunlight) and abaxial (adjacent to the sediment). Temperature, pH and total alkalinity were measured, and other chemical parameters were calculated with the CO_2Sys software. Mean ± standard-deviation (n=5). DIC (dissolved inorganic carbon) was calculated by adding HCO_3^-, CO_3^{-2} and CO_2. Symbols indicate that the initial values (stock water) are higher (>), lower (<) or equal (=) to curve values. Saturation state (Ω).

Results of the ANOVA factorial are shown in Table 12. Among the photosynthetic parameters (Table 12), calculated from the light curve (O_2 versus irradiance), only the maximum net photosynthesis (P_{net}^{max}) per cm² exhibited significant variation in relation to the rhodoliths collection site (rhodoliths and rhodoliths/seagrass). These significant variations were not detected by Newman-Keuls post hoc test, as shown in Table 13.

Tabela 12 - Summary of factorial ANOVA for rhodoliths collected outside and within seagrass meadows, and both faces: adaxial (exposed to sunlight) and abaxial (adjacent to the sediment).

Factor	Site		Face		Site*Face	
	F	p-value	F	p-value	F	p-value
Photosynthesis (O_2)						
P_{gross}^{max} (µmol O_2 cm^{-2} h^{-1})	2.96	0.107	0.06	0.802	0.51	0.486
P_{net}^{max} (µmol O_2 cm^{-2} h^{-1})	5.34	**0.037**	0.02	0.890	1.81	0.199
R_d (µmol O_2 cm^{-2} h^{-1})	0.26	0.614	0.09	0.759	0.49	0.493
α	0.15	0.698	0.56	0.463	0.45	0.509
E_k (µmol photons m^{-2} s^{-1})	0.08	0.779	0.00	0.942	0.45	0.509
E_c (µmol photons m^{-2} s^{-1})	1.34	0.264	0.07	0.795	0.11	0.739
DPP (µmol O_2 cm^{-2} h^{-1})	2.96	0.107	0.06	0.802	0.51	0.485
Photosynthesis (O_2)						
P_{gross}^{max} (µmol O_2 g^{-1} DW h^{-1})	0.03	0.858	0.05	0.825	0.12	0.724
P_{net}^{max} (µmol O_2 g^{-1} DW h^{-1})	1.55	0.233	0.03	0.847	0.86	0.369
R_d (µmol O_2 g^{-1} DW h^{-1})	1.08	0.313	0.02	0.880	0.00	0.928
α	0.56	0.466	0.04	0.844	0.11	0.738
E_k (µmol photons m^{-2} s^{-1})	0.00	0.943	0.95	0.344	2.40	0.141
E_c (µmol photons m^{-2} s^{-1})	1.33	0.266	0.07	0.795	0.11	0.738
DPP (µmol O_2 g^{-1} DW h^{-1})	0.05	0.819	0.03	0.853	0.00	0.960
CO_2 fixation						
FCO_{2gross}^{max} (µmol CO_2 cm^{-2} h^{-1})	2.19	0.159	0.31	0.588	5.30	**0.036**
FCO_{2net}^{max} (µmol CO_2 cm^{-2} h^{-1})	0.07	0.797	0.88	0.361	0.00	0.946
R_{dCO2} (µmol CO_2 cm^{-2} h^{-1})	8.79	**0.010**	0.00	0.995	6.69	**0.021**
α	4.81	**0.045**	0.49	0.497	4.43	0.052
E_k (µmol photons m^{-2} s^{-1})	4.79	**0.045**	25.39	**0.000**	3.87	0.068
E_c (µmol photons m^{-2} s^{-1})	32.06	**0.000**	12.35	**0.004**	15.05	**0.002**
DPP (µmol CO_2 cm^{-2} h^{-1})	0.15	0.701	2.39	0.142	1.37	0.258
CO_2 fixation						
FCO_{2gross}^{max} (µmol CO_2 g^{-1} DW h^{-1})	0.04	0.830	0,04	0,829	0,43	0,519
FCO_{2net}^{max} (µmol CO_2 g^{-1} DW h^{-1})	0,23	0,632	0,58	0,454	0.01	0.893
R_{dCO2} (µmol CO_2 g^{-1} DW h^{-1})	0.68	0.421	0.01	0.918	3.41	0.084
α	0.78	0.387	0.84	0.372	0.61	0.443
E_k (µmol photons m^{-2} s^{-1})	4.78	**0.045**	25.35	**0.000**	3.88	0.067
E_c (µmol photons m^{-2} s^{-1})	31.98	**0.000**	12.35	**0.003**	15.03	**0.001**
DPP (µmol CO_2 g^{-1} DW h^{-1})	0.04	0.830	0.04	0.829	0.43	0.519
Calcification ($CaCO_3$)						
G^{max}(µmol $CaCO_3$ cm^{-2} h^{-1})	0.35	0.563	46.43	**0.000**	0.77	0.393
G_d (µmol $CaCO_3$ cm^{-2} h^{-1})	45.09	**0.000**	55.34	**0.000**	1.73	0.208
α	0.03	0.854	45.38	**0.000**	3.76	0.072

Factor	Site		Face		Site*Face	
	F	p-value	F	p-value	F	p-value
E_k (µmol photons m^{-2} s^{-1})	4.04	**0.062**	14.07	**0.001**	8.68	**0.009**
E_c (µmol photons m^{-2} s^{-1})	18.58	**0.001**	73.67	**0.000**	11.81	**0.006**
DGR (µmol $CaCO_3$ cm^{-2} h^{-1})	37.79	**0.000**	0.37	0.551	0.67	0.423
Calcification ($CaCO_3$)						
G^{max} (µmol $CaCO_3$ g^{-1} DW h^{-1})	0.37	0.547	5.60	**0.031**	0.22	0.639
G_d (µmol $CaCO_3$ g^{-1} DW h^{-1})	23.16	**0.000**	33.45	**0.000**	1.23	0.286
α	0.30	0.589	22.13	**0.000**	4.97	0.040
E_k (µmol photons m^{-2} s^{-1})	12.86	**0.002**	16.96	**0.001**	20.99	**0.000**
E_c (µmol photons m^{-2} s^{-1})	11.53	**0.006**	20.92	**0.001**	7.61	**0.019**
DGR (µmol $CaCO_3$ g^{-1} DW h^{-1})	28.17	**0.000**	0.00	0.967	0.00	0.986
Pigments (µg cm^{-2})						
Phycocyanin (PC)	3.35	0.086	0.02	0.874	1.92	0.184
Phycoerythrin (PE)	4.69	**0.048**	14.48	**0.002**	0.48	0.497
Allophycocyanin (APC)	1.36	0.260	1.33	0.266	1.91	0.185
phycobiliproteins (PBP)	4.43	0.054	10.24	**0.006**	0.76	0.398
PE:PC ratio	10.09	**0.007**	57.85	**0.000**	20.37	**0.000**
Chlorophyll a (Chla)	8.54	**0.011**	1.77	0.204	0.18	0.672
Carotenes	13.83	**0.002**	28.46	**0.000**	0.91	0.355
PBP:Chla ratio	24.72	**0.000**	28.72	**0.000**	8.83	**0.011**
Mycosporine-like amino acids (MAAs) (mg cm^{-2})						
Palythine	0.06	0.799	1.31	0.269	0.89	0.358
Palythinol	10.16	**0.007**	0.67	0.425	2.43	0.141
Shinorine	10.37	**0.006**	1.58	0.227	0.00	0.926
Total MAAs	8.14	**0.012**	0.62	0.443	3.76	0.072

Dependent variables included the parameters calculated from response curves or light curves (O_2, CO_2 and $CaCO_3$ versus irradiance), pigments and mycosporine-like amino acids (MAAs). The p-value<0.05 are indicated in bold. Data were normalized per g of dry biomass (DW) or per cm² (photosynthetic area) per hour (h). P_{gross}^{max} and P_{net}^{max} (maximum gross and net O_2 production), $FCO2_{gross}^{max}$ and $FCO2_{net}^{max}$ (maximum gross and net CO_2 fixation), G^{max} (maximum calcification), R_d and Rd_{CO2} (dark respiration), G_d (dark calcification), α (photosynthetic efficiency), E_k (saturation irradiance), E_c (compensation irradiance), DPP (daily primary productivity), DGR (daily calcification rates).

Table 13 exhibit detailed parameters of the primary production of *Lithophyllum hibernicum*. Maximum gross CO_2 fixation ($FCO2_{gross}^{max}$), dark respiration in terms of CO_2 release (R_{dCO2}) and alpha (α) showed significant differences among the conditions evaluated when the data were normalized by the photosynthetic area (cm^2) (Tables 12 and 13), although statistical differences were not detected by Newman-Keuls post hoc test for $FCO2_{gross}^{max}$ (Table 13). R_{dCO2} was higher in rhodoliths/adaxial (0.60 µmol CO_2 cm^{-2} h^{-1}) compared to rhodoliths/seagrass/adaxial (0.38 µmol CO_2 cm^{-2} h^{-1}), and α was the highest in rhodoliths/seagrass/abaxial (-0.0039 µmol CO_2 cm^{-2} h^{-1}), but statistically different only of rhodoliths/abaxial (-0.0030 µmol CO_2 cm^{-2} h^{-1}). Saturation (E_k) and compensation irradiance (E_c) exhibited differences for the normalized data by area (cm²) and dry biomass (g). E_k and E_c were higher in rhodoliths/adaxial, reaching values of 445.24 and 445.44 µmol photons m^{-2} s^{-1} and 167.14 and 167.18 µmol photons m^{-2} s^{-1}, respectively (Table 13).

Photosynthesis (O_2 and CO_2 fluxes) versus irradiance curves showed similar pattern among rhodoliths collected inside and outside seagrass meadows and both faces adaxial and abaxial (Figure 52 A, B, C and D). O_2 production and CO_2 fixation exhibited a high relationship with irradiance, R^2 varied from 0.94 to 0.97. Comparing the O_2 and CO_2 curves in Figure 52, it is possible to observe that the assimilation of CO_2 was slightly higher than the production of O_2 by the photosynthesis of *L. hibernicum*, independent of the site or face.

Tabela 13 - Primary production of rhodoliths collected outside and within seagrass meadow, both faces: adaxial (exposed to sunlight) and abaxial (adjacent to the sediment).

Conditions	**Primary production**					
Photosynthesis (O_2)	P_{gross}^{max} (µmol O_2 cm^{-2} h^{-1})	P_{net}^{max} (µmol O_2 cm^{-2} h^{-1})	R_d (µmol O_2 cm^{-2} h^{-1})	α	E_k (µmol photons m^{-2} s^{-1})	E_c (µmol photons m^{-2} s^{-1})
Rhodoliths/adaxial	0.88 ± 0.08[a]	0.66 ± 0.07[a]	-0.21 ± 0.05[a]	0.003 ± 0.001[a]	346.70 ± 39.56[a]	78.87 ± 13.68[a]
Rhodoliths/abaxial	0.90 ± 0.09[a]	0.71 ± 0.07[a]	-0.19 ± 0.05[a]	0.002 ± 0.000[a]	355.59 ± 16.45[a]	78.33 ± 13.07[a]
Rhodoliths/seagrass/adaxial	0.83 ± 0.08[a]	0.63 ± 0.08[a]	-0.21 ± 0.04[a]	0.002 ± 0.000[a]	360.90 ± 25.81[a]	84.73 ± 16.68[a]
Rhodoliths/seagrass/abaxial	0.79 ± 0.12[a]	0.58 ± 0.07[a]	-0.22 ± 0.05[a]	0.002 ± 0.001[a]	349.83 ± 36.53[a]	89.04 ± 19.69[a]
Photosynthesis (O_2)	P_{gross}^{max} (µmol O_2 g^{-1} DW h^{-1})	P_{net}^{max} (µmol O_2 g^{-1} DW h^{-1})	R_d (µmol O_2 g^{-1} DW h^{-1})	α	E_k (µmol photons m^{-2} s^{-1})	E_c (µmol photons m^{-2} s^{-1})
Rhodoliths/adaxial	2.97 ± 0.72[a]	2.23 ± 0.45[a]	-0.63 ± 0.21[a]	0.008 ± 0.002[a]	329.62 ± 51.43[a]	78.88 ± 13.67[a]
Rhodoliths/abaxial	3.01 ± 0.58[a]	2.36 ± 0.39[a]	-0.65 ± 0.23[a]	0.008 ± 0.002[a]	378.17 ± 52.42[a]	78.34 ± 13.07[a]
Rhodoliths/seagrass/adaxial	3.13 ± 0.74[a]	2.17 ± 0.38[a]	-0.73 ± 0.21[a]	0.009 ± 0.002[a]	360.83 ± 25.64[a]	84.70 ± 16.70[a]
Rhodoliths/seagrass/abaxial	2.96 ± 0.62[a]	1.98 ± 0.11[a]	-0.74 ± 0.13[a]	0.008 ± 0.002[a]	349.76 ± 36.64[a]	89.03 ± 19.69[a]
CO_2 fixation	FCO_{2gross}^{max} (µmol CO_2 cm^{-2} h^{-1})	FCO_{2net}^{max} (µmol CO_2 cm^{-2} h^{-1})	R_{dCO2} (µmol CO_2 cm^{-2} h^{-1})	α	E_k (µmol photons m^{-2} s^{-1})	E_c (µmol photons m^{-2} s^{-1})
Rhodoliths/adaxial	-1.507 ± 0.17[a]	-0.91 ± 0.11[a]	0.60 ± 0.09[a]	-0.0033 ± 0.000[ab]	445.24 ± 33.82[a]	167.14 ± 14.36[a]
Rhodoliths/abaxial	-1.287 ± 0.17[a]	-0.85 ± 0.15[a]	0.49 ± 0.09[ab]	-0.0030 ± 0.001[b]	342.27 ± 27.53[b]	129.80 ± 11.16[b]
Rhodoliths/seagrass/adaxial	-1.216 ± 0.16[a]	-0.92 ± 0.16[a]	0.38 ± 0.10 [b]	-0.0034 ± 0.001[ab]	384.18 ± 34.18[b]	118.95 ± 6.63[b]
Rhodoliths/seagrass/abaxial	-1.351 ± 0.16[a]	-0.87 ± 0.13[a]	0.48 ± 0.04[ab]	-0.0039 ± 0.000[a]	339.03 ± 30.52[b]	120.79 ± 8.24[b]
CO_2 fixation	FCO_{2gross}^{max} (µmol CO_2 g^{-1} DW h^{-1})	FCO_{2net}^{max} (µmol CO_2 g^{-1} DW h^{-1})	R_{dCO2} (µmol CO_2 g^{-1} DW h^{-1})	α	E_k (µmol photons m^{-2} s^{-1})	E_c (µmol photons m^{-2} s^{-1})
Rhodoliths/adaxial	-4.68 ± 1.19[a]	-3.09 ± 0.80[a]	1.81 ± 0.49[a]	-0.012 ± 0.00[a]	445.44 ± 34.05[a]	167.18 ± 14.40[a]
Rhodoliths/abaxial	-4.30 ± 0.81[a]	-2.83 ± 0.54[a]	1.47 ± 0.52[a]	-0.012 ± 0.00[a]	342.22 ± 27.52[b]	129.79 ± 11.16[b]
Rhodoliths/seagrass/adaxial	-4.49 ± 0.91[a]	-3.20 ± 0.66[a]	1.30 ± 0.30[a]	-0.012 ± 0.00[a]	384.20 ± 34.22[b]	118.97 ± 6.65[b]
Rhodoliths/seagrass/abaxial	-4.68 ± 0.87[a]	-3.01 ± 0.59[a]	1.67 ± 0.32[a]	-0.014 ± 0.00[a]	339.03 ± 30.53[b]	120.80 ± 8.24[b]

Table parameters were obtained from light curves (O_2 and CO_2 versus irradiance) and expressed as µmol O_2 or CO_2 per g of dry biomass (DW) or per cm² (photosynthetic area) per hour (h). Mean ± standard-deviation (n=5). Significant differences are indicated by superscript letters (ANOVA, Newman-Keuls post hoc, $p<0.05$). P_{gross}^{max} and P_{net}^{max} (maximum gross and net photosynthesis), FCO_{2gross}^{max} and FCO_{2net}^{max} (maximum gross and net CO_2 fixation), R_d and Rd_{CO2} (dark respiration), α (photosynthetic efficiency), E_k (saturation irradiance), E_c (compensation irradiance).

Figura 52 - Irradiance versus net primary production expressed by O_2 and CO_2 fluxes.

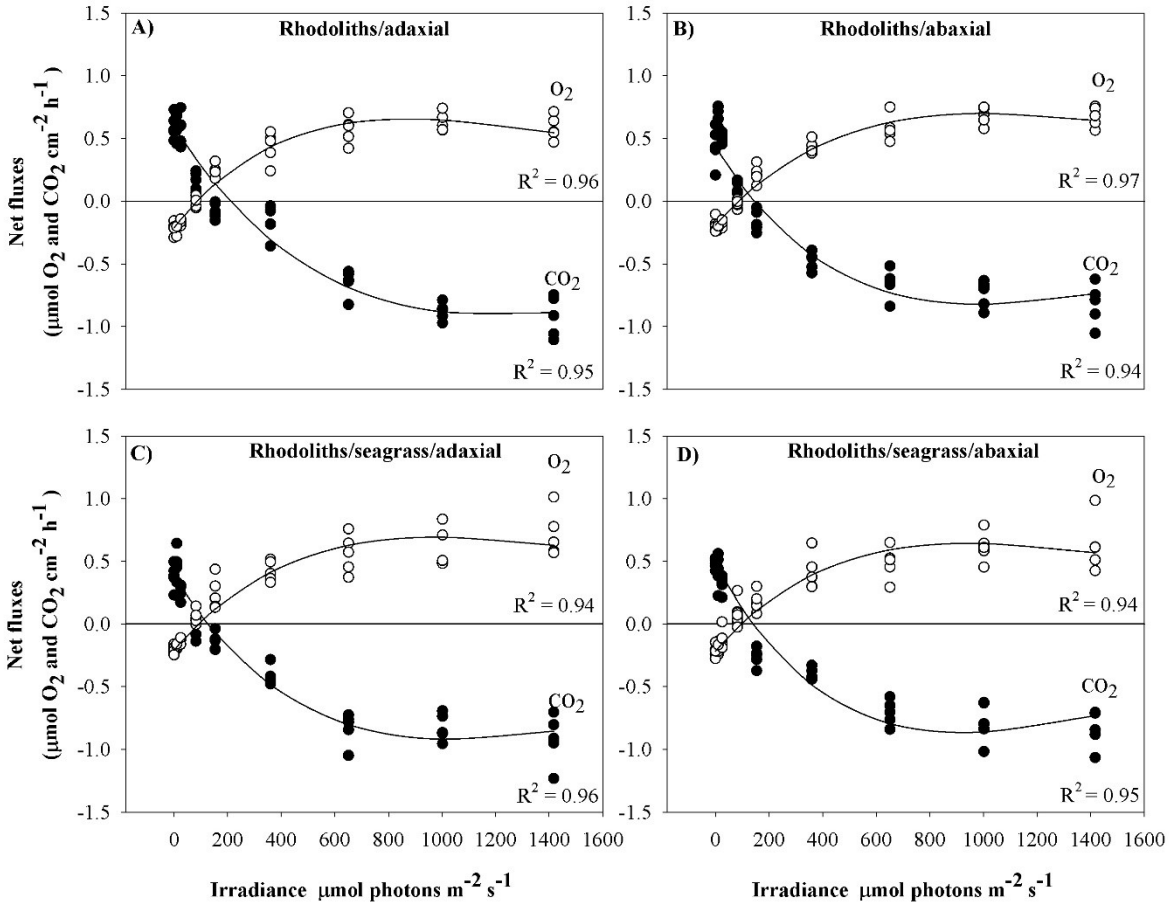

Metabolic responses of rhodoliths collected outside and within seagrass meadow, both faces: adaxial (exposed to sunlight) and abaxial (adjacent to the sediment). Lines represented the curve fit according Platt et al. (Platt, Gallegos, and Harrison 1980). R^2 was obtained from nonlinear regression.

Maximum calcification (G^{max}) was lower in rhodoliths/abaxial (0.60 µmol $CaCO_3$ cm^{-2} h^{-1}), although statically similar to rhodoliths/seagrass/abaxial (0.63 µmol $CaCO_3$ cm^{-2} h^{-1}). G^{max} in rhodoliths/adaxial and rhodoliths/seagrass/adaxial was 0.77 and 0.76 µmol $CaCO_3$ cm^{-2} h^{-1}, respectively. When G^{max} is normalized by g, there is no statistical difference. Calcification was negative for rhodoliths/adaxial in the dark (-0.12 µmol $CaCO_3$ cm^{-2} h^{-1} and -0.40 µmol $CaCO_3$ g^{-1} DW h^{-1}). Significatively higher calcification values were observed for other conditions in darkness, such as rhodoliths/abaxial (0.15, µmol $CaCO_3$ cm^{-2} h^{-1}, 0.58 µmol $CaCO_3$ g^{-1} DW h^{-1}), rhodoliths/seagrass/adaxial (0.13, µmol $CaCO_3$ cm^{-2} h^{-1}, 0.44 µmol $CaCO_3$ g^{-1} DW h^{-1}), and rhodoliths/seagrass/abaxial (0.32, µmol $CaCO_3$ cm^{-2} h^{-1}, 1.11 µmol $CaCO_3$ g^{-1} DW h^{-1}). Saturation irradiance (E_k) was greater for rhodoliths/seagrass/abaxial (676 and 753 µmol photons m^{-2} s^{-1}), as well as the compensation irradiance (E_c) (406 and 349 µmol photons m^{-2} s^{-1}) (Table 14).

Tabela 14 - Rhodoliths calcification data collected outside and within seagrass meadow, both faces: adaxial (exposed to sunlight) and abaxial (adjacent to the sediment).

Conditions	Calcification parameters				
	G^{max} (µmol $CaCO_3$ cm^{-2} h^{-1})	G_d (µmol $CaCO_3$ cm^{-2} h^{-1})	α	E_k (µmol photons m^{-2} s^{-1})	E_c (µmol photons m^{-2} s^{-1})
Rhodoliths/adaxial	0.77 ± 0.02^{a}	-0.12 ± 0.09^{c}	0.002 ± 0.000^{a}	377.16 ± 40.69^{b}	31.37 ± 12.75^{c}
Rhodoliths/abaxial	0.60 ± 0.06^{b}	0.15 ± 0.08^{b}	0.001 ± 0.000^{b}	418.81 ± 130.22^{b}	180.91 ± 61.29^{b}
Rhodoliths/seagrass/adaxial	0.76 ± 0.07^{a}	0.13 ± 0.04^{b}	0.002 ± 0.000^{a}	328.59 ± 37.57^{b}	56.75 ± 19.40^{c}
Rhodoliths/seagrass/abaxial	0.63 ± 0.03^{b}	0.32 ± 0.05^{a}	0.001 ± 0.000^{b}	675.61 ± 190.86^{a}	406.10 ± 109.02^{a}
	G^{max} (µmol $CaCO_3$ g^{-1} DW h^{-1})	G_d (µmol $CaCO_3$ g^{-1} DW h^{-1})	α	E_k (µmol photons m^{-2} s^{-1})	E_c (µmol photons m^{-2} s^{-1})
Rhodoliths/adaxial	2.62 ± 0.67^{a}	-0.40 ± 0.40^{c}	0.007 ± 0.001^{ab}	377.08 ± 40.65^{b}	31.37 ± 12.74^{b}
Rhodoliths/abaxial	1.93 ± 0.56^{a}	0.58 ± 0.39^{b}	0.005 ± 0.002^{bc}	354.51 ± 106.41^{b}	103.65 ± 91.67^{b}
Rhodoliths/seagrass/adaxial	2.66 ± 0.53^{a}	0.44 ± 0.13^{b}	0.008 ± 0.002^{a}	328.55 ± 37.61^{b}	56.74 ± 19.39^{b}
Rhodoliths/seagrass/abaxial	2.20 ± 0.37^{a}	1.11 ± 0.25^{a}	0.003 ± 0.001^{c}	752.96 ± 184.22^{a}	348.80 ± 147.81^{a}

Table parameters were obtained from light curves ($CaCO_3$ versus irradiance) and expressed as µmol $CaCO_3$ per g of dry biomass (DW) or per cm^2 (photosynthetic area) per hour (h). Mean ± standard-deviation (n=5). Significant differences are indicated by superscript letters (ANOVA, Newman-Keuls post hoc, $p<0.05$). G^{max} (maximum calcification), G_d (dark calcification), α (photosynthetic efficiency), E_k (saturation irradiance), E_c (compensation irradiance).

Less upward curves were observed for rhodoliths/abaxial and rhodoliths/seagrass/abaxial compared to rhodoliths/adaxial and rhodoliths/seagrass/adaxial (Figure 53). Calcification versus irradiance showed a lower relationship in rhodoliths/abaxial and rhodoliths/seagrass/abaxial (R^2 = 0.87 and 0.85) than in rhodoliths/adaxial and rhodoliths/seagrass/adaxial (R^2 = 0.90 and 0.93). Only rhodoliths/adaxial exhibited negative values in darkness (Figure 53).

Figura 53 - Irradiance versus calcification of rhodoliths collected outside and within seagrass meadow, both faces: adaxial (exposed to sunlight) and abaxial (adjacent to the sediment).

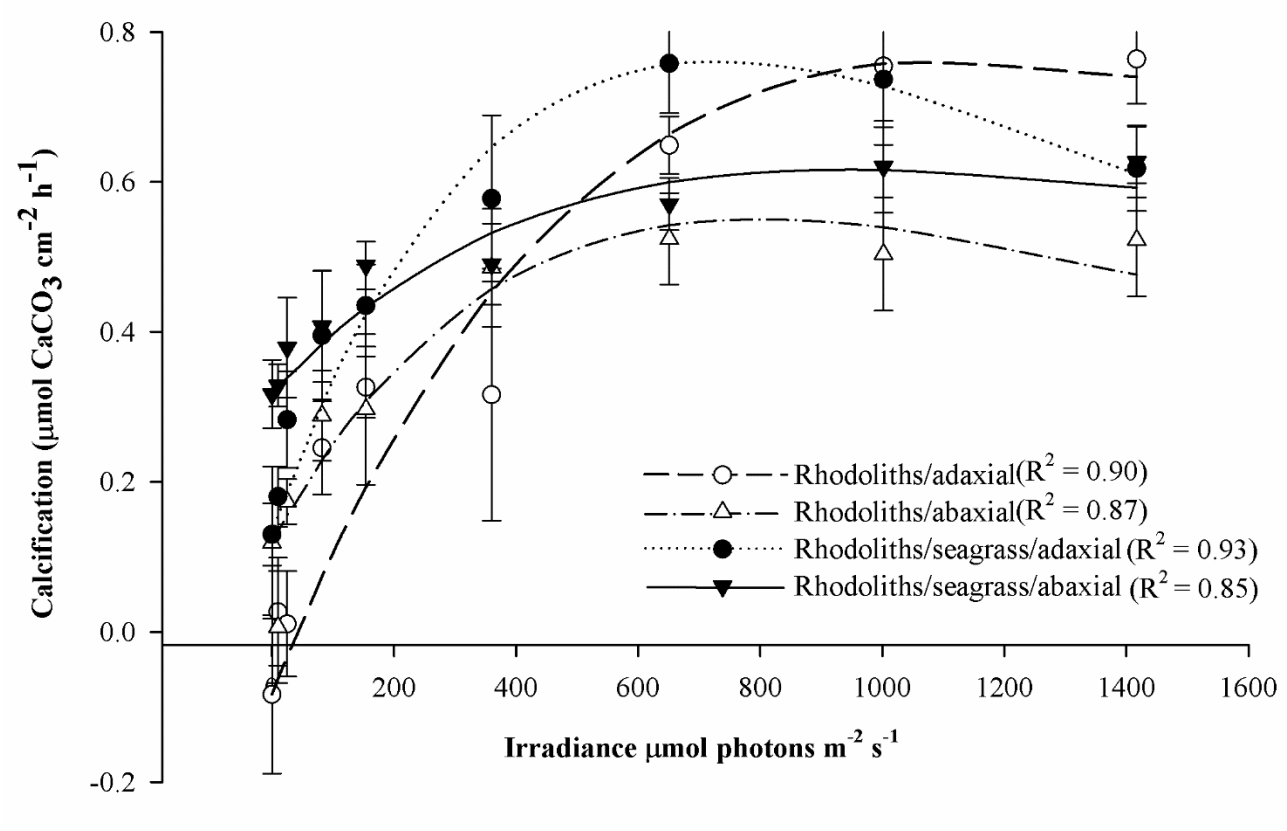

Data expressed as µmol of $CaCO_3$ per cm² (photosynthetic area). Mean ± standard-deviation (n=5). Lines represented the curve fit according Platt et al. (PLATT; GALLEGOS; HARRISON, 1980). R^2 was obtained from nonlinear regression.

The daily productivity of O_2 production and CO_2 fixation did not present significant differences among the evaluated conditions, the average values obtained were around 10 µmol O_2 cm^{-2} d^{-1} and 16 µmol CO_2 cm^{-2} d^{-1}, respectively (Table 15). Daily calcification rates were around 8 µmol $CaCO_3$ cm^{-2} d^{-1} for rhodoliths/adaxial and rhodoliths/abaxial and around 10 µmol $CaCO_3$ cm^{-2} d^{-1} for rhodoliths/seagrass/adaxial and rhodoliths/seagrass/abaxial, respectively (Table 15).

Tabela 15 - Daily primary productivity (O_2 and CO_2) and daily calcification rates ($CaCO_3$) of rhodoliths collected outside and within seagrass meadow, both faces: adaxial (exposed to sunlight) and abaxial (adjacent to the sediment).

Conditions	Daily productivity (O_2)	Daily productivity (CO_2)	Daily calcification ($CaCO_3$)
	(µmol O_2 cm^{-2} d^{-1})	(µmol CO_2 cm^{-2} d^{-1})	(µmol $CaCO_3$ cm^{-2} d^{-1})
Rhodoliths/adaxial	10.5 ± 1.0[a]	18.1 ± 2.0[a]	8.2 ± 1.2[b]
Rhodoliths/abaxial	10.8 ± 1.1[a]	15.4 ± 2.1[a]	8.1 ± 1.1[b]
Rhodoliths/seagrass/adaxial	10.0 ± 0.9[a]	16.6 ± 2.4[a]	10.7 ± 1.1[a]
Rhodoliths/seagrass/abaxial	9.5 ± 1.4[a]	16.2 ± 2.0[a]	11.4 ± 0.6[a]
	(µmol O_2 g^{-1} DW d^{-1})	(µmol CO_2 g^{-1} DW d^{-1})	(µmol $CaCO_3$ g^{-1} DW d^{-1})
Rhodoliths/adaxial	35.6 ± 8.7[a]	56.19 ± 14.29[a]	24.4 ± 4.3[b]
Rhodoliths/abaxial	36.1 ± 7.0[a]	51.63 ± 9.70[a]	24.6 ± 6.3[b]
Rhodoliths/seagrass/adaxial	34.6 ± 6.9[a]	53.90 ± 10.89[a]	39.6 ± 4.8[a]
Rhodoliths/seagrass/abaxial	35.5 ± 7.4[a]	56.18 ± 10.45[a]	39.7 ± 7.1[a]

The calculations were performed considering a daily cycle of 12h light and 12h dark. Data expressed as µmol of O_2, CO_2 or $CaCO_3$ per g of dry biomass (DW) and per cm^2 (photosynthetic area) per day (d). Mean ± standard-deviation (n=5). Significant differences are indicated by superscript letters (ANOVA, Newman-Keuls post hoc, $p<0.05$).

Permanova results showed a significant interaction between factors: site versus face and face versus irradiance ($p<0.05$), P(MC) = 0.023 and 0.015, respectively. There was no significant interaction between site versus face versus irradiance ($p = 0.615$) (ANEXO D, Table S. 7). The PCO showed that irradiance was the main factor easily associated to PCO axis 1. The data were separated from lower to higher irradiances following the axis. The separation of faces (adaxial and abaxial) indicated that some variables respond differently when irradiance was higher than 82 µmol photons m^{-2} s^{-1}. Moreover, it was possible to verify that variables, such as temperature, pH, calcification, net O_2 flux, CO_3^{-2}, Ω calcite and Ω aragonite were greater under high irradiance and inversely related to AT, DIC, net CO_2 flux, HCO_3^-, CO_2 and pCO_2 (Figure 54). The variables most strongly correlated to axis 1 (PCO1) were pCO_2 (0.97), HCO_3^- (0.98), CO_2 (0.98), DIC (0.95), and net CO_2 flux (0.96). To axis 2 (PCO2), the variables CO_3^{-2} (0.20), Ω calcite (0.20) and Ω aragonite (0.19), AT (0.47), and DIC (0.20) were most correlated.

Figura 54 - Results of the Principal Coordinates Analysis (PCO).

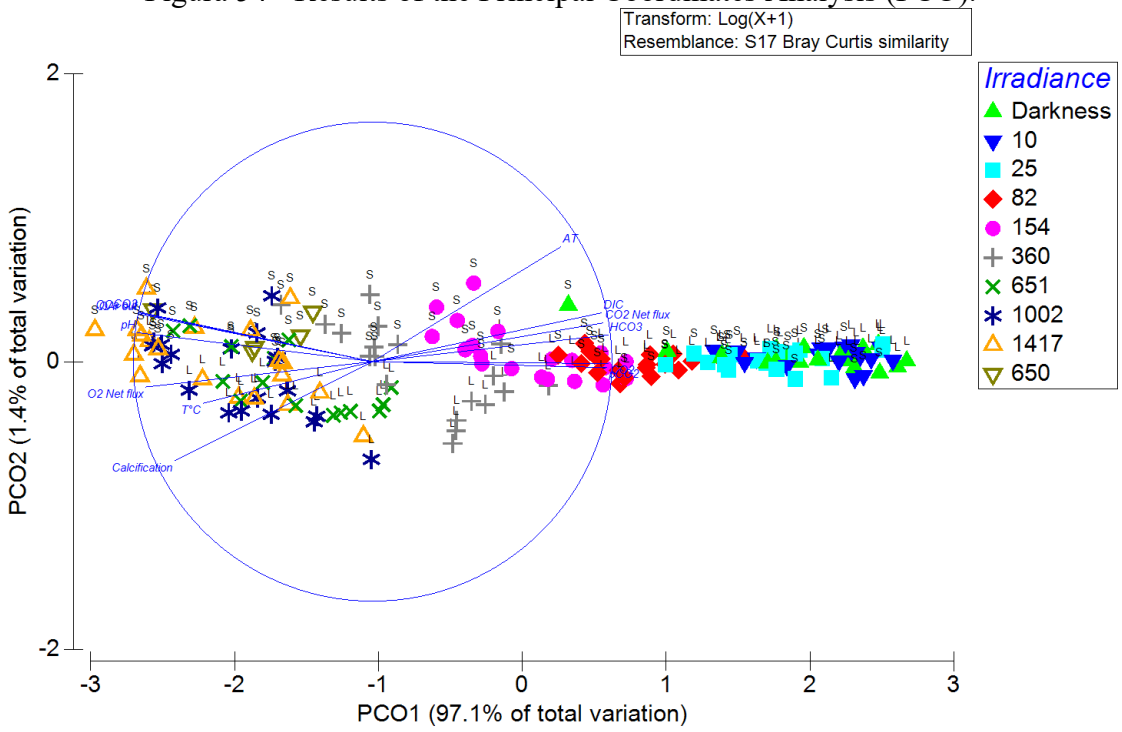

The variables analyzed were temperature, pH, total alkalinity (AT), pCO_2, HCO_3^-, CO_3^{-2}, CO_2, DIC (dissolved inorganic carbon), calcite and aragonite saturation (Ω), Net fluxes (µmol CO_2 and O_2 cm^2 h^{-1}) and calcification (µmol $CaCO_3$ cm^{-2} h^{-1}), under different irradiances (darkness, 10, 25, 82, 154, 360, 651, 1002 and 1417 µmol photons m^{-2} s^{-1}). S = face adjacent to the sediment (abaxial face), L = face exposed to sunlight (adaxial face).

The pigments from *L. hibernicum* showed significant differences between site collection and faces (Tables 12 and 16). Total phycobiliproteins (PBP) and Phycoerythrin (PE) were found in higher concentrations in rhodoliths/seagrass/abaxial (66.8 µg cm^{-2}) compared to other conditions, especially in relation to rhodoliths/adaxial (25.3 µg cm^{-2}) (Table 16). Phycocyanin (PC) and allophycocyanin (APC) concentrations showed no statistic difference among sites and faces, although slightly higher values were found for rhodoliths/seagrass/abaxial compared to other conditions. The concentrations of chlorophyll *a* (Chl*a*) and carotenoids were higher in rhodoliths/adaxial, with values of 10.6 and 10.7 µg cm^{-2}, respectively. Rhodoliths/abaxial and rhodoliths/seagrass/adaxial presented values from 8 to 10 µg cm^{-2} for Chl*a* and from 6 to 8 µg cm^{-2} for carotenoids. Rhodoliths/seagrass/abaxial showed the lowest values for both Chl*a* and carotenoids, 7.0 and 5.0 µg cm^{-2}, respectively. The PBP: Chl*a* ratio was about 13 for rhodoliths/seagrass/abaxial, while the other conditions showed values below 6 (Table 16).

Tabela 16 - Phycobiliproteins, chlorophyll and carotenoids concentration of rhodoliths collected outside and within seagrass meadow, both faces: adaxial (exposed to sunlight) and abaxial (adjacent to the sediment).

Conditions	PC	PE	APC	PBP	PE: PC	Chl*a*	Carotenoids	PBP: Chl*a*
Rhodoliths/adaxial	3.1 ± 1.1^{a}	25.3 ± 3.3^{a}	4.6 ± 1.0^{a}	32.9 ± 3.9^{a}	9.8 ± 2.7^{a}	10.6 ± 1.9^{b}	10.7 ± 1.6^{c}	3.1 ± 0.7^{a}
Rhodoliths/abaxial	2.2 ± 0.6^{a}	46.9 ± 9.6^{ab}	4.3 ± 1.6^{a}	52.8 ± 11.5^{ab}	23.7 ± 1.3^{b}	9.8 ± 2.4^{ab}	6.7 ± 1.4^{ab}	5.6 ± 1.6^{a}
Rhodoliths/seagrass/adaxial	3.5 ± 2.4^{a}	35.5 ± 16.9^{a}	4.4 ± 2.5^{a}	43.4 ± 21.2^{a}	11.4 ± 2.7^{a}	8.5 ± 1.6^{ab}	7.8 ± 1.2^{b}	5.2 ± 2.7^{a}
Rhodoliths/seagrass/abaxial	4.6 ± 2.0^{a}	66.8 ± 19.6^{b}	6.8 ± 2.7^{a}	78.2 ± 23.9^{b}	14.9 ± 2.5^{c}	7.0 ± 1.2^{a}	5.0 ± 0.9^{a}	13.7 ± 2.3^{b}

Mean ± standard-deviation (n=5), expressed as µg cm^{-2}. Significant differences are indicated by superscript letters (ANOVA, Newman-Keuls post hoc). PC (phycocyanin), PE (phycoerythrin), APC (allophycocyanin), PBP (total phycobiliproteins), PE: PC (phycoerythrin to phycocyanin ratio), Chl*a* (Chlorophyll *a*), PBP: Chl*a* (phycobiliproteins total to chlorophyll a ratio).

The total concentration of mycosporine-like amino acids (MAAs) was of 1.39 mg cm^{-2} for rhodoliths/seagrass/abaxial, this was the lowest concentration observed (Table 17). The other conditions showed values of total MAAs between 2 and 5 mg cm^{-2}. Among MAAs, palythine was found in small amounts in all conditions, with an average value of 0.02 mg cm^{-2}. Shinorine and palythinol were found in lower concentration in rhodoliths/seagrass/abaxial, with values of 0.79 and 0.58 mg cm^{-2}, respectively. Values from 1.0 to 3.0 mg cm^{-2} of shinorine and from 0.9 to 3.0 mg cm^{-2} of palythinol were found for rhodoliths/adaxial, rhodoliths/abaxial and rhodoliths/seagrass/adaxial.

Tabela 17 - Mycosporine-like amino acids (MAAs) concentration of rhodoliths collected outside and within seagrass meadow, both faces: adaxial (exposed to sunlight) and abaxial (adjacent to the sediment).

Conditions	Palythine	Palythinol	Shinorine	MAAs total
Rhodoliths/adaxial	0.02 ± 0.01^{a}	1.64 ± 1.39^{ab}	2.16 ± 1.03^{a}	2.75 ± 2.21^{ab}
Rhodoliths/abaxial	0.02 ± 0.01^{a}	2.72 ± 1.32^{a}	1.81 ± 0.75^{ab}	4.54 ± 1.72^{a}
Rhodoliths/seagrass/adaxial	0.03 ± 0.02^{a}	0.91 ± 0.55^{b}	1.21 ± 0.51^{ab}	2.14 ± 1.02^{ab}
Rhodoliths/seagrass/abaxial	0.02 ± 0.01^{a}	0.58 ± 0.17^{b}	0.79 ± 0.18^{b}	1.39 ± 0.14^{b}

Mean ± standard-deviation (n=5), expressed as mg cm^{-2}. Significant differences are indicated by superscript letters (ANOVA, Newman-Keuls post hoc). The data represent mean ± SD (n=5).

7.5 DISCUSSION

We evaluated the effect of different light intensities on the photosynthesis, respiration, and calcification of *Lithophyllum hibernicum*, which was collected inside and outside of seagrass meadows and presented two differently pigmented faces. Table 11 shows the variation of the carbonate system before and after *L. hibernicum* incubations in the dark and under different light intensities. The changes observed in parameters from Table 11 were driven by physiological processes of alga, such as photosynthesis, respiration, and calcification. After 30 min in the dark, the

amount of CO_2 increased compared to the initial value due to algae respiration. When *L. hibernicum* was exposed to increasing light intensities, CO_2 was gradually fixed by photosynthesis. While CO_2 decreased, parameters such as pH, CO_3^{-2} ions and saturation (Ω) of aragonite and calcite increased (Table 11). The increase in these parameters favors the calcification process (DONEY et al., 2009; HOFMANN; BISCHOF, 2014). We compared the variation of the carbonate system in Table 11 with the results of calcification in Table 14 and Figure 53. Rhodoliths/adaxial was the condition in which the reduction in CO_2 and the increase in pH occurred more slowly, i.e., these parameters achieved the initial values (pH 8.2 and 10.0 µmol kg^{-1}) only after exposure to 360 µmol photons m^{-2} s^{-1} of light. Meanwhile, rhodoliths/abaxial and rhodoliths/seagrass/abaxial reestablished the initial values after exposure to 82 µmol photons m^{-2} s^{-1} and rhodoliths/seagrass/adaxial after 154 µmol photons m^{-2} s^{-1} of light. The slow increase in pH in rhodoliths/adaxial may be related to the negative rates of calcification in the dark (G_d, -0.12 µmol $CaCO_3$ cm^{-2} h^{-1}) and in the first light intensities, while the other conditions evaluated exhibited positive G_d values (Table 14 and Figure 53). The negative G_d indicates dissolution of calcium carbonate and was observed in *Ellisolandia elongata* when collected in winter (EGILSDOTTIR; OLAFSSON; MARTIN, 2016). Negative G_d was also observed in *Phymatolithon lusitanicum* (SORDO et al., 2018). On the other hand, rhodoliths/seagrass/abaxial exhibited the highest value of G_d (0.32 µmol $CaCO_3$ cm^{-2} h^{-1}), being 2-3-fold higher than the other conditions evaluated. Some authors suggest that dark calcification is a late biological process, which occurs after the transition of the alga from light to darkness (CHISHOLM, 2000; EL HAÏKALI et al., 2004). However, Martin et al. (MARTIN; CHARNOZ; GATTUSO, 2013) reported that the calcification rates of *Lithophyllum cabiochae* remained high even after a long period of exposure of algae to the dark.

Table 18 summarizes the results of this study and others performed with coralline algae. In a study performed with *Lithophyllum incrustans* (QUI-MINET et al., 2019), it was possible to verify that the maximum calcification rate (G^{max}) obtained in the summer (2.27 $CaCO_3$ g^{-1} DW h^{-1}) was similar to the obtained in this study for rhodoliths/seagrass/abaxial (2.20 $CaCO_3$ g^{-1} DW h^{-1}). Martin et al. (MARTIN; CHARNOZ; GATTUSO, 2013) evaluated photosynthesis, respiration, and calcification of the coralline alga *L. cabiochae*. This alga was collected at 25 m depth, under maximum irradiance of 60 µmol photons m^{-2} s^{-1}. G^{max} values of *L. cabiochae* were 0.37 µmol $CaCO_3$ cm^{-2} h^{-1}, while in this study the values varied between 0.60 and 0.77 µmol $CaCO_3$ cm^{-2} h^{-1}.

Maximum gross O_2 production (P_{gross}^{max}) found in the present study was consistent with the values obtained in winter for *Lithothamnion corallioides*, *Phymatolithon calcareum* and *L. incrustans*. Although in summer, these species produced 2-fold more O_2 compared to our results, mainly *L. incrustans* (QUI-MINET et al., 2019). *L. cabiochae* exhibited maximum gross and net O_2 production higher in summer and lower in winter compared to our results (MARTIN et al., 2013). In

terms of O_2 consumption, the dark respiration (R_d) of *L. cabiochae* was similar to observed in this study for *L. hibernicum.* Maximum gross and net CO_2 fixation ($FCO_2^{max}_{gross}$ and $FCO_2^{max}_{net}$) exhibited by *L. hibernicum* in this study were 2-fold higher compared to the values found for *L. cabiochae* in winter. In the summer, $FCO_2^{max}_{gross}$ was slightly higher for *L. hibernicum* and $FCO_2^{max}_{net}$ was similar between species (MARTIN et al., 2013). Dark respiration (R_{dCO2}), in terms of CO_2 release, was higher for *L. hibernicum* in comparison with *L. cabiochae* (MARTIN; CHARNOZ; GATTUSO, 2013), see Table 18.

We obtained significantly higher values of saturation (E_k) and compensation (E_c) irradiance compared to other studies, see Table 18 (EGILSDOTTIR; OLAFSSON; MARTIN, 2016; MARTIN et al., 2013; MARTIN; CASTETS; CLAVIER, 2006; MARTIN; CHARNOZ; GATTUSO, 2013; QUI-MINET et al., 2019). *Lithothamnion corallioides* was collected between 1 and 8 m depth, with surface irradiances ranged between 1300 and 2500 µmol m^{-2} s^{-1}. During incubations, this alga was exposed to irradiances between 50 and 824 µmol m^{-2} s^{-1}, exhibiting E_k values of 179 µmol photons m^{-2} s^{-1} for CO_2 fixation and 102 µmol photons m^{-2} s^{-1} for calcification (MARTIN; CASTETS; CLAVIER, 2006). In this study, we collected *L. hibernicum* in intertidal pools during low tide. The average irradiance obtained at the pool surface was 1044 µmol photons m^{-2} s^{-1}. The high E_k and E_c can indicate that *L. hibernicum* was acclimated to high irradiance levels, even the rhodoliths collected inside seagrass meadows. E_k values > 300 µmol photons m^{-2} s^{-1} were exhibited for photosynthesis, CO_2 fixation and calcification. Rhodoliths/seagrass/abaxial showed mean value > 600 µmol photons m^{-2} s^{-1} for calcification. In the study of Qui-Minet et al. (QUI-MINET et al., 2019), *L. incrustans* presented E_k values 2-3-fold lower than our E_k results. The authors collected *L. incrustans* in the Roz maerl bed, located in the Bay of Brest, where the depth varies from 0.7 to 8 m, with maximum irradiances of 645 µmol photons m^{-2} s^{-1} in the summer.

Tabela 18 - Primary production (O_2 and CO_2) and rates calcification of different species coralline algae, such as: *Lithothamnion corallioides*, *Lithophyllum cabiochae*, *Ellisolandia elongata*, *Phymatolithon calcareum*, *Lithophyllum incrustans,* and *Lithophyllum hibernicum* (present study).

Species	Condition	P^{max}_{gross}			P^{max}_{net}			R_d			E_k	E_c	Reference
		cm²	g dw	g wt	cm²	g dw	g wt	cm²	g dw	g wt	cm²	cm²	
L. corallioides	winter	-	-	-	-	-	0.77	-	-	-0.07	143	15	(MARTIN; CASTETS; CLAVIER, 2006)
L. corallioides	summer	-	-	-	-	-	1.61	-	-	-0.32	159	35	
L. cabiochae	winter	0.52	-	-	0.43	-	-	-	-	-	10	1.7	*(MARTIN et al., 2013)
L. cabiochae	summer	1.16	-	-	0.90	-	-	-	-	-	30	6.9	
L. cabiochae	-	1.00	-	3.26	0.75	-	2.41	-0.25	-	-0.85	31	8.4	(MARTIN; CHARNOZ; GATTUSO, 2013)
E. elongata	winter	-	20.3	-	-	19.4	-	-	-0.92	-	30	1.4	(EGILSDOTTIR; OLAFSSON; MARTIN, 2016)
E. elongata	summer	-	62.2	-	-	50.2	-	-	-12.01	-	82	15	
L. corallioides		-	3.5	-	-	-	-	-	-	-	37	-	*(QUI-MINET et al., 2019)
P. calcareum	winter	-	3.3	-	-	-	-	-	-	-	34	-	
L. incrustans		-	4.0	-	-	-	-	-	-	-	56	-	
L.corallioides		-	7.7	-	-	-	-	-	-	-	75	-	
P. calcareum	summer	-	5.6	-	-	-	-	-	-	-	99	-	
L. incrustans		-	8.0	-	-	-	-	-	-	-	120	-	
L. hibernicum	I	0.88	2.97	-	0.66	2.23	-	-0.21	-0.63	-	346	78	Present study
	II	0.90	3.01	-	0.71	2.36	-	-0.19	-0.65	-	355	78	
	III	0.83	3.13	-	0.63	2.17	-	-0.21	-0.73	-	360	84	
	IV	0.79	2.96	-	0.58	1.98	-	-0.22	-0.74	-	349	89	

Species	Condition	FCO_{2gross}^{max}			FCO_{2net}^{max}			R_{dCO2}			E_k	E_c	References
		cm²	g dw	g wt	cm²	g dw	g wt	cm²	g dw	g wt	cm²	cm²	
L. corallioides	winter	-	-	-	-	-	-0.68	-	-	0.07	125	12	(MARTIN; CASTETS; CLAVIER, 2006)
L. corallioides	summer	-	-	-	-	-	-1.48	-	-	0.30	179	40	
L. cabiochae	winter	-0.43	-	-	-0.37	-	-	-	-	-	9	1.3	*(MARTIN et al., 2013)
L. cabiochae	summer	-1.11	-	-	-0.84	-	-	-	-	-	29	7	
L. cabiochae	-	-1.01	-	-3.25	-0.81	-	-2.56	0.20	-	0.69	43	8	(MARTIN; CHARNOZ; GATTUSO, 2013)
E. elongata	winter	-	-20.4	-	-	-20.0	-	-	0.44	-	29	0.6	(EGILSDOTTIR; OLAFSSON; MARTIN, 2016)
E. elongata	summer	-	-69.1	-	-	-52.2	-	-	16.90	-	89	19	
L. hibernicum	I	-1.50	-4.68	-	-0.91	-3.09	-	0.60	1.81	-	445	167	Present study
	II	-1.28	-4.30	-	-0.85	-2.83	-	0.49	1.47	-	342	129	
	III	-1.21	-4.49	-	-0.92	-3.20	-	0.38	1.30	-	384	118	
	IV	-1.35	-4.68	-	-0.87	-3.01	-	0.48	1.67	-	339	120	

Species	Condition	-			G^{max}			G_d			E_k	E_c	References
		-	-	-	cm²	g dw	g wt	cm²	g dw	g wt	cm²	cm²	
L. corallioides	winter	-	-	-	-	-	-0.38	-	-	0.03	123	-9	(MARTIN; CASTETS; CLAVIER, 2006)
L. corallioides	summer	-	-	-	-	-	-0.60	-	-	0.07	102	-12	
L. cabiochae	winter	-	-	-	0.05	-	-	-	-	-	8	-	*(MARTIN et al., 2013)
L. cabiochae	summer		-	-	0.42	-	-	-	-	-	46	-	
L. cabiochae	-	-	-	-	0.37	-	1.26	0.08	-	0.28	36	-	(MARTIN; CHARNOZ; GATTUSO, 2013)
E. elongata	winter	-	-	-	-	2.29	-	-	-0.24	-	31	1.7	(EGILSDOTTIR; OLAFSSON; MARTIN, 2016)
E. elongata	summer	-	-	-	-	6.3	-	-	1.35	-	65	-	
L. corallioides	winter	-	-	-	-	0.64	-	-	-	-	87	-	*(QUI-MINET et al., 2019)

Species	Condition	P_{gross}^{max}			P_{net}^{max}			R_d			E_k	E_c	Reference
		cm^2	g dw	g wt	cm^2	g dw	g wt	cm^2	g dw	g wt	cm^2	cm^2	
P. calcareum		-	-	-	-	0.43	-	-	-	-	104	-	
L. incrustans		-	-	-	-	1.05	-	-	-	-	125	-	
L.corallioides		-	-	-	-	1.3	-	-	-	-	97	-	
P. calcareum	summer	-	-	-	-	0.65	-	-	-	-	129	-	
L. incrustans		-	-	-	-	2.27	-	-	-	-	122	-	
L. hibernicum	I	-	-	-	0.77	2.62	-	-0.12	-0.40	-	377	31	Present study
	II	-	-	-	0.60	1.93	-	0.15	0.58	-	419	180	
	III	-	-	-	0.76	2.66	-	0.13	0.44	-	329	56	
	IV	-	-	-	0.63	2.20	-	0.32	1.11	-	676	406	

P_{gross}^{max} and P_{net}^{max} (maximum gross and net O_2 production), FCO_{2gross}^{max} and FCO_{2net}^{max} (maximum gross and net CO_2 fixation), G^{max} (maximum calcification), R_d and Rd_{CO2} (dark respiration), G_d (dark calcification), E_k (saturation irradiance), E_c (compensation irradiance). Values were normalized by photosynthetic area or thallus area (µmol O_2 or CO_2 or $CaCO_3$ cm^{-2} h^{-1}), by dry biomass (µmol O_2 or CO_2 or $CaCO_3$ g^{-1} DW h^{-1}), or by wet biomass (µmol O_2 or CO_2 or $CaCO_3$ g^{-1} WT h^{-1}). E_k and E_c are in µmol photons m^{-2} s^{-1}.

Unreported values (-). Present study conditions are I (rhodoliths/adaxial), II (rhodoliths/abaxial), III (rhodoliths/seagrass/adaxial) and IV (rhodoliths/seagrass/abaxial).

*Photosynthesis and calcification data were obtained from the control (environmental conditions).

Considering daily primary productivity and daily calcification rates (Table 15), we found no statistical differences between the conditions evaluated for O_2 production and CO_2 fixation, although our daily calcification rates varied. Both faces of the rhodoliths collected outside seagrass meadow (rhodoliths/adaxial and rhodoliths/abaxial) showed the lowest values of calcification around 8 μmol $CaCO_3$ cm^{-2} d^{-1}. Meanwhile, both faces of the rhodoliths collected within seagrass meadow (rhodoliths/seagrass/adaxial and rhodoliths/seagrass/abaxial) exhibited values above 10 μmol $CaCO_3$ cm^{-2} d^{-1}. For better understanding, daily calcification calculations considered 12h of calcification plus 12h of dark calcification (G_d). Although rhodoliths/adaxial showed high calcification under light, in the dark the values were negative, dissolving $CaCO_3$ (Table 14). On the other hand, rhodoliths/seagrass/abaxial showed a low value of calcification and the highest value of G_d, resulting in the highest daily calcification rates (11.4 μmol $CaCO_3$ cm^{-2} d^{-1} and 39.7 μmol $CaCO_3$ g^{-1} DW d^{-1}), see Tables 14 and 15. Our daily calcification rates in rhodoliths/seagrass/abaxial were significantly higher compared to the rates obtained for *L. corallioides* (9.7 μmol $CaCO_3$ g^{-1} DW d^{-1}) in the summer at 1m depth and *L. cabiochae* (13.7 $CaCO_3$ g^{-1} DW d^{-1}) at 25 m depth (MARTIN; CASTETS; CLAVIER, 2006; MARTIN; CHARNOZ; GATTUSO, 2013).

The differently pigmented faces of rhodoliths showed different amounts of phycobiliproteins (PBP), mainly phycoerythrin. Thus, the abaxial faces showed a higher amount of this pigment compared to the adaxial faces. The highest concentration of phycoerythrin was observed in rhodoliths/seagrass/abaxial, as we expected because the abaxial face of the rhodoliths collected within seagrass meadow was visibly more pigmented than the other faces. (Table 16). On the other hand, rhodoliths/adaxial showed the highest concentration of chlorophyll *a* (Chl*a*), especially when compared to rhodoliths/seagrass/abaxial. These differences are clearly expressed in the PBP:Chl*a* ratio (Table 16). The pigment composition of red algae can vary depending on the quality and intensity of light. This process is known as chromatic adaptation occurring both in cyanobacteria and red algae (FIGUEROA; AGUILERA; NIELL, 1995; KIRK, 2011b; SANFILIPPO et al., 2019; TALARICO; MARANZANA, 2000). Rhodoliths with their faces fully exposed to the sun receive the entire spectrum of radiation, which contains the wavelengths that are absorbed by chlorophyll *a*, the main photosynthetic pigment. In seagrass meadows, light reaches the surface of rhodoliths after passing through the seagrass leaves. Thus, the quality of light reaching the rhodoliths is variable and possibly better absorbed by phycobiliproteins. As a result, the abaxial face of rhodoliths associated with seagrasses showed a higher concentration of phycobiliproteins and a lower

concentration of chlorophyll *a* compared to both faces of rhodoliths outside of seagrass meadows.

Rhodoliths/adaxial exhibited the highest concentration of carotenes, while rhodoliths/abaxial showed the highest of mycosporine-like amino acids (MAAs) (Tables 16 and 17). In both conditions, rhodoliths were collected outside seagrass meadows, i.e., they were more exposed to the sun than those inside seagrass meadows. Carotenoids are accessory pigments in light-harvesting, they also have antioxidant and photoprotective properties (RASTOGI et al., 2010). MAAs are small molecules, usually colorless, soluble in water and absorb UV-A and UV-B wavelengths. These molecules are found in several marine organisms, including red algae. Among other functions, MAAs are efficient antioxidants and heat dissipators, they can also contribute to the osmotic balance under ionic stress. For these and other characteristics, MAAs are considered photoprotective compounds (LA BARRE; ROULLIER; BOUSTIE, 2014; RASTOGI et al., 2010; SUN et al., 2020).

In summary, we verified a complex relationship between the carbonate system and the physiological processes of *L. hibernicum*. The changes in the forms of dissolved inorganic carbon (DIC) happened gradually, as the algae was exposed to the dark and to different intensities of light. The increase in irradiance caused an increase in photosynthesis and calcification. Both processes showed a positive relationship in previous studies (MARTIN et al., 2013; MARTIN; CASTETS; CLAVIER, 2006; SORDO et al., 2018). PCO results showed that temperature, pH, calcification, net O_2 flux, CO_3^{-2}, Ω calcite and Ω aragonite were greater under high irradiance and inversely related to AT, DIC, net CO_2 flux, HCO_3^-, CO_2 and pCO_2. The rates of daily primary productivity (CO_2 and O_2) were not affected by the face or place of collection. On the other hand, the rates of daily calcification were different between rhodoliths collected outside and inside seagrass meadow. The differences were due to dark calcification (G_d), which was significantly different mainly between rhodoliths/adaxial and rhodoliths/seagrass/abaxial. That is, the face most exposed to light presented negative G_d and the least exposed to light presented G_d 2-3-fold higher. These differences can be the result of acclimatization mechanisms to the conditions in which the rhodoliths were exposed before collection, i.e., in the field. Figure 53 shows the calcification versus irradiance, being possible to verify the differences in the behavior of the curves of the different conditions evaluated. Assuming that, in the field, rhodoliths outside seagrass meadows exhibit greater dissolution of calcium carbonate at night compared to rhodoliths within seagrass meadows, then the deposition of this carbon form can be significantly different between these ecosystems.

However, further studies are needed to clarify dark calcification, since some authors cite G_d as a late physiological process due to the transition of algae from light to dark. Considering the differently pigmented faces, our results confirm the pigment content differences. Abaxial faces of the rhodoliths showed a higher concentration of phycoerythrin than adaxial faces. These and other differences found in the concentration of pigments did not reflect directly on the physiological processes, especially photosynthesis (O_2 production).

8 DISCUSSÃO GERAL

As algas produzem substâncias químicas diversas, com estruturas complexas e algumas difíceis de serem sintetizadas. O potencial das algas para serem utilizadas como fontes de compostos depende de uma alta produção natural ou de fatores que induzam essa produção. No **Capítulo I** desta tese foi realizada uma bioprospecção incluindo 22 espécies de algas (pardas, vermelhas e verdes) e um líquen. Os extratos obtidos desses organismos foram avaliados quanto as características bioquímicas e potencial de fotoproteção.

As algas vermelhas se destacaram por apresentar alto conteúdo de aminoácidos tipo micosporinas (MAAs), especialmente as espécies *Bangia atropurpurea* e *Porphyra umbilicalis*. Esta última também se destacou na quantidade de polifenóis. Os MAAs e os polifenóis atuam como antioxidantes e substâncias de fotoproteção (ABDALA-DÍAZ et al., 2014; CHAROENSIDDHI et al., 2017a; LA BARRE; ROULLIER; BOUSTIE, 2014; MACHU et al., 2015; PANGESTUTI; SIAHAAN; KIM, 2018; SCHMID; SCHÜRCH; ZÜLLI, 2004). Consequentemente, a espécie *P. umbilicalis* também se destacou nos parâmetros utilizados para determinar a capacidade de fotoproteção (%ESAR e EPI).

As algas pardas apresentaram alto conteúdo de polifenóis, especialmente *Carpodesmia tamariscifolia* e *Sargassum vulgare*. Os compostos fenólicos de algas pardas exibem altos teores de florotaninos que podem representar até 14% da biomassa seca (CHAROENSIDDHI et al., 2017a). Além disso, o pigmento fucoxantina que confere a colocaração às algas pardas também foi identificado neste estudo pelo pico proeminante presente na porção vísivel do espectro (em torno de 450 nm). Tanto os florotaninos como a fucoxantina apresentam atividade antioxidante e de fotoproteção (ABDALA-DÍAZ et al., 2014; ANDRADE et al., 2013; CELIS-PLÁ et al., 2016; JASWIR et al., 2013; NURJANAH et al., 2017; PANGESTUTI; SIAHAAN; KIM, 2018). *S. vulgare* se destacou em ambos os parâmetros utilizados para avaliar a capacidade de fotoproteção, %ESAR e EPI.

As algas verdes apresentaram baixo conteúdo de compostos fenólicos, MAAs e pouca atividade antioxidante. A espécie *Ulva lactuca* se destacou dentre todas que foram avaliadas. Na varredura UV, *U. lactuca* apresentou um pico em 290 nm, enquanto no espectro visível picos foram observados entre 400 e 500 nm e entre 600 e 700 nm para todas as algas verdes. Os picos observados na porção visível do espectro coincidem com as regiões de absorção dos pigmentos fotossintéticos, incluindo clorofilas e carotenoides (GRAHAM et al., 2016a). As

algas verdes não se destacaram nas outras análises quando comparada com espécies de algas vermelhas e pardas.

O líquen (*Lichina pygmaea*) avaliado se destacou para polifenóis e MAAs, mostrando também alta atividade antioxidante, porém não foi analisado quanto ao potencial de fotoproteção por apresentar quantidades muito baixas de biomassa. *L. pygmaea* apresentou duas micosporinas (glicina e serinol) interessantes que absorvem em 310 nm, região UV-B do espectro. Estes MAAs já foram anteriormente descritos na literatura para esta espécie (LA BARRE; ROULLIER; BOUSTIE, 2014).

Os **Capítulos II** e **III** tiveram como objetivo verificar respostas fisiológicas e bioquímicas induzidas por diferentes qualidades de radiação UV-Visível e mediadas por fotorreceptores não fotossintéticos nas algas vermelhas *Osmundea pinnatifida* e *Gracilaria cornea*. O delineamento experimental foi baseado na literatura (BRITZ; SAGER, 1990; SEGOVIA; GORDILLO; FIGUEROA, 2003; THOMAS; DICKINSON, 1979). Os tratamentos foram realizados com uma fonte de luz de alta intensidade, a fim de saturar a fotossíntese, e radiações monocromáticas complementares de baixa intensidade (radiação ultravioleta UV-A e UV-B e ≈ 20 μmol fótons m^{-2} s^{-1} de azul, verde e vermelho), com objetivo de ativar fotorreceptores sem causar grandes mudanças na fotossíntese. A luz de alta intensidade foi fornecida por uma lâmpada SOX (lâmpada de sódio de baixa pressão). O espectro de emissão desta lâmpada apresentava um pico estreito no amarelo/laranja (590 nm), assim a luz emitida não poderia interferir com fotorreceptores sensíveis às radiações complementares.

No **Capítulo II**, a radiação UV-A (SOX+UVA) pareceu influenciar positivamente o crescimento em *O. pinnatifida,* assim como em outros estudos (ALTAMIRANO; FLORES-MOYA; FIGUEROA, 2000; GAO; XU, 2008; HENRY; ALSTYNE, 2004). No **Capítulo III**, o crescimento de *G. cornea* também foi afetado positivamente pelo tratamento SOX+UVA após oito dias de experimento. O tratamento SOX+UVA continha um pico de luz azul, o qual pode ter influenciado nos resultados. O pico de luz azul presente nos tratamentos UV (SOX+UVA e SOX+UVA+UVB) apresentava emissão máxima em 436 nm, enquanto o tratamento SOX+B tinha luz azul com um pico de emissão em 459 nm. *G. cornea* sob o tratamento SOX+B também mostrou maior crescimento em relação à luz SOX sozinha após 8 dias. Tanto a radiação UV-A quanto a luz azul são detectadas por um fotorreceptor, o criptocromo (JIANG; LI, 2015). Este sensor de luz está associado com fotoenzimas conhecidas por reparar danos ao DNA (BJÖRN, 2015b; OLIVERI et al., 2014a). Além disso, outros estudos mostraram que a radiação UV-A e PAR podem atuar no reparo de dímeros de timina e fotoprodutos após exposição à radiação

UV-B em algas vermelhas (PAKKER et al., 2000; PAKKER; BEEKMAN; BREEMAN, 2000). Assim, é possível que o efeito positivo da radiação UV-A e do pico de luz azul (436 nm) sobre o crescimento de *O. pinnatifida* e *G. cornea* tenha ocorrido de forma indireta pelo favorecimento de vias de fotoproteção, uma vez que todos os tratamentos receberam luz de alta fluência da lâmpada SOX. Além disso, sob SOX+UVA *G. cornea* também produziu alguns compostos em maior quantidade que SOX sozinha, tais como: o carotenoide zeaxantina e o MAA palitina.

Quanto aos efeitos radiação UV-B (SOX+UVA+UVB), ambas as espécies, *O. pinnatifida* e *G. cornea*, mostram um declínio no crescimento após 8 dias. Efeitos negativos da radiação UV-B foram verificados em outros estudos, os autores observaram uma melhora no crescimento quando a radiação UV-B era cortada dos tratamentos, mantendo somente PAR e UV-A (ALTAMIRANO; FLORES-MOYA; FIGUEROA, 2000; GAO; XU, 2008). Se por um lado a radiação UV-B prejudica o crescimento, por outro lado ela parece favorecer o acúmulo de compostos, tais como MAAs e carotenoides. O acúmulo de compostos em resposta a radiação UV-B foi verificado em outras algas (BONOMI-BARUFI et al., 2020; KRÄBS et al., 2002).

O. pinnatifida e *G.cornea* apresentaram os carotenoides do ciclo das xantofilas (XC) a violaxantina, zeaxantina e anteraxantina. O XC é responsável por dissipar o excesso de anergia absorvido pelo aparato fotossintético. Este ciclo reduz a geração de espécies reativas que possam causar danos, liberando energia na forma de calor (BJÖRN, 2015a). Violaxantina foi observada em menor quantidade em ambas as espécies, enquanto zeaxantina foi observada em maior quantidade em *O. pinnatifida*, principalmente no tratamento SOX+UVA+UVB após 15 dias. *G. cornea* apresentou maior quantidade de anteraxantina após 8 dias, principalmente em SOX+UVA+UVB. A quantidade de zeaxantina também foi significativa em *G. cornea,* mas especialmente em SOX+UVA após 15 dias. A presença de carotenoides do XC pode indicar que este ciclo esteja operando, embora em algas vermelhas sua existência é discutida (DAUTERMANN; LOHR, 2017; SCHUBERT; GARCÍA-MENDOZA; PACHECO-RUIZ, 2006). De qualquer forma, em ambas as espécies estes carotenoides podem ter atuado na fotoproteção, uma vez que o acúmulo de zeaxantina sob estresse de luz foi relatado em estudos anteriores (SCHUBERT; GARCÍA-MENDOZA, 2008; SCHUBERT; GARCÍA-MENDOZA; PACHECO-RUIZ, 2006). A zeaxantina é capaz de absorver o excesso de energia a partir da Chl*a*, dissipando na forma de calor (BJÖRN, 2015a).

Os MAAs também são considerados compostos de fotoproteção e variam conforme a qualidade de radiação (KARSTEN et al., 1999b; LA BARRE; ROULLIER; BOUSTIE, 2014; SUN et al., 2020). Os MAAs foram detectados nas algas *O. pinnatifida* e *G. cornea*. Em *O. pinnatifida*, a quantidade total de MAAs variou em relação aos tratamentos, embora esta variação não tenha sido significativa. Além disso, em todos os tratamentos o conteúdo de MAAs decresceu em relação aos valores iniciais. Em *G. cornea,* os MAAs aumentaram em todos os tratamentos em relação aos valores iniciais. O MAA palitine foi encontrado em maior quantidade no tratamento SOX+UVA+UVB após 15 dias de cultivo, embora as concentrações deste MAA foram as menores dentre os demais MAAs.

No **Capítulo IV**, o objetivo foi investigar a fotossíntese, a respiração e a calcificação sob diferentes irradiâncias na alga coralina vermelha *Lithophyllum hibernicum*. Diferentes condições foram avaliadas, uma vez que esta alga ocorre dentro e fora de prados de ervas marinhas no local onde foi coletada. Além disso, *L. hibernicum* apresentava no momento da coleta duas faces diferentemente pigmentadas, em função da baixa hidrodinâmica do local. As algas coralinas apresentam importantes papéis ecológicos. Dentre eles, influenciam o ciclo de carbono por meio da fotossíntese e da calcificação (GRAHAM et al., 2016b). A compreensão desses processos nas macroalgas ainda é incompleta. A luz é essencial para o processo fotossintético, o qual está positivamente relacionado com a calcificação. Embora, além de influenciar a fotossíntese, a luz parece ativar bombas complexas de íons que atuam na captação de carbono inorgânico e na calcificação(HOFMANN; KOCH; BEER, 2016).

Para entender melhor a produção primária e a calcificação de *L. hibernicum,* foi realizada uma curva de luz com diferentes intensidades. Como esperado, no escuro ocorre a liberação do CO_2 pela respiração e um declínio no pH, resultando em valores negativos na calcificação de alguns espécimes de *L. hibernicum* (aqueles coletados fora dos prados de ervas marinhas, face adaxial). Esses valores negativos indicam descalcificação. Quando as algas foram expostas a irradiâncias crescentes, ocorre um declínio do pCO_2 e da alcalinidade total, enquanto o pH, os íons carbonato (CO_3^{-2}) e o estado de saturação da calcita e aragonita aumentam. Isso leva a um incremento nas taxas de calcificação (DONEY et al., 2009; HOFMANN; BISCHOF, 2014). A fotossíntese retira CO_2 da água propiciando condições favoráveis para calcificação. Ambos os processos atingem um valor máximo em uma irradiância específica e depois ocorre uma estabilização, seguida de um leve declínio. Para os rodolitos aclimatados às condições dos prados de ervas marinhas, a calcificação no escuro é positiva, portanto, a produtividade diária é maior. Para alguns autores, a calcificação no escuro

é um processo biológico atrasado, que ocorre após a transição da alga da luz para o escuro (CHISHOLM, 2000; EL HAÏKALI et al., 2004). Entretanto, as coralinas do gênero *Clathromorphum* continuam a crescer na escuridão do Ártico, usando possivelmente fotossintátos estocados (ADEY; HALFAR; BRANWEN, 2013). As ervas marinhas podem alterar parâmetros como luz e pH no ambiente circundante. Em campo, foi possível verificar valores de pH maiores dentro dos prados (pH médio 8,16) do que em áreas adjacentes onde as gramas marinhas estavam ausentes (pH médio 8,09). Entretanto, não é possível afirmar que as condições nas quais os rodolitos estavam aclimatados do campo são de fato responsáveis pelas taxas de calcificação obtidas no escuro em laboratório.

A análise de pigmentos confirmou a presença de faces. As faces abaxiais apresentaram maior quantidade de ficobiliproteínas, especialmente, ficoeritrina. Os rodolitos coletados fora dos prados de ervas marinhas apresentaram maior quantidade de clorofila, carotenoides e MAAs. Os carotenoides e os MAAs são considerados compostos de fotoproteção (LA BARRE; ROULLIER; BOUSTIE, 2014; RASTOGI et al., 2010).

9 CONCLUSÕES GERAIS

No **Capítulo I** foi possível identificar espécies que se distinguem na quantidade e qualidade de compostos. As algas *S. vulgare*, *C. tamariscifolia*, *P. umbilicalis* e o líquen *L. pygmaea* se destacaram pela quantidade de polifenóis e pela atividade antioxidante. *P. umbilicalis* e *L. pygmaea* também se destacaram pela quantidade de MAAs. Dentre as espécies, *S. vulgare* e *P. umbilicalis* apresentam os melhores valores, por isso, foram consideradas como fontes potenciais de compostos antioxidantes e de fotoproteção.

Nos **Capítulo II e III**, foi possível verificar que a radiação UV atua sobre o crescimento e o acúmulo de compostos em *O. pinnatifida* e *G. cornea*. A radiação UV-A juntamente com a luz azul parece favorecer o crescimento, como ambas as qualidades de radiação são percebidas pelo criptocromo, pode ser que as respostas positivas em relação ao crescimento sejam consequências indiretas da ativação de vias de fotoproteção. Além disso, sob UV-A e luz azul (SOX+UVA) alguns compostos são produzidos em maior quantidade (carotenoides e MAAs em *G. cornea*) e isso não parece afetar o crescimento. Já com relação a radiação UV-B, esta parece favorecer o acúmulo de compostos às custas do crescimento. Um fotorreceptor UVR parece estar envolvido nessas respostas, embora seja necessário o uso de ferramentas de sequenciamento para identificá-lo. Em outro estudo (FERNÁNDEZ et al., 2016), o UVR8 foi identificado como um fotorreceptor sensível à radiação UV-B, embora seja encontrado somente em algas verdes.

No **Capítulo IV**, foi possível verificar uma relação complexa entre o sistema carbonato e as respostas fisiológicas de *L. hibernicum.* As mudanças na química do carbono ocorrem em resposta a respiração, fotossíntese e calcificação da alga exposta ao escuro e às diferentes intensidades de luz. A fotossíntese retira CO_2 do sistema, aumentando o pH e o estado de saturação da calcita e aragonita, assim a calcificação é favorecida. A calcificação diária dos rodolitos coletados dentro dos bancos de gramas marinhas foi maior, em função da calcificação no escuro. Isso pode ser resultado da aclimatação dos rodolitos às condições mais sombreadas e com pH maior, como observado em campo. A presença de faces nos rodolitos foi confirmada pela análise de pigmentos. A coloração diferenciada ocorre em função das ficobiliproteínas, principalmente a ficoeritrina, que ocorreu em maior concentração nas faces abaxiais. Os carotenoides e MAAs ocorreram em maior concentração nas faces adaxiais, possivelmente, porque além de outras funções são também compostos de fotoproteção.

De forma geral, foi possível concluir que as macroalgas podem ser importantes fontes de compostos de interesse, conforme verificado no processo de prospecção que identificou *S. vulgare* e *P. umbilicalis* como espécies relevantes. Além disso, as macroalgas podem ser reguladas em suas respostas fisiológicas e bioquímicas como foi visto para *O. pinnatifida* e *G. cornea,* especialmente em relação a radiação UV e luz azul. É importante destacar ainda que a fisiologia das algas precisa ser mais bem compreendida como foi observado para a alga coralina *L. hibernicum,* a qual foi exposta ao escuro e a diferentes intensidade de luz em uma "light curve". Desta forma, esta tese contribui sobre o entendimento de compostos produzidos por macroalgas, regulação dos mesmos e aspectos ecofisiológicos da alga coralina *L. hibernicum*.

REFERÊNCIAS

ABDALA-DÍAZ, R. T. et al. Intra-thallus variation of phenolic compounds, antioxidant activity, and phenolsulphatase activity in *Cystoseira tamariscifolia* (Phaeophyceae) from southern Spain. **Ciencias Marinas**, v. 40, n. 1, p. 1–10, 30 mar. 2014.

ADAMS III, W. W. et al. Energy Dissipation and Photoinhibition: A Continuum of Photoprotection. In: DEMMIG-ADAMS, B.; ADAMS, W. W.; MATTOO, A. K. (Eds.). . **Photoprotection, Photoinhibition, Gene Regulation, and Environment**. Dordrecht: Springer, 2008. p. 49–64.

ADEY, W. H.; HALFAR, J.; BRANWEN, W. **The coralline genus *Clathromorphum* Foslie emend. AdeySmithsonian Institution Scholarly Press**Washington, D.C, 2013. Disponível em: <https://repository.si.edu/bitstream/handle/10088/21560/SCMS-0040.web.pdf>. Acesso em: 29 set. 2021

AGUILERA, J.; FIGUEROA, F. L.; NIELL, F. X. Photocontrol of short-term growth in *Porphyra leucosticta* (Rhodophyta). **British Phycological Society**, v. 32, n. 4, p. 417–424, 1997.

AGUIRRE, J.; BRAGA, J. C.; BASSI, D. Rhodoliths and rhodolith beds in the rock record. In: RIOSMENA-RODRÍGUEZ, R.; NELSON, W.; AGUIRRE, J. (Eds.). . **Rhodolith/Maërl Beds: A Global Perspective**. [s.l.] Coastal Research Library, Springer, 2017. v. 15p. 105–138.

ALLORENT, G.; PETROUTSOS, D. Photoreceptor-dependent regulation of photoprotection. **Current Opinion in Plant Biology**, v. 37, p. 102–108, 1 jun. 2017.

ALTAMIRANO, M.; FLORES-MOYA, A.; FIGUEROA, F. L. Long-Term Effects of Natural Sunlight under Various Ultraviolet Radiation Conditions on Growth and Photosynthesis of Intertidal *Ulva rigida* (Chlorophyceae) Cultivated In Situ. **Botanica Marina**, v. 43, n. 2, p. 119–126, 8 jan. 2000.

ÁLVAREZ-GÓMEZ, F. et al. Combined effects of UVR and nutrients on cell ultrastructure, photosynthesis and biochemistry in *Gracilariopsis longissima* (Gracilariales, Rhodophyta). **Algal Research**, v. 26, p. 190–202, 1 set. 2017.

ÁLVAREZ-GÓMEZ, F. et al. UV photoprotection, cytotoxicity and immunology capacity of red algae extracts. **Molecules**, v. 24, n. 2, p. 341, 18 jan. 2019.

ÁLVAREZ-GÓMEZ, F.; KORBEE-PEINADO, N.; FIGUEROA, F. L. Analysis of antioxidant capacity and bioactive compounds in marine macroalgal and lichenic extracts using different solvents and evaluation methods. **Ciencias Marinas**, v. 42, n. 4, p. 271–288, 15 dez. 2016.

ÁLVAREZ-GÓMEZ, F.; KORBEE, N.; FIGUEROA, F. L. Effects of UV Radiation on Photosynthesis, Antioxidant Capacity and the Accumulation of Bioactive Compounds in *Gracilariopsis longissima* , *Hydropuntia cornea* and *Halopithys incurva* (Rhodophyta). **Journal of Phycology**, v. 55, n. 6, p. 1258–1273, 19 dez. 2019.

ANDRADE, P. B. et al. Valuable compounds in macroalgae extracts. **Food Chemistry**, v. 138, n. 2–3, p. 1819–1828, 1 jun. 2013.

ANTONIOU, C. et al. Sunscreens - what's important to know. **Journal of the European Academy of Dermatology and Venereology**, v. 22, n. 9, p. 1110–8, maio 2008.

ARAÚJO, S. A. C.; DEMINICIS, B. B. Fotoinibição da Fotossíntese. **Revista Brasileira de Biociências**, v. 7, n. 4, p. 463–472, 2009.

AVILA, M. et al. Cultivation of the red alga Chondracanthus chamissoi: sexual reproduction and seedling production in culture under controlled conditions. **Journal of Applied Phycology 2010 23:3**, v. 23, n. 3, p. 529–536, 25 nov. 2010.

AYYAD, S. N. et al. Antioxidant, cytotoxic, antitumor, and protective DNA damage metabolites from the red sea brown alga *Sargassum* sp. **Pharmacognosy research**, v. 3, n. 3, p. 160–5, jul. 2011.

BARSANTI, L.; GUALTIERI, P. **Anatomy, Biochemistry, and Biotechnology**. 1st Editio ed. Boca Raton: [s.n.].

BARUFI, J. B. et al. Effects of N supply on the accumulation of photosynthetic pigments and photoprotectors in *Gracilaria tenuistipitata* (Rhodophyta) cultured under UV radiation. **Journal of Applied Phycology**, v. 23, n. 3, p. 457–466, 20 jun. 2011a.

BARUFI, J. B. et al. Effects of N supply on the accumulation of photosynthetic pigments and photoprotectors in *Gracilaria tenuistipitata* (Rhodophyta) cultured under UV radiation. **Journal of Applied Phycology**, v. 23, n. 3, p. 457–466, 20 jun. 2011b.

BARUFI, J. B. et al. Nitrate reduces the negative effect of UV radiation on photosynthesis and pigmentation in *Gracilaria tenuistipitata* (Rhodophyta): The photoprotection role of mycosporine-like amino acids. **Phycologia**, v. 51, n. 6, p. 636–648, nov. 2012.

BARUFI, J. B. et al. Effects of light quality on reproduction, growth and pigment content of *Gracilaria birdiae* (Rhodophyta: Gracilariales). **Scientia Marina**, v. 79, n. 1, p. 15–24, 30 mar. 2015.

BEDOUX, G. et al. Production and properties of mycosporine-like amino acids isolated from seaweeds. In: BOURGOUGNON, N. (Ed.). . **Advances in Botanical Research**. [s.l.] Academic Press Inc., 2020. v. 95p. 213–245.

BEER, S.; ESCHEL, A. Determining phycoerythrin and phycocyanin concentrations in aqueous crude extracts of red algae. **Marine and Freshwater Research**, v. 36, n. 6, p. 785, 1985.

BIKKER, P. et al. Biorefinery of the green seaweed *Ulva lactuca* to produce animal feed, chemicals and biofuels. **Journal of Applied Phycology**, v. 28, n. 6, p. 3511–3525, 1 dez. 2016.

BIRD, C. J.; DEOLIVEIRA, E. C.; MCLACHLAN, J. *Gracilaria cornea*, the correct name for the western Atlantic alga hitherto known as *G. debilis* (Rhodophyta, Gigartinales). **Canadian Journal of Botany**, v. 64, n. 9, p. 2045–2051, 1986.

BISCHOF, K.; HANELT, D.; WIENCKE, C. Effects of ultraviolet radiation on photosynthesis and related enzyme reactions of marine macroalgae. **Planta**, v. 211, n. 4, p. 555–562, 2000.

BISSETT, D. L.; HANNON, D. P.; ORR, T. V. Wavelength dependence of histological, physical, and visible changes in chronically UV-irradiated hairless mouse skin. **Photochemistry and Photobiology**, v. 50, n. 6, p. 763–769, dez. 1989.

BJÖRN, L. O. The nature of light and its interaction with matter. In: BJÖRN L.O. (Ed.). . **Photobiology: The Science of Life and Light**. 2. ed. New York: Springer , 2008. p. 20.

BJÖRN, L. O. Hints for teaching experiments and demonstrations. In: BJÖRN L.O. (Ed.). . **Photobiology: The Science of Life and Light**. 3. ed. New York: Springer, 2015a. p. 421–436.

BJÖRN, L. O. Photoactive proteins. In: BJÖRN L. (Ed.). . **Photobiology: The Science of Light and Life**. 3. ed. New York: Springer , 2015b. p. 139–150.

BJÖRN, L. O.; GHIRADELLA, H. Spectral Tuning in Biology I: Pigments. In: BJÖRN, L. O. (Ed.). . **Photobiology: The Science of Light and Life**. 3. ed. New York: Springer, 2015. p. 97–117.

BLOIS, M. S. Antioxidant Determinations by the Use of a Stable Free Radical. **Nature 1958**

181:4617, v. 181, n. 4617, p. 1199–1200, 1958.

BONOMI-BARUFI, J. **Fotoproteção em *Gracilaria tenuistipitata* (Rhodophyta): uma abordagem fisiológica e molecular**. [s.l.] Universidade de São Paulo, 2010.

BONOMI-BARUFI, J. et al. How macroalgae can deal with radiation variability and photoacclimation capacity: The example of *Gracilaria tenuistipitata* (Rhodophyta) in laboratory. **Algal Research**, v. 50, p. 102007, 1 set. 2020.

BOSELLINI, A.; GINSBURG, R. N. Form and Internal Structure of Recent Algal Nodules (Rhodolites) from Bermuda. **The Journal of Geology**, v. 79, n. 6, p. 669–682, 29 nov. 1971.

BOSENCE, D. W. J. The Occurrence and Ecology of Recent Rhodoliths — A Review. In: PERYT, T. M. (Ed.). . **Coated Grains**. Berlin, Heidelberg: Springer , 1983. p. 225–242.

BRADFORD, M. M. A rapid and sensitive method for the quantitation of microgram quantities of protein utilizing the principle of protein-dye binding. **Analytical Biochemistry**, v. 72, n. 1–2, p. 248–254, 7 maio 1976.

BRAND-WILLIAMS, W.; CUVELIER, M. E.; BERSET, C. Use of a free radical method to evaluate antioxidant activity. **LWT - Food Science and Technology**, v. 28, n. 1, p. 25–30, 1 jan. 1995.

BRIGGS, W. R. Blue/UV-A receptors: historical overview. In: SCHÄFER, E.; NAGY, F. (Eds.). . **Photomorphogenesis in Plants and Bacteria**. 3. ed. Netherlands: Springer, 2006. p. 171–197.

BRITO, T. V. et al. Anti-inflammatory effect of a sulphated polysaccharide fraction extracted from the red algae Hypnea musciformis via the suppression of neutrophil migration by the nitric oxide signalling pathway. **Journal of Pharmacy and Pharmacology**, v. 65, n. 5, p. 724–733, 1 maio 2013.

BRITZ, S. J.; SAGER, J. C. Photomorphogenesis and photoassimilation in soybean and sorghum grown under broad spectrum or blue-deficient light sources. **Plant physiology**, v. 94, n. 2, p. 448–54, 1 out. 1990.

BRODY, M.; EMERSON, R. The effect of wavelength and intensity of light on the proportion of pigments in *Porphyridium cruentum*. **American Journal of Botany**, v. 46, n. 6, p. 433–440, 1 jun. 1959.

BUSCHMANN, A. H. et al. Experimental indoor cultivation of the carrageenophytic red alga

*Gigartina skottsbe*rgii. **Aquaculture**, v. 241, n. 1–4, p. 357–370, 26 nov. 2004.

CAI, J. et al. **Seaweeds and microalgae: an overview for unlocking their potential in global aquaculture developmentSeaweeds and microalgae: an overview for unlocking their potential in global aquaculture development**Rome, ItalyFAO, , 16 jul. 2021.

CARDOZO, K. H. M. et al. Metabolites from algae with economical impact. **Comparative Biochemistry and Physiology Part C: Toxicology & Pharmacology**, v. 146, n. 1–2, p. 60–78, 1 jul. 2007.

CARR, H.; BJORK, M. A methodological comparison of photosynthetic oxygen evolution and estimated electron transport rate in tropical *Ulva* (Chlorophyceae) species under different light and inorganic carbon conditions. **Journal of Phycology**, v. 39, n. 6, p. 1125–1131, 1 dez. 2003.

CARRILLO, J. M. A.; ACEDO, M. S. **Algas, hongos y fanerógamas marinas de las Islas Canarias : clave analítica**. [s.l.] Servicio de Publicaciones, Universidad de La Laguna, 1999.

CASTRO-VARELA, P. A. et al. Photobiological Effects on Biochemical Composition in *Porphyridium cruentum* (Rhodophyta) with a Biotechnological Application. **Photochemistry and Photobiology**, 2021.

CAVALCANTI, G. S. et al. Physiologic and metagenomic attributes of the rhodoliths forming the largest CaCO3 bed in the South Atlantic Ocean. **ISME Journal**, v. 8, n. 1, p. 52–62, 29 jan. 2014.

CELIS-PLÁ, P. S. M. et al. Seasonal biochemical and photophysiological responses in the intertidal macroalga *Cystoseira tamariscifolia* (Ochrophyta). **Marine Environmental Research**, v. 115, p. 89–97, 1 abr. 2016.

CHAROENSIDDHI, S. et al. **The development of seaweed-derived bioactive compounds for use as prebiotics and nutraceuticals using enzyme technologiesTrends in Food Science and Technology**Elsevier, , 1 dez. 2017a.

CHAROENSIDDHI, S. et al. The development of seaweed-derived bioactive compounds for use as prebiotics and nutraceuticals using enzyme technologies. **Trends in Food Science and Technology**, v. 70, p. 20–33, 1 dez. 2017b.

CHISHOLM, J. R. M. Calcification by crustose coralline algae on the northern Great Barrier Reef, Australia. **Limnology and Oceanography**, v. 45, n. 7, p. 1476–1484, 1 nov. 2000.

COCKELL, C. S.; KNOWLAND, J. Ultraviolet radiation screening compounds. **Biological Reviews**, v. 74, n. 3, p. 311–345, 1999.

COLIPA. **Method for In Vitro Determination of UVA Protection, 2011, COLIPA (European Cosmetic, Toiletry and Perfumery Association). In Vitro Method for the Determination of the UVA Protection Factor and "Critical Wavelength" Values of Sunscreen ProductsGuidelines**, 2011.

COLLÉN, J. et al. Genome structure and metabolic features in the red seaweed *Chondrus crispus* shed light on evolution of the Archaeplastida. **Proceedings of the National Academy of Sciences of the United States of America**, v. 110, n. 13, p. 5247–52, 26 mar. 2013.

CORINALDESI, C. et al. Impact of inorganic UV filters contained in sunscreen products on tropical stony corals (*Acropora* spp.). **Science of The Total Environment**, v. 637–638, p. 1279–1285, 1 out. 2018.

COSGROVE, D. J. Photomodulation of growth. In: KENDRICK, R. E.; KRONENBERG, G. H. M. (Eds.). . **Photomorphogenesis in Plants**. [s.l.] Springer Netherlands, 1994. p. 631–658.

DANOVARO, R. et al. Sunscreens Cause Coral Bleaching by Promoting Viral Infections. **Environmental Health Perspectives**, v. 116, n. 4, p. 441–447, abr. 2008.

DARKO, E. et al. Photosynthesis under artificial light: the shift in primary and secondary metabolism. **Philosophical Transactions of the Royal Society B: Biological Sciences**, v. 369, n. 1640, p. 20130243–20130243, 3 mar. 2014.

DAUTERMANN, O.; LOHR, M. A functional zeaxanthin epoxidase from red algae shedding light on the evolution of light-harvesting carotenoids and the xanthophyll cycle in photosynthetic eukaryotes. **The Plant Journal**, v. 92, n. 5, p. 879–891, 1 dez. 2017.

DE BEER, D.; LARKUM, A. W. D. Photosynthesis and calcification in the calcifying algae *Halimeda discoidea* studied with microsensors. **Plant, Cell and Environment**, v. 24, n. 11, p. 1209–1217, 1 nov. 2001.

DE GRUIJL, F. R. Biological Action Spectra. **Radiation Protection Dosimetry**, v. 91, n. 1, p. 57–63, 2 set. 2000.

DE LA COBA, F. et al. Antioxidant activity of mycosporine-like amino acids isolated from three red macroalgae and one marine lichen. **Journal of Applied Phycology**, v. 21, n. 2, p. 161–169, 21 abr. 2009.

DE LA COBA, F. et al. UVA and UVB photoprotective capabilities of topical formulations containing mycosporine-like amino acids (MAAs) through different Biological Effective Protection Factors (BEPFs). **Marine Drugs**, v. 17, n. 1, p. 55, 14 jan. 2019.

DIFFEY, B. L. Solar ultraviolet radiation effects on biological systems. **Physics in Medicine and Biology**, v. 36, n. 3, p. 299–328, mar. 1991.

DIFFEY, B. L. et al. In vitro assessment of the broad-spectrum ultraviolet protection of sunscreen products. **Journal of the American Academy of Dermatology**, v. 43, n. 6, p. 1024–1035, dez. 2000.

DONEY, S. C. et al. Ocean acidification: The other CO2 problem. **Annual Review of Marine Science**, v. 1, p. 169–192, 25 mar. 2009.

DRING, M. J. Photocontrol of Development in Algae. **Annual Review of Plant Physiology and Plant Molecular Biology**, v. 39, n. 1, p. 157–174, 28 jun. 1988.

DUARTE, C. M. Nutrient concentration of aquatic plants: Patterns across species. **Limnology and Oceanography**, v. 37, n. 4, p. 882–889, jun. 1992.

DUNLAP, W. C.; CHALKER, B. E.; OLIVER, J. K. Bathymetric adaptations of reef-building corals at Davies Reef, Great Barrier Reef, Australia. III. UV-B absorbing compounds. **Journal of Experimental Marine Biology and Ecology**, v. 104, n. 1–3, p. 239–248, 31 dez. 1986.

EGILSDOTTIR, H.; OLAFSSON, J.; MARTIN, S. Photosynthesis and calcification in the articulated coralline alga *Ellisolandia elongata* (Corallinales, Rhodophyta) from intertidal rock pools. **European Journal of Phycology**, v. 51, n. 1, p. 59–70, 2 jan. 2016.

EL HAÏKALI, B. et al. Estimation of photosynthesis and calcification rates of *Corallina elongata* Ellis and Solander, 1786, by measurements of dissolved oxygen, pH and total alkalinity. **Scientia Marina**, v. 68, n. 1, p. 45–56, 30 mar. 2004.

ENGELMANN, T. W. Ueber Sauerstoffausscheidung von Pflanzenzellen im Mikrospektrum. **Pflüger, Archiv für die Gesammte Physiologie des Menschen und der Thiere**, v. 27, n. 1, p. 485–489, dez. 1882.

ENRÍQUEZ, S.; SCHUBERT, N. Direct contribution of the seagrass *Thalassia testudinum* to lime mud production. **Nature Communications**, v. 5, n. 1, p. 1–12, 22 maio 2014.

ESTEBAN, R. et al. Carotenoid composition in Rhodophyta: insights into xanthophyll

regulation in *Corallina elongata*. **European Journal of Phycology**, v. 44, n. 2, p. 221–230, maio 2009.

FABO, E. C. DE; KRIPKE, M. L. Wavelength Dependence and Dose-Rate Independence of UV Radiation-Induced Immunologic Unresponsiveness of Mice to a UV-Induced Fibrosarcoma. **Photochemistry and Photobiology**, v. 32, n. 2, p. 183–188, 1980.

FAO. The state of world fisheries and aquaculture 2020. **The State of World Fisheries and Aquaculture (SOFIA)**, n. SOFIA 2020, p. 244, 1 jun. 2020.

FAO. **Top 10 species groups in global aquaculture 2019.** Disponível em: <www.fao.org/3/cb5186en/cb5186en.pdf>.

FAO. **Top 10 species groups in global, regional and national aquaculture 2019. No Title**. Disponível em: <www.fao.org/3/cb5012en/cb5012en.pdf>.

FERNÁNDEZ, M. B. et al. A Comprehensive Phylogeny Reveals Functional Conservation of the UV-B Photoreceptor UVR8 from Green Algae to Higher Plants. **Frontiers in Plant Science**, v. 7, p. 1698, 15 nov. 2016.

FIGUEROA, F. L. et al. Detection of Some Conserved Domains in Phytochrome-like Proteins from Algae. **Journal of Plant Physiology**, v. 136, n. 4, p. 484–487, 1 jul. 1990.

FIGUEROA, F. L. et al. Growth, pigment synthesis and nitrogen assimilation in the red alga *Porphyra* sp. (Bangiales, Rhodophyta) under blue and red light. **Scientia Marina**, v. 59, p. 9–20, 1995.

FIGUEROA, F. L. et al. Effects of short-term irradiation on photoinhibition and accumulation of mycosporine-like amino acids in sun and shade species of the red algal genus Porphyra. **Journal of Photochemistry and Photobiology B: Biology**, v. 69, n. 1, p. 21–30, 2003.

FIGUEROA, F. L. et al. Effects of nutrient supply on photosynthesis and pigmentation in *Ulva lactuca* (Chlorophyta): responses to short-term stress. **Aquatic Biology**, v. 7, n. 1–2, p. 173–183, 22 out. 2009.

FIGUEROA, F. L. et al. Effect of nutrient supply on photosynthesis and pigmentation to short-term stress (UV radiation) in *Gracilaria conferta* (Rhodophyta). **Marine Pollution Bulletin**, v. 60, n. 10, p. 1768–1778, 1 out. 2010.

FIGUEROA, F. L.; AGUILERA, J.; NIELL, F. X. Red and blue light regulation of growth and photosynthetic metabolism in *Porphyra umbilicalis* (Bangiales, Rhodophyta). **European**

Journal of Phycology, v. 30, n. 1, p. 11–18, fev. 1995.

FIGUEROA, F. L.; CONDE-ÁLVAREZ, R.; GÓMEZ, I. Relations between electron transport rates determined by pulse amplitude modulated chlorophyll fluorescence and oxygen evolution in macroalgae under different light conditions. **Photosynthesis Research**, v. 75, n. 3, p. 259–275, 2003.

FIGUEROA, F. L.; NIELL, F. X. Effects of light quality on chlorophyll and biliprotein accumulation in seaweeds. **Marine Biology**, v. 104, n. 2, p. 321–327, jun. 1990.

FLINT, S. D.; CALDWELL, M. M. A biological spectral weighting function for ozone depletion research with higher plants. **Physiologia Plantarum**, v. 117, n. 1, p. 137–144, jan. 2003.

FOLIN, O.; CIOCALTEU, V. On tyrosine and trytophane determinations in proteins. **Journal of Biological Chemistry**, v. LXXIII, n. 2, p. 627–650, 1927.

FOSTER, M. S. Rhodoliths: between rocks and places. **Journal of Phycology**, v. 37, n. 5, p. 659–667, 1 out. 2001.

FOSTER, M. S. et al. Rhodoliths and Rhodolith Beds. **Smithsonian Contr. Mar. Sci.**, n. 39, p. 143– 55, 2013.

FRANKLIN, L. A.; BADGER, M. R. A comparison of photosynthetic electron transport rates in macroalgae measured by pulse amplitude modulated chlorophyll fluorometry and mass spectrometry. **Journal of Phycology**, v. 37, n. 5, p. 756–767, 1 out. 2001.

FRANKLIN, L. A.; KRÄBS, G.; KUHLENKAMP, R. Blue light and UV-A radiation control the synthesis of mycosporine-like amino acids in *Chondrus crispus* (Florideophyceae). **Journal of Phycology**, v. 37, n. 2, p. 257–270, 2001a.

FRANKLIN, L. A.; KRÄBS, G.; KUHLENKAMP, R. Blue light and UV-A radiation control the synthesis of mycosporine-like amino acids in *Chondrus crispus* (Florideophyceae). **Journal of Phycology**, v. 37, n. 2, p. 257–270, 18 abr. 2001b.

FREILE-PELEGRÍN, Y.; ROBLEDO, D. Effects of season on the agar content and chemical characteristics of *Gracilaria cornea* from Yucatan, Mexico. **Botanica Marina**, v. 40, n. 4, p. 285–290, 1997.

GAO, K.; XU, J. Effects of solar UV radiation on diurnal photosynthetic performance and

growth of *Gracilaria lemaneiformis* (Rhodophyta). **European Journal of Phycology**, v. 43, n. 3, p. 297–307, ago. 2008.

GATES, F. L. Study of the bactericidal action of ultra violet light: I. The reaction to monochromatic radiations. **Journal of General Physiology**, v. 13, n. 2, p. 231–248, 20 nov. 1929a.

GATES, F. L. Study of the bactericidal action of ultra violet light: II. The effect of various environmental factors and conditions. **Journal of General Physiology**, v. 13, n. 2, p. 249–260, 20 nov. 1929b.

GATES, F. L. A study of the bactericidal action of ultra violet light: III. the absorption of ultra violet light by bacteria. **Journal of General Physiology**, v. 14, n. 1, p. 31–42, 20 set. 1930.

GHEDIFA, A. BEN et al. Effects of light quality on the photosynthetic activity and biochemical composition of *Gracilaria gracilis* (Rhodophyta). **Journal of Applied Phycology 2021**, p. 1–13, 10 jul. 2021.

GLEASON, D. F. Differential effects of ultraviolet radiation on green and brown morphs of the Caribbean coral *Porites astreoides*. **Limnology and Oceanography**, v. 38, n. 7, p. 1452–1463, 1 nov. 1993.

GÓMEZ, I.; HUOVINEN, P. Induction of phlorotannins during UV exposure mitigates inhibition of photosynthesis and DNA damage in the kelp *Lessonia nigrescens*. **Photochemistry and Photobiology**, v. 86, n. 5, p. 1056–1063, 1 set. 2010.

GORTON, H. L. **Biological action spectra**. Disponível em: <http://photobiology.info/Gorton.html>. Acesso em: 24 jan. 2020.

GRAHAM, L. E. et al. Introduction to the Algae. In: **Algae**. Third Edit ed. [s.l: s.n.]. p. 1–17.

GRAHAM, L. E. et al. The Roles of Algae in Biogeochemistry. In: GRAHAM, L. E. et al. (Eds.). . **Algae**. 3. ed. [s.l.] LJLM Press, 2016b. p. 1–23.

GRAHAM, L. E. et al. Cyanobacteria. In: GRAHAM, L. E. et al. (Eds.). . **Algae**. 3. ed. [s.l: s.n.]. p. 1–27.

GRASSHOFF, K.; EHRHARDT, M.; KREMLING, K. **Methods of Seawater Analysis**. 2. ed. New York: Verlag Chemie Weinhein, 1983.

GREER, D. H.; BERRY, J. A.; BJÖRKMAN, O. Photoinhibition of photosynthesis in intact bean leaves: role of light and temperature, and requirement for chloroplast-protein synthesis

during recovery. **Planta**, v. 168, n. 2, p. 253–260, jun. 1986.

GROSSMAN, A. R. et al. The phycobilisome, a light-harvesting complex responsive to environmental conditions. **Microbiological reviews**, v. 57, n. 3, p. 725–49, 1 set. 1993.

GRZYMSKI, J.; JOHNSEN, G.; SAKSHAUG, E. The significance of intracellular self-shading on the bio optical properties of brown, red, and green macroalgae. **Journal of Phycology**, v. 33, n. 3, p. 408–414, 1 jun. 1997.

GUIHÉNEUF, F.; GIETL, A.; STENGEL, D. B. Temporal and spatial variability of mycosporine-like amino acids and pigments in three edible red seaweeds from western Ireland. **Journal of Applied Phycology**, v. 30, n. 4, p. 2573–2586, 1 ago. 2018.

GUIRY, M. D.; GUIRY, G. M. ***Osmundea pinnatifida* (Hudson) Stackhouse**. Disponível em: <http://www.algaebase.org>. Acesso em: 9 jul. 2019.

GUIRY, M. D.; GUIRY, G. M. ***Crassiphycus corneus* (J.Agardh) Gurgel, J.N.Norris & Fredericq 2018**. Disponível em: <https://www.algaebase.org/search/species/detail/?species_id=170841>. Acesso em: 20 jan. 2021.

HÄDER, D. P. et al. European light dosimeter network (ELDONET): 1998 data. **Helgoland Marine Research**, v. 55, n. 1, p. 35–44, 1 mar. 2001.

HAXO, F. T.; BLINKS, L. R. Photosynthetic action spectra of marine algae. **The Journal of general physiology**, v. 33, n. 4, p. 389–422, 1950.

HE, T. et al. Toxicological effects of two organic ultraviolet filters and a related commercial sunscreen product in adult corals. **Environmental Pollution**, v. 245, p. 462–471, 1 fev. 2019.

HEGEMANN, P. Algal Sensory Photoreceptors. **Annual Review of Plant Biology**, v. 59, n. 1, p. 167–189, 29 jun. 2008.

HENRY, B. E.; ALSTYNE, K. L. V. Effects of UV radiation on growth and phlorotannins in *Fucus gardneri* (phaeophyceae) juveniles and embryos. **Journal of Phycology**, v. 40, n. 3, p. 527–533, 1 jun. 2004.

HERNANDEZ-KANTUN, J. J. et al. Sequencing type material resolves the identity and distribution of the generitype Lithophyllum incrustans, and related European species L. hibernicum and L. bathyporum (Corallinales, Rhodophyta). **Journal of Phycology**, v. 51, n.

4, p. 791–807, 1 ago. 2015.

HOFMANN, L. C.; BISCHOF, K. Ocean acidification effects on calcifying macroalgae. **Aquatic Biology**, v. 22, p. 261–279, 20 nov. 2014.

HOFMANN, L. C.; KOCH, M.; BEER, D. DE. Biotic Control of Surface pH and Evidence of Light-Induced H+ Pumping and Ca2+-H+ Exchange in a Tropical Crustose Coralline Alga. **PLOS ONE**, v. 11, n. 7, p. e0159057, 1 jul. 2016.

HOFMANN, L. C.; SCHOENROCK, K.; DE BEER, D. Arctic Coralline Algae Elevate Surface pH and Carbonate in the Dark. **Frontiers in Plant Science**, v. 9, p. 1416, 25 set. 2018.

HORNECK, G. Quantification of the biological effectiveness of environmental UV radiation. **Journal of Photochemistry and Photobiology, B: Biology**, v. 31, n. 1–2, p. 43–49, 1995.

HOYER, K.; KARSTEN, U.; WIENCKE, C. Induction of sunscreen compounds in Antarctic macroalgae by different radiation conditions. **Marine Biology**, v. 141, n. 4, p. 619–627, 2002.

HWANG, E. K.; PARK, C. S.; BAEK, J. M. Artificial seed production and cultivation of the edible brown alga, *Sargassum fulvellum* (Turner) C. Agardh: Developing a new species for seaweed cultivation in Korea. **Eighteenth International Seaweed Symposium**, p. 25–31, 6 maio 2006.

IBTISSAM, C. et al. Screening of antibacterial activity in marine green and brown macroalgae from the coast of Morocco. **African Journal of Biotechnology**, v. 8, n. 7, p. 1258–1262, 2009.

JASWIR, I. et al. Analysis of fucoxanthin content and purification of all-trans-fucoxanthin from *Turbinaria turbinata* and *Sargassum plagyophyllum* by SiO2 open column chromatography and reversed phase-HPLC. **Journal of Liquid Chromatography & Related Technologies**, v. 36, n. 10, p. 1340–1354, 1 abr. 2013.

JIANG, L.; LI, S. Signaling cross talk under the control of plant photoreceptors. In: BJÖRN, L. (Ed.). . **Photobiology: The Science of Light and Life**. 3. ed. New York: Springer , 2015. p. 177–187.

JIAO, Y.; LAU, O. S.; DENG, X. W. **Light-regulated transcriptional networks in higher plantsNature Reviews Genetics**Nature Publishing Group, , mar. 2007. Disponível em: <https://www.nature.com/articles/nrg2049>. Acesso em: 6 ago. 2020

JOFRE, J.; NAVARRO, N. P.; PLASTINO, E. M. Physiological assessment of 2 color strains of *Crassiphycus corneus* (J. agardh) gurgel, j.n. norris et fredericq (gracilariales, rhodophyta):

Effects of temperature and irradiance. **Ciencias Marinas**, v. 46, n. 2, p. 119–132, 26 jun. 2020.

KARSTEN, U. et al. Natural ultraviolet radiation and photosynthetically active radiation induce formation of mycosporine-like amino acids in the marine macroalga *Chondrus crispus* (Rhodophyta). **Planta**, v. 205, n. 2, p. 257–262, 18 maio 1998.

KARSTEN, U. et al. The effect of ultraviolet radiation on photosynthesis and ultraviolet-absorbing substances in the endemic Arctic macroalga *Devaleraea ramentacea* (Rhodophyta). **Physiologia Plantarum**, v. 105, n. 1, p. 58–66, 4 jan. 1999a.

KARSTEN, U. et al. The effect of ultraviolet radiation on photosynthesis and ultraviolet-absorbing substances in the endemic Arctic macroalga *Devaleraea ramentacea* (Rhodophyta). **Physiologia Plantarum**, v. 105, n. 1, p. 58–66, 4 jan. 1999b.

KARSTEN, U. Defense strategies of slgae and cyanobacteria against solar ultraviolet radiation. In: AMSLER, C. D. (Ed.). . **Algal Chemical Ecology**. Berlin, Heidelberg: Springer Berlin Heidelberg, 2008. p. 273–296.

KARSTEN, U.; ESCOUBEYROU, K.; CHARLES, F. The effect of re-dissolution solvents and HPLC columns on the analysis of mycosporine-like amino acids in the eulittoral macroalgae *Prasiola crispa* and *Porphyra umbilicalis*. **Helgoland Marine Research**, v. 63, n. 3, p. 231–238, 14 set. 2009.

KIANIANMOMENI, A.; HALLMANN, A. Algal photoreceptors: in vivo functions and potential applications. **Planta**, v. 239, n. 1, p. 1–26, 1 jan. 2014.

KIRILOVSKY, D.; KERFELD, C. A. The Orange Carotenoid Protein: a blue-green light photoactive protein. **Photochemical & Photobiological Sciences**, v. 12, n. 7, p. 1135, jul. 2013.

KIRK, J. T. O. Concepts of hydrologic optics. In: KIRK, J. T. O. (Ed.). . **Light and Photosynthesis in Aquatic Ecosystems**. 3. ed. New York: Cambridge University Press, 2010. p. 3–27.

KIRK, J. T. O. The photosynthetic apparatus of aquatic plants. In: KIRK, J. T. O. (Ed.). . **Light and photosynthesis in aquatic ecosystems**. 3. ed. [s.l.] Cambridge University Press, 2011a. p. 265–307.

KIRK, J. T. O. **Light and photosynthesis in aquatic ecosystems**. [s.l.] Cambridge University Press, 2011b.

KIRK, J. T. O. Ecological strategies. In: KIRK, J. T. O. (Ed.). . **Light and photosynthesis in aquatic ecosystems**. 3. ed. [s.l.] Cambridge University Press, 2011c. p. 453–538.

KLEITOU, P.; KLETOU, D.; DAVID, J. Is Europe ready for integrated multi-trophic aquaculture? A survey on the perspectives of European farmers and scientists with IMTA experience. **Aquaculture**, v. 490, p. 136–148, 1 mar. 2018.

KORBEE-PEINADO, N. **Fotorregulación y efecto del nitrógeno inorgánico en la acumulación de aminoácidos tipo micosporina en algas rojas.** [s.l.] Servicio de Publicaciones de la Universidad de Málaga, 2004.

KORBEE-PEINADO, N. et al. Ammonium and UV radiation stimulate the accumulation of mycosporine-like amino acids in *Porphyra columbina* (Rhodophyta) from Patagonia, Argentina. **Journal of Phycology**, v. 40, n. 2, p. 248–259, abr. 2004.

KORBEE, N. et al. Availability of ammonium influences photosynthesis and the accumulation of mycosporine-like amino acids in two *Porphyra* species (Bangiales, Rhodophyta). **Marine Biology**, v. 146, n. 4, p. 645–654, 11 mar. 2005.

KORBEE, N.; FIGUEROA, F. L.; AGUILERA, J. Effect of light quality on the accumulation of photosynthetic pigments, proteins and mycosporine-like amino acids in the red alga Porphyra leucosticta (Bangiales, Rhodophyta). **Journal of Photochemistry and Photobiology B: Biology**, v. 80, n. 2, p. 71–78, 1 ago. 2005.

KRÄBS, G. et al. Wavelength-dependent induction of UV-absorbing mycosporine-like amino acids in the red alga *Chondrus crispus* under natural solar radiation. **Journal of Experimental Marine Biology and Ecology**, v. 268, n. 1, p. 69–82, 1 fev. 2002.

KRÄBS, G.; WATANABE, M.; WIENCKE, C. A Monochromatic Action Spectrum for the Photoinduction of the UV-Absorbing Mycosporine-like Amino Acid Shinorine in the Red Alga *Chondrus crispus*¶. **Photochemistry and Photobiology**, v. 79, n. 6, p. 515, jun. 2004.

KURSAR, T. A.; VAN DER MEER, J.; ALBERTE, R. S. Light-Harvesting System of the Red Alga *Gracilaria tikvahiae* . **Plant Physiology**, v. 73, n. 2, p. 353–360, 1 out. 1983.

LA BARRE, S.; ROULLIER, C.; BOUSTIE, J. Mycosporine-Like Amino Acids (MAAs) in Biological Photosystems. In: **Outstanding Marine Molecules**. Weinheim, Germany: Wiley-VCH Verlag GmbH & Co. KGaA, 2014. p. 333–360.

LALEGERIE, F. et al. Photo-protective compounds in red macroalgae from Brittany:

Considerable diversity in mycosporine-like amino acids (MAAs). **Marine Environmental Research**, v. 147, p. 37–48, 1 maio 2019.

LARSON, R. A.; BEREBAUM, M. R. Environmental phototoxicity: Solar ultraviolet radiation affects the toxicity of natural and man-made chemicals. **Enrivonmental Science Technology**, v. 22, n. 4, p. 354–360, abr. 1988.

LAWRENCE, K. P. et al. Molecular photoprotection of human keratinocytes in vitro by the naturally occurring mycosporine-like amino acid palythine. **British Journal of Dermatology**, v. 178, n. 6, p. 1353–1363, 1 jun. 2017.

LEE, T. M.; SHIU, C. T. Implications of mycosporine-like amino acid and antioxidant defenses in UV-B radiation tolerance for the algae species *Ptercladiella capillacea* and *Gelidium amansii*. **Marine Environmental Research**, v. 67, n. 1, p. 8–16, fev. 2009.

LEGRAND, E. et al. Grazers increase the sensitivity of coralline algae to ocean acidification and warming. **Journal of Sea Research**, v. 148–149, p. 1–7, 1 jun. 2019.

LEY, A. C.; BUTLER, W. L. Effects of Chromatic Adaptation on the Photochemical Apparatus of Photosynthesis in *Porphyridium cruentum* . **Plant Physiology**, v. 65, n. 4, p. 714–722, 1 abr. 1980.

LIGNELL, Å.; PEDERSÉN, M. Agar composition as a function of morphology and growth rate. Studies on some morphological strains of *Gracilaria secundata* and Gracilaria verrucosa (Rhodophyta). **Botanica Marina**, v. 32, n. 3, p. 219–228, 1989.

LONG, S. P.; HUMPHRIES, S.; FALKOWSKI, P. G. Photoinhibition of Photosynthesis in Nature. **Annual Review of Plant Physiology and Plant Molecular Biology**, v. 45, n. 1, p. 633–662, 28 jun. 1994.

LÓPEZ-FIGUEROA, F. et al. Detection of a Phytochrome-like Protein in Macroalgae. **Botanica Acta**, v. 102, n. 2, p. 178–180, 1 maio 1989.

LÓPEZ-FIGUEROA, F. Red, green and blue light photoreceptors controlling chlorophyll a , biliprotein and total protein synthesis in the red alga Chondrus crispus. **British Phycological Journal**, v. 26, n. 4, p. 383–393, 24 dez. 1991.

LUBIÁN, L. M.; MONTERO, O. Excess light-induced violaxanthin cycle activity in *Nannochloropsis gaditana* (Eustigmatophyceae): effects of exposure time and temperature. **Phycologia**, v. 37, n. 1, p. 16–23, 6 jan. 1998.

LÜNING, K.; DRING, M. J. Action spectra and spectral quantum yield of photosynthesis in marine macroalgae with thin and thick thalli. **Marine Biology**, v. 87, n. 2, p. 119–129, jan. 1985.

MACHÍN-SÁNCHEZ, M. et al. Species diversity of the genus *Osmundea* (Ceramiales, Rhodophyta) in the Macaronesian region. **Journal of Phycology**, v. 52, n. 4, p. 664–681, 1 ago. 2016.

MACHÍN-SÁNCHEZ, M.; GIL-RODRÍGUEZ, M. C. Phylogeography of the Red Algal *Laurencia complex* in the Macaronesia Region and Nearby Coastal Areas: Recent Advances and Future Perspectives. **Diversity**, v. 10, n. 1, p. 10, 5 fev. 2018.

MACHU, L. et al. Phenolic content and antioxidant capacity in algal food products. **Molecules**, v. 20, n. 1, p. 1118–1133, 12 jan. 2015.

MARTIN, S. et al. One-year experiment on the physiological response of the Mediterranean crustose coralline alga, *Lithophyllum cabiochae* , to elevated *p* CO_2 and temperature. **Ecology and Evolution**, v. 3, n. 3, p. 676–693, 1 mar. 2013.

MARTIN, S.; CASTETS, M. D.; CLAVIER, J. Primary production, respiration and calcification of the temperate free-living coralline alga *Lithothamnion corallioides*. **Aquatic Botany**, v. 85, n. 2, p. 121–128, 1 ago. 2006.

MARTIN, S.; CHARNOZ, A.; GATTUSO, J. P. Photosynthesis, respiration and calcification in the Mediterranean crustose coralline alga *Lithophyllum cabiochae* (Corallinales, Rhodophyta). **European Journal of Phycology**, v. 48, n. 2, p. 163–172, maio 2013.

MASCHEK, J. A.; BAKER, B. J. The Chemistry of Algal Secondary Metabolism. In: AMSLER, C. D. (Ed.). . **Algal Chemical Ecology**. Berlin, Heidelberg: Springer Berlin Heidelberg, 2008. p. 1–24.

MAXWELL, K.; JOHNSON, G. N. Chlorophyll fluorescence—a practical guide. **Journal of Experimental Botany**, v. 51, n. 345, p. 659–668, 1 abr. 2000.

MCCLUNEY, W. **Introduction to Radiometry and Photometry**. 1st editio ed. [s.l: s.n.]. v. 1

MCCONNAUGHEY, T. Calcification in *Chara corallina* : CO_2 hydroxylation generates protons for bicarbonate assimilation. **Limnology and Oceanography**, v. 36, n. 4, p. 619–628, 1 jun. 1991.

MCHUGH, D. J. A guide to the seaweed industry. In: **Fisheries Technical Paper**. Rome: FOA,

2003. v. 441p. 105.

MCKINLEY, A. F.; DIFFEY, B. L. A reference action spectrum for ultraviolet-induced erythema in human skin. In: PASSCHIER, W. F.; BOSNJAKOVIC, B. F. M. (Eds.). . **Human Exposure to Ultraviolet Radiation: Risks and Regulations**. Amsterdam: Excerpta Medica, 1987. p. 83–87.

MERCURIO, D. G. et al. In vivo photoprotective effects of cosmetic formulations containing UV filters, vitamins, *Ginkgo biloba* and red algae extracts. **Journal of Photochemistry and Photobiology B: Biology**, v. 153, p. 121–126, 1 dez. 2015.

MONTGOMERY, H.; TIPTON, M. Matters of life and death: Change beyond planetary homeostasis. **Experimental Physiology**, v. 104, n. 12, p. 1749–1750, 1 dez. 2019.

MORLIERE, P.; MOYSAN, A.; TIRACHE, I. Action spectrum for UV-induced lipid peroxidation in cultured human skin fibroblasts. **Free Radical Biology and Medicine**, v. 19, n. 3, p. 365–371, 1995.

MOYAL, D.; CHARDON, A.; KOLLIAS, N. UVA protection efficacy of sunscreens can be determined by thepersistent pigment darkening (PPD) method. . **Photodermatology, Photoimmunology and Photomedicine**, v. 16, n. 6, p. 250–255, dez. 2000.

NAVARRO, N. P. et al. Short-term effects of solar UV radiation and NO3- supply on the accumulation of mycosporine-like amino acids in *Pyropia columbina* (Bangiales, Rhodophyta) under spring ozone depletion in the sub-Antarctic region, Chile. **Botanica Marina**, v. 57, n. 1, p. 9–20, 1 fev. 2014.

NAVARRO, N. P. et al. Mycosporine-like amino acids form red algae to develop natural UV sunscreens. In: Sunscreens: source, formulation, efficacy and recommendations. In: RASTOGI, R. P. (Ed.). . **Biochemistry Research Trends: Nova Science Publishers Inc.** [s.l: s.n.]. p. 99–129.

NEORI, A. et al. A novel three-stage seaweed (*Ulva lactuca*) biofilter design for integrated mariculture. **Journal of Applied Phycology**, v. 15, n. 6, p. 543–553, nov. 2003.

NEORI, A. Essential role of seaweed cultivation in integrated multi-trophic aquaculture farms for global expansion of mariculture: an analysis. In: BOROWITZKA, M. A. et al. (Eds.). . **Nineteenth International Seaweed Symposium. Developments in Applied Phycology**. [s.l.] Springer, Dordrecht, 2007. v. Vol. 2p. 117–120.

NOISETTE, F. et al. Physiological responses of three temperate coralline algae from contrasting habitats to near-future ocean acidification. **Journal of Experimental Marine Biology and Ecology**, v. 448, p. 179–187, 1 out. 2013.

NURJANAH et al. Identification of Bioactive Compounds of Seaweed *Sargassum* sp. and *Eucheuma cottonii* Doty as a Raw Sunscreen Cream. **Proceedings of the Pakistan Academy of Sciences: Pakistan Academy of Sciences B. Life and Environmental Sciences**, v. 54, n. 4, p. 311–318, 2017.

OLIVERI, P. et al. The Cryptochrome/Photolyase Family in aquatic organisms. **Marine Genomics**, v. 14, p. 23–37, 1 abr. 2014a.

OLIVERI, P. et al. The Cryptochrome/Photolyase Family in aquatic organisms. **Marine Genomics**, v. 14, p. 23–37, 1 abr. 2014b.

PAGELS, F. et al. Light quality triggers biochemical modulation of *Cyanobium* sp.—photobiology as tool for biotechnological optimization. **Journal of Applied Phycology**, p. 1–11, 13 jul. 2020.

PAKKER, H. et al. Effects of temperature on the photoreactivation of ultraviolet-b-induced DNA damage in Palmaria palmata (Rhodophyta). **Journal of Phycology**, v. 36, n. 2, p. 334–341, 25 dez. 2000.

PAKKER, H.; BEEKMAN, C.; BREEMAN, A. Efficient photoreactivation of UVBR-induced DNA damage in the sublittoral macroalga *Rhodymenia pseudopalmata* (Rhodophyta). **European Journal of Phycology**, v. 35, n. 2, p. 109–114, 1 maio 2000.

PAN, Z. et al. Adverse Effects of Titanium Dioxide Nanoparticles on Human Dermal Fibroblasts and How to Protect Cells. **Small**, v. 5, n. 4, p. 511–520, 20 fev. 2009.

PANGESTUTI, R.; SIAHAAN, E. A.; KIM, S. K. **Photoprotective substances derived from marine algaeMarine Drugs**Multidisciplinary Digital Publishing Institute (MDPI), , 23 out. 2018.

PARSONS, T. R.; STRICKLAND, J. D. H. Discussion of spectrophotometric determination of marine-plant pigments, with revised equations for ascertaining chlorophylls and carotenoids. **Journal Marine Research**, p. 105–156, 1963.

PEREIRA-FILHO, G. H. et al. Extensive Rhodolith Beds Cover the Summits of Southwestern Atlantic Ocean Seamounts. **https://doi.org/10.2112/11T-00007.1**, v. 28, n. 1, p. 261–269, 1

jan. 2012a.

PEREIRA-FILHO, G. H. et al. Extensive Rhodolith Beds Cover the Summits of Southwestern Atlantic Ocean Seamounts. **Journal of Coastal Research**, v. 279, n. 1, p. 261–269, 1 jan. 2012b.

PEREIRA, B. S. M. et al. Prospeção dos bancos dea lgas marinhas do estado do Rio Grande do Norte. 2a. Parte: profundidade de 10 a 45 metros. In: **Projecto Algas, Estado do Rio Grande do Norte**. Recife, Brazil: SUDENE, Estudos de Pesca 9, 1981. p. 25–81.

PÉREZ-LLORÉNS, J. L. et al. **Flora marina del litoral gaditano biología, ecología, usos y guía de identificación**. [s.l.] Universidad de Cádiz. Servicio de Publicaciones, 2012.

PÉREZ-RODRÍGUEZ, E.; AGUILERA, J.; FIGUEROA, F. L. Tissular localization of coumarins in the green alga *Dasycladus vermicularis* (Scopoli) Krasser: a photoprotective role? **Journal of Experimental Botany**, v. 54, n. 384, p. 1093–1100, 1 mar. 2003.

PETROUTSOS, D. et al. A blue-light photoreceptor mediates the feedback regulation of photosynthesis. **Nature**, v. 537, n. 7621, p. 563–566, 14 set. 2016.

PIERROT, D. E.; LEWIS, E.; WALLACE, D. W. R. **MS Excel Program Developed for CO2 System Calculations. ORNL/CDIAC-105a.**Oak Ridge, TennesseeCarbon Dioxide Information Analysis Center, Oak Ridge National Laboratory, U.S. Department of Energy, , 2006.

PLATT, T.; GALLEGOS, C. L.; HARRISON, W. G. Photoinhibition of photosynthesis in natural assemblages of marine phytoplankton. **Journal of Marine Research**, v. 38, p. 103–111, 1980.

PLAZA, M.; CIFUENTES, A.; IBÁÑEZ, E. In the search of new functional food ingredients from algae. **Trends in Food Science & Technology**, v. 19, n. 1, p. 31–39, 1 jan. 2008.

POULSEN, J. T. et al. Dermal elastosis in hairless mice after UV-B and UV-A applied simultaneously, separately or sequentially. **British Journal of Dermatology**, v. 110, n. 5, p. 531–538, 29 jul. 1984.

QIAN, P. Y. et al. Integrated cultivation of the red alga *Kappaphycus alvarezii* and the pearl oyster Pinctada martensi. **Aquaculture**, v. 147, n. 1–2, p. 21–35, 20 nov. 1996.

QUI-MINET, Z. N. et al. Combined effects of global climate change and nutrient enrichment

on the physiology of three temperate maerl species. **Ecology and Evolution**, v. 9, n. 24, p. 13787–13807, 5 dez. 2019.

RAJAURIA, G.; FOLEY, B.; ABU-GHANNAM, N. Identification and characterization of phenolic antioxidant compounds from brown Irish seaweed *Himanthalia elongata* using LC-DAD–ESI-MS/MS. **Innovative Food Science & Emerging Technologies**, v. 37, p. 261–268, 1 out. 2016.

RASTOGI, R. P. et al. Photoprotective compounds from marine organisms. **Journal of Industrial Microbiology and Biotechnology**, v. 37, n. 6, p. 537–558, 2010.

RAVEN, P. H.; EVERT, R. F.; EICHHORN, S. E. **Biologia Vegetal**. 8. ed. Rio de Janeiro: Guanabara Koogan S.A., 2014.

RE, R. et al. Antioxidant activity applying an improved ABTS radical cation decolorization assay. **Free Radical Biology and Medicine**, v. 26, n. 9–10, p. 1231–1237, 1 maio 1999.

REINOSA, J. J. et al. Hierarchical nano ZnO-micro TiO2 composites: High UV protection yield lowering photodegradation in sunscreens. **Ceramics International**, v. 44, n. 3, p. 2827–2834, 15 fev. 2018.

RIBEIRO, J. et al. Seasonal, tidal and diurnal changes in fish assemblages in the Ria Formosa lagoon (Portugal). **Estuarine, Coastal and Shelf Science**, v. 67, n. 3, p. 461–474, 1 abr. 2006.

RITCHIE, R. J. Consistent sets of spectrophotometric chlorophyll equations for acetone, methanol and ethanol solvents. **Photosynthesis Research**, v. 89, n. 1, p. 27–41, 9 jul. 2006.

RITCHIE, R. J. Universal chlorophyll equations for estimating chlorophylls a, b, c, and d and total chlorophylls in natural assemblages of photosynthetic organisms using acetone, methanol, or ethanol solvents. **Photosynthetica**, v. 46, n. 1, p. 115–126, mar. 2008.

ROCKWELL, N. C. et al. Eukaryotic algal phytochromes span the visible spectrum. **Proceedings of the National Academy of Sciences**, v. 111, n. 10, p. 3871–3876, 11 mar. 2014.

RODRÍGUEZ-PRIETO, C. et al. **Guía de las macroalgas y fanerógamas marinas del Mediterráneo Occidental**. [s.l.] Omega, 2013.

SAFAFAR, H. et al. Carotenoids, Phenolic Compounds and Tocopherols Contribute to the Antioxidative Properties of Some Microalgae Species Grown on Industrial Wastewater. **Marine Drugs**, v. 13, n. 12, p. 7339–7356, 11 dez. 2015.

SANFILIPPO, J. E. et al. Chromatic acclimation in cyanobacteria: A diverse and widespread

process for optimizing photosynthesis. **Annual Review of Microbiology**, v. 73, p. 407–433, 2019.

SANJEEWA, K. K. A. et al. **Bioactive properties and potentials cosmeceutical applications of phlorotannins isolated from brown seaweeds: A reviewJournal of Photochemistry and Photobiology B: Biology**, set. 2016.

SCHMID, D.; SCHÜRCH, C.; ZÜLLI, F. UV-A sunscreen from red algae for protection against premature skin aging. **Cosmetics and toiletries manufacture worldwide**, n. 2004, p. 139–143, 2004.

SCHMID, D.; SCHÜRCH, C.; ZÜLLI, F. Mycosporine-like Amino Acids from Red Algae Protect against Premature Skin-Aging. **Euro Cosmetics**, v. 9, 1 jan. 2006.

SCHNEIDER, G. et al. Photoprotection properties of marine photosynthetic organisms grown in high ultraviolet exposure areas: Cosmeceutical applications. **Algal Research**, v. 49, p. 101956, 1 ago. 2020a.

SCHNEIDER, G. et al. Physiological and biochemical responses driven by different UV-visible radiation in: *Osmundea pinnatifida* (Hudson) Stackhouse (Rhodophyta). **Photochemical and Photobiological Sciences**, v. 19, n. 12, p. 1650–1664, 1 dez. 2020b.

SCHNEIDER, S. L.; LIM, H. W. Review of environmental effects of oxybenzone and other sunscreen active ingredients. **Journal of the American Academy of Dermatology**, v. 80, n. 1, p. 266–271, 1 jan. 2019.

SCHUBERT, N.; GARCÍA-MENDOZA, E. Photoinhibition in red algal species with different carotenoid profiles. **Journal of Phycology**, v. 44, n. 6, p. 1437–1446, 1 dez. 2008.

SCHUBERT, N.; GARCÍA-MENDOZA, E.; PACHECO-RUIZ, I. Carotenoid composition of marine red algae. **Journal of Phycology**, v. 42, n. 6, p. 1208–1216, 16 dez. 2006.

SEGOVIA, M.; GORDILLO, F. J. L.; FIGUEROA, F. L. Cyclic-AMP levels in the lichen *Evernia prunastri* are modulated by light quantity and quality. **Journal of Photochemistry and Photobiology B: Biology**, v. 70, n. 3, p. 145–151, 1 jul. 2003.

SEMESI, I. S.; BEER, S.; BJÖRK, M. Seagrass photosynthesis controls rates of calcification and photosynthesis of calcareous macroalgae in a tropical seagrass meadow. **Marine Ecology Progress Series**, v. 382, p. 41–47, 30 abr. 2009.

SILVA, J. et al. Physiological Responses of *Zostera marina* and *Cymodocea nodosa* to Light-Limitation Stress. **PLoS ONE**, v. 8, n. 11, p. e81058, 28 nov. 2013.

SILVA, J. P. et al. Antioxidant and antitumor potential of wild and IMTA-cultivated *Osmundea pinnatifida*. **Journal of Oceanology and Limnology**, v. 37, n. 3, p. 825–835, 1 maio 2019.

SILVA, J.; SANTOS, R. Daily variation patterns in seagrass photosynthesis along a vertical gradient. **Marine Ecology Progress Series**, v. 257, p. 37–44, 7 ago. 2003.

SINGH, S. P. et al. Mycosporine-like amino acids (MAAs): Chemical structure, biosynthesis and significance as UV-absorbing/screening compounds. **Indian Journal of Experimental Biology**, v. 46, p. 7–17, 2008.

SINGH, S. P. et al. **Uncovering potential applications of cyanobacteria and algal metabolites in biology, agriculture and medicine: Current status and future prospectsFrontiers in Microbiology**, 25 abr. 2017.

SMITH, S. V.; KEY, G. S. Carbon dioxide and metabolism in marine environments. **Limnology and Oceanography**, v. 20, n. 3, p. 493–495, 1 maio 1975.

SORDO, L. et al. High CO_2 decreases the long-term resilience of the free-living coralline algae *Phymatolithon lusitanicum*. **Ecology and Evolution**, v. 8, n. 10, p. 4781–4792, 1 maio 2018.

STAHL, W.; SIES, H. Antioxidant activity of carotenoids. **Molecular Aspects of Medicine**, v. 24, n. 6, p. 345–351, 1 dez. 2003.

STELLER, D. L. et al. Effect of temperature on photosynthesis, growth and calcification rates of the free-living coralline alga *Lithophyllum margaritae*. **Ciências Marinas**, v. 33, n. 4, p. 441–456, 4 dez. 2007.

SUN, Y. et al. Distribution, contents, and types of mycosporine-like amino acids (MAAs) in marine macroalgae and a database for Maas based on these characteristics. **Marine Drugs**, v. 18, n. 1, p. 1–43, 7 jan. 2020.

TAKANO, S.; DAISUKE, U.; YOSHIMASA, H. Isolation and structure of a new amino acid, palythine, from the zoanthid *Palythoa tuberculosa*. **Tetrahedron Letters**, v. 19, p. 2229–2300, 1978.

TAKANO, S.; UEMURA, D.; HIRATA, Y. Isolation and structure of two new amino acids, palythinol and palythene, from the zoanthid *Palythoa tubercolosa*. **Tetrahedron Letters**, v. 19, n. 49, p. 4909–4912, 1 jan. 1978.

TALARICO, L.; MARANZANA, G. Light and adaptive responses in red macroalgae: an overview. **Journal of Photochemistry and Photobiology B: Biology**, v. 56, n. 1, p. 1–11, 1 jun. 2000.

TEICHERT, S.; FREIWALD, A. Polar coralline algal CaCO3-production rates correspond to intensity and duration of the solar radiation. **Biogeosciences**, v. 11, n. 3, p. 833–842, 11 fev. 2014.

THOMAS, B.; DICKINSON, H. G. Evidence for two photoreceptors controlling growth in de-etiolated seedlings. **Planta**, v. 146, n. 5, p. 545–550, out. 1979.

TORRES, A. et al. Porphyra-334, a potential natural source for UVA protective sunscreens. **Photochemical & Photobiological Sciences**, v. 5, n. 4, p. 432, 3 abr. 2006.

TORRES, P. B. et al. Mycosporine-like amino acids from *Gracilariopsis tenuifrons* (Gracilariales, Rhodophyta) and its variation under high light. **Journal of Applied Phycology**, v. 28, n. 3, p. 2035–2040, 1 jun. 2015.

TSUJINO, I.; YABE, K.; SEKIKAWA, I. Isolation and structure of a new amino acid, shinorine, from the red alga *Chondrus yendoi*. **Bot. Mar.**, v. 23, p. 65–68, 1980.

VALENTE, L. M. P. et al. Carotenoid deposition, flesh quality and immunological response of Nile tilapia fed increasing levels of IMTA-cultivated *Ulva* spp. **Journal of Applied Phycology**, v. 28, n. 1, p. 691–701, 1 fev. 2016.

VEGA, J. et al. Mycosporine-Like Amino Acids from Red Macroalgae: UV-Photoprotectors with Potential Cosmeceutical Applications. **Applied Sciences 2021, Vol. 11, Page 5112**, v. 11, n. 11, p. 5112, 31 maio 2021.

WAKEFIELD, G. et al. Modified titania nanomaterials for sunscreen applications – reducing free radical generation and DNA damage. **Materials Science and Technology**, v. 20, n. 8, p. 985–988, 18 ago. 2004.

WANG, H. M. D. et al. **Potential biomedical applications of marine algaeBioresource Technology**Elsevier, , 1 nov. 2017.

WEBB, A. R.; DECOSTA, B. R.; HOLICK, M. F. Sunlight Regulates the Cutaneous Production of Vitamin D3 by Causing Its Photodegradation. **The Journal of Clinical Endocrinology & Metabolism**, v. 68, n. 5, p. 882–887, maio 1989.

WIENCKE, C. et al. Impact of UV-radiation on viability, photosynthetic characteristics and DNA of brown algal zoospores: implications for depth zonation. **Marine Ecology Progress Series**, v. 197, p. 217–229, 12 maio 2000.

WOLF-GLADROW, D. A. et al. Total alkalinity: The explicit conservative expression and its application to biogeochemical processes. **Marine Chemistry**, v. 106, n. 1- 2 SPEC. ISS., p. 287–300, 1 jul. 2007.

WU, H. Effect of different light qualities on growth, pigment content, chlorophyll fluorescence, and antioxidant enzyme activity in the red alga *Pyropia haitanensis* (Bangiales, Rhodophyta). **BioMed Research International**, v. 2016, p. 1–8, 2016.

WULF, H. C. et al. Narrow-band UV radiation and induction of dermal elastosis and skin cancer. **Photo-dermatology**, v. 6, n. 1, p. 44–51, fev. 1989.

YAO, W.; BYRNE, R. H. Simplified seawater alkalinity analysis: use of linear array spectrometers. **Deep-Sea Research Part I: Oceanographic Research Papers**, v. 45, n. 8, p. 1383–1392, 1 ago. 1998.

YE, K. et al. A Review of Pigments Derived from Marine Natural Products. **Israel Journal of Chemistry**, v. 59, n. 5, p. 327–338, 28 maio 2019.

ZHANG, T.; MARUHNICH, S. A.; FOLTA, K. M. Green light induces shade avoidance symptoms. **Plant physiology**, v. 157, n. 3, p. 1528–36, 1 nov. 2011.

ANEXO A – Material suplementar (Capítulo I)

Figura S. 1 - Effective solar absorption radiation (ESAR, in %) by hydroethanolic algal extracts.

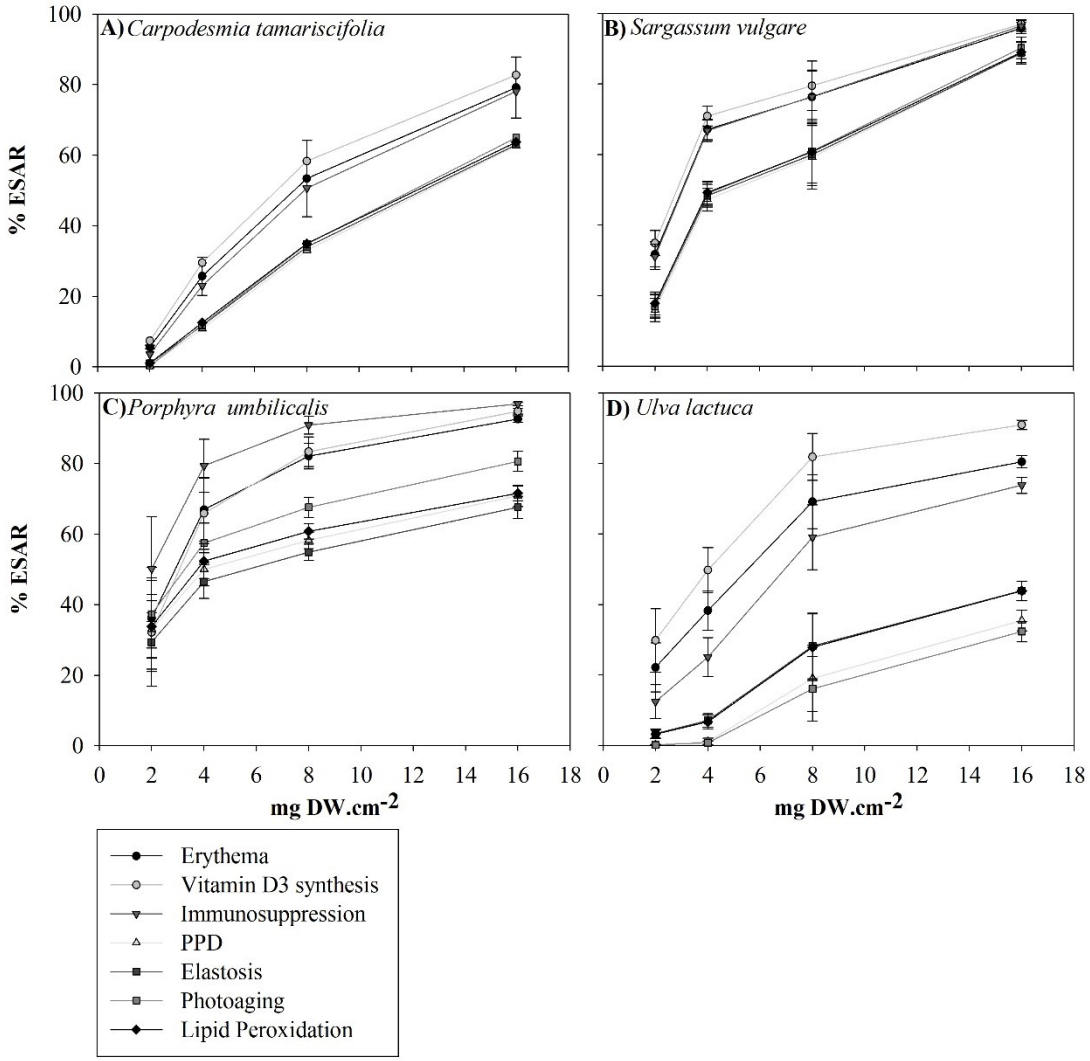

Different extract concentrations were tested, and %ESAR was calculated to a solar spectrum on a summer day in Malaga and applying action spectra for diverse UV-driven responses, such as erythematic responses, vitamin D3 synthesis, immunosuppression, persistent pigment darkening (PPD), elastosis, photoaging, and lipid peroxidation. A. *Carpodesmia tamariscifolia*, B. *Sargassum vulgare*, C. *Porphyra umbilicalis*, and D. *Ulva lactuca*. Comparisons among concentrations for each responses resulted in values from $2<4<8<16$ mg cm^{-2}, with the exception of %ESAR for PPD, elastosis, photoaging and lipid peroxidation of *U. lactuca*, where $2=4<8<16$ mg cm^{-2}, according to the Newman-Keuls a posteriori test ($p<0.05$).

Table S. 1. Results of one-way analyses of variance (ANOVA) of biochemical variables evaluated in this study.

Dependent variable	Source of variation	df	SS	MS	F-value	P-value
Phenolic compounds	Species	22	6715.90	305.27	351.67	**<0.0001**
Total MAAs	Species	23	434.79	18.90	84.12	**<0.0001**
Myc-Glyc	Species	23	0.04	0.00	32.80	**<0.0001**
Serinol	Species	23	0.21	0.01	68.52	**<0.0001**
Asterina-330	Species	23	156.98	6.83	124.19	**<0.0001**
Palythine	Species	23	6.20	0.27	47.57	**<0.0001**
Palythinol	Species	23	58.49	2.54	42.42	**<0.0001**
Shinorine	Species	23	2.00	0.09	93.66	**<0.0001**
Porphyra-334	Species	23	56.53	2.46	161.97	**<0.0001**
Antioxidant activity	Species	23	38355.47	1667.63	232.46	**<0.0001**

The sources of variation were the different species. Dependent variables included phenolic content; total MAAs (mycosporine-like amino acids) and individual MAA contents (Myc-Glyc as mycosporine-glycine, serinol, asterina-330, palythine, palythinol, shinorine and porphyra-334); and antioxidant activity (ABTS). Values in bold indicate significant differences (P <0.05). SS, sum of squares; df, degrees of freedom; MS, mean of squares.

Table S. 2. Results from one-way analyses of variance (ANOVA) of effective solar absorption radiation (%ESAR). The sources of variation were the different species and concentrations.

Dependent variable	Source of variation	df	SS	MS	F-value	P-value
Carpodesmia tamariscifolia						
Immunosuppression	Concentration	3	25395.79	8465.26	113.46	**<0.0001**
Elastosis	Concentration	3	18039.68	6013.23	105.07	**<0.0001**
Erythema	Concentration	3	24808.71	8269.57	121.68	**<0.0001**
Lipid peroxidation	Concentration	3	18340.48	6113.49	109.91	**<0.0001**
Persistent Pigment Darkening	Concentration	3	18225.53	6075.18	101.81	**<0.0001**
Photoaging	Concentration	3	19538.13	6512.71	98.39	**<0.0001**
Vitamin D3 synthesis	Concentration	3	26060.08	8686.69	122.91	**<0.0001**
Porphyra umbilicalis						
Immunosuppression	Concentration	3	10370.24	3456.75	48.72	**<0.0001**
Elastosis	Concentration	3	6174.42	2058.14	76.78	**<0.0001**
Erythema	Concentration	3	14499.70	4833.23	63.89	**<0.0001**
Lipid peroxidation	Concentration	3	6109.53	2036.51	70.51	**<0.0001**
Persistent Pigment Darkening	Concentration	3	6034.86	2011.62	78.72	**<0.0001**
Photoaging	Concentration	3	8022.02	2674.01	76.69	**<0.0001**
Vitamin D3 synthesis	Concentration	3	17929.21	5976.40	66.76	**<0.0001**
Sargassum vulgare						
Immunosuppression	Concentration	3	13562.36	4520.79	211.28	**<0.0001**
Elastosis	Concentration	3	16656.54	5552.18	191.93	**<0.0001**
Erythema	Concentration	3	12995.17	4331.72	213.03	**<0.0001**
Lipid peroxidation	Concentration	3	16440.81	5480.27	192.57	**<0.0001**
Persistent Pigment Darkening	Concentration	3	17338.02	5779.34	190.77	**<0.0001**
Photoaging	Concentration	3	17521.65	5840.55	190.54	**<0.0001**
Vitamin D3 synthesis	Concentration	3	12189.05	4063.02	220.01	**<0.0001**
Ulva lactuca						
Immunosuppression	Concentration	3	19706.62	6568.87	182.07	**<0.0001**
Elastosis	Concentration	3	8652.05	2884.02	115.46	**<0.0001**
Erythema	Concentration	3	17473.33	5824.44	166.20	**<0.0001**
Lipid peroxidation	Concentration	3	8712.87	2904.29	114.31	**<0.0001**
Persistent Pigment Darkening	Concentration	3	6744.13	2248.04	91.18	**<0.0001**
Photoaging	Concentration	3	5559.57	1853.19	79.44	**<0.0001**

Dependent variable	Source of variation	df	SS	MS	F-value	P-value
Vitamin D3 synthesis	Concentration	3	19292.66	6430.89	153.77	**<0.0001**
Immunosuppression [2]	Species	3	10110.60	3370.20	47.29	**<0.0001**
Elastosis [2]	Species	3	4105.06	1368.35	62.66	**<0.0001**
Erythema [2]	Species	3	4198.21	1399.40	18.47	**<0.0001**
Lipid peroxidation [2]	Species	3	5487.14	1829.05	73.19	**<0.0001**
Persistent Pigment Darkening [2]	Species	3	5811.34	1937.11	96.48	**<0.0001**
Photoaging [2]	Species	3	7406.37	2468.79	90.39	**<0.0001**
Vitamin D3 synthesis [2]	Species	3	3570.19	1190.06	12.69	**<0.0001**
Immunosuppression [4]	Species	3	19884.82	6628.27	142.83	**<0.0001**
Elastosis [4]	Species	3	11659.93	3886.64	236.67	**<0.0001**
Erythema [4]	Species	3	10468.12	3489.37	68.61	**<0.0001**
Lipid peroxidation [4]	Species	3	13721.59	4573.86	266.56	**<0.0001**
Persistent Pigment Darkening [4]	Species	3	14961.45	4987.15	331.35	**<0.0001**
Photoaging [4]	Species	3	18353.60	6117.87	322.93	**<0.0001**
Vitamin D3 synthesis [4]	Species	3	8357.37	2785.79	44.04	**<0.0001**
Immunosuppression [8]	Species	3	7764.83	2588.28	34.28	**<0.0001**
Elastosis [8]	Species	3	5769.56	1923.19	26.55	**<0.0001**
Erythema [8]	Species	3	3707.37	1235.79	18.76	**<0.0001**
Lipid peroxidation [8]	Species	3	7081.44	2360.48	32.85	**<0.0001**
Persistent Pigment Darkening [8]	Species	3	9321.41	3107.14	41.12	**<0.0001**
Photoaging [8]	Species	3	13628.50	4542.83	57.01	**<0.0001**
Vitamin D3 synthesis [8]	Species	3	3303.51	1101.17	17.74	**<0.0001**
Immunosuppression [16]	Species	3	3516.71	1172.24	77.04	**<0.0001**
Elastosis [16]	Species	3	8105.12	2701.71	102.03	**<0.0001**
Erythema [16]	Species	3	1705.60	568.53	45.74	**<0.0001**
Lipid peroxidation [16]	Species	3	8406.13	2802.04	116.82	**<0.0001**
Persistent Pigment Darkening [16]	Species	3	11818.03	3939.34	138.77	**<0.0001**
Photoaging [16]	Species	3	15465.02	5155.01	179.31	**<0.0001**
Vitamin D3 synthesis [16]	Species	3	942.10	314.03	33.20	**<0.0001**

Dependent variables included the biological responses driven by UV, such as immunosuppression, elastosis, erythema, lipid peroxidation, persistent pigment darkening, photoaging, and vitamin D3 synthesis. Values of biological responses were obtained using %ESAR. These values were compared among the extract concentrations in each selected species (*Carpodesmia tamariscifolia, Porphyra umbilicalis, Sargassum vulgare* and *Ulva lactuca)*, and among species in different concentrations, which are indicated in the table by the numbers in brackets (2, 4, 8 and 16 mg cm^{-2} DW). Values in bold indicate significant differences ($P < 0.05$). SS, sum of squares; df, degrees of freedom; MS, mean of squares.

ANEXO B – Material suplementar (Capítulo II)

Table S. 3. Results of factorial ANOVA (analyses of variance).

Dependent variable	Source of variation	SS	df	MS	F	p-value
Growth rate	Time	1.92	1	1.92	84.0	**0.000**
	Treatment	2.22	5	0.44	19.4	**0.000**
	Time*treatment	0.48	5	0.10	4.2	**0.010**
Fv/Fm	Time	0.04	4	0.01	14.7	**0.000**
	Treatment	0.01	5	0.00	3.5	**0.008**
	Time*Treatment	0.04	20	0.00	2.8	**0.001**
ETR	Time	21.05	4	5.26	9.6	**0.000**
	Treatment	36.15	5	7.23	13.2	**0.000**
	Time*Treatment	23.21	20	1.16	2.1	**0.013**
α_{ETR}	Time	0.00	1	0.00	0.7	0.404
	Treatment	0.00	5	0.00	2.8	**0.042**
	Time*Treatment	0.00	5	0.00	3.3	**0.021**
ETR_{max}	Time	176.26	1	176.26	19.6	**0.000**
	Treatment	325.29	5	65.06	7.2	**0.000**
	Time*Treatment	230.19	5	46.04	5.1	**0.003**
Ek_{ETR}	Time	10931.00	1	10931.00	22.3	**0.000**
	Treatment	4819.00	5	964.00	2.0	0.125
	Time*Treatment	14811.00	5	2962.00	6.1	**0.001**
Phycocyanin (PC)	Time	0.00	1	0.00	0.5	0.506
	Treatment	0.07	5	0.01	1.4	0.274
	Time*Treatment	0.01	5	0.00	0.2	0.956
Phycoerythrin (PE)	Time	0.05	1	0.05	5.2	**0.036**
	Treatment	0.71	5	0.14	13.9	**0.000**
	Time*Treatment	1.06	5	0.21	20.8	**0.000**
Phenolic compounds	Time	90.27	1	90.27	30.6	**0.000**
	Treatment	122.08	5	24.42	8.3	**0.000**
	Time*Treatment	311.48	5	62.30	21.1	**0.000**
Soluble proteins	Time	0.03	1	0.03	0.0	0.863
	Treatment	6.85	5	1.37	1.5	0.217
	Time*Treatment	12.36	5	2.47	2.8	**0.043**
Total MAAs	Time	0.89	1	0.89	10.3	**0.004**
	Treatment	0.39	5	0.08	0.9	0.498
	Time*treatment	0.99	5	0.20	2.3	0.075
Asterina-330	Time	0.07	1	0.07	17.4	**0.000**
	Treatment	0.02	5	0.00	1.2	0.323
	Time*treatment	0.17	5	0.03	8.4	**0.000**
Palythine	Time	0.01	1	0.01	3.4	0.081
	Treatment	0.01	5	0.00	1.5	0.248
	Time*treatment	0.04	5	0.01	4.9	**0.004**
Palythinol	Time	0.21	1	0.21	15.2	**0.001**
	Treatment	0.07	5	0.01	1.0	0.454
	Time*treatment	0.25	5	0.05	3.7	**0.013**
Shinorine	Time	0.00	1	0.00	0.5	0.480
	Treatment	0.00	5	0.00	2.6	**0.049**
	Time*treatment	0.00	5	0.00	1.3	0.309
Porphyra-334	Time	0.02	1	0.02	10.0	**0.004**
	Treatment	0.01	5	0.00	1.1	0.387

Dependent variable	Source of variation	SS	df	MS	F	p-value
	Time*treatment	0.02	5	0.00	2.2	0.085
ABTS assay	Time	0.62	1	0.62	1.6	0.214
	Treatment	10.02	5	2.00	5.3	**0.003**
	Time*Treatment	5.91	5	1.18	3.1	**0.029**

The variation sources were time (8^{th} and 15^{th} days) and radiation treatments. Dependent variables included growth rate (% FW Day^{-1}); parameters of chlorophyll *a* fluorescence of *O. pinnatifida*, such as Fv/Fm (maximum quantum yield of PSII), ETR (electron transport rate, µmol electrons m^{-2} s^{-1}), α_{ETR} (photosynthetic efficiency), ETR_{max} (maximum electron transport rate, µmol electrons m^{-2} s^{-1}) and $E_{k\ ETR}$ (saturation irradiance, µmol photons m^{-2} s^{-1}); phycobiliproteins, such as phycocyanin (PC) and phycoerythrin (PE) (mg g^{-1} DW); phenolic compounds (mg g^{-1} DW); soluble proteins (mg g^{-1} DW); mycosporine-like amino acids (MAAs) from whole thalli, such as asterina-330, palythine, palythinol, shinorine, porphyra-334 (mg g^{-1} DW); and antioxidant activity by ABTS assay (μM_{TE} g^{-1} DW). Bold values indicate significant differences ($P < 0.05$). SS, sun of squares; df, degrees of freedom; MS, mean of squares.

Table S. 4. Results of one-way ANOVA (analyses of variance). for analyses performed on the 15^{th} day of experiment. squares.

Dependent variable	Source of variation	SS	df	MS	F	p-value
Carotenoid and chlorophyll pigments						
Chlorophyll *a*	Treatment	13544.70	5	2708.90	17.9	**<0.0001**
Violaxanthin	Treatment	11.72	5	2.34	5.1	**0.0140**
Anteraxanthin	Treatment	33.68	5	6.74	1.0	0.477
Zeaxanthin	Treatment	4665.58	5	933.12	11.4	**0.0010**
Lutein	Treatment	4.99	5	1.00	7.6	**0.0030**
β-carotene	Treatment	605.50	5	121.10	45.6	**<0.0001**
MAAs from apex thallus						
Total MAAs	Treatment	0.08	5	0.02	1.0	0.473
Asterina-330	Treatment	0.02	5	0.00	1.4	0.307
Palythine	Treatment	0.00	5	0.00	0.7	0.648
Palythinol	Treatment	0.01	5	0.00	1.3	0.322
Shinorine	Treatment	0.00	5	0.00	1.1	0.406
Porphyra-334	Treatment	0.01	5	0.00	2.9	0.058
Carbon	Treatment	1072	5	214	2.0	0.137
Nitrogen	Treatment	14.8	5	2.9	0.8	0.548
C:N	Treatment	10.5	5	2.1	0.8	0.517

The variation sources were radiation treatments. Dependent variables included carotenoid and chlorophyll pigments, such as chlorophyll *a,* violaxanthin, antheraxanthin, zeaxanthin, lutein, β-carotene (µg g^{-1} DW); carbon (C), nitrogen (N) and C:N ratio (mg g^{-1} DW), mycosporine-like amino acids (MAAs) extracted from apex of *O. pinnatifida,* such as asterina-330, palythine, palythinol, shinorine, porphyra-334 (mg g^{-1} DW). Bold values indicate significant differences ($P < 0.05$). SS, sun of squares; df, degrees of freedom; MS, mean of

ANEXO C – Material suplementar (Capítulo III)

Table S. 5. Nutrient concentrations measured in the culture water from different treatments during o experiment.

Treatments	Time	PO_4^{2-} (µM)			NO_3^- (µM)		
		1th to 4th day					
Stock water	**1st day**	**6.32**	**±**	**2.18**	**161.64**	**±**	**12.00**
SOX	4th day	<0.05	±	-	41.35	±	5.40
SOX+R	4th day	<0.05	±	-	50.88	±	9.60
SOX+G	4th day	0.17	±	0.26	40.70	±	10.13
SOX+B	4th day	0.23	±	0.36	34.02	±	19.17
SOX+UVA	4th day	0.17	±	0.14	18.50	±	9.89
SOX+UVA+UVB	4th day	0.13	±	0.22	33.70	±	20.03
		4th to 8th day					
Stock water	**4th day**	**3.45**	**±**	**0.52**	**166.65**	**±**	**6.89**
SOX	8th day	0.30	±	0.03	<0.05	±	-
SOX+R	8th day	0.25	±	0.24	<0.05	±	-
SOX+G	8th day	0.08	±	0.13	0.33	±	0.52
SOX+B	8th day	1.10	±	0.68	<0.05	±	-
SOX+UVA	8th day	0.22	±	0.10	<0.05	±	-
SOX+UVA+UVB	8th day	0.78	±	1.02	<0.05	±	-
		8th to 11th day					
Stock water	**8th day**	**7.52**	**±**	**0.24**	**161.74**	**±**	**12.28**
SOX	11th day	0.05	±	0.08	1.63	±	2.38
SOX+R	11th day	0.40	±	0.00	0.28	±	0.10
SOX+G	11th day	0.18	±	0.21	0.35	±	0.17
SOX+B	11th day	0.18	±	0.22	0.13	±	0.05
SOX+UVA	11th day	0.22	±	0.34	0.48	±	0.75
SOX+UVA+UVB	11th day	<0.05	±	0.00	31.97	±	41.13
		11th to 15th day					
Stock water	**11th day**	**8.45**	**±**	**0.64**	**146.80**	**±**	**1.41**
SOX	15th day	<0.05	±	-	1.13	±	0.36
SOX+R	15th day	<0.05	±	-	0.80	±	0.09
SOX+G	15th day	<0.05	±	-	0.73	±	0.14
SOX+B	15th day	<0.05	±	-	0.97	±	0.19
SOX+UVA	15th day	1.73	±	2.70	0.87	±	0.31
SOX+UVA+UVB	15th day	<0.05	±	-	1.23	±	0.37

The measureds were carried out on the 1st (stock water) and 4th day (final); 4th day (stock water) and 8th day (final); 8th day (stock water) and 11th day (final); 11th day (stock water) and 15th day (final). Mean ± standard-deviation (n=3). Detection limit 0.05 µM (indicated as <0.05).

Table S. 6. Results of factorial and one-way ANOVA (analyses of variance).

	Dependent variables	Source of variation	SS	df	MS	F-ratio	p-value
	Growth rate	Time	13.8	1	13.8	210.55	**0.0000**
		Treatment	22.9	5	4.6	70	**0.0000**
		Time*treatment	6.7	5	1.3	20.35	**0.0000**
Parameters of chlorophyll a fluorescence	F_v/F_m	Time	0.2	4	0.040	28.72	**0.0000**
		Treatment	0.1	5	0.021	14.95	**0.0000**
		Time*Treatment	0.0	20	0.002	1.79	**0.0436**
	ETR	Time	50.3	4	12.6	22.55	**0.0000**
		Treatment	20.5	5	4.1	7.36	**0.0000**
		Time*Treatment	63.0	20	3.1	5.64	**0.0000**
	α_{ETR}	Time	0.000	1	0.000	0.51	0.4815
		Treatment	0.001	5	0.000	2.32	0.0760
		Time*Treatment	0.001	5	0.000	2.44	0.0646
	ETR_{max}	Time	8.6	1	8.6	1.06	0.3137
		Treatment	275.3	5	55.1	6.78	**0.0006**
		Time*Treatment	39.3	5	7.9	0.96	0.4579
	Ek_{ETR}	Time	1542.0	1	1542.0	0.79	0.3833
		Treatment	34038.0	5	6808.0	3.49	**0.0178**
		Time*Treatment	48451.0	5	9690.0	4.97	**0.0034**
	Chlorophyll *a*	Time	113472.0	1	113472.0	383.64	0.0000
		Treatment	29965.0	5	5993.0	20.26	**0.0000**
		Time*Treatment	5702.0	5	1140.0	3.85	**0.0140**
Carotenoid pigments	Violaxanthin	Time	313.7	1	313.7	381.02	**0.0000**
		Treatment	101.2	5	20.2	24.58	**0.0000**
		Time*Treatment	39.7	5	7.9	9.64	**0.0001**
	Anteraxanthin	Time	7571.4	1	7571.4	513.34	**0.0000**
		Treatment	576.0	5	115.2	7.81	**0.0003**
		Time*Treatment	199.3	5	39.9	2.70	**0.0489**
	Zeaxanthin	Time	1778.5	1	1778.5	60.97	**0.0000**
		Treatment	1713.4	5	342.7	11.7	**0.0001**
		Time*Treatment	305.9	5	61.2	2.09	0.1157
	β-carotene	Time	32.2	1	32.2	150.41	**0.0000**
		Treatment	10.6	5	2.1	9.90	**0.0000**
		Time*Treatment	3.5	5	0.7	3.28	**0.0231**
Phycobiliproteins	Phycocyanin (PC)	Time	0.06	1	0.06	88.0	**0.0000**
		Treatment	0.01	5	0.00	3.7	**0.0122**
		Time*Treatment	0.01	5	0.00	3.7	**0.0121**
	Phycoerythrin (PE)	Time	1.86	1	1.86	37.3	**0.0000**
		Treatment	0.61	5	0.12	2.4	0.0622
		Time*Treatment	0.59	5	0.12	2.3	0.0709
Mycosporine-like	Total MAAs	Time	0.106	1	0.106	0.23	0.6331
		Treatment	1.481	5	0.296	0.65	0.6600

	Time*treatment	0.722	5	0.144	0.31	0.8961
	Time	0.000	1	0.000	3.36	0.0794
Palythine	Treatment	0.008	5	0.002	65.82	**0.0000**
	Time*treatment	0.001	5	0.000	8.15	**0.0002**
	Time	0.001	1	0.001	0.06	0.7937
Palythinol	Treatment	0.233	5	0.047	4.09	**0.0078**
	Time*treatment	0.185	5	0.037	3.25	**0.0221**
	Time	0.022	1	0.022	0.56	0.4587
Shinorine	Treatment	0.385	5	0.077	2.01	0.1124
	Time*treatment	0.128	5	0.026	0.67	0.6491
	Time	0.044	1	0.044	0.28	0.5959
Porphyra-334	Treatment	0.260	5	0.052	0.34	0.8803
	Time*treatment	0.239	5	0.048	0.31	0.8976
	Time	25.2	1	25.2	17.85	**0.0003**
Phenolic compounds	Treatment	36.1	5	7.2	5.11	**0.0029**
	Time*Treatment	28.4	5	5.7	4.02	**0.0096**
	Time	39.2	1	39.2	22.37	**0.0001**
Soluble proteins	Treatment	26.8	5	5.4	3.05	**0.0306**
	Time*Treatment	53.2	5	10.6	6.06	**0.0011**
	Time	1.2	1	1.2	2.00	0.1716
ABTS assay	Treatment	93.1	5	18.6	31.59	**0.0000**
	Time*Treatment	18.7	5	3.7	6.36	**0.0010**
	Time	15.6	1	15.6	8.95	**0.0065**
DPPH assay	Treatment	21.5	5	4.3	2.46	0.0630
	Time*Treatment	24.7	5	4.9	2.84	**0.0388**
Carbon (C)	Treatment	3653.7	5	730.7	47.47	**0.0000**
Nitrogen (N)	Treatment	28.0	5	5.6	3.045	0.0575
Ratio C:N	Treatment	17.0	5	3.4	2.371	0.1150

The variation sources were time (8^{th} and 15^{th} days) and radiation treatments. Dependent variables for factorial ANOVA included growth rate (% FW Day^{-1}); parameters of chlorophyll *a* fluorescence, such as F_v/F_m (maximum quantum yield of PSII), ETR (electron transport rate, µmol electrons m^{-2} s^{-1}), α_{ETR} (photosynthetic efficiency), ETR_{max} (maximum electron transport rate, µmol electrons m^{-2} s^{-1}), Ek_{ETR} (saturation irradiance, µmol photons m^{-2} s^{-1}); chlorophyll *a* (µg g^{-1} DW); carotenoids as violaxanthin, anteraxanthin, zeaxanthin, and β-carotene (µg g^{-1} DW); phycobiliproteins, such as phycocyanin (PC) and phycoerythrin (PE) (mg g^{-1} DW); mycosporine-like amino acids (MAAs), such as palythine, palythinol, shinorine, porphyra-334 (mg g^{-1} DW); phenolic compounds (mg g^{-1} DW); soluble proteins (mg g^{-1} DW); and antioxidant activity by ABTS and DPPH assays (µM_{TE} g^{-1} DW). Dependent variables for one-way ANOVA included nitrogen and elemental carbon. Bold values indicate significant differences ($P < 0.05$). SS, sum of squares; df, degrees of freedom; MS, mean of squares.

ANEXO D – Material suplementar (Capítulo IV)

Table S. 7. Permanova results for interaction between site and face and irradiance. The p-value < 0.05 are indicated in bold.

Source	df	SS	Pseudo-F	P(perm)	P(MC)
Site	1	2.36	11.53	0.002	0.002
Face	1	12.04	58.65	0.001	0.001
Irradiance	9	450.04	243.71	0.001	0.001
Site * face	1	1.00	4.91	**0.023**	0.030
Site * irradiance	8	3.12	1.90	0.066	0.060
Face * irradiance	8	4.03	2.45	**0.015**	0.014
Site * face * irradiance	7	1.11	0.77	0.615	0.636

df: degrees of freedom; SS: sum of squares; Pseudo-F: F value by permutation, P(perm): p-values based on 999 permutations.